Title
THE CORROSION OF A ZINC ROTATING DISK IN ONE MOLAR HYDROCHLORIC ACID

Author
Hauser, A.K.

Publication Date
1984-04-01

Lawrence Berkeley Laboratory
UNIVERSITY OF CALIFORNIA

Materials & Molecular Research Division

THE CORROSION OF A ZINC ROTATING DISK IN ONE MOLAR HYDROCHLORIC ACID

A.K. Hauser
(M.S. Thesis)

April 1984

Prepared for the U.S. Department of Energy under Contract DE-AC03-76SF00098

DISCLAIMER

The Corrosion of a Zinc Rotating Disk in One Molar Hydrochloric Acid

Alan Hauser

Master's Thesis

Materials and Molecular Research Division
Lawrence Berkeley Laboratory

and

Department of Chemical Engineering
University of California
Berkeley, CA 94720

April 20, 1984

The Corrosion of a Zinc Rotating Disk in One Molar Hydrochloric Acid

Alan Hauser

Materials and Molecular Research Division, Lawrence Berkeley Laboratory
and Department of Chemical Engineering, University of California
Berkeley, CA 94720

April 20, 1984

Abstract

The corrosion of a zinc rotating disk in one molar hydrochloric acid has been studied using a potentiodynamic polarization method. The relationship between the electrochemical behavior of zinc and its corrosion rate in an oxygen–free, aqueous solution is described. The principles of the corrosion process presented here emphasize how important it is that engineers understand the underlying fundamental electrochemical concepts. Both experimental and theoretical treatments of the corrosion process have been investigated.

Experimental rotating–disk data at a rotation speed of 1600 rpm are presented. The polarization curves are analyzed to determine the transfer coefficients and rate constants for the anodic zinc dissolution and cathodic hydrogen evolution reactions. The set of parameters that may be used to fit best the experimental data were compared to those reported in the literature, and significant differences are apparent for the corrosion of zinc. Electrolyte and electrode impurities are possible causes for the differences.

It is of interest to use the experimentally determined kinetic parameters in a mathematical model to predict corrosion rates. A modified Butler–Volmer equation is used to describe the kinetics of the zinc and hydrogen charge–transfer reactions accounting for the forward and back terms of each reaction. Mass transfer of the electroactive and complexed

zinc species is accounted for assuming that the homogeneous reactions are in equilibrium.

The experimental polarization curve shows good agreement with that predicted theoretically provided the back reactions are neglected. However, when the modified Butler–Volmer equation is used, the cathodic polarization sweep away from the open–circuit potential is significantly different from what was expected owing to the effect of the cathodic zinc reaction. The results of the model are compared to conventional polarization techniques which underestimate the corrosion–current density. This indicates the importance of the model.

If my troubles and griefs were weighed on scales,
they would weigh more than the sands of the sea,
so my wild words should not surprise you.

Job, 6: 1

Acknowledgements

I would like to thank Professor John Newman for taking me into his research group. He contributed significantly to my understanding of electrochemical engineering, and his suggestions and criticisms along the way are greatly appreciated. Discussions with my committee members Fiona Doyle–Garner and Jim Michaels were also beneficial and appreciated.

I have benefitted from discussions with my research colleagues, and the friendships that have been made while in Berkeley will always be remembered. My family has been most encouraging and their support has made my work here possible.

This work was supported by the Assistant Secretary of Conservation and Renewable Energy, Office of Energy Systems Research, Energy Storage Division of the U.S. Department of Energy under Contract DE–AC03–76SF00098.

Contents

Chapter 1. Introduction

The deterioration of metallic engineering materials cost the U.S.A. $15 billion a year ten years ago. Today corrosion is a serious and even more costly materials science problem. The future importance of corrosion will only increase in the years ahead as our resources are increasingly utilized to the limits of practicality. To meet future demands, it is necessary for corrosion engineers to develop materials of increased corrosion resistance. Improved corrosion resistance requires research to characterize surface phenomena, to elucidate corrosion mechanisms, to predict the behavior of materials in specific corrosive environments, and to identify materials and processes which control the rate of corrosion reactions. Electrochemical methods will have a significant role in better corrosion control and prevention.

1. Purpose of Thesis

Corrosion is a well established electrochemical process, and new developments leading to a better understanding and to the eventual control of corrosion phenomena will come from the application of current electrochemical analysis. Information about the nature of electrochemical processes is usually obtained in the laboratory where research provides a unique opportunity to separate and investigate experimental variables. Through studies of transport properties of electrolytic solutions, electrode kinetics, and double-layer effects, many electrochemical systems have been well characterized. Similar work must be continued to understand and to deduce mechanisms for corrosion processes. Only then may our materials problems be solved.

The design of critical experiments to evaluate material/environment compatibility depends on a knowledge of the underlying fundamental concepts of the electrochemical nature of corrosion. Researchers, out of the necessity to collect fast, accurate, and reproducible experimental data, have developed systems which are well defined from the standpoint of hydrodynamics, current distribution, and mass transfer. Among the most commonly used is the versatile rotating–disk electrode. The rotating disk may be used in conjunction with potentiodynamic polarization techniques to accelerate the corrosion process. These methods improve the cost effectiveness of corrosion research, which otherwise tends to be both time consuming and expensive. The ability to increase carefully or control the oxidizing potential of an environment and thereby reveal specific characteristics of a material is another advantage of this electrochemical technique.

A combination of theoretical understanding coupled with modern scientific instrumentation is necessary to characterize the electrochemical nature of corrosion processes. The principles governing electrochemical phenomena have been presented by Newman,[1] who assesses the fundamental equations as well as giving a general method of solution of these problems. Next, the experimental data must be related to these theoretical treatments. Combining the two becomes unavoidable in order to simulate situations as close to the actual physical processes as possible. However, due to the intricate coupling of charge–transfer reactions at the surface and mass transfer in the presence of a nonuniform electric field in the solution, the interpretation of experimental data turns out to be more complicated than is usually anticipated. For this reason, rigorously bridging the gap between experimental and theoretical analysis to date has been limited.

This thesis attempts to investigate the relationship between experimental data and theory. Relating measured potentials to the proper theoretical potential difference is fundamental to this work. The ability to do this is important and would have a significant effect on the analysis of not only corrosion processes, but all electrochemical systems. This work is a small step toward the eventual coupling of experimental data with high powered numerical methods for solving sophisticated models. Eventually, with further technological advancements, desk–top computers will be able to collect experimental data and simultaneously determine the physical parameters that best match the experimental data. Computerized data acquisition and a corresponding mathematical model to analyze the data such as proposed here could bring about a change in the present methods of electrochemical research.

2. Structure of Thesis

The specific problem that is to be studied is the anodic dissolution of zinc in a de–aerated one molar aqueous, hydrochloric acid solution. The objective of the work is to demonstrate the experimental and theoretical aspects of an electrochemical approach as applied to a corrosion system. Before giving these results, background information pertaining to corrosion in general and electrochemical engineering analysis is presented.

Chapter 2 gives a historical perspective of the development of the electrochemical theory of corrosion, followed by a discussion of the applications that zinc has in anodic dissolution processes. The third chapter is fundamental in nature and applies thermodynamic and kinetic principles to the analysis of practical electrochemical reactions. A rigorous treatment of potentials is given attempting to relate measured quantities to hypothetical terms with underlying theoretical meaning. The definitions of the surface overpotential, thermodynamic reversible potential,

concentration overpotential, diffusion potential, solution ohmic potential drop, and liquid junction potential are given. This section is long and rather detailed. The most pertinent equations developed there will be given in the following chapters for specific applications.

Chapter 4 describes the standard electrochemical polarization technique used to characterize the zinc corrosion process. An iterative scheme to determine the kinetic parameters from the experimental rotating–disk data is given. The general transport equations are described in chapter 5. However, only diffusion in a stagnant, Nernst boundary layer coupled with charge–transfer reactions at the electrode, and equilibrium zinc complexing reactions next to the surface are accounted for in the present model. The emphasis is on the methodology that will enable the measured potentials to be related to the theoretical potential differences and to show their effect. In chapter 6 the results of the model are compared to conventional corrosion analysis. Limitations to the traditional ways are pointed out.

Chapter 2. Corrosion and the Role of Zinc in Anodic Dissolution Processes

1. Introduction

One only has to contemplate that the pocket flashlight and the portable transistor radio are commonly driven by the Leclanché dry cell to realize that metallic corrosion is electrochemical in origin. Roughly 10 mg of zinc are electrochemically oxidized every second a small flashlight is operated. If we assume that one quarter of the world's population owns a Leclanché–battery–operated device and has it switched on for an average of one hour a day, then some 30 metric tons of zinc are dissolved daily in this way. Clearly, metallic corrosion can amount to electrochemistry on a grand scale.[2]

In this chapter, a historical perspective of the electrochemical nature of corrosion analysis will be given followed by a general review of corrosion prevention techniques. The emphasis in the latter section however will be on specific applications that zinc has for control and protection. The last section of the chapter will discuss the role of the zinc electrode as the anode of primary and secondary batteries.

2. Historical Perspective

It was long questioned whether the most familiar manifestations of immersed metallic corrosion are electrochemical. Hoar with Evans[3] in 1932 accomplished this by proving that the rusting of iron is quantitatively faradaic. Agar's more elaborate experiments[4] with zinc in 1939 finally secured the electrochemical basis for corrosion.

Pourbaix in 1938 developed diagrams to represent that the equilibrium potential of a metal in an aqueous solution depends not only on the activity of the relevant metal ions in solution, but also on the hydrogen ion activity as conveniently expressed by pH. Out of this essentially thermodynamic approach, the potential/pH diagram has become attractive educationally for summarizing in easy visual style a diversity of metals' performance in aqueous conditions. The diagram is extremely useful to know if a metal is immune to corrosion in given circumstances. However, practical situations most often subject metals to corrosive risks, and the rate of corrosion, which is not apparent from the potential/pH diagram, then becomes of great importance.

From about the turn of the century, the pioneer corrosion workers gave considerable attention to corrosion–rate measurements, but the advent of polarization curves in corrosion science waited until Evans and Hoar[3] had demonstrated that the current in a corrosion cell could be equated to the metal loss. It was the concept of mixed potential introduced by Wagner and Traud[5] in 1938 that has been invoked at some time by almost every electrochemist working in corrosion science. The acceptance of the potentiostat and the importance of the anodic polarization curve were most significant to the advance of corrosion science.

The polarization curves allow the electrochemical kinetics of corrosion reactions to be studied. Probing the meaning of Tafel lines for corroding metals and connecting this with the dissolution of the metal has become a standard tool in corrosion analysis. Almost twenty years later, Stern and Geary[8] were able to elaborate on the Russian electrochemical approach of Frumkin established in the 1940's. By this time advances in electrochemical kinetics had produced a detailed two–term expression for the current of a reaction for the entire potential range starting from the reversible

potential.[7] Stern and Geary showed by extrapolating the straight sections of the Tafel lines of the anodic metal dissolution reaction and the cathodic hydrogen evolution reaction back to the rest potential the current at this conjunction could be identified with the corrosion rate of the metal. By making these simplifying assumptions for the kinetic expressions, they obtained a convenient and convincing expression for the metallic corrosion current giving the constant of proportionality between polarization resistance and corrosion rate.

Response to the Stern–Geary equation has been mixed since its introduction in 1957. More rigorous treatments of its theoretical basis have been published, leading to more complexity. On the other hand, many practical corrosion workers trust the original Stern–Geary equation and the corrosion rates calculated from it. Mansfeld and Oldham[8] have examined theoretically the effect on the reliability of the Stern–Geary equation of making the original assumptions. They show that the simplified equation can yield wrong results under certain conditions. Therefore, the Stern–Geary equation should be used with much circumspection, and the observer should always prove first by independent measurement, *i.e.*, weight–loss experiments, that the Stern–Geary equation is suitable for use with the system of interest.

3. Corrosion Prevention

Corrosion of metallic materials is a major limitation in the chemical industry. In a variety of processes, dissolution of metal occurs at high rates from locally active anodic regions leading to equipment failure or contamination of the final product. Because of zinc's stability and highly protective nature in aqueous media, it has an important role in corrosion prevention.[9] Zinc is more negative than hydrogen on the EMF scale and is more active than most common metals. Therefore, zinc would be expected

to undergo spontaneous dissolution by reacting with water to release hydrogen. However, zinc dissolves very slowly except in strongly acid or alkaline solutions.[10] The high hydrogen overpotential ostensibly exhibited by zinc in near neutral solutions is deduced directly from this experimental observation. Important results of this stability include the ability to use zinc as a battery anode material and for corrosion prohibition and galvanizing.

3.1. Electrochemical Protection

Electrochemical protection is applied by one of two methods, power–impressed current or sacrificial anodes. In the latter method, a galvanic couple is formed when the sacrificial anode is attached to the protected structure. In order to utilize this method, the anode must have a potential that is more negative than that of the protected structure. When connected, the structure is polarized cathodically, and the sacrificial anode is polarized anodically, and the two reach the same potential, provided the resistance of the electrolyte is sufficiently low. The sacrificial anode is consumed by dissolution during protection of the cathode and requires periodic replacement. For maximum efficiency of protection, the self–corrosion of the anode should be a minimum.

Zinc's standard potential is more negative than all of the more common metals of construction except aluminum and magnesium. When zinc coats any of the more noble metals, a sacrificial electrochemical reaction may occur with the active zinc forming the anode. While this action leads to increased zinc corrosion, it provides the basis for the protection of metal structures by coupling them to zinc metal. Pure zinc must be utilized to obtain good efficiencies for cathodic protection. Because of the low driving force for potential, cathodic protection of ships' hulls, pipes, and other structures using zinc finds application mainly in seawater and in more

conductive soil environments. The use of zinc may not be practical in environments requiring high currents or involving high resistance.[11]

Power–impressed current protection, whether anodic or cathodic, is another important electrochemical method because it is easy to apply and control. The impressed–current method operates by the maintenance of the electrode potential of the object at a level where the corrosion rate is low. Cathodic protection, *i.e.*, controlling the potential in the cathodic region, is presently being adopted instead of galvanic protection whenever electric power is available. Impressed current is widely used today for internal and external protection of pipelines and ships' external hulls. The amount of current required to protect a metal depends on the corrosion rate and the area of the surface. Anodic protection, which functions by the control of the potential in the anodic region at a level where passivation is obtained, is used mainly for titanium and for stainless steel in contact with sulfuric acid.[12]

3.2. Inhibitors and Alloys

A corrosion inhibitor is a chemical substance which, when added in small concentrations to an environment, decreases, or prevents the reaction of the metal with the environment. Most inhibitors are used in liquid systems, *i.e.*, alcohols and amines are common cathodic inhibitors, but vapor corrosion inhibitors which prevent corrosion in the atmosphere also exist. Even though the use of inhibitors is of great practical importance, their widespread use has been limited because of the lack of general understanding and the poor information available on specific commercial inhibitor products.[12] Corrosion prevention by inhibitors often seems risky today, and considerable efforts are needed to bridge the gap existing between scientific work conducted in the laboratory and actual service problems. Future work needs to be done to develop simple and quick

electrochemical methods for the evaluation of a given inhibitor. Then corrosion inhibitors might become an effective tool more generally employed in the fight against corrosion.

The protective nature of zinc depends on, in part, the hydrogen overpotential characteristics which control the rate of zinc corrosion in aqueous solutions. Again, pure zinc possesses a very high hydrogen overpotential, implying a low exchange–current density for hydrogen on zinc. The presence of impurities (e.g., iron, copper, and nickel) with low hydrogen overpotentials either in the zinc or in the environment drastically increases the corrosion rate. Therefore, control of zinc corrosion rests on control of the hydrogen evolution reaction. Alloying with higher hydrogen overpotential metals (e.g. mercury and tin) decreases the corrosion rate.

3.3. Protective Coatings

The most common method of corrosion prevention is the application of protective coatings.[11] The success of zinc coatings rests on the low cost of zinc, the ease of application, and its high corrosion resistance. The two main reasons for zinc's excellent protective coating have previously been stated. The first is the natural resistance of zinc itself against corrosion in the atmosphere and in most natural waters. The second is the fact that zinc's standard potential is negative to iron and can protect it sacrificially.

The protective nature of the corrosion film results from a layer of non–conducting zinc hydroxide and oxides as well as basic carbonates and salts, making the hydrogen evolution reaction negligible. The exact composition of the protective film depends on the nature of the environment. In aqueous solution the pH of the environment governs the formation of the protective film. In alkaline and acid solutions, the formation of protective layers is lessened, and corrosion increases at both high and low pH. A conductive medium increases the protection provided by

the zinc coating because it provides a low resistance electrolytic path between zinc and base metal.

The natural resistance of zinc is its most important property in relation to zinc coatings. The electrochemical property becomes important when the zinc coating is damaged in any way to expose the metal. The sacrificial corrosion of the zinc then occurs, and the more noble metal is thereby protected. Moreover, the corrosion product of the zinc normally fills the break in the coating and prevents or retards further corrosion of the exposed metal. As the protective value of the zinc coating depends largely on the corrosion resistance of zinc, the life of the coating is governed almost entirely by its thickness and by the severity of the corrosion conditions to which it is exposed. The principal method for applying zinc coatings to iron and steel is hot-dip galvanizing. Other methods include spraying, plating, and painting with zinc-rich paints.

Galvanizing

It is estimated that approximately 40% of the world production of zinc is consumed in hot-dip galvanizing of iron and steel, and this adequately demonstrates the world-wide use of zinc as a protective coating.[13] The oldest and most familiar of commercial processes used for applying metallic coatings to other metals is hot dipping. Hot dipping refers to immersion in molten metal. Zinc coating by hot dipping is known as the galvanizing process. Galvanized, as applied to zinc-coated iron, had its origin in the concept of the galvanic protection from corrosion afforded iron by zinc in contact with it. The coating is not uniform in composition, but is made up of layers of zinc-iron alloys becoming progressively richer in zinc towards the surface, so that the actual surface layer is composed of more or less pure zinc. Because of this alloy formation, there is a strong bond between the coating and the steel resulting in a successful coating given by the

hot–dipping process. The process produces a thick coating which thoroughly covers the work, sealing all edges, rivets, seams, and welds when fabricated articles are treated. Hot–dip galvanizing is the most widely used method for coating with zinc.

Plating

There are many books and reviews dealing with electroplating as a commercial technology and as an interesting process for scientific enquiry. However, it is mentioned here because the production of electroplated coatings can be used for the control of corrosion. Zinc coatings produced by plating have the advantage that the thickness can be accurately controlled according to the protection desired. The coating is of uniform composition throughout, containing no alloy layer, and is united with the underlying surface by a metal/metal bond. The process is more expensive, and plating is confined to much smaller objects than those of the other methods given. Thus, corrosion control is not the sole function of electroplated coatings. Other virtues of plating are decoration, reflectivity, wear resistance, solderability, and low contact resistance.

Metal spraying

The advantage which the metal spraying process possesses over almost any other is that zinc coatings can be applied to very large structures, such as bridges. In this method there is no alloy formation, and the bond is primarily mechanical. Although porous, the coating is protective as discussed before partly due to the zinc corrosion products which soon block up the pores, stifling further attack. Sprayed deposits of zinc and aluminum have protective properties proportional to their thickness. Therefore, if the zinc coating has sufficient weight per unit area, it will give complete protection.

Painting

Antirust painting accounts for a major proportion of the total corrosion budget.[12] The main use is to protect structural steel–work, ships' hulls, and vulnerable parts of car bodies, and to repair damage to other zinc coatings. Paints capable of protecting steel prepared with zinc dust function satisfactorily only in the presence of an electrolyte. The metallic pigment paints are quite porous, and water containing a trace of salt or acid completes the circuit formed by the two metals. The useful life of the paint is not limited to the life of the electronic contact between the zinc particles, because of the formation of hydroxyl ions at the steel surface. Consequently as mentioned before, the surface becomes coated with these deposits, which block the pores in the film and render it very compact, adherent, and impervious. Thus, although metallic contact between the steel and the zinc dust particles is essential in the early stages of exposure, the paints provide good protection after that contact has been lost. As was stated previously, the metal spraying process provides a method of treating steel with coatings of zinc or aluminum which can afterwards be painted. Outstanding virtues of zinc–rich paints are simplicity of application and a combination of a metallic primer and a good silicate–bonded zinc–dust paint is the most effective means of combating corrosion of constructional steelwork at a reasonable cost that is known yet.[11]

In the same way as for an unprotected surface, the corrosion of a painted metal surface proceeds by the action of an electrochemical corrosion cell. The cathodic reaction is the reduction of oxygen permeating through the paint film to the metal surface. The paint film which includes absorbed water, constitutes an essential part of the electrolyte. Thus the overall corrosion mechanism on a painted metal surface might be entirely different than in plain metal–solution systems. Knowledge of the

mechanism of corrosion on painted metal would provide a good basis for the development of a rapid test method for anticorrosion paints. Such a method is urgently needed, as even in this case the conventional field tests require too long exposure times, and the accelerated test methods now being employed are often far from representative of the exposure in practice. In fact, a quick and reliable method for the evaluation of anticorrosion paints is essential for rational development work in this field.

4. Battery Anodes

Zinc is the anode in many commercially important primary cells and in several high–energy–density secondary cells. In the primary Leclanché cell, zinc dissolves anodically into the separator layer as the simple ion, which then forms complexes with the near–neutral electrolyte. Zinc corrosion and its effects on cell water balance constitute important limitations on the storage or shelf life of the Leclanché cell.

In battery production, the zinc container for primary batteries and zinc electrodes for silver–zinc cells are usually amalgamated with mercury to keep the corrosion of metallic zinc at a very low rate. A zinc battery is very easily destroyed if a salt containing ions of a metal with a high exchange–current density is put into the battery electrolyte. This results from the corrosion of zinc with common impurities being 10,000 times larger than that of amalgamated zinc.[14]

Aqueous zinc halide batteries, such as $ZnCl_2$–KCl–H_2O or $ZnBr_2$–KCl–H_2O, are being investigated for electrical vehicles and utility load–leveling purposes. The major considerations are overall energy efficiency and system cost. To maximize energy efficiency, cell design is aimed at reducing coulombic and voltaic losses in cells. Parasitic hydrogen generation at the zinc electrode and irreversibility of the zinc electrode are two losses that may be overcome through fundamental kinetic studies.

Included in the cost issue is component stability and reliability, which affect life cycle cost of the system. Again, corrosion and instability of the zinc anode are problems that possibly can be solved only with more research.

Chapter 3. Electrochemical Reaction Fundamentals

1. Introduction

As was stated in chapter 1, the objective of this work is to understand corrosion processes by emphasizing fundamentals. The purpose of this chapter is to present the theoretical tools so that the electrochemical reactions of a corrosion process may be studied and further understood. In order to obtain useful information about the reactions from experimental data, it is necessary to relate the measured quantities to idealized, hypothetical quantities with underlying fundamental concepts. This requires the use of thermodynamics, kinetics, and transport phenomena, and will be presented in the next two sections. However, before proceeding with the details of the fundamental equations, it is necessary to understand how to analyze the electrochemical cell used in this experimental study.

An electrochemical cell consisting of two electrodes separated by a conducting, electrolytic solution is represented in figure 3–1. Because it is of interest to study the corrosion process at the negative zinc electrode, it is indicated on the schematic as the working electrode. The secondary electrode chosen is chemically inert platinum and is specified as the counterelectrode. Since the platinum electrode potential is positive relative to the zinc electrode potential and platinum has a low hydrogen overpotential, hydrogen evolution will occur at the counterelectrode when the electrodes are connected externally. When electrons are allowed to pass from the negative to the positive electrode through the external circuit, the circuit is completed by ionic, chemical species transfer across the cell through the electrolyte. The change from electronic conduction to ionic conduction occurs at the electrode surfaces. The electrodes must be

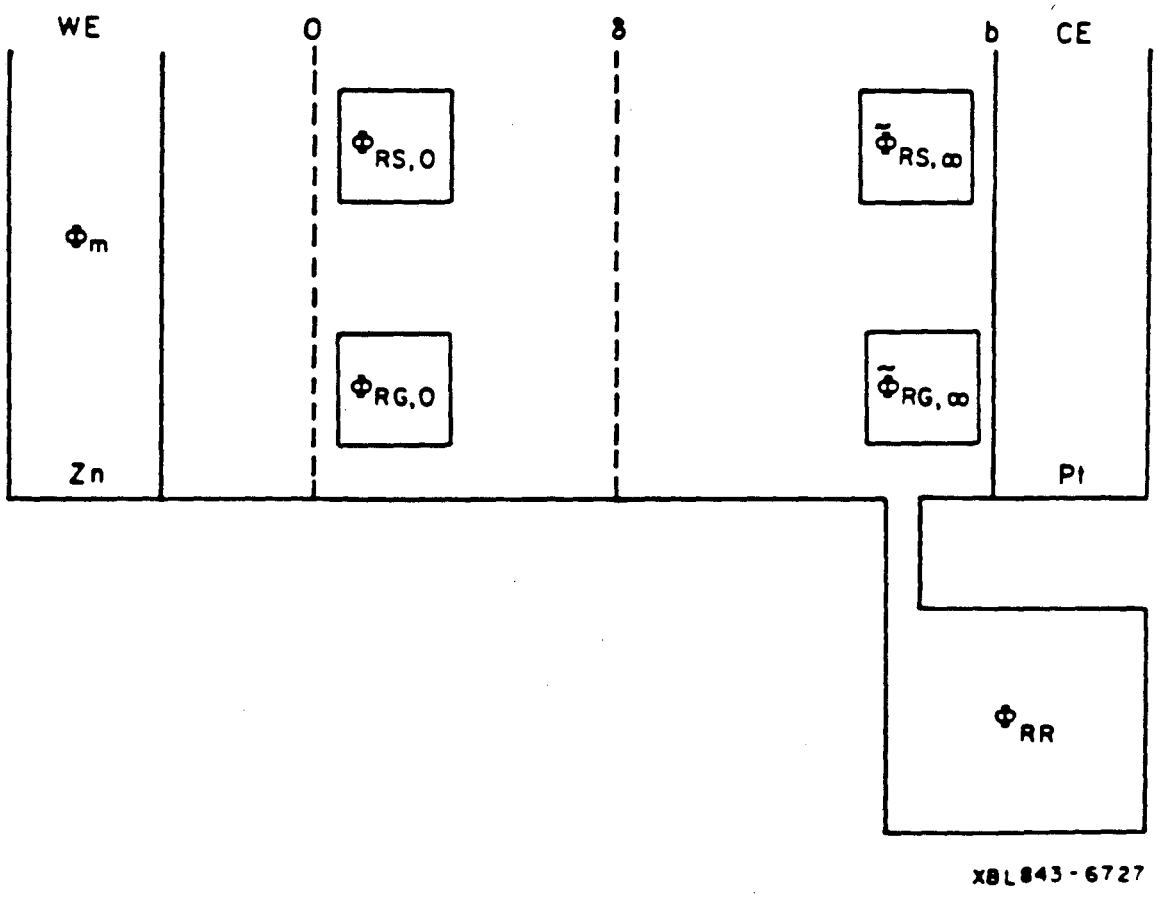

Figure 3–1. The electrochemical cell.

electronic conductors to assure that electrons can get to or from sites at which the electrochemical reaction takes place. It is these electrochemical or faradaic reactions that are of interest to study at the working electrode.

It should be noted that it is possible also for electronic and ionic charge to accumulate at an electrode without any chemical reactions occurring. This capacitance effect occurs next to the working electrode in the diffuse double layer. The outer edge of the double layer is denoted with a 0 in figure 3–1. This thin region actually is part of the electrode–electrolyte interface and is about 1 to 10 nm thick. At steady–state, the double layer is charged, and the measured potential difference is independent of the capacitance.

In addition to electrons getting to and from reaction sites, species in the electrolytic solution must get to and from the reaction site. The solution–phase transport gives rise to concentration variations near reaction sites which affect the rate of reaction. All concentration gradients may be assumed to be within a region next to the electrode interface, and the bulk solution therefore has a constant concentration. The diffusion layer is shown in figure 3–1 with thickness δ. For this system, as for most aqueous solutions with excess supporting electrolyte, the Schmidt number $Sc = \nu / D_i$ is 1000 or higher. High Schmidt numbers result in thin diffusion layers (of the order of 10 μm thick) relative to the hydrodynamic boundary layer.

An important technique used to investigate cell behavior is to insert a reference electrode into the cell. The purpose of the reference electrode is to measure the potential in the solution. It should be pointed out that the current flow is between the working electrode and the counterelectrode, and the reference electrode with its high input impedance is used only to sense the potential at a given solution composition and position within the cell. The reference electrode should be reversible and reproducible, and its potential should remain constant over the course of an experiment. The

reference electrode should be chosen so that its electrolytic solution, which is usually in its own separate compartment, is as similar as possible to the electrolytic solution being measured. This minimizes contamination and complicating liquid–junction effects. By careful placement of the reference electrode, it is possible to determine how the cell potential changes with varying operating conditions.

Also shown in figure 3–1 are five different reference electrodes which may be used to assess the potential difference between the working electrode and the solution at some distance from the working electrode. There are four imaginary reference electrodes and one real reference electrode. The potential difference that may be measured, $\Phi_m - \Phi_{RR}$, is the potential of the metal Φ_m minus the potential of an actual reference electrode of a real kind Φ_{RR} placed in the bulk solution. However, if thermodynamics is to be of any help in the analysis, it is necessary to break down the overall measured potential into potentials with a theoretical basis. This is done by the introduction of hypothetical reference electrodes. The potentials of the hypothetical reference electrodes that are shown in figure 3–1 are designated by $\Phi_{RS,0}$, $\tilde{\Phi}_{RS,-}$, $\Phi_{RC,0}$, and $\tilde{\Phi}_{RC,-}$. Each is defined here and will be discussed further in sections 3.2, 3.3, and the appendix.

$\Phi_{RS,0}$ and $\Phi_{RC,0}$ are potentials which would be measured by reference electrodes placed next to the working electrode just outside the diffuse double layer. The difference between them is that $\Phi_{RS,0}$ is the potential as sensed by a reference electrode of the same kind as the working electrode. The imaginary reference electrode $\Phi_{RS,0}$ is defined so that at a given position, the electrolytic composition of the reference electrode is at the same composition as the electrolytic solution that is being measured. Therefore, no concentration differences or liquid–junction regions may exist between this highly idealized reference electrode and the solution. $\Phi_{RC,0}$ is the

potential given by a reference electrode of given kind. Its reference electrode compartment usually will have a composition different from the solution being measured. However, any liquid–junction potential which might exist between the solution in question and that within the reference–electrode compartment is corrected for by definition of the ideal reference electrode. "Corrected for liquid–junction potentials" means making the (perhaps imaginary) requirement that the electrical states of the two solutions be equal.[1]

$\tilde{\Phi}_{RS,\infty}$ and $\tilde{\Phi}_{RG,\infty}$ are the potentials of reference electrodes of the same and given kinds, respectively, at a large distance from the working electrode and are for all practical purposes at infinity. The potentials indicated with tildes represent the potential that would exist at the specified position if the concentration everywhere were that of the bulk solution. These potentials satisfy Ohm's law and therefore are the solution of Laplace's equation

$$\nabla^2\tilde{\Phi} = 0 \quad , \tag{3–1}$$

for the potential variation in a solution with uniform concentration.

The measured potential difference may be rewritten

$$\begin{aligned} V^{\infty} &= \Phi_m - \Phi_{RR} \\ &= (\Phi_m - \Phi_{RS,0}) + (\Phi_{RS,0} - \tilde{\Phi}_{RS,\infty}) + (\tilde{\Phi}_{RS,\infty} - \Phi_{RR}) \end{aligned} \tag{3–2}$$

using the reference electrode potentials defined above. As will be shown later, this is equivalent to

$$V^{\infty} = \eta_{sj} + \Delta\Phi_{RS} + U''_{j/RR,\infty} \quad . \tag{3–3}$$

The potential difference between electrode reaction j, evaluated at the species' bulk concentrations, and a real reference electrode, $U''_{j/RR,\infty} = \tilde{\Phi}_{RS,\infty} - \Phi_{RR}$, is calculated using principles of local equilibrium and transport equations because a junction region exists between the bulk solution and the actual reference electrode's solution compartment. The remaining terms on the right side of equation 3–3 are potential losses which

are non–zero when current flows. The surface overpotential for reaction j, $\eta_{sj} = \Phi_m - \Phi_{RS,0}$, is associated with the energy losses that accompany driving the charge–transfer reaction j at the reaction sites. Energy also is required to transport electrons, ions, and neutral species to and from reaction sites. The decrease in cell potential resulting from concentration variations is the concentration overpotential, η_c. Added to the concentration overpotential is the energy necessary to drive ions through the solution to carry electrical current, which is the solution resistance loss or ohmic loss, $\Delta\tilde{\Phi}_{ohm}$. Both of these energy losses go into $\Delta\Phi_{RS} = \Phi_{RS,0} - \tilde{\Phi}_{RS,-}$. Therefore, the potential difference across the cell as measured by two reference electrodes of the same type placed just outside the diffuse double layer and in the bulk solution. may be given by $\Delta\Phi_{RS} = \eta_c + \Delta\tilde{\Phi}_{ohm}$, where $\Delta\tilde{\Phi}_{ohm}$ is the potential difference which would exist if there were the same current distribution but no concentration gradient in the diffusion layer.

Since the bulk concentration of the cation being produced is quite often zero for a corrosion process, the concentration overpotential and the potential $\tilde{\Phi}_{RS,-}$ are undesirable to use, as will be shown later. One can rewrite V^* as

$$V^* = (\Phi_m - \Phi_{RS,0}) + (\Phi_{RS,0} - \Phi_{RC,0}) + (\Phi_{RC,0} - \tilde{\Phi}_{RC,-}) + (\tilde{\Phi}_{RC,-} - \Phi_{RR}) \quad (3\text{–}4)$$

This will be shown to be equivalent to

$$V^* = \eta_{sj} + U'_{j/RC,0} + \Delta\Phi_{RC} + U''_{RC/RR,-} \quad . \quad (3\text{–}5)$$

The potential difference V^* as measured between the metal and a real reference electrode in the bulk is the same no matter how the cell is divided. In equation 3–5, the surface overpotential η_{sj} is the same as is given in equation 3–3. However, the remaining potential terms on the right of equation 3–5 are defined differently.

$U'_{j/RC,0} = \Phi_{RS,0} - \Phi_{RC,0}$ is a thermodynamic potential difference that assesses the electrical state of the working electrode reaction j relative to

the given reference electrode RG evaluated at the same species surface concentrations. Since the potential difference is defined by imaginary reference electrodes, it contains no liquid–junction potentials. The potential difference, $\Delta\Phi_{RG} = \Phi_{RG,0} - \tilde{\Phi}_{RG,-}$, is the potential of a reference electrode of a given kind placed next to the working electrode minus the potential of another reference electrode of a given kind in the bulk. It may be rewritten as $\Delta\Phi_{RG} = \Delta\Phi_{diff} + \Delta\Phi_{ohm}$, where $\Delta\Phi_{diff}$ is the diffusion potential and $\Delta\Phi_{ohm}$ is the ohmic potential drop of the solution with concentration variations. The potential difference $U''_{RG/RR,-} = \tilde{\Phi}_{RG,-} - \Phi_{RR}$ between a hypothetical reference electrode of a given kind $\tilde{\Phi}_{RG,-}$ placed in the bulk solution (not containing a liquid junction) and a real reference electrode Φ_{RR} placed in the same bulk solution is established by the activity gradients of species across the junction, and transport equations are necessary to treat this problem.

It is the purpose of the remaining sections of this chapter to define carefully the variables in equations 3–3 and 3–5 in terms of thermodynamics, kinetics, and the laws of diffusion taking into account the method of forming the junction.† The results will be of a general nature, but only the applications specifically for the anodic zinc dissolution and the cathodic hydrogen evolution reactions as they occur in the corrosion process of zinc in dilute, aqueous hydrochloric acid will be presented.

2. Cell Potential for Corrosion Processes

The expression developed in section 1 for the measured cell potential particularly for a corrosion process is given by

$$V'' = \eta_{sj} + U'_{j/RG,0} + \Delta\Phi_{RG} + U''_{RG/RR,-} \qquad (3\text{–}6)$$

Before proceeding to give expressions for each of these terms, it is

† The notation used in section 40 of reference 1 to define reference electrodes of a given kind will be followed. Newman uses U and U' to denote cell potentials without and with junction regions, respectively.

necessary to understand better the relationship between each of the imaginary reference electrodes that have been introduced. Figure 3–2 qualitatively gives the potential profiles within the electrochemical cell shown in figure 3–1. Because three types of reference electrodes are used, it is interesting to compare the results given by each. The potentials Φ_{RS} of the reference electrodes of the same type as the reaction of interest occurring on the working electrode are shown by dotted lines just below the potential Φ_m of the working electrode. The potentials Φ_{RG} of the reference electrode of a given kind are given below. The potential of the real reference electrode Φ_{RR} is given at the bottom of the figure.

The significance of figure 3–2 is that it shows qualitatively how the measured cell potential $V = \Phi_m - \Phi_{RR}$ may be subdivided using the hypothetical reference electrodes Φ_{RS} and Φ_{RG} into a number of potential differences that are given on the right of the figure. The potential difference that is shown first from the top is the kinetic potential driving force or surface overpotential

$$\eta_{sj} = \Phi_m - \Phi_{RS,0} \quad . \tag{3–7}$$

At equilibrium,† this overpotential equals zero since $\Phi_m = \Phi_{RS,0}$. Next, the potential difference between reference electrodes $\Phi_{RS,0}$ and $\Phi_{RG,0}$, when both are placed just outside the diffuse–double layer, is the thermodynamic potential $U'_{j/RG,0}$ between the two different reference electrode reactions j and RG. As we move down the figure, $\Delta\Phi_{RG}$ is the potential difference between the two ideal reference electrodes of a given kind, where one is placed next to the electrode surface and the other in the bulk. This difference includes the diffusion potential $\Delta\Phi_{diff}$ and ohmic resistance of the solution. Finally, the potential difference between the imaginary reference electrode of a given kind and the real reference electrode is shown at the

† It will be shown later in this chapter that the corrosion process does not reach an equilibrium state.

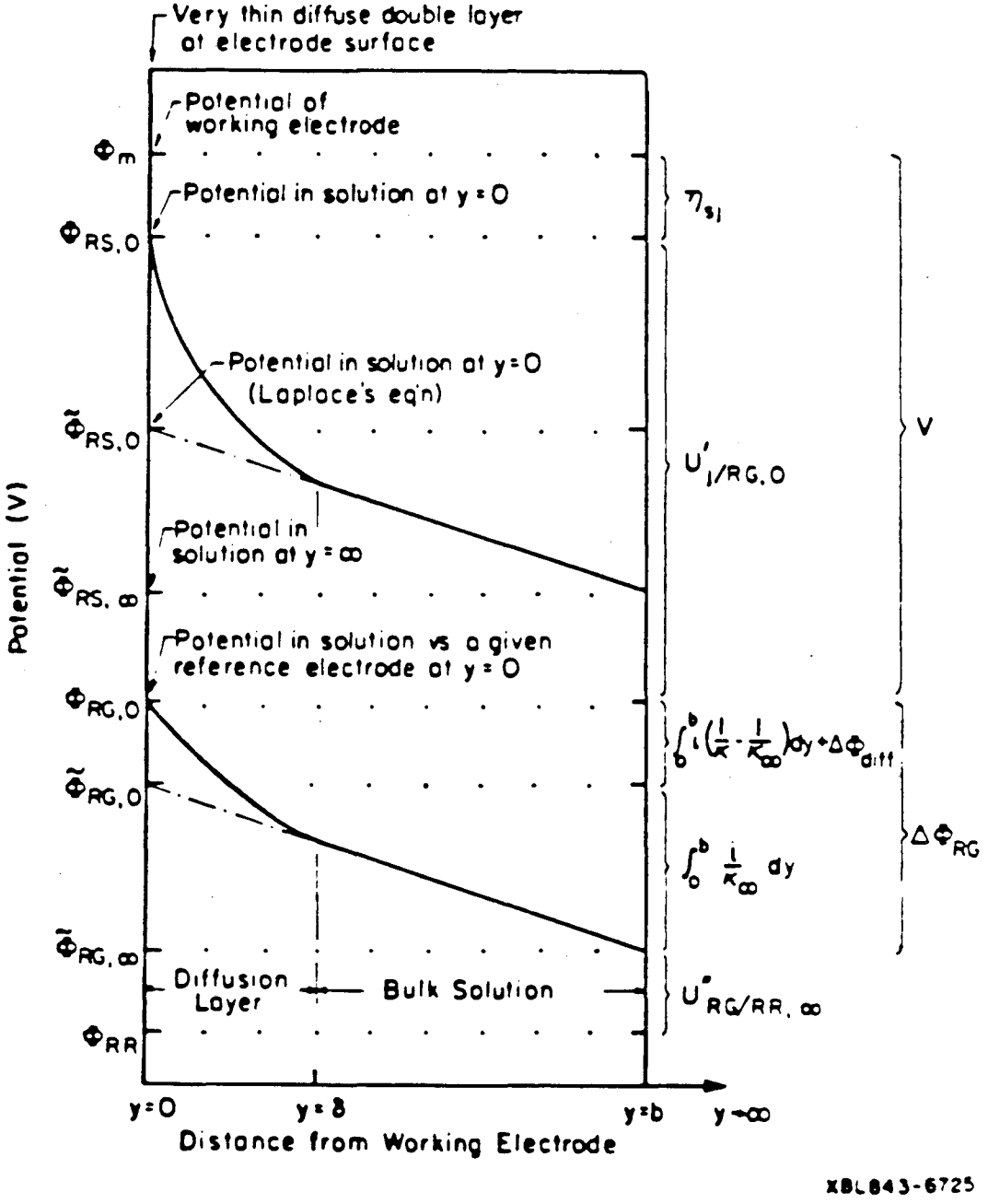

Figure 3-2. Potential distributions. This figure applies to the case where the reactant concentration does not go to zero in the bulk solution.

bottom of the figure to be $U''_{RG/RR,\infty}$.

It should be noted that two additional potentials are shown in this figure that were not given in figure 3–1. $\tilde{\Phi}_{RS,0}$ and $\tilde{\Phi}_{RG,0}$ are the potentials of the solution adjacent to the working electrode as measured by the two hypothetical reference electrodes as if there were no concentration gradients across the diffusion layer. If the conductivity is constant across the diffusion layer, the difference between the reference electrodes of a given kind $\Phi_{RG,0}$ and $\tilde{\Phi}_{RG,0}$ reduces to the diffusion potential. This potential difference should be compared to the potential difference $\Phi_{RS,0} - \tilde{\Phi}_{RS,0}$ between the two reference electrodes of the same kind as electrochemical reaction j. The latter potential difference is the definition of the concentration overpotential. More will be said about it later, but for now it should be pointed out that the zinc reference electrode is very sensitive to the potential difference across the diffusion boundary layer since the difference in the zinc ion concentration is large. The reference electrode of a given kind, a saturated calomel electrode (SCE),† is less sensitive to the concentration difference across the boundary layer. For this reason, the concentration overpotential is larger in magnitude than the diffusion potential. For example, if the zinc bulk concentration is zero, then the concentration overpotential is positive infinity. Each of these potential differences will be discussed further in the following sections.

Figure 3–3 is a helpful representation of the cell potential V' measured between the zinc working electrode and an actual saturated calomel electrode placed in the bulk. Two of the terms in equation 3–6, $U'_{j/RG,0}$ and $U''_{RG/RR,\infty}$, may be determined by constructing hypothetical electrochemical cells as shown in the figure, and then by applying local equilibrium concepts.

† For this work, the calomel electrode is chosen as the reference electrode because the chloride ion, which participates in the reversible calomel reaction, is common with the electrolyte (reducing the junction potential) and has an invariant internal concentration within the reference electrode compartment.

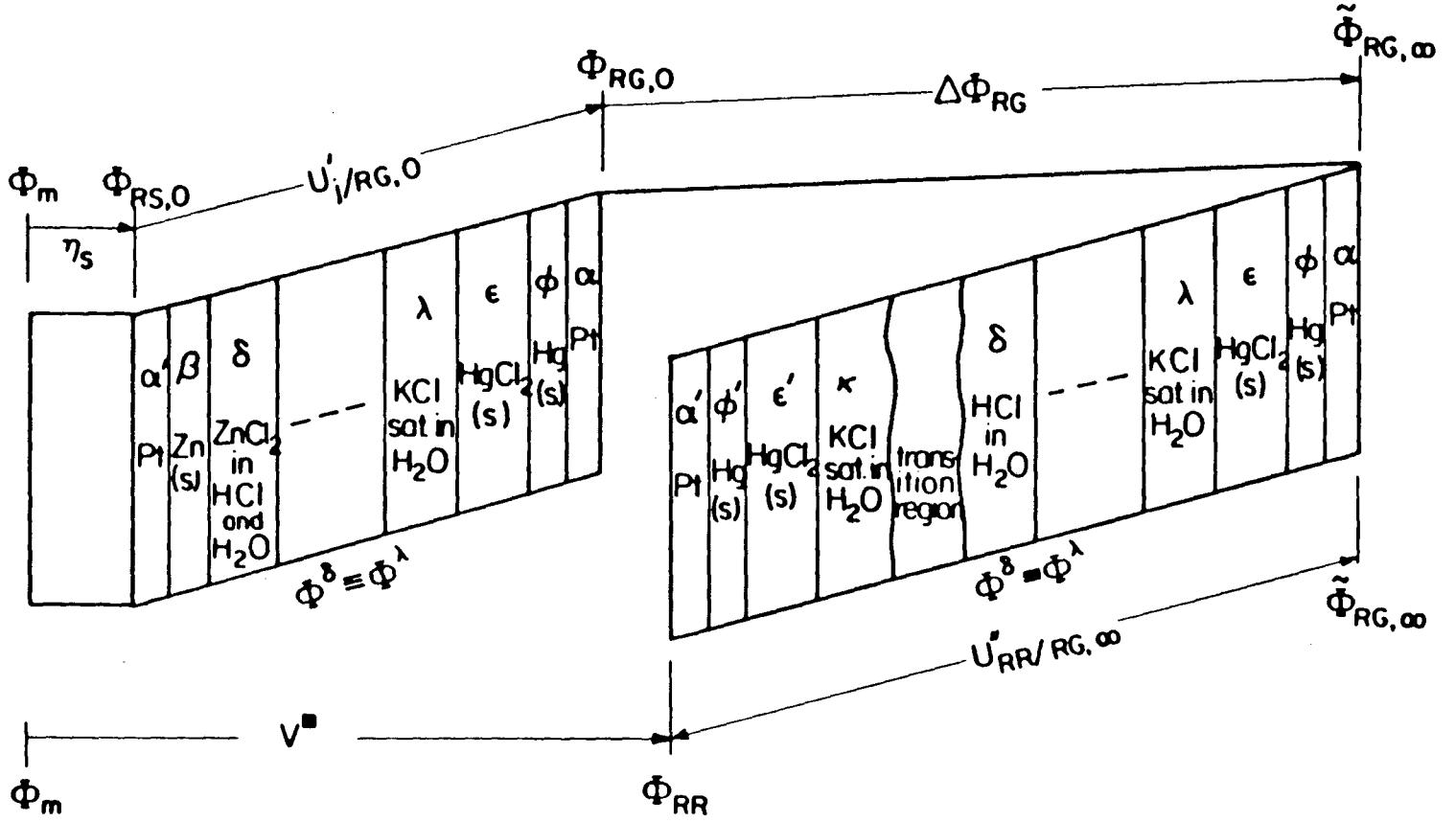

Figure 3–3. Schematic of the measured cell potential.

The thermodynamic potential $U'_{j/RG,0}$ refers to the conceptualized cell potential difference between two electrode reactions at a given position (adjacent to the working electrode) in the actual cell. For this case, the zinc reaction occurring at the electrode surface is shown relative to the calomel electrode, where the potentials of the δ and λ phases are equal by definition. When the potential of the bulk solution is assessed, a potential difference $U''_{RR/RG,\infty}$ results from using a real reference electrode in the place of an ideal reference electrode of a given kind. This difference between the two types of calomel electrodes includes a junction or transition region and is represented on the right of the figure.

The other two potential differences shown in figure 3–3 are η_{sj} and $\Delta\Phi_{RG}$. Again, the surface overpotential η_{sj} is shown to be the difference between the working electrode and an ideal reference electrode Φ_{RS} placed adjacent to the working electrode. $\Delta\Phi_{RG}$ is the potential difference across the cell as given by two reference electrodes of a given kind placed outside the diffuse–double layer and in the bulk solution. This difference includes the potential variation with position due to activity gradients and ohmic resistance of the solution. Transport processes must be considered to obtain an equation for $\Delta\Phi_{RG}$. In the next three sections, we should like to give explicit expressions for each term in the measurable cell potential equation 3–6.

2.1. Cell Potentials Relative to a Given Reference Electrode

The theoretical thermodynamic potential difference between the electrode reaction j and the reference electrode reaction RG is given by $U'_{j/RG,0} = \Phi_{RS,0} - \Phi_{RG,0}$, where 0 denotes the position next to the electrode surface shown in figure 1. An expression may be derived for this potential difference by mentally constructing an electrochemical cell for the zinc corrosion process as follows:

α	φ	ε	λ	δ	β	α'
Pt	Hg(s)	Hg_2Cl_2(s)	4.1 M KCl saturated in H_2O	$ZnCl_2$ and HCl, in H_2O	Zn(s)	Pt

The corrosion of zinc in zinc chloride and dilute, aqueous, hydrochloric acid electrolyte is represented here. A saturated calomel electrode is shown on the left of the cell. This ideal reference electrode of a given kind with potential $\Phi_{RC,0}$ is used to access the potential $\Phi_{RS,0}$ of the electrode reaction j. The dashed line does not denote a junction region; instead we make the requirement that the electrical states of solutions λ and δ are equal in this hypothetical cell so that thermodynamics alone may be applied.

The calculation of a finite cell potential $U'_{j/RC}$ may be carried out by applying the concept of local equilibrium as shown by Newman.[1] It is assumed that equilibrium exists between the reacting species and the metal so that the sum of the electrochemical potentials of the electrode reactants equals the sum of the electrochemical potentials of the products. The mercury–mercurous chloride reference electrode reaction at the left of the cell shown above is

$$2Hg + 2Cl^- = Hg_2Cl_2 + 2e^- \quad , \tag{3–8}$$

and one possible reaction at the right electrode is

$$Zn = Zn^{2+} + 2e^- \quad . \tag{3–9}$$

Another reaction that occurs at the working electrode is hydrogen evolution and will be given following this treatment of the zinc cell potential.

The local equilibrium relationship for reactions 3–8 and 3–9 are given as

$$2\mu^{\varphi}_{Hg} + 2\mu^{\lambda}_{Cl^-} = \mu^{\varepsilon}_{Hg_2Cl_2} + 2\mu^{\alpha}_{e^-} \tag{3–10}$$

and

$$\mu^{\beta}_{Zn} = \mu^{\delta}_{Zn^{2+}} + 2\mu^{\alpha'}_{e^-} \quad . \tag{3-11}$$

These equations relate the electrochemical potential of electrons in the leads to the electrochemical potentials of reactants in the solution adjacent to the electrodes. The thermodynamic cell potential $U'_{j/RC}$, taken to denote the potential of the right relative to the left, then may be expressed as

$$FU'_{j/RC} = \mu^{\alpha}_{e^-} - \mu^{\alpha'}_{e^-} \quad , \tag{3-12}$$

which is in terms of the electrochemical potentials of the electrons.

The electrical potential is related to the thermodynamic properties using the phase-equilibrium equations 3-10 and 3-11 in equation 3-12 yielding

$$FU'_{Zn/RC,0} = \mu^{\beta}_{Hg} - \frac{1}{2}\mu^{\beta}_{Hg_2Cl_2} + \mu^{\lambda}_{Cl^-} + \frac{1}{2}\mu^{\delta}_{Zn^{2+}} - \frac{1}{2}\mu^{\beta}_{Zn} \quad . \tag{3-13}$$

The electrochemical potential is given as

$$\mu_i = RT \ln \lambda_i = \mu_i^{\phi} + RT \ln a_i \quad , \tag{3-14}$$

where $\lambda_i = \lambda_i^{\phi} a_i$ is the dimensionless absolute activity and a_i is the activity of species i expressed in mol/kg. The standard state chemical potential is given by $\mu_i^{\phi} = RT \ln \lambda_i^{\phi}$, where λ_i^{ϕ} is a property expressing the secondary reference state in kg/mol and is independent of composition and electrical state. Substitution of the electrochemical potential given by equation 3-14 for each species into equation 3-13 for the thermodynamic cell potential yields

$$U'_{Zn/RC,0} = U^{\phi}_{Zn/RC} + \frac{RT}{2F} \ln \left[a^{\delta}_{Zn^{2+}} \left(a^{\lambda}_{Cl^-} \right)^2 \right] \quad , \tag{3-15a}$$

where

$$FU^{\phi}_{Zn/RC} = \mu^{\beta}_{Hg} - \frac{1}{2}\mu^{\beta}_{Hg_2Cl_2} - \frac{1}{2}\mu^{\beta}_{Zn} + RT \ln \lambda^{\phi}_{Cl^-} \lambda^{\phi^{1/2}}_{Zn^{2+}} \quad , \tag{3-15b}$$

because the chemical potential of a pure phase simply is equal to its standard state chemical potential μ_i^0.

Now we should like to relate the activity of the solute species to the

concentration and electrical state of the solution.† It is desired to follow the concepts and notation of previous workers in the thermodynamics field. For example, the electrochemical potential of an ionic species is frequently split into an electrical term and a "chemical" term,

$$\mu_i = \mu_i^{\text{chem}} + z_i F\Phi = RT \ln \lambda_i^{\circ} m_i \Gamma_i + z_i F\Phi \quad , \qquad (3\text{–}16)$$

where Φ is the "electrostatic" potential, m_i is the molality, and Γ_i is the activity coefficient which now is supposed to be independent of the electrical state of the phase. The electrostatic potential Φ could be defined so that it is measurable or unmeasurable. Depending upon how well defined Φ is, Γ_i is just as well or poorly defined. In order to avoid proceeding with only a vague concept of the electrostatic potential as supplied by electrostatic theory, Newman's analysis given in his text[1] will be followed.

It should be pointed out that for a purely thermodynamic problem, the introduction of the quasi–electrostatic potential is not necessary; the electrostatic potential can be avoided, since it is not directly related to reversible work. However, the beauty of Newman's approach lies in the way that it may be applied to the determination of potentials of non–thermodynamic cells containing liquid–junction regions. A brief outline of his method is given, and the determination of the thermodynamic zinc electrode potential relative to a saturated calomel electrode should provide a simple example illustrating the computational ease of using Newman's definition of the quasi–electrostatic potential.

The chemical or electrochemical potential, depending on whether the solute species i is neutral or ionic, respectively, may be written in terms of the molality or molar concentration c_i' as

$$\mu_i = RT \ln \lambda_i^{\circ} m_i \gamma_i = RT \ln a_i^{\circ} c_i' f_i \quad . \qquad (3\text{–}17)$$

The primes on the concentrations are used to indicate that the

† As an aside, much of the motivation required for writing this terribly long introductory chapter was a result of the effort to do just that.

concentration is expressed in mol/l.† The secondary reference state, which again is taken to be at infinite dilution, is characterized by the molarity constant α_i° expressed in l/mol. Since the absolute activity, $\lambda_i = \lambda_i^\circ m_i \gamma_i = \alpha_i^\circ c_i f_i$, depends on electrical state for an ionic species, the dimensionless activity coefficients γ_i and f_i must also depend on this state. This convention is different from that of splitting the electrochemical potential into a chemical potential term, where the activity coefficient is independent of the electrical state of the phase. However, the advantage of the present method should become apparent as we proceed.

The electrochemical potential μ_i can be related to the electrical state of a phase by using an ingenious concept introduced by Newman[15],[1] By selecting an ionic species n (for the present example, the chloride ion is a good choice), the electrochemical potential can be expressed as

$$\mu_n = RT \ln c_n + z_n F\Phi \quad , \tag{3-18}$$

where Φ is defined as the quasi-electrostatic potential of the phase relative to species n. Then, the electrochemical potential of any other species (for example, the zinc divalent ion) can be expressed as

$$\mu_i = RT \ln (c_i f_{i,n} \alpha_{i,n}^\circ) + z_i F\Phi \quad , \tag{3-19}$$

where the neutral combination of molar activity coefficients is given by

$$f_{i,n} = f_i \,/\, f_n^{z_i/z_n} \quad ,$$

and the property expressing the secondary reference state is

$$\alpha_{i,n}^\circ = \alpha_i^\circ \,/\, \alpha_n^{\circ z_i/z_n}$$

for species i relative to species n. Next, it is necessary to give equation 3-19 in terms of λ_i° which characterizes the secondary reference state so that the tables of standard potentials such as those given by Newman[1] may be used. By our definition of the secondary reference states, the molar and molal secondary-reference-state constants are related by $\alpha_i^\circ = \lambda_i^\circ / \rho_C$ (see

† Later in the text, C will be used to indicate the units mol/cm^3.

appendix A), where the density of pure solvent water ρ_0 is 1 g/cm^3. Therefore,

$$a_{i,n}^{\delta} = \lambda_{i,n}^{\delta} / \rho_0^{(1 - z_i/z_n)} \quad , \tag{3-20}$$

where

$$\lambda_{i,n}^{\delta} = \lambda_i^{\delta} / \lambda_n^{\delta z_i/z_n} \quad .$$

Finally, we are in a position to achieve our desired, well-defined relationship between the activity, concentration, and electrical state. Even though Newman never writes an equation for a_i, such an equation may be obtained by substituting equation 3-20 into 3-19. When this result and equation 3-18 are compared to equation 3-14, the following equations for the activity

$$\begin{aligned} a_n &= \frac{c_n'}{\lambda_n^{\delta}} \exp\left[\frac{z_n F}{RT}\Phi\right] \\ a_i &= \left[\frac{c_i' f_{i,n}}{\rho_0 (\lambda_n^{\delta}/\rho_0)^{z_i/z_n}}\right] \exp\left[\frac{z_i F}{RT}\Phi\right] \quad , \end{aligned} \tag{3-21}$$

are implied directly from the basic definitions given here.

We may now use equation 3-21 for the activity of solute species i and n in equation 3-15 to obtain the theoretical thermodynamic cell potential $U'_{Zn/RC,0}$, where the prime again implies the junction region is assumed not to exist. The same equation may also be determined by substituting the expressions given here for μ_n and μ_i into equation 3-13. The electrochemical potential of the chloride ions in phase λ is given by equation 3-18. Equations 3-19 and 3-20 may be used to give the electrochemical potential of the zinc species in phase δ relative to the chloride ion. Thus, equation 3-13, after making these substitutions, becomes

$$U'_{Zn/RC,0} = U^{\delta}_{Zn/RC} + \frac{RT}{2F} \ln\left[\frac{c'^{\delta}_{Zn^{2+}} \left(c'^{\lambda}_{Cl^-,sat}\right)^2 f^{\delta}_{Zn^{2+},Cl^-}}{\rho_0^3}\right]_0 \quad . \tag{3-22}$$

where $FU^{\delta}_{Zn/RC}$ is given by equation 3-15b. The value of the standard cell potential for the zinc reaction relative to the calomel electrode at 25°C is

$$U^{\circ}_{Zn/RC} = U^{\circ}_{Zn} - U^{\circ}_{RC} = -0.7628 - 0.2676 = -1.0304\ V \quad .$$

The brackets subscripted with 0 in equation 3–22 indicate that each species is at its surface concentration. It should be pointed out that the quasi–electrostatic potential difference between phases λ and δ does not appear in equation 3–22 because our definition of a reference electrode of a given kind implies $\Phi^{\delta} = \Phi^{\lambda}$. Appendices A, B, and C give a more thorough and general description of these thermodynamic properties of the electrochemical potential for determining cell potentials.

The zinc reaction is not the only electrode process occurring during corrosion. Hydrogen evolution

$$H^{+} + e- = \tfrac{1}{2} H_2 \qquad (3\text{–}23)$$

simultaneously takes place with the anodic zinc dissolution. The same procedure is used to obtain the cell potential of the hydrogen reaction relative to a reference electrode of a given kind as was obtained for the zinc reaction. Therefore, the hydrogen potential is given by

$$FU'_{H_2/RC,0} = \mu^{\beta}_{H_2} - \frac{1}{2}\mu^{\beta}_{Hg_2Cl_2} + \mu^{\lambda}_{Cl^-} + \mu^{\delta}_{H^+} - \frac{1}{2}\mu^{\beta}_{H_2} \quad . \qquad (3\text{–}24)$$

In addition to the expressions given above for the electrochemical potentials of solids and solutes, the partial pressure or fugacity of hydrogen must be related to the standard potentials. The chemical potential of a real gas in a multicomponent system is given by

$$\mu_i = \mu_i^{\circ}(T) + RT \ln (p_i \varphi_i) \quad , \qquad (3\text{–}25)$$

where $p_i = y_i p$ is the partial pressure of species i, and φ_i is the fugacity coefficient describing departures from the ideal state and approaches one in low–pressure mixtures. The potential difference $U'_{H_2/RC,0} = \Phi_{RS} - \Phi_{RC,0}$ for the hydrogen reaction relative to an imaginary saturated calomel electrode may be determined using equation 3–24 to be

$$U'_{H_2/RC,0} = U^{\circ}_{H_2/RC} + \frac{RT}{F} \ln \left[\frac{c'^{\delta}_{H^+} c'^{\lambda}_{Cl^-,sat} f^{\delta}_{H^+,Cl^-}}{\rho^{\delta}} \right]_0 - \frac{RT}{2F} \ln \left[p_{H_2} \varphi_{H_2} \right]_0^{\delta} \quad (3\text{–}26)$$

where

$$FU^{\circ}_{H_2/RC} = \mu^{\circ}_{Hg} - \frac{1}{2}\mu^{\circ}_{Hg_2Cl_2} - \frac{1}{2}\mu^{\circ}_{H_2} + RT \ln \lambda^{\circ}_{H^+,Cl^-} \quad . \quad (3\text{–}27)$$

The value of the standard cell potential for hydrogen relative to the calomel electrode at 25°C is

$$U^{\circ}_{H_2/RC} = U^{\circ}_{H_2} - U^{\circ}_{RC} = 0.0 - 0.2676 = -0.2676\ V. \quad (3\text{–}28)$$

A general equation for the cell potential of an electrode reaction j relative to a reference electrode of a given kind is developed in appendix C. A discussion of the Nernst equation is given there as well.

The expressions for the cell potential of both the zinc and hydrogen reactions contain activity coefficients of the solute i relative to the chloride ion. An equation for a neutral combination of molar activity coefficients $f_{i,n}$ is given in chapter 4 of Newman[1] as follows:

$$\ln f_{i,n} = - \frac{\alpha' z_i (z_i - z_n) \sqrt{I'}}{1 + B'\alpha \sqrt{I'}} + 2 \sum_{j \neq 0} \left[\beta'_{ij} - \frac{z_i}{z_n} \beta'_{nj} \right] c'_j \quad . \quad (3\text{–}29)$$

where the sum is over solute species. The coefficient for ion–ion specific interactions, β'_{ij}, can be taken to be zero for a pair of ions of like charge, and $\beta'_{ij} = \beta'_{ji}$. Thus, $\beta'_{HCl} = 0.27 l/\text{mol}$, and $\beta'_{ZnCl_2} = 0.20 l/\text{mol}$. I' is the molar ionic strength, and $B'\alpha$ is a Debye–Hückel parameter that is given the same value of 1 $(l/\text{mol})^{1/2}$ for all electrolytes, which corresponds to a mean diameter of ions, $\alpha = 3.04$ Å, for aqueous solutions at 25°C. For each electrolyte, there is only one adjustable parameter α', which can be fit by linear regression. At 25°C, $\alpha' = 1.1779$ for aqueous solutions. It should be pointed out that the activity coefficient is small in dilute solutions and in most cases may be neglected.

2.2. $\Delta\Phi_{RC}$

The third term in equation 3–6 $\Delta\Phi_{RC} = \Phi_{RC,0} - \Phi_{RC,\infty}$ is the potential of a reference electrode of a given kind placed in the solution adjacent to the working electrode minus the potential of another reference electrode of a given kind in the bulk. A general expression for this potential difference is given by[1]

$$V_r = \int_0^b \frac{i_y}{\kappa}\,dy + \frac{RT}{n_j F}\sum_i s_{ij} \ln \frac{(c_i f_{i,n})_\infty}{(c_i f_{i,n})_0} + \frac{RT}{F}\int_0^b \sum_p \frac{t_p^0}{z_p}\,\frac{\partial \ln c_p f_{p,n}}{\partial y}\,dy \qquad (3\text{–}30)$$

where V_r strictly speaking is the potential of a movable reference electrode of the same kind as the electrode reaction relative to a fixed reference electrode. The transference number for species p relative to the velocity of the solvent is given by t_p^0, s_{ij} is the stoichiometric coefficient of species i in electrode reaction j, and κ is the conductivity of the electrolyte.. The integration is performed from the electrode surface to the bulk solution denoted as b. The first term on the right of this equation is the ohmic potential drop, and the second depends on the specific electrode reaction j. The last term represents the diffusion potential resulting from concentration gradients of all species p in the solution excluding the solvent. The last two terms are obtained by integrating the gradients of the electrochemical potentials of neutral combinations of ions across the diffusion layer. In the absence of concentration, they are zero, in which case κ is a constant.

We should like to use equation 3–30 for the potential difference $\Delta\Phi_{RC}$ of two reference electrodes of a given kind. The electrode reaction for the reference electrodes *RG* is the mercury–mercurous chloride reaction given by equation 3–8. The chloride ion is the reference species n, and because the concentration of the reference electrode compartment is the same (4.1 M saturated KCl) at the surface and in the bulk, the second term of equation 3–30 is zero. Therefore, equation 3–30 reduces to

$$\Delta\Phi_{RC} = V_{rg} = \int_0^b \frac{i_y}{\kappa}\,dy + \frac{RT}{F}\int_0^b \sum_p \frac{t_p^0}{z_p}\,\frac{\partial \ln c_p f_{p,n}}{\partial y}\,dy \quad , \qquad (3\text{–}31)$$

where V_{rg} now represents the potential difference of a movable electrode of a given kind relative to a fixed reference electrode of a given kind. For dilute solutions, the activity coefficients may be neglected, and the transference number is replaced with a conductivity term resulting in

$$\Delta\Phi_{RC} = \int_0^b \frac{i_y}{\kappa}\,dy + F\int_0^b \sum_p \frac{z_p D_p}{\kappa}\,\frac{\partial c_p}{\partial y}\,dy \quad , \qquad (3\text{–}32)$$

where D_p is the diffusion coefficient of species p. Further simplifications may be made for solutions with an excess of supporting electrolyte by neglecting conductivity variations in the diffusion layer. Then equation 3–32 for $\Delta\Phi_{RC}$ becomes

$$\Delta\Phi_{RC} = \int_0^b \frac{i_y}{\kappa_\infty}\,dy + \frac{F}{\kappa_\infty}\sum_p z_p D_p (c_{p\infty} - c_{p0}) \quad . \qquad (3\text{–}33)$$

At open circuit, the current density is zero so that $\Delta\Phi_{RC}$ reduces to the diffusion potential $\Delta\Phi_{diff}$ which is given by the last term on the right in equations 3–31, 3–32, and 3–33. This difference of potential is zero by electroneutrality if all the diffusion coefficients are equal. The diffusion potential has the advantage of not approaching infinity as the bulk concentrations go to zero. More will be said about this important point in a later section.

It may be desirable to break down the potential variation across the cell as shown in figure 2 to be

$$\Delta\Phi_{RC} = (\Phi_{RC,0} - \tilde{\Phi}_{RC,0}) + (\tilde{\Phi}_{RC,0} - \tilde{\Phi}_{RC,\infty}) \quad . \qquad (3\text{–}34)$$

The second term on the right is the ohmic potential drop across the cell calculated as though there were no concentration gradients across the diffusion layer and is given by

$$\Delta\tilde{\Phi}_{ohm} = \tilde{\Phi}_{RC,0} - \tilde{\Phi}_{RC,\infty} = \int_0^b \frac{i_y}{\kappa_\infty}\,dy \quad . \qquad (3\text{–}35)$$

Therefore, the first term gives the difference between $\Phi_{RC,0}$ and $\tilde{\Phi}_{RC,0}$ as

$$\Phi_{RC,0} - \tilde{\Phi}_{RC,0} = \int_0^b \left[i_y \left(\frac{1}{\kappa} - \frac{1}{\kappa_\infty} \right) + \frac{RT}{F} \sum_p \frac{t_p^0}{z_p} \frac{\partial \ln c_p f_{\pm,n}}{\partial y} \right] dy \quad (3\text{–}36)$$

This equation shows that in a well–supported solution there is a negligible difference between $\Phi_{RC,0}$ and $\tilde{\Phi}_{RC,0}$.

2.3. Potential of Junction Region

The final term in equation 3–6 $U''_{RC/RR,\infty} = \tilde{\Phi}_{RC,\infty} - \Phi_{RP}$, where the double primes again indicate a cell potential that contains a liquid–junction potential, may be evaluated by mentally constructing another cell shown as:

φ	ε	λ	δ	κ	ε'	φ'
Hg(s)	Hg_2Cl_2(s)	4.1 M KCl saturated in H_2O	– – – HCl in H_2O	4.1 M *KCl* saturated in H_2O	Hg_2Cl_2(s)	Hg(s)

Here, we have represented the potential difference† $U''_{RR/RC,\infty}$ between a real reference electrode shown on the right placed in the bulk solution and a hypothetical reference electrode of a given kind placed in the same bulk solution, phase δ. The reference electrode of a given kind (saturated calomel electrode) is shown on the left, and as previously done, the dashed line represents the region between the imaginary electrode and the bulk solution where the liquid–junction potential is assumed to be zero since $\Phi^\lambda = \Phi^\delta$ by definition of a reference electrode of a given kind. The electrode on the right, which is used to measure experimentally the potential of the solution phase δ, is also a saturated calomel electrode. Because of the difference in composition between the bulk solution and reference electrode compartment κ, a liquid junction or transition region exists which is

† Note the change from $U''_{RC/RR,\infty}$ to $U''_{RR/RC,\infty}$ so that the same notation previously used for potentials relative to an ideal reference electrode of a given kind may be applied.

illustrated by the wavy vertical lines.

The same electrode reaction, equation 3–8, takes place on each side of the cell, therefore the expression for the cell potential as shown becomes

$$F\ddot{U}_{RR/\,RC,\blacksquare} = \mu_{e^-}^{\alpha} - \mu_{e^-}^{\alpha'} = \mu_{Cl^-,\blacksquare}^{\lambda} - \mu_{Cl^-,\blacksquare}^{\kappa} \quad . \tag{3–37}$$

Equation 3–14 for the chloride ion may be substituted into 3–37 yielding

$$\ddot{U}_{RR/\,RC,\blacksquare} = \Phi^{\kappa} - \Phi^{\lambda} \quad . \tag{3–38}$$

The chloride concentration does not appear in this equation, because the two calomel reference electrodes are both arbitrarily chosen to have the same composition of saturated 4.1 M KCl. By definition of an electrode of a given kind, $\Phi^{\lambda} = \Phi^{\delta}$, equation 3–38 becomes

$$\ddot{U}_{RR/\,RC,\blacksquare} = \Phi^{\kappa} - \Phi^{\delta} \quad . \tag{3–39}$$

Therefore, the last term in equation 3–6 $\ddot{U}_{RC/\,RR,\blacksquare}$ is equal to the negative of equation 3–39 and is the liquid–junction potential $\Delta\Phi_{LJ}$ given by

$$\ddot{U}_{RC/\,RR,\blacksquare} = \Delta\Phi_{LJ} = \Phi^{\delta} - \Phi^{\kappa} \quad . \tag{3–40}$$

Thermodynamics alone is not enough to solve this problem. Some knowledge of how the junction is formed and its concentration profile are needed to evaluate the liquid–junction potential. A simple and popular model of the liquid junction is the continuous–mixture junction. At all points in the junction, the concentrations are assumed to be linear combinations of those of the solutions at the ends of the junction. This assumption obviates the problem of calculating the concentration profiles by the laws of diffusion. Assuming a continuous–mixture junction, the Henderson formula[16],[1] may be used to get an estimate for the potential difference across the transition region. The liquid–junction potential is then given by

$$\Phi^{I} - \Phi^{II} = -\frac{RT}{F} A \frac{\ln \dfrac{B^{I}}{B^{II}}}{B^{I} - B^{II}} \quad , \tag{3–41}$$

where I stands for the δ phase and II for the κ phase, and

$$A = \sum_i z_i D_i (c_i^I - c_i^{II}), \quad B^I = \sum_i z_i^2 D_i c_i^I, \quad B^{II} = \sum_i z_i^2 D_i c_i^{II} \quad . \qquad (3\text{–}42)$$

This potential difference may be calculated since the composition of the δ phase would be known for any given experimental conditions as well as the composition of the actual reference electrode compartment, phase κ. If a continuous junction does not exists or is not appropriate, then Smyrl and Newman's[15] more thorough treatment of the subject may be applied.

A final expression may now be written for the cell potential V^* by substituting equations 3–22, 3–33 and 3–40 into equation 3–6. This result is an extension of the expressions that are given for the open–circuit potential U given in section 40 of reference 1. The desire to elaborate on that section initiated much of the work presented in this chapter.

3. Cell Potential for General Process

Next, for completeness, an expression for the measured cell potential in more conventional terms is desired using the concentration overpotential. Equation 3–3 that was developed in section 1

$$V^* = \eta_{sj} + \Delta\Phi_{RS} + U''_{j/RR,*} \qquad (3\text{–}43)$$

is the starting point. Figure 3–4 is useful to see the potential distribution as it applies to this equation. The surface overpotential η_{sj} and the potential variation across the cell as sensed by reference electrodes of the same type as the reaction of interest j occurring at the working electrode $\Delta\Phi_{RS}$ are shown. The potential difference, $U''_{j/RR,*} = \tilde{\Phi}_{RS,*} - \Phi_{RR}$, between reactions j and RR may be broken down as

$$U''_{j/RR,*} = (\tilde{\Phi}_{RS,*} - \tilde{\Phi}_{RC,*}) + (\tilde{\Phi}_{RC,*} - \Phi_{RR}) = U'_{j/RC,*} + U''_{RC/RR,*} \quad . \qquad (3\text{–}44)$$

An expression for $U''_{RC/RR,*}$ has already been obtained and is given by equation 3–40. Equation 3–22 could be used for $U'_{j/RC,*}$ for the zinc reaction simply by evaluating it at the bulk concentrations instead of surface concentrations. However, another more general approach will be given in the next section for the derivation of cell potentials with liquid junctions.

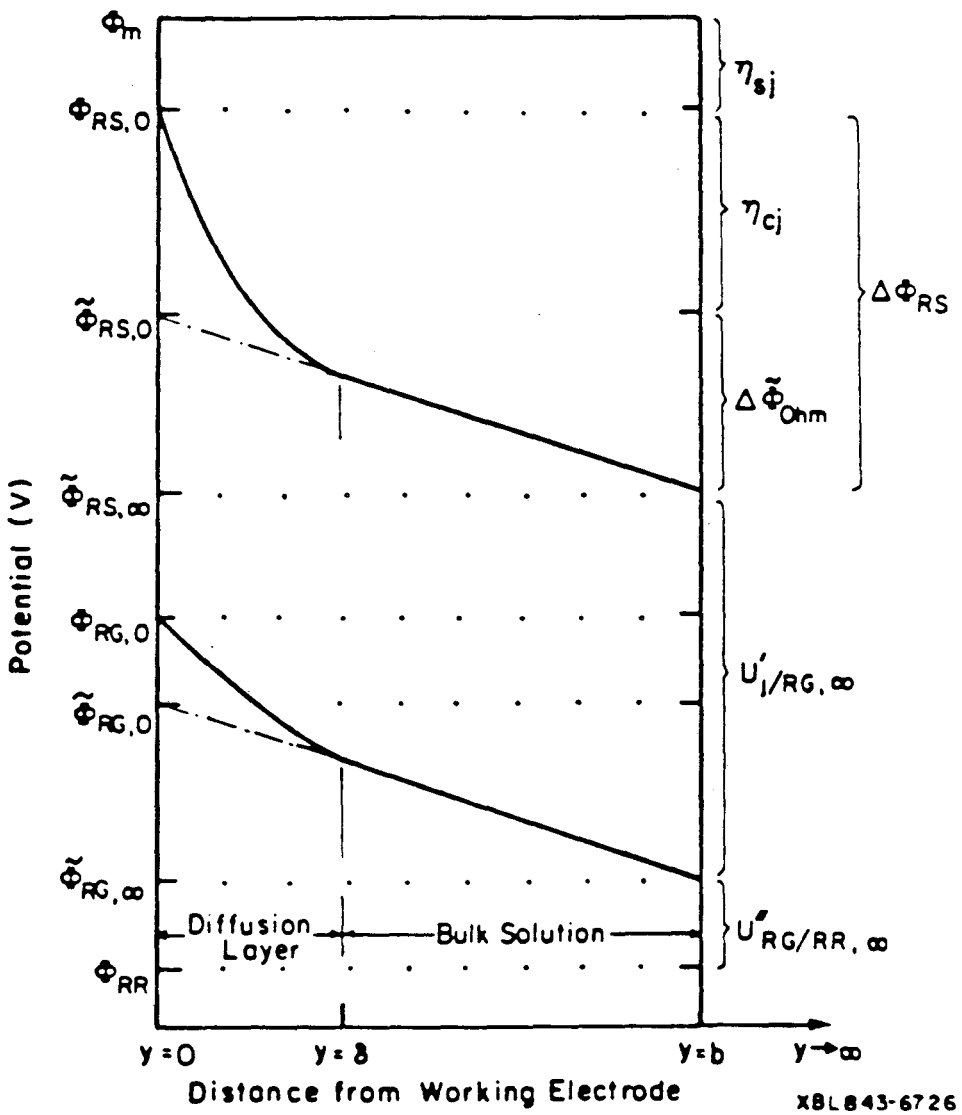

Figure 3–4. Potential distribution. This figure applies to the case where the reactant concentration does not go to zero in the bulk solution.

The purpose of the next two sections is to derive expressions for each of the terms in equation 3–43.

3.1. Cell Potential with a Liquid Junction

In order to demonstrate further capabilities of the local equilibrium concept, an expression for the potential difference $U''_{j/RR,-} = \tilde{\Phi}_{RS,-} - \Phi_{RR}$ may be obtained by mentally constructing an electrochemical cell as follows:

α	φ	ε	κ		δ	β	α'
Pt	Hg(s)	Hg_2Cl_2(s)	4.1 M KCl saturated in H_2O	junction region	$ZnCl_2$ in HCl and H_2O	Zn(s)	Pt

The ideal zinc reference electrode on the right with a potential denoted as $\tilde{\Phi}_{RS,-}$ is placed in the bulk solution, and its electrolytic solution must be of the same composition as the bulk electrolyte. The left electrode represents the actual saturated calomel electrode of potential Φ_{RR}. The potential difference across this cell must account for the transition region in which concentration gradients exist between the δ and κ phases. The treatment of the open–circuit potential of electrochemical cells of this nature involves first the description of phase equilibria between the electrodes and the solutions or solids adjacent to them, followed by a consideration of the junction region that is likely to exist between the solutions adjacent to the electrodes. The reactions occurring at the left and right electrodes are given by equations 3–8 and 3–9, respectively. The development of an expression for the cell potential is like that given in section 2.1 except that an actual reference electrode is being used in the place of a given kind. Therefore, the cell potential is obtained by substituting the expressions given for the electrochemical potential into an equation like 3–13 yielding

$$U''_{Zn/\,RR,\infty} = U^{\circ}_{Zn/\,RC} + \frac{RT}{2F}\ln\left[\frac{c'^{\delta}_{Zn^{2+}}\left(c'^{\kappa}_{Cl^-,sat}\right)^2 f^{\delta}_{Zn^{2+},Cl^-}}{\rho^{\delta}}\right]_{\infty} + \left(\Phi^{\delta} - \Phi^{\kappa}\right)_{\infty} \quad (3\text{–}45)$$

which contains the liquid–junction potential $\Phi^{\delta} - \Phi^{\kappa}$. This expression should be compared with the equation that is obtained by substituting equation 3–22 when evaluated at the bulk concentrations and equation 3–40 into equation 3–44. In each hypothetical cell that was constructed, the λ and κ phases make reference to the calomel electrode compartment. Because each solution is saturated 4.1 M KCl, equation 3–45 is identical to the result obtained by using the previously derived cell potentials. This confirms the power of the local equilibrium and quasi–electrostatic potential concepts.

An equation for the hydrogen cell potential with a liquid junction $U''_{H_2/\,RR}$ may be obtained in a similar manner as shown here for the zinc reaction. $U''_{H_2/\,RR}$ is given by equation 3–26 plus the liquid–junction potential $\Phi^{\delta} - \Phi^{\kappa}$. A general expression for the cell potential with a liquid junction also is developed in appendix D. Table 1 in appendix D gives equations for the electrochemical potential of different types of species using the quasi–electrostatic potential. For other examples of this procedure, Trainham and Newman[17] give results for waste–water, ion–removal reactions.

3.2. $\Delta\Phi_{RS}$

The potential difference $\Delta\Phi_{RS} = \Phi_{RS,0} - \Phi_{RS,\infty}$ as measured by reference electrodes of the same type as the reaction of interest j placed near the working electrode and in the bulk is $\Delta\Phi_{RS} = V_{rs}$, where V_{rs} is given by equation 3–30. This potential may be broken down as

$$\Delta\Phi_{RS} = \left(\Phi_{RS,0} - \tilde{\Phi}_{RS,0}\right) + \left(\tilde{\Phi}_{RS,0} - \tilde{\Phi}_{RS,\infty}\right) \quad . \quad (3\text{–}46)$$

where the first term is the concentration overpotential η_c and the second is the ohmic drop $\Delta\tilde{\Phi}_{ohm}$ that would exist if there were no concentration

gradients. Equation 3–46 may be rewritten as

$$\Delta\Phi_{RS} = \eta_c + \int_0^b \frac{i_y}{\kappa_\infty}\, dy \qquad (3\text{–}47)$$

At zero–current conditions, the potential difference $\Delta\Phi_{RS}$ reduces to the concentration overpotential. From equations 3–30 for V_{rs} and 3–47, the concentration overpotential for reaction j is

$$\eta_c = \int_0^b i_y \left(\frac{1}{\kappa} - \frac{1}{\kappa_\infty}\right) dy + \frac{RT}{n_j F} \sum_i s_{ij} \ln \frac{(c_i f_{i,n})_\infty}{(c_i f_{i,n})_0} + \frac{RT}{F} \int_0^b \sum_j \frac{t_j^0}{z_j} \frac{\partial \ln c_j f_{j,n}}{\partial y} dy \qquad (3\text{–}48)$$

Hence, one can see why the concentration overpotential is defined as the potential difference between a reference electrode of the same kind as the working electrode located adjacent to it and one of the same kind located in the bulk solution, minus the potential drop between these reference electrodes in the absence of concentration variations. It reduces to

$$\eta_c = i_n \int_0^b \left(\frac{1}{\kappa} - \frac{1}{\kappa_\infty}\right) dy + \frac{RT}{n_j F} \sum_i s_{ij} \ln \frac{c_{i\infty}}{c_{i0}} + F \int_0^b \sum_p \frac{z_p D_p}{\kappa} \frac{\partial c_p}{\partial y} dy \qquad (3\text{–}49)$$

for dilute solutions. Surface concentrations are needed to determine a value for η_c. Also, if anyone of the bulk concentrations is zero, then the concentration overpotential becomes undefined. This is the reason such an expression should be avoided for corrosion processes if the bulk concentration of any of the corrosion products is zero.

At zero–current conditions, the potential difference $\Delta\Phi_{RS}$ reduces to the concentration overpotential. Therefore, the final expression for the measured cell potential V in terms of the concentration overpotential now can be written if equations 3–45, 3–47, and 3–49 are substituted into equation 3–43. The resulting equation may be evaluated after the surface concentrations are specified.

4. Equilibrium Constant for Electrochemical Reactions

Strictly speaking, thermodynamic equilibrium calculations are for no net current and uniform equilibrium composition conditions such that the concentration at the surface and in the bulk are the same. This is written $c_{i,0}' = c_{i,\infty}' = c_{i,*}'$, where * represents the equilibrium state. In an electrochemical process this implies that the two electrode half reactions are balanced so that there are no temperature, pressure, or concentration gradients acting as driving forces for change. Before continuing the development for determining an expression for the electrochemical reaction equilibrium constant, we should obtain an expression for the thermodynamic potential difference $U_{j/l}$ between two half reactions at equilibrium so that the equilibrium conditions may be assessed.

4.1. Chemical Reaction Equilibrium Constant

In the zinc corrosion process, we know that two electrochemical reactions take place on the zinc surface. The anodic zinc dissolution reaction 3–9 simultaneously occurs with the hydrogen evolution reaction 3–23. The second reaction may be subtracted from the first to obtain the chemical reaction

$$Zn + 2H^{+} = Zn^{2+} + H_2 \,. \tag{3–50}$$

The Gibbs energy for a chemical reaction m is related to the potential difference between the two electrochemical reactions by

$$\Delta G_m = nFU_{j/l} \,. \tag{3–51}$$

We previously have shown with equation 3–12 that the thermodynamic cell potential $U_{j/l}$ may be expressed in terms of the electrochemical potentials of the electrons so that the Gibbs energy for reaction 3–50 is

$$\Delta G = -2\left(\mu_{e^-,Zn} - \mu_{e^-,H_2}\right) \,. \tag{3–52}$$

Again, the electrical potential is related to the thermodynamic properties

using the phase–equilibrium equations 3–11 for zinc and a similar equation for hydrogen in equation 3–52 yielding

$$\Delta G = \mu_{Zn^{2+}} + \mu_{H_2} - \mu_{Zn} - 2\mu_{H^+} \qquad (3\text{–}53)$$

At equilibrium, ΔG must equal zero, and equation 3–52 requires that the two reactions occur at the same electrode potential.

The chemical and electrochemical potentials μ_i of species i have been given previously and may be substituted into the chemical reaction equilibrium equation 3–53 with $\Delta G = 0$ yielding

$$K = \frac{(\lambda^{\circ}_{H^+})^2 \lambda^{\rho}_{Zn}}{\lambda^{\circ}_{Zn^{2+}} \lambda^{\bullet}_{H_2}} = \frac{(c_i f_i)_{Zn^{2+}} (p_i \varphi_i)_{H_2} \rho_0}{(c_i f_i)^2_{H^+}} \qquad (3\text{–}54)$$

The chemical equilibrium constant defined by this equation may be rewritten in terms of the standard Gibbs energy of the chemical reaction or as a function of the difference in the standard electrode potentials of the two electrochemical half reactions as

$$K = \exp\left[-\frac{\Delta G^{\circ}}{RT}\right] = \exp\left[-\frac{2F}{RT}\left(U^{\circ}_{Zn} - U^{\circ}_{H_2}\right)\right] , \qquad (3\text{–}55)$$

where $\Delta G^{\circ} = \sum_i \nu_i G^{\circ}_f = \sum_i \nu_i \mu^{\circ}_i$ is the standard Gibbs energy of a chemical reaction. Values of the standard Gibbs energy of formation G°_f of each species may be obtained from the *NBS Technical Note* 270–3.[18]

K is determined to be 6.23×10^{25} atm–kg/mol using standard potentials of -0.76 and 0.0 V for the zinc and hydrogen reactions, respectively. For a hydrogen partial pressure of 1 atm and 1 M hydrogen ion concentration, the equilibrium zinc ion concentration would be 6.23×10^{25} M, ignoring activity coefficients. Hence, the corrosion process never reaches thermodynamic equilibrium, and a steady–state uniform equilibrium concentration distribution will not be obtained for each species.

4.2. Electrochemical Reaction Equilibrium Constant

In this section, we should like to develop a general expression for the equilibrium constant for an electrochemical reaction. This is somewhat different than in the previous section, where an equilibrium constant was given for a chemical reaction, because of the appearance of the electrochemical potential of electrons in, for example, reactions 3–10 and 3–11. This is difficult to deal with because of the arbitrariness in the reference state for electrons. Therefore, we shall continue the analysis here to develop an expression for the equilibrium constant of the zinc and hydrogen electrochemical reactions relative to the saturated calomel electrode despite the fact that an equilibrium state for the zinc corrosion process is not reached. It should also be pointed out that this method is not limited solely to the SCE.

The purpose of this exercise will become apparent in the next section, where the kinetics of electrode reactions will be discussed. For now, one should keep in mind that if the ratio of kinetic rate constants of an electrochemical reaction may be related to the thermodynamic properties of the species, then only one of the two rate constants needs to be measured. Thus, we have a convenient method for reducing the number of experiments that must be carried out to characterize a given system.

Equation 3–45 for the potential difference of an electrochemical cell with a liquid junction may be rewritten as

$$U''_{Zn/\,RR} = \frac{RT}{2F} \ln \left[\frac{k_c'}{k_a'} \right]_{Zn} + \frac{RT}{2F} \ln \left[\frac{c'_{Zn^{2+}} f_{Zn^{2+},Cl^-}}{\rho_0} \right]^{\delta} + (\Phi^{\delta} - \Phi^{\kappa}) \quad , \quad (3\text{–}56)$$

where

$$\ln \left[\frac{k_c'}{k_a'} \right]_{Zn} = \frac{2F}{RT} U^{\beta}_{Zn/\,RC} + 2 \ln \frac{c'^{\kappa}_{Cl^-,sat}}{\rho_0} \quad . \quad (3\text{–}57)$$

The superscripted brackets refer to the bulk solution phase δ evaluated at

the hypothetical equilibrium conditions. An equation for the hydrogen reaction relative to a real reference electrode is as follows:

$$U''_{H_2/RC} = \frac{RT}{F} \ln \left(\frac{k'_c}{k'_a} \right)_{H_2} - \frac{RT}{F} \ln \left[\frac{\left(\varphi_{H_2} p_{H_2} \right)^{1/2} \rho_0}{c'_{H^+} f_{H^+,Cl^-}} \right]^{\delta} + (\Phi^{\delta} - \Phi^{\kappa}) \quad , \qquad (3\text{–}58)$$

where

$$\ln \left(\frac{k'_c}{k'_a} \right)_{H_2} = \frac{F}{RT} U^{\circ}_{H_2/RC} + \ln \left[\frac{c'^{\kappa}_{Cl^-,sat}}{\rho_0} \right] . \qquad (3\text{–}59)$$

Equation 3–58 is similar to equation 3–26 for the thermodynamic potential difference $U'_{H_2/RC}$, but in addition to it, 3–58 contains the liquid–junction potential. One can see from these two equations that the equilibrium constants (k'_c / k'_a) are independent of the equilibrium concentrations in the cell. The value of the constant is dependent on the choice of reference electrode and the composition of the electrolytic solution in the reference electrode compartment. Therefore, equations 3–57 and 3–59 remain valid for nonequilibrium conditions.

Equations 3–57 and 3–59 define the equilibrium constant for the zinc and hydrogen reactions, respectively, but the correct units are not easily seen. After rearranging these equations, the following expressions for the zinc reaction

$$\left(\frac{k'_c}{k'_a} \right)_{Zn} = \frac{\rho_0}{c'_{Zn^{2+}} f_{Zn^{2+},Cl^-}} \exp \left[\frac{2F}{RT} \left(U''_{Zn/RR} - (\Phi^{\delta} - \Phi^{\kappa}) \right) \right] , \qquad (3\text{–}60)$$

and the hydrogen reaction

$$\left(\frac{k'_c}{k'_a} \right)_{H_2} = \frac{\left(\varphi_{H_2} p_{H_2} \right)^{1/2} \rho_0}{c'_{H^+} f_{H^+,Cl^-}} \exp \left[\frac{F}{RT} \left(U''_{H_2/RR} - (\Phi^{\delta} - \Phi^{\kappa}) \right) \right] , \qquad (3\text{–}61)$$

are useful to determine quickly the units for the equilibrium constant. For the two electron–transfer zinc reaction 3–9 at 25°C and a chloride species concentration of 4.1 M in the reference electrode compartment, the equilibrium constant as given by equation 3–57 is 2.414×10^{-34} kg/ mol . The

one electron–transfer hydrogen reaction 3–23 at the same conditions has an equilibrium constant equal to 1.228×10^{-4} atm^{½}–kg/ mol .

5. Electrode Kinetics

Up to this point, only thermodynamics and limited transport phenomena have been discussed. However, the thermodynamics of a reaction does not indicate how fast the reaction occurs. If so, zinc would instantaneously corrode in an aqueous environment due to its very negative or corrosive active standard electrode potential favoring anodic oxidation. But we know that this is not the case, due to zinc's large overpotential for the hydrogen evolution reaction. Thus, zinc is used for cathodic protection of other metals with more positive standard potentials, *i.e.*, steels. In a corrosion process, it is usually the rate of the electrode reactions which is controlling. Therefore, understanding and characterizing the charge transfer or faradaic reactions are of primary importance in many electrochemical systems of practical importance. Newman's[1] chapter 8 on electrode kinetics will be the basis for this analysis.

The rate of a single electrode reaction j occurring at steady–state is related by Faraday's law to the current density as $r_j = i_j / n_j F$ and depends on the nature and previous treatment of the electrode surface. Second, the rate of reaction depends on the composition of the electrolytic solution adjacent to the electrode, just outside the double layer. The diffuse part of the double layer is regarded as part of the interface. Because of the high ionic strength of the solution, the double layer is too thin to probe adequately, and the theory of the diffuse layer is a microscopic model rather than a macroscopic theory. Finally, the rate of reaction depends on the electrode potential. The potential change across the interface results from the distribution of potential in the double layer and may be written as

$$V^{+} = \Phi_{m} - \Phi_{soln} \quad . \tag{3-62}$$

Φ_m is the electrostatic potential of the electrode and Φ_{soln} is the electrostatic potential of the solution just outside the double layer. This is not usually a well-defined potential so a different potential driving force for electrode reactions

$$V = \Phi_{m} - \Phi_{RC,0} \tag{3-63}$$

may be used. This potential difference which was introduced in the previous sections is relative to an imaginary reference electrode of a given kind placed just outside the double layer so that there is no ohmic drop between it and the metal. More specifically, $\Phi_{RC,0}$ is the potential of an ideally reversible electrode that by definition contains no liquid-junction potential that actually might exist between it and the ionically conducting phase in which it is placed.

The basic theory of relating the rate constants to the potential difference V was given by Eyring *et al.* [19] For the zinc reaction 3-9, the following kinetic expression may be written provided that the reaction order is proportional to to the reaction stoichiometry

$$r_{Zn} = \frac{i_{Zn}}{2F} = k_{a,Zn} \exp\left[\frac{(1-\beta_{Zn})2F}{RT} V\right] - k_{c,Zn}\, c_{Zn^{2+},0} \exp\left[-\frac{\beta_{Zn}2F}{RT} V\right] \tag{3-64}$$

In order to make such an assumption, the zinc oxidation reaction is taken to be a simple, elementary reaction. This might not be true; but if so, the symmetry factor β has quantum mechanical significance. Finally, because the rate is given in mol/(cm^2-s), the units of the rate constants for zinc, k_a and k_c are mol/(cm^2-s) and cm/s , respectively provided the concentration is expressed in mol/cm^3.

The expression for the rate of the hydrogen reaction 3-23 may be written

$$r_{H_2} = \frac{i_{H_2}}{F} = k_{a,H_2} p_{H_2,0}^{\frac{1}{2}} \exp\left[\frac{(1-\beta_{H_2})F}{RT} V\right] - k_{c,H_2} c_{H^+,0} \exp\left[-\frac{\beta_{H_2} F}{RT} V\right] \quad (3-65)$$

The "derivation" of this equation is discussed in chapter 4. The units of the anodic and cathodic rate constant are $mol/(atm^{\frac{1}{2}}cm^2-s)$ and cm/s, respectively. The rate constants are independent of concentration in each of these kinetic equations.

At the hypothetical equilibrium conditions, the concentrations are uniform, and the net current density is zero, so that equation 3–64 yields

$$\begin{aligned} i_{0,Zn} &= 2F\, k_{a,Zn} \exp\left[\frac{(1-\beta_{Zn})2F}{RT} V^0\right] \\ &= 2F\, k_{c,Zn}\, c_{Zn^{2+}} \exp\left[-\frac{\beta_{Zn} 2F}{RT} V^0\right], \end{aligned} \quad (3-66)$$

where $i_{0,Zn}$ is the exchange–current density and V^0 is the equilibrium potential. The two terms on the right of equation 3–66 can be rearranged to obtain

$$V^0 = \frac{RT}{2F} \ln\left[\frac{k_c}{k_a}\right] + \frac{RT}{2F} \ln c_{Zn^{2+}} \quad . \quad (3-67)$$

and the substitution of this equation for V^0 back into equation 3–66 yields

$$i_{0,Zn} = 2F k_a^{\beta} k_c^{1-\beta} c_{Zn^{2+}}^{1-\beta} \quad . \quad (3-68)$$

Another way of expressing the concentration dependence of the exchange–current density is given by

$$i_{0,Zn} = \left[\frac{c_{Zn^{2+}}}{c_{Zn^{2+},=}}\right]^{(1-\beta)} i_{0,Zn}\Big|_{c_{Zn^{2+},=}} \quad . \quad (3-69)$$

Finally, equation 3–64 can be rewritten in terms of the exchange–current density and the equilibrium potential with the result

$$i_{Zn} = i_{0,Zn}\left\{\exp\left[\frac{(1-\beta_{Zn})2F}{RT}(V-V^0)\right] - \exp\left[-\frac{\beta_{Zn}2F}{RT}(V-V^0)\right]\right\} \quad . (3-70)$$

The potential difference driving force in this equation may be written using equation 3–63 as

$$V - V^0 = (\Phi_m - \Phi_{RG,0}) - (\Phi_m - \Phi_{RG,0})_{\bullet} \quad (3-71)$$

At equilibrium, $\Phi_m = \Phi_{RS,0}$ so

$$V - V^0 = \Phi_m - \Phi_{RS,0} = \eta_{sj} \quad (3-72)$$

Here we have defined the surface overpotential as the potential difference between the working electrode and an imaginary reference electrode placed just outside the diffuse–double layer of the working electrode. This reference electrode is of the same type as the working electrode and contains no ohmic potential drop or liquid–junction potentials. Now equation 3–70 may be written

$$i_{Zn} = i_{0,Zn}\left\{ \exp\left[\frac{(1-\beta_{Zn})2F}{RT}\eta_{s,Zn} \right] - \exp\left[-\frac{\beta_{Zn}2F}{RT}\eta_{s,Zn} \right] \right\}, \quad (3-73)$$

which is the Butler–Volmer equation. This expression gives the dependence of the current density on the surface overpotential and the composition adjacent to the electrode surface for steady–state conditions.

Next, the kinetic rate–constant ratio should be compared with the thermodynamic equilibrium constant derived in the previous section. The equilibrium cell potential, $V^0 = (\Phi_m - \Phi_{RG,0})_{\bullet}$, is the same as the previously defined thermodynamic potential difference, $U'_{j/RG,\bullet} = \Phi_{RS,\bullet} - \Phi_{RG,\bullet}$, since $\Phi_m = \Phi_{RS,0}$ at the theoretical equilibrium potential. Even though equation 3–67 was simplified from equation 3–66 for equilibrium conditions, it maintains a general nature as a result of the concentration–independent rate constants. When the kinetic equilibrium equation 3–67 which contains the kinetic rate constant ratio k_c / k_a is equated with equation 3–22 for the thermodynamic potential difference without a liquid junction followed by substitution of the result into equation 3–57 which defines the thermodynamic equilibrium constant k'_c / k'_a, the final result is

$$\left[\frac{k_c}{k_a}\right]_{Zn} = \left[\frac{k_c'}{k_a'}\right]_{Zn}\left[\frac{f_{Zn^{2+},Cl^-}}{\rho_0'}\right] \quad . \tag{3-74}$$

Because the kinetic expression 3–67 contains c_i in mol/cm^3 and the thermodynamic equation 3–22 contains c_i' in mol/l, the density of the pure solvent ρ_0' must be expressed in kg/cm^3. This equation relates the thermodynamic equilibrium constant that may be easily calculated using standard electrode potentials with the desired kinetic ratio of the anodic and cathodic rate constants that may be used in equation 3–64 for the zinc reaction.

We are now in a position to relate the actual cell potential V^* to the current density. With the aid of the introduction of highly conceptual reference potentials with theoretical basis, equation 3–5 for the measured potential of a corrosion process was obtained and will be used here. The potential driving force, $V = \Phi_m - \Phi_{RC,0}$, used in the kinetic expression 3–64 may be rewritten as

$$V = (\Phi_m - \Phi_{RS,0}) + (\Phi_{RS,0} - \Phi_{RC,0}) = \eta_{sj} + U_{j/RC,0}' \quad . \tag{3-75}$$

Hence, the substitution of equation 3–5 and 3–31 into 3–75 after rearrangement yields

$$V = V^* - \Delta\Phi_{ohm} - \Delta\Phi_{diff} - U_{RC/RR,-}'' \tag{3-76}$$

for the kinetic potential driving force. The ohmic potential drop $\Delta\Phi_{ohm}$ and the diffusion potential $\Delta\Phi_{diff}$ are given by the first and second terms in equation 3–31, respectively. The junction region potential difference $U_{RC/RR,-}''$ is given by equation 3–40. The following equation

$$\eta_{sj} = V^* - U_{j/RC,0}' - \Delta\Phi_{ohm} - \Delta\Phi_{diff} - U_{RC/RR,-}'' \tag{3-77}$$

for the surface overpotential in terms of the measured cell potential may be substituted into equation 3–73 for the current density. This gives the relationship that was desired at the beginning of this chapter in terms of clear, well–defined expressions.

Chapter 4. Experimental Study of the Corrosion of Zinc

1. Introduction

The results of an experimental study of the corrosion of zinc are presented in this chapter. The purpose of the work is to determine the kinetic parameters of the reactions of interest and to quantify the corrosion rate in a one molar hydrochloric acid solution. Again, the most common metals have much lower hydrogen overpotentials than zinc. This means zinc will corrode at a smaller rate than those metals even though its negative standard reduction potential makes it thermodynamically favorable for instantaneous corrosion. Characterizing the effect that the hydrogen overpotential has on zinc corrosion is desired. The kinetic information obtained gives a better understanding of the corrosion process and more specifically the protective nature of zinc. A brief review of the experimental method is presented next. Then, the equipment, details of the procedure, and results will be described.

2. Experimental Method

Information about a corrosion process may be obtained in a number of ways. For example, one could do a series of tests simply allowing zinc to corrode in various concentrations of hydrochloric acid over a long period of time. Afterwards, the measured weight loss may be related to the corrosion rate by Faraday's law which states that for every equivalent of electrical charge passed through an electrochemical cell, one equivalent of chemical reactant is consumed at each electrode. However, accelerated electrochemical tests allow corrosion rate information to be obtained if the zinc dissolution and hydrogen evolution reactions can be treated independently. Each reaction essentially can be studied separately using

standard electrochemical polarization techniques. We shall be concerned with these methods.

2.1. Polarization Technique

The study of electrode kinetics has been done by means of polarization methods. Sweeping the potential into the Tafel region is a useful technique for determining the kinetic parameters. Graphical extrapolation from the Tafel region back to the corrosion potential is a common way of determining the corrosion–current density. The Stern–Geary[6] linear polarization method and modifications thereof by Mansfeld *et al.* [8] are other common methods of determining the corrosion–current density. Each will be discussed in more detail in chapter 6.

The linear and Tafel polarization methods may be carried out potentiostatically or potentiodynamically. The latter is a potential sweep method, and only a quasi–steady state is obtained. Potentiostatic experiments allow a true steady–state current to be reached at each potential before the next I–V datum is recorded. The potentiodynamic method has the advantage that the information may be obtained in a much shorter time, therefore allowing the electrode surface to maintain its original surface longer. This method has become the most common in recent years and will be used in this study. The result of the accelerated electrochemical test just described is the polarization curve. These polarization curves allow electrode–kinetic information about each independent reaction to be obtained.

2.2. Rotating–Disk Electrode

The rotating–disk electrode is a common tool for studying the kinetics of moderately fast electrode reactions because the hydrodynamics[20], [21], [22] and the mass–transfer characteristics[23] are well understood. A rotating

disk provides an uniformly accessible surface. This means that if a heterogeneous reaction is carried out at the disk, the mass–transfer rate is uniform to all parts of the surface. This is important if one wants to study the heterogeneous reaction uncomplicated by mass–transfer effects. Also, the strong forced convection eliminates the effects of natural convection. However, the rotating disk has one serious disadvantage. The current density at the disk is not uniform, because of the nonuniform ohmic potential drop. The degree of nonuniformity of the current distribution was assessed by Newman[24] and will be discussed in more detail later.

3. Equipment

3.1. Design and Description of the Electrodes

Rotating Disk The size and the shape of the rotating–disk electrode is important since it may affect the flow pattern. In a review on the rotating–disk system, Riddiford[25] has summarized the various designs and recommended several design criteria based on theoretical and experimental considerations. These criteria attempt to attain the theoretical hydrodynamic model and concentration profile by minimizing the edge effects and ensuring laminar flow. In practice however, shape and alignment factors are usually not troublesome, especially at low rotation speeds used in this work.

The rotating–disk electrode is shown in figure 4–1. The 5 mm diameter, active disk is embedded in a rod of insulating Teflon® with a 20 mm diameter. Only the central portion of the lower surface of the disk is 99.99% high–purity zinc. The electrode shaft and interchangeable, screw–on, zinc disk electrodes were obtained from Pine Instruments.

Since the rugosity of the disk surface should be considerably less than the momentum–boundary–layer thickness ($\sim 5 \times 10^{-2}$ cm), the disk surface

CBB 839-8210

Figure 4–1. Picture of the rotating–disk electrode.

was subjected to the following treatment before each run:

1. The electrodes were polished using a Buehler Econmet III grinder/polisher with 600 grit silicon carbide paper until all previous traces of corrosion were gone. The maximum scratch on the surface is then on the order of 10 μm.
2. The electrode finally was rinsed with distilled water.

Reference Electrode A mercury–mercurous chloride reference electrode saturated with a potassium chloride solution was used. This quartz–fiber saturated calomel electrode was obtained from Beckman Instruments, Inc. The use of this reference electrode was desirable since the chloride ion is common to both solutions, and this reduces the liquid–junction potential.

Counterelectrode A platinum–rhodium screen served as the counterelectrode, providing an area much larger than the working electrode for the purpose of minimizing the cathodic overpotential.

3.2. Electrochemical Cell

A schematic of the pyrex glass cell is shown in figure 4–2. The cell holds approximately 150 ml of electrolyte. The reference electrode and counterelectrode compartments each are separated from the central portion of the cell by two connections. The connections contain porous glass frits which eliminate convective flow to the reference electrode. The placement of the reference electrode in such a manner has been shown by Newman[26] to be essentially at infinity relative to the working electrode. The counterelectrode should be separated so any reaction occurring at its surface will not interfere or its products will contaminate the electrolyte next to the working electrode.

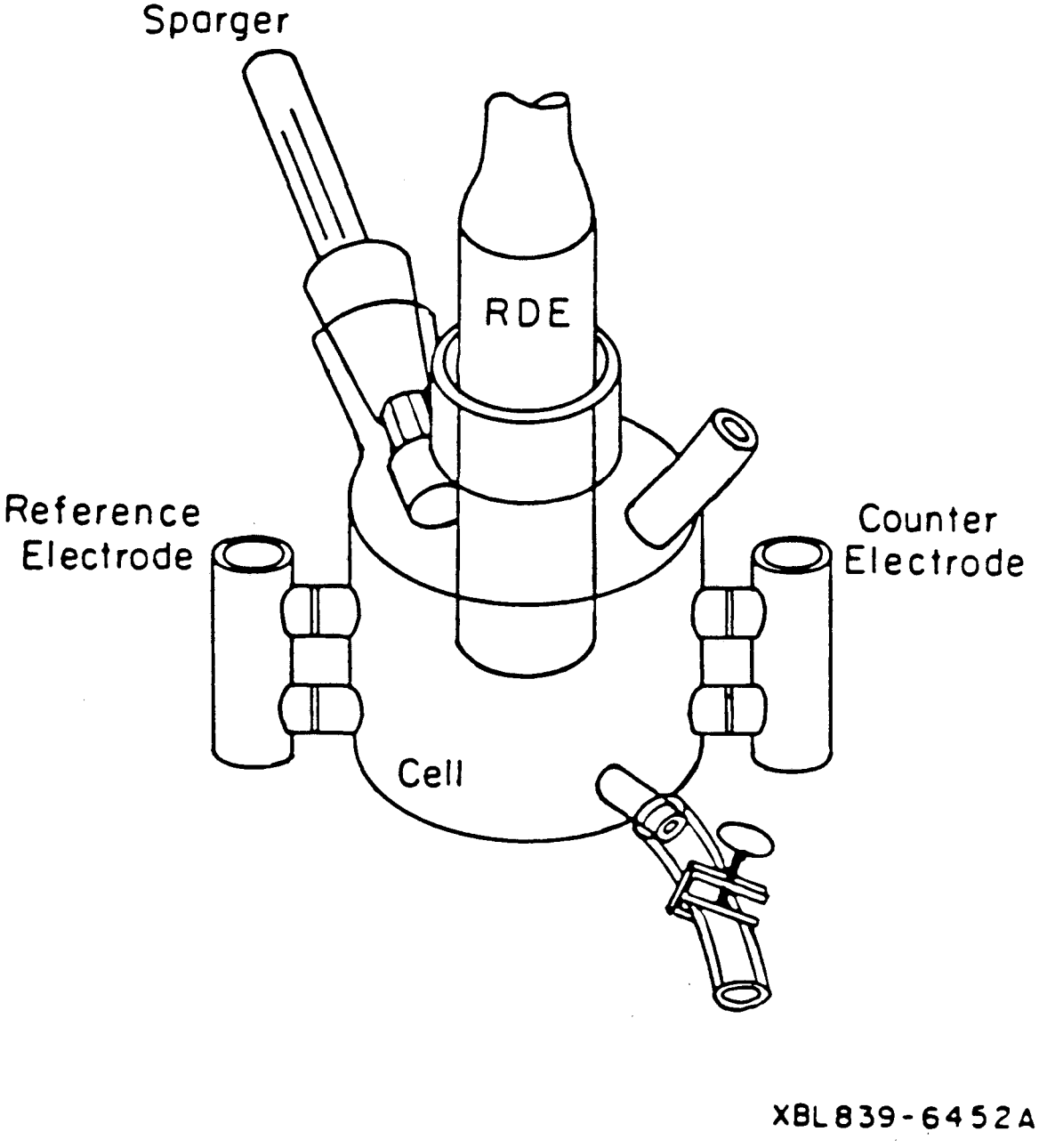

Figure 4–2. Schematic representation of the electrochemical cell.

The electrolyte is one molar hydrochloric acid prepared using Mallinckrodt analytical–reagent–grade concentrated acid, and purified water having a specific resistance of 17 MΩ–cm. The water was purified using a SYBRON/Barnstead NANOpure distilling apparatus with charcoal filters to remove organics. The solution was de–aerated for at least two hours before starting the experiments using Liquid Carbonic high–purity nitrogen. Nitrogen bubbling was continued at a much slower rate during the experiments so that the bubbles would not disturb the hydrodynamics. The experiments were carried out at room temperature.

3.3. Electrical Set–Up

Figure 4–3 is a schematic of the experimental apparatus used in the dc–polarization study. The electrochemical cell is shown on the left consisting of the working electrode, reference electrode, and counterelectrode. A Pine Instrument Company, Model PIR, rotating–disk assembly was used. The electrical connection was made to the rotating–disk electrode by means of a carbon–silver brush contact and a slip ring. No observable noise was detected in the current response of the electrode as a result of this contact for the steady–state dc experiments. The electrode shaft is attached to a 1/15 horsepower hysteresis synchronous motor (Bodine Electric Company) directly by a belt–drive system. The pulley arrangement allows different rotation speeds to be obtained, and the speed of rotation is determined using a Shimpo Digitacho DT–103B digital tachometer with an accuracy of ±1%.

The potential between the working and saturated calomel reference electrodes was potentiostatically controlled by a Stonehart, Model BC1200, potentiostat. This high performance instrument has a 1.2 A capability and was used in four–terminal operation. There are two leads from the potentiostat to the working electrode and one each to the counterelectrode

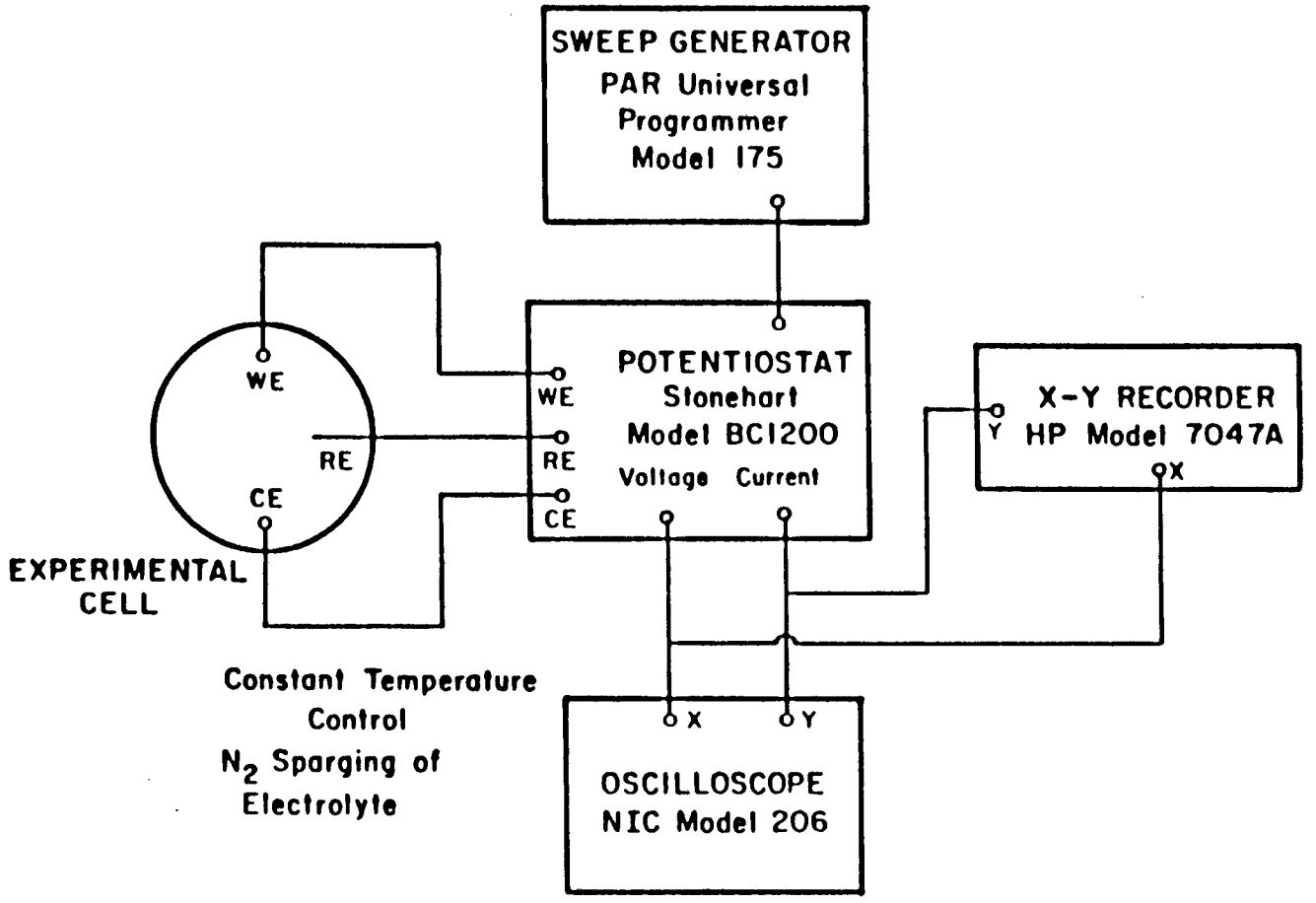

Figure 4–3. Schematic representation of the experimental apparatus.

and reference electrode. This allows the potentiostat to have a differential input which will subtract out the noise and inductance effects. The stability controls and ac attenuation were set at a minimum. The external measuring resistor was selected to be 10 ohm.

An IR bridge is available on the potentiostat to correct electronically a percentage of a fixed resistance for the ohmic drop in solution. Results from this method were compared to the results obtained from calculating the ohmic drop and making the subtraction after the experiment. The latter technique for ohmic correction is preferred, and all the results will be presented using this procedure. The advantages and the disadvantages for not using the IR–bridge feature of the potentiostat will be discussed in the results section.

The time dependence of the open–circuit potential was recorded from the potentiostat output. A Hewlett-Packard, Model 3456A, digital voltmeter also was used to confirm the readings. The potential could be ramped at a constant rate from open circuit using a Princeton Applied Research Model 175 universal programmer. Various scan rates were used ranging from 1 mV/s to 50 mV/s in order to determine the optimum rate. It is desired to have as fast a scan rate as possible so that the time for anodic dissolution is kept to a minimum. However, the rate must be slow enough so that a quasi–equilibrium state is maintained throughout the sweep. For the work being reported, a sweep velocity of 1 mV/s was used so that the anodic polarization required 300 s to reach a 300 mV overpotential from the measured open–circuit potential. The choice of the proper scan rate will be discussed in the results section.

The current and potential output were recorded with a Nicolet Model 206 digital oscilloscope as functions of time. Floppy disks were used to store the data with 2048 points each for the potential and the current so that the

recording speed was 200 ms/pt. A Hewlett-Packard, Model 7047A, analog X–Y recorder was used to record the current–potential polarization curve. A bucking box was used (not shown in figure 4–3) to subtract out the open–circuit cell potential in order that the polarization curve could be recorded full scale. A picture of the equipment is shown in figure 4–4.

4. Experimental Results

4.1. Open–Circuit Potential Data

The corrosion of a zinc rotating disk at 1600 rpm in 1.0 M hydrochloric acid was studied. Prior to any experiment, the electrode was held at zero current for the given angular velocity of the disk till the corrosion potential was stabilized. Under these conditions, the open-circuit cell potential was measured to be -1.05 V after a hold time of twenty minutes had elapsed for the electrochemical system to reach steady state. After twenty minutes, the surface becomes dulled, so that the polarization sweep was not made using the original polished surface. For this reason, polishing was not as critical as it might be in other experiments. Figure 4–5 shows the time dependence of the open-circuit cell potential prior to two polarization sweep experiments. The solid line 1, where circles represent the measured open–circuit potentials, shows the time dependency prior to the anodic dissolution polarization sweep. The solid line 2, with triangles, gives the results preceding the cathodic hydrogen evolution scan. These variations in the open–circuit potential are a concern for both dc work and future ac work. If the open–circuit potential shifts during polarization, then the corrosion potential becomes less well–defined. Even though these shifts are important, the subject will not be discussed further at this time.

4.2. Polarization Curves

The potentiodynamic polarization curves were obtained for the experimental conditions described above and summarized in table 4–1.

Table 4–1. Experimental conditions for the zinc corrosion process.

Zinc disk radius	r_0	0.25 cm
Rotation speed	Ω	167.55 rad/s (1600 rpm)
Scan rate	S	1 mV/s
1 M HCl, 25°C, 150 ml electrochemical cell		
20 min hold time for steady–state achievement		
2 hours of sparging with N_2 prior to experiment		

The system's current response to a change in potential was found to be rather slow; therefore, if a quasi–steady state is to be obtained, a slow scan rate is required. A number of scan rates were used, but 1 mV/s appears to be the best.

Ac–impedance data† may be used to confirm the proper choice of scan or sweep rate in dc–polarization measurements. Mansfeld[27] reported a criterion for the optimum scan rate. The maximum scan rate S_{max} can be calculated by

$$S_{max} = \pi V_{pp} f_{max} \quad . \tag{4–1}$$

where V_{pp} is the peak–to–peak amplitude of the voltage perturbation, and f_{max} is the maximum frequency characteristic of the scan rate. The value of f_{max} can be determined from a Bode plot of the magnitude of the impedance versus the frequency of perturbation. From unpublished ac–impedance data[28] for zinc corrosion in 1 M HCl, f_{max} is approximately 40 Hz using a

† Neither the theory of ac impedance nor the electrochemical impedance–measurement technique will be discussed here. Only the pertinent results will be used.

0.07 mV peak-to-peak perturbation applied to the open-circuit potential. Therefore, S_{max} is found to be 10 mV/s, which implies that the chosen scan rate is well below the maximum rate suggested by Mansfeld. However, it should be pointed out that if we strive to reach zero scan rate, other problems will be encountered. For example, the length of the experiment becomes longer, and the disk surface may significantly change. Therefore, a trade off must be made between the errors associated with a scan rate that is too fast (no longer a quasi-steady state), and a scan rate that is too slow. More work must be done to confirm the data presented here. For example, ac-impedance data in the Tafel regions of both the zinc and hydrogen reactions are needed to verify the proper scan rate.

The potentiodynamic polarization curve for a scan rate of 1 mV/s is shown in figure 4-6. The current density versus the measured potential V_{meas} is represented by triangles in both the anodic and cathodic sweeps. The open-circuit potential for the anodic sweep is -1.058 V. The curve for the zinc reaction appears to be linear due to the uncompensated resistance. The ohmic drop contains contributions from the electrolyte resistance between the working electrode and reference electrode, surface films, the bulk electrical resistance of the test electrode and its lead. Figure 4-6 also shows the results after sweeping the potential cathodically from the open-circuit potential of -1.049 V. (The differences in the open-circuit potential were illustrated in figure 4-1.) The polarization curve for the hydrogen reaction also appears to be linear as a result of the ohmic-potential drop in the solution. The line with circles represents the ohmic corrected potential difference, $V_{meas} - IR_{\Omega}$, where R_{Ω} is the ohmic resistance. Only selected data points were used for the ohmic correction procedure. This will be explained in more detail in the next section.

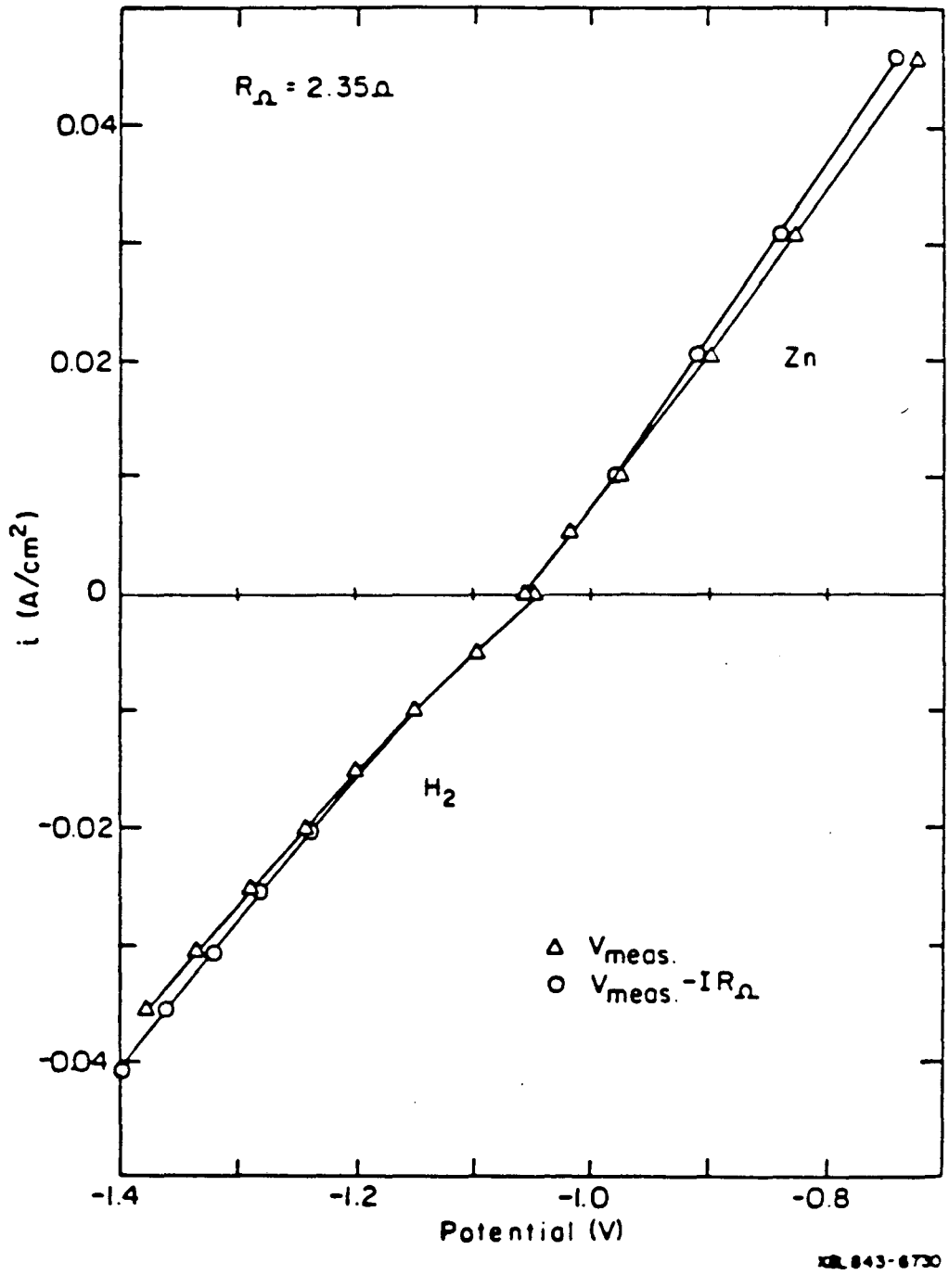

Figure 4-6. Experimental potentiodynamic polarization curve for the corrosion of zinc in 1 M HCl. Both the anodic and the cathodic potential sweeps showing the current densities relative to the measured potential and the ohmic-corrected measured potential difference. Sweep rate is 1 mV/s and rotation speed is 1600 rpm.

5. Reduction of Data

5.1. Ohmic Compensation

One should compensate for the ohmic drop to obtain meaningful kinetic parameters for the zinc and hydrogen reactions. For corroding systems, the electrode and electrolyte resistance is potential–dependent due to changes of electrolyte conductivity, surface–layer formation, and gas–bubble evolution, in addition to the potential–dependent kinetic resistance. Ideally, the variations of the solution resistance should be accounted for and be electronically subtracted as the potential sweep–measurements are made. Compensation of the ohmic drop with a preset value of R_Ω determined either at the beginning of the test or by calculation can therefore lead to only partial compensation or to over–compensation and potentiostat instability.[28] In the case of a changing solution resistance, compensation is in principal impossible due to the effect of the nonuniform current distribution. An interrupter technique[29] should be used.

If one assumes that the electrolyte resistance is potential–independent, then it is possible to correct an experimental polarization curve such as figure 4–6 for the ohmic drop by subtracting a given value for the uncompensated ohmic potential after the test. Even though for the work presented here the reference electrode is placed at a finite distance from the disk, it is assumed the reference electrode is positioned at infinity relative to the working electrode. Therefore, the necessary correction is rather simple to accomplish since one can assume without significant error that the primary distribution prevails in the bulk of the solution. This method of eliminating the linear distortion of polarization curves is preferable to positive feedback compensation of IR_Ω–drop where potentiostat oscillation is used as a criterion for correct compensation.[30] However, the technique of ohmic subtraction after the experiment does not eliminate the

effect of the uncompensated ohmic potential on the true scan rate. This is a problem with potentiodynamic polarization techniques. Uncompensated ohmic drop not only alters the shape of the polarization curve, but also produces a varying effective scan rate which depends on potential. Depending on the shape of the polarization curve, the effective scan rate S_{eff} can be larger or smaller than the applied scan rate S_{appl}. The relative error associated with the scan rate due to uncompensated ohmic drop[31] must be determined to verify the correctness of this procedure. The results of this test will be given in the next section after the kinetic parameters are presented.

The ohmic drop in the solution may be estimated from

$$\Delta\tilde{\Phi}_{ohm} = IR_\Omega = i\pi r_0^2 R_\Omega \quad , \tag{4-2}$$

where r_0 is the radius of the active disk electrode, and R_Ω is the primary resistance of the bulk solution. I is the measured net current, and i is the corresponding current density. Newman[26] showed that the resistance for a disk electrode embedded in an infinite insulating plane with the counterelectrode in the form of a hemisphere at infinity is

$$R_\Omega = \frac{1}{4\kappa_- r_0} \quad , \tag{4-3}$$

where κ_- is the conductivity of the bulk solution. This resistance was obtained from applying a separation-of-variables technique and Fourier series and integrals. Later, Newman[32] gives a thorough review of the applications of potential theory in order to determine the primary current distribution for a rotating disk including the method of Hankel transforms which Nanis and Kesselman[33] had used. The error associated with assuming an infinite cell for the primary distribution calculation is discussed by Pierini and Newman.[34] They indicate that a carefully designed disk and cell can approach conditions which allow calculations for infinite cells to be applied to finite laboratory sized cells without correction. The authors

specify a design criteria for which the uncorrected calculations are accurate.

Law and Newman[35] and more recently Russell and Newman[36] use a more general form for the resistance of a disk electrode surrounded by an infinite insulating plane depending on if either a uniform or nonuniform–primary current distribution exists. A more general form is given here by

$$R_\Omega = \frac{\varepsilon}{4\kappa r_0} \quad , \tag{4–4}$$

where ε is given by

$$\varepsilon = \begin{cases} 1 & \text{primary current distribution} \\ 8/\pi^2 & \text{uniform current distribution at the edge} \\ 4/\pi & \text{uniform current distribution at the center of the disk} \end{cases} \tag{4–5}$$

The experimental conditions of the measurements determine if the current distribution is approximated more closely by a primary or uniform distribution. Both will be used to identify which is the most appropriate. The error in using either of these equations may be assessed by introducing the dimensionless parameter[1]

$$J = \frac{ni_0 Fr_0}{RT\kappa} \quad , \tag{4–6}$$

for a disk electrode. This linear polarization parameter characterizes the corrosion process, when the electrode kinetic equation is replaced by a linear relation between the surface overpotential and the potential derivative at the electrode. For $J \to \infty$, one obtains the primary current distribution. Then the ohmic resistance dominates over the kinetic resistance at the interface. For any finite value of J, the distribution is more nearly uniform and is finite at the edge of the disk. For $J \to 0$, the distribution is uniform, but the average current must be small for the linear polarization law still to apply.

The conductivity of the bulk solution is needed in order to determine the ohmic resistance and the dimensionless parameter J. The specific conductivity is given by

$$\kappa = z_+ \nu_+ c \Lambda \quad , \tag{4-7}$$

where z_+ is the charge number and ν_+ is the number of cations into which a molecule of electrolyte dissociates. The concentration of electrolyte c is expressed in mol/ cm^3. The equivalent conductance Λ of a single salt is the sum of the values of the two ionic equivalent conductances, λ_+ and λ_-, which is given by

$$\Lambda = \lambda_+ + \lambda_- \quad . \tag{4-8}$$

The equivalent conductance of an electrolyte containing more than one salt, to a good approximation for dilute solutions, is equal to the sum of Λ for each salt. Table 75–1 in Newman[1] gives values of ionic equivalent conductances at infinite dilution in water at 25°C. For HCl, Λ = 426.1 mho–cm^2/ equiv using the infinite dilution data. So for a one molar solution, the conductivity is 0.4261 mho/cm. This should be compared with data given by Chapman and Newman,[67] where a measured conductivity of 0.3347 mho/cm is reported for a one molar hydrochloric acid solution. The difference can be attributed to the effect of concentration on the conductivity. The infinite dilution data simply gives an estimate for the conductivity. Finally, the primary and uniform ohmic resistances, R_Ω and R'_Ω, are determined to be 2.35 and 2.99 Ω, respectively, using the former conductivity. The uniform current distribution is taken to be at the center of the disk, and $\varepsilon = 4/\pi$. Unless stated otherwise, the primary resistance will be used for the remainder of the work, and this value is assumed to be constant over the entire polarization range shown in figure 4–6.

5.2. Kinetic Equations

As was stated earlier, the potentiodynamic polarization curve given in figure 4–6 may be of value for analysis only after the elimination of the linear ohmic distortion. Kinetic parameters for the corrosion process are determined from such a corrected polarization curve. First however, a kinetic expression describing the current response of the potential sweep must be established based on an assumed corrosion mechanism. The dissolution of the zinc metal is taken to be a one step, two electron–transfer elementary reaction given by

$$Zn = Zn^{2+} + 2e^- \quad . \tag{4–9}$$

It is accompanied by the reduction of hydrogen ions given by the following overall reaction

$$H^+ + e^- = \tfrac{1}{2}H_2 \quad . \tag{4–10}$$

For this work, reaction 4–10 is assumed to be the only cathodic reaction occurring, because of the low pH and the deoxygenated solution.

The logarithm of the measured current density should be plotted versus the theoretical potential difference, $V = \Phi_m - \Phi_{RC,0}$, where Φ_m is the potential of the metal rotating–disk electrode, and $\Phi_{RC,0}$ is the potential of an ideal reference electrode placed just outside the double layer. This potential driving force is used in the kinetic rate expressions for the zinc reaction 4–9

$$r_{Zn} = \frac{i_{Zn}}{2F} = k_{a,Zn} \exp\left[\frac{2(1-\beta_{Zn})F}{RT} V\right] - k_{c,Zn}\, c_{Zn^{2+},0} \exp\left[-\frac{2\beta_{Zn}F}{RT} V\right] , \tag{4–11}$$

where the rate r has units of mol/cm^2–s . The symmetry factor β is used, and k_a and k_c are the anodic and cathodic rate constants, respectively. The kinetic rate constants are assumed to be independent of concentration, and the reaction order is taken to be proportional to the stoichiometry of the reaction. It is quite possible that the two electron–transfer zinc reaction is

not an elementary step, but for the present analysis this assumption will suffice.

The cathodic hydrogen evolution reaction given by equation 4–10 is the most thoroughly investigated electrode process. This electrochemical reaction seems to be simple although its mechanism has not yet been clarified in a fully satisfactory manner. The mechanism that is used here is the Volmer–Tafel mechanism:

$$S + H^+ + e^- = H_{ads} \qquad (4-12)$$

$$2H_{ads} = H_2 + 2S \quad . \qquad (4-13)$$

The first step is the Volmer reaction reported by Erdey–Grúz and Volmer.[70] The solvated hydrogen ion is discharged at an available surface site S by an electron from the metal to form atomic hydrogen, which remains adsorbed on the metal surface. After the charge–transfer reaction, the formation of a hydrogen molecule from two adsorbed hydrogen atoms may occur by direct combination, as was originally discussed by Tafel,[71] leaving behind two vacant surface sites. The hydrogen molecules are then dissolved in water, and their removal in the form of bubbles is a mass–transfer effect not closely related to the electrode process.

The reaction mechanism and rate determining step change depending on the nature of the metal, the condition of the surface, and other factors such as electrode potential, current density, and temperature. According to Erdey–Grúz,[52] the rate of the hydrogen evolution reaction is limited by the transfer of electrons from the metal to ions in solution. The reaction of hydrogen atoms with each other to form hydrogen molecules may therefore be taken to reach equilibrium rapidly.

Reaction 4–12 is assumed to be an elementary step, so the reaction order is again taken to be proportional to the reaction stoichiometry. Therefore, the kinetic expression for the hydrogen reduction reaction is as

follows:

$$r_H = \frac{i_H}{F} = k_{a,H}\,\theta_H \exp\left[\frac{(1-\beta_H)F}{RT}V\right] - k_{c,H}\,(1-\theta_H)\,c_{H^+,0}\exp\left[-\frac{\beta_H F}{RT}V\right], \tag{4-14}$$

where θ_H is the degree of surface coverage of hydrogen atoms which is proportional to the actual surface concentration of atomic hydrogen. The cathodic reaction 4–12 occurs only at the part of the surface which is not covered by adsorbed hydrogen atoms. This fraction is $1-\theta_H$ and is multiplied by the concentration of hydrogen ions at the surface. Again, the rate constants are assumed to be independent of concentration, and β is the symmetry factory.

The kinetics of the overall hydrogen electrode reaction are also influenced by the desorption process given by equation 4–13, in addition to the relationship between the concentration of hydrogen atoms formed as a result of electron transfer and the coverage of the surface by hydrogen atoms. The amount of gas adsorbed, after equilibrium is established, depends on the nature of the surface, the temperature, and the pressure. At constant temperature, an adsorption isotherm relates the amount of adsorption to the partial pressure of the gas. Langmuir's isotherm[72] applies to the ideal case of chemisorption on a perfectly smooth surface with no interactions between adsorbed molecules.

The desorption process involves reaction between two adsorbed atoms. The rate is therefore proportional to the square of the fraction of surface covered which is given by $k_d\theta_H^2$, where k_d is the desorption constant. The reverse of reaction 4–13, the dissociation of H_2 into two species H, must be considered to be a reaction between the gas molecule and two surface sites. The rate of adsorption may therefore be written as $k_{ad}p_{H_2,0}(1-\theta_H)^2$, where k_{ad} is the adsorption constant. At equilibrium, the rates are equal, giving

$$\frac{\theta_H}{1-\theta_H} = K p_{H_2,0}^{1/2} \quad . \tag{4-15}$$

where $K = k_{ad}/k_d$ is the chemisorption equilibrium constant. When the surface coverage is sufficiently small (the partial pressure must also be very small), the fraction covered is simply proportional to $p_{H_2}^{1/2}$. These assumptions lead to the following kinetic expression for the overall hydrogen reaction 4-10

$$\begin{aligned} i_{H_2} = {} & F k_{a,H_2} p_{H_2,0}^{1/2} \exp\left[\frac{(1-\beta_{H_2})F}{RT} V\right] \\ & - F k_{c,H_2} c_{H^+,0} \exp\left[-\frac{\beta_{H_2} F}{RT} V\right]. \end{aligned} \tag{4-16}$$

where again, the degree of coverage is assumed to be small compared to unity so that the $1 - \theta_H$ term in equation 4-14 reduces simply to unity. The rate constants are independent of concentration, and k_{a,H_2} contains the chemisorption equilibrium constant.

The potential V may be rewritten in terms of the measured cell potential shown in figure 4-6, $V_{meas} = \Phi_m - \Phi_{RR}$, where Φ_{RR} is the potential as measured by an actual saturated calomel electrode placed in the bulk solution far enough away that it may be treated as infinity. Equation 3-76 written for the measured cell potential V_{meas} is

$$V = V_{meas} - \Delta\Phi_{ohm} - \Delta\Phi_{diff} - U_{RC/RR}^{\infty} \quad . \tag{4-17}$$

where the ohmic potential drop is given by

$$\Delta\Phi_{ohm} = \int_0^{\delta} \frac{i_y}{\kappa} dy \quad . \tag{4-18}$$

and y is the normal direction away from the disk. Equation 4-2 may be used for the ohmic drop if there are no concentration gradients across the cell. The diffusion potential $\Delta\Phi_{diff}$ is given by the second term on the right of equation 3-31, and the junction-region potential difference $U_{RC/RR}^{\infty}$ is given by equation 3-40. For dilute solutions with excess of supporting electrolyte, conductivity variations in the diffusion layer may be neglected, and the

diffusion potential is given by

$$\Delta\Phi_{diff} = \frac{F}{\kappa_\infty} \sum_p z_p D_p (c_{p\infty} - c_{p0}) \quad . \tag{4-19}$$

where D_p is the diffusion coefficient of species p. The equation for the potential of the junction region is

$$U''_{RC/RR,\infty} = \Phi^\delta - \Phi^\kappa \quad . \tag{4-20}$$

This is simply the liquid-junction potential $\Delta\Phi_{LJ,\infty}$; the δ phase represents the bulk solution compartment, and the κ phase is the reference electrode compartment where the saturated calomel electrode has a 4.1 M concentration of chloride ions. No concentration terms appear directly in this equation, because the same reference electrode is used for the ideal given kind and for the actual reference electrode.

5.3. Tafel Polarization Curves

In the previous section, kinetic expressions describing the current response to potential were given based on the assumption that the individual steps of the suggested mechanism were elementary reactions. The theoretical potential driving force was then related to the measured potential difference in terms of unknown surface concentrations. We would now like to analyze the experimental polarization curves and verify our proposed corrosion mechanism. A plot of log i versus V, known as a Tafel plot, is useful for this. Simplified Tafel equations will be introduced here, which allow the kinetic parameters to be evaluated. The kinetic parameters that result from our analysis of the measured data will then be presented in the following section.

Figure 4-7 is a semi-logarithmic plot of the measured current density given in figure 4-6 versus the measured cell potential corrected for the solution ohmic drop, $V \approx V_{meas} - IR_\Omega$. For a first approximation, the potential across the junction is assumed to be negligible, and the diffusion potential is

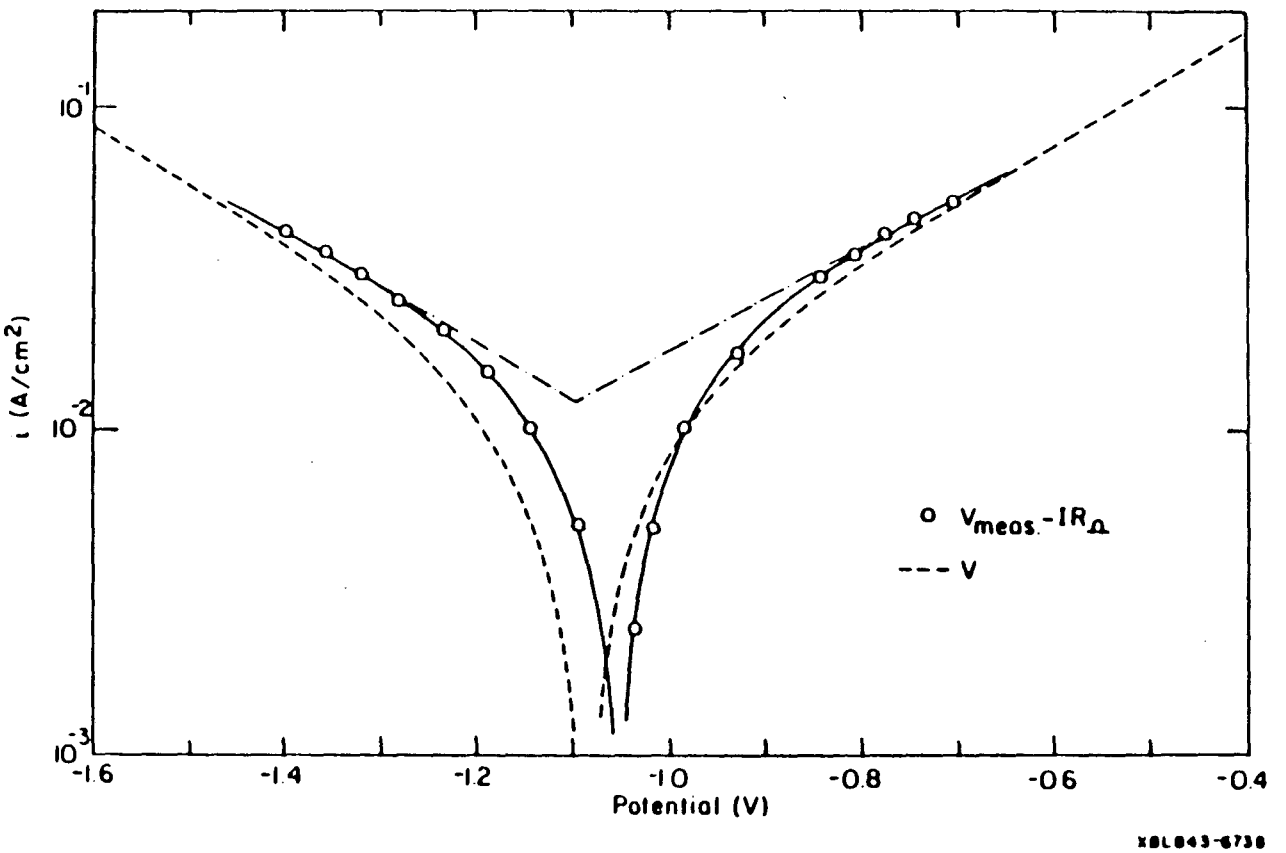

Figure 4–7. Potentiodynamic polarization curve for the corrosion of zinc. Both the logarithm of the anodic zinc dissolution and the cathodic hydrogen evolution current densities are shown relative to the ohmic–corrected measured potential difference. The regression best fit parameters were used to generate the curves given by the dotted line.

neglected because the surface concentrations of zinc and hydrogen are not known. This assumption is most valid for high rotation speeds where the mass–transfer boundary layer is thin and concentration variations are small. On such a plot, the two linear regions to the left and right of the open-circuit potential correspond to Tafel kinetics for the hydrogen evolution and zinc dissolution reactions, respectively. The symmetry factors are not equal, and therefore, the two curves are not symmetric. This is seen on the plot with the cathodic part of the curve decreasing more sharply because of its larger slope.

Near the open-circuit potential, the polarization curves have been extrapolated from the Tafel regions so that the corrosion current is shown to be 1.2×10^{-2} A/ cm^2. Allowing the Tafel law to remain valid all the way to the open-circuit potential is simply an assumption. The error in making such an approximation should be quantitatively assessed. This will be done in chapter 5, where a mathematical model of the corrosion process will be developed. However, kinetic parameters used in a model to determine the corrosion current must be obtained from the experimental polarization curves.

An equation that is commonly used to reduce polarization data is the Tafel[71] equation introduced in 1905. This simplified, yet successful model of electrode kinetics, allows the kinetic parameters to be determined easily. The equation governing the Tafel region for the zinc reaction is given by the first term on the right of equation 4–11. It may be rewritten as

$$\log |i_{Zn}| = (1/b_{a,Zn})\, V + \log (2Fk_{a,Zn}) \quad , \tag{4–21}$$

where the anodic Tafel slope $1/b_{a,Zn}$ is given by

$$\frac{1}{b_{a,Zn}} = \frac{\partial \log i_{Zn}}{\partial V} = \frac{2(1-\beta_{Zn})F}{2.303RT} \quad . \tag{4–22}$$

Again, it should be pointed out that equation 4–11 is based on the assumption that the zinc reaction is a two electron–transfer elementary

step. Thus, the symmetry factor is used.

The Tafel region for the hydrogen reaction is described by the cathodic second term on the right of equation 4–16. This equation resulted from a two–step mechanism for hydrogen evolution, where the one electron–transfer reaction is also assumed to be an elementary step. The Tafel equation for the hydrogen reaction is written as

$$\log |i_{H_2}| = -(1/b_{c,H_2})\, V + \log (Fk_{c,H_2} c_{H^+,0}) \quad . \tag{4–23}$$

where the cathodic Tafel slope is given by

$$\frac{1}{b_{c,H_2}} = \frac{\beta_{H_2} F}{2.303RT} \quad . \tag{4–24}$$

An extension of Tafel's work was introduced in 1938 by Stern and Geary.[8] They showed that to a good approximation the net current density in de–aerated solutions is the sum of the Tafel term of the anodic metal dissolution reaction and the Tafel term of the cathodic evolution of hydrogen reaction. Equations 4–21 and 4–23 are summed giving

$$i_{net} = 2Fk_{a,Zn} \exp\left[\frac{2(1-\beta_{Zn})F}{RT} V\right] - Fk_{c,H_2} c_{H^+,0} \exp\left[-\frac{\beta_{H_2} F}{RT} V\right]. \tag{4–25}$$

for the net current density.

The i_{net} versus V curves that are given by the dotted lines in figure 4–7 are generated using the Stern–Geary equation 4–25. The kinetic parameters used in this equation were determined by applying linear regression to the two Tafel portions of the experimental curves and were adjusted after roundoff. The details of this procedure are given in appendix E. It is clear that a good fit is not obtained over the entire polarization range. Therefore, another method is presented in the next section for determining the kinetic parameters.

5.4. Kinetic Parameters

Kinetic parameters for the zinc dissolution and hydrogen evolution reactions in one molar hydrochloric acid are to be presented. Various methods may be used to analyze the data to determine these parameters. The simplest method is a linear regression fit to calculate the zinc and hydrogen transfer coefficients and rate constants. Another approach utilizes a routine called FIT that is based on the Stern–Geary equation. However, before discussing FIT, let us briefly summarize the results obtained using the linear regression fit method. The physical significance of the measurable quantities should become more evident by taking the time to review the regression analysis.

The Tafel polarization curves were given in figure 4–7. The slope of the anodic zinc dissolution curve is determined by linear regression to be 1.715 V^{-1} or $b_a = 583\,mV/decade$. The measured Tafel slope is given by $b = 2.303RT/\alpha F$, where α is the transfer coefficient for the overall (anodic or cathodic) process. The transfer coefficient may therefore be determined without having to make any assumptions about the reaction mechanism. The anodic α_a for the zinc reaction is 0.102. Now if the two–electron–transfer reaction 4–9 is truly an elementary step, then equation 4–22 allows the anodic transfer coefficient to be written as $\alpha_a = (1 - \beta)n$, where $n = 2$. Hence, the symmetry factor is $\beta_{Zn} = 0.949$. The symmetry factor should have a more theoretical underlying meaning, because quantum mechanical concepts may be used to interpret it for an individual step of complex reactions. However, we will not be concerned with such analysis, and the overall experimentally measured transfer coefficient will be incorporated into the kinetic expressions for the remainder of the work instead of symmetry factors.

The transfer coefficient may be determined in a similar fashion for the hydrogen evolution reaction. The Tafel slope of the cathodic hydrogen curve in figure 4–7 is 643 mV/decade. A cathodic transfer coefficient of 0.092 results. The hydrogen symmetry factor is given by $\alpha_c = \beta n$ if equation 4–24 is used. This kinetic expression is based on the two–step reaction mechanism given by equations 4–12 and 4–13. The one electron–transfer reaction 4–12 is assumed to be an elementary step. Hence, the symmetry factor is also equal to 0.092.

The regression analysis may also be used to determine the intercepts of the best Tafel lines through the experimental i versus $V_{meas} - IR_\Omega$ polarization curves. This allows the anodic and cathodic rate constants for the zinc and hydrogen reactions, respectively to be calculated. The Tafel expression 4–21 for the zinc dissolution reaction yields the anodic rate constant which is determined from the log $(2Fk_{a,Zn})$ intercept of figure 4–7. Equation 4–23 may be used to calculate the cathodic rate constant for the hydrogen reaction assuming the surface concentration of the hydrogen ions is the same as the bulk concentration of 0.001 mol/cm^3. Because the proper rate constant is very sensitive to slight changes in the Tafel slope, round–off errors must be considered. A discussion of this sensitivity is given in the appendix. Its importance warrants pointing out that two additional significant figures will be reported because of the computational errors that arise from round off. However, one should at the same time keep in mind that the accuracy of the data is not good enough to justify writing the extra significant figures.

Next, we should like to discuss the curve fitting program, FIT, which is based on the Stern–Geary equation 4–25. We are interested in the using this equation to determine new kinetic parameters that will predict the entire polarization curve. Three experimental data points may be incorporated

into this equation by using $i-V$ points of the zinc and hydrogen Tafel regions and zero current at the corrosion potential. A trial and error procedure is used by initially assuming a value for the anodic zinc transfer coefficient. The cathodic hydrogen transfer coefficient, and the anodic and cathodic rate constants for the zinc and hydrogen reactions then may be determined iteratively. The polarization curves generated with the Stern–Geary equation by different sets of parameters are compared to the experimental curves to obtain the best graphical fit. This procedure can be carried out simply and effectively without having to use a more expensive non–linear, multivariate least–squares fitting routine. The approach used here does sacrifice a more statistically meaningful method for finding the kinetic parameters.

The results of using FIT for three cases are shown in figure 4–8. A reasonable fit for the entire polarization curve is obtained from the set which is determined based on a transfer coefficient of 0.10. This curve is represented with a dotted line in the figure. The FIT routine is also used to determine the best set of kinetic parameters based on transfer coefficients of 0.15 and 0.05. The larger α_a implies a larger Tafel slope and yields poor agreement with the experimental data as shown by the dashed line. The solid line is generated using an anodic transfer coefficient of 0.05 and surprisingly gives the best fit of the experimental data, which are represented with circles. Therefore, this set will be used in the remaining discussion of the results. Tables 4–2 and 4–3 give the best kinetic parameters obtained from FIT. An interesting point should be made about these results. The "best fit" transfer coefficients imply Tafel slopes that are significantly different from the linear regression fitted slopes previously mentioned. It is true that the parameters given in tables 4–2 and 4–3 give a good fit over the entire polarization range; however, their departure from

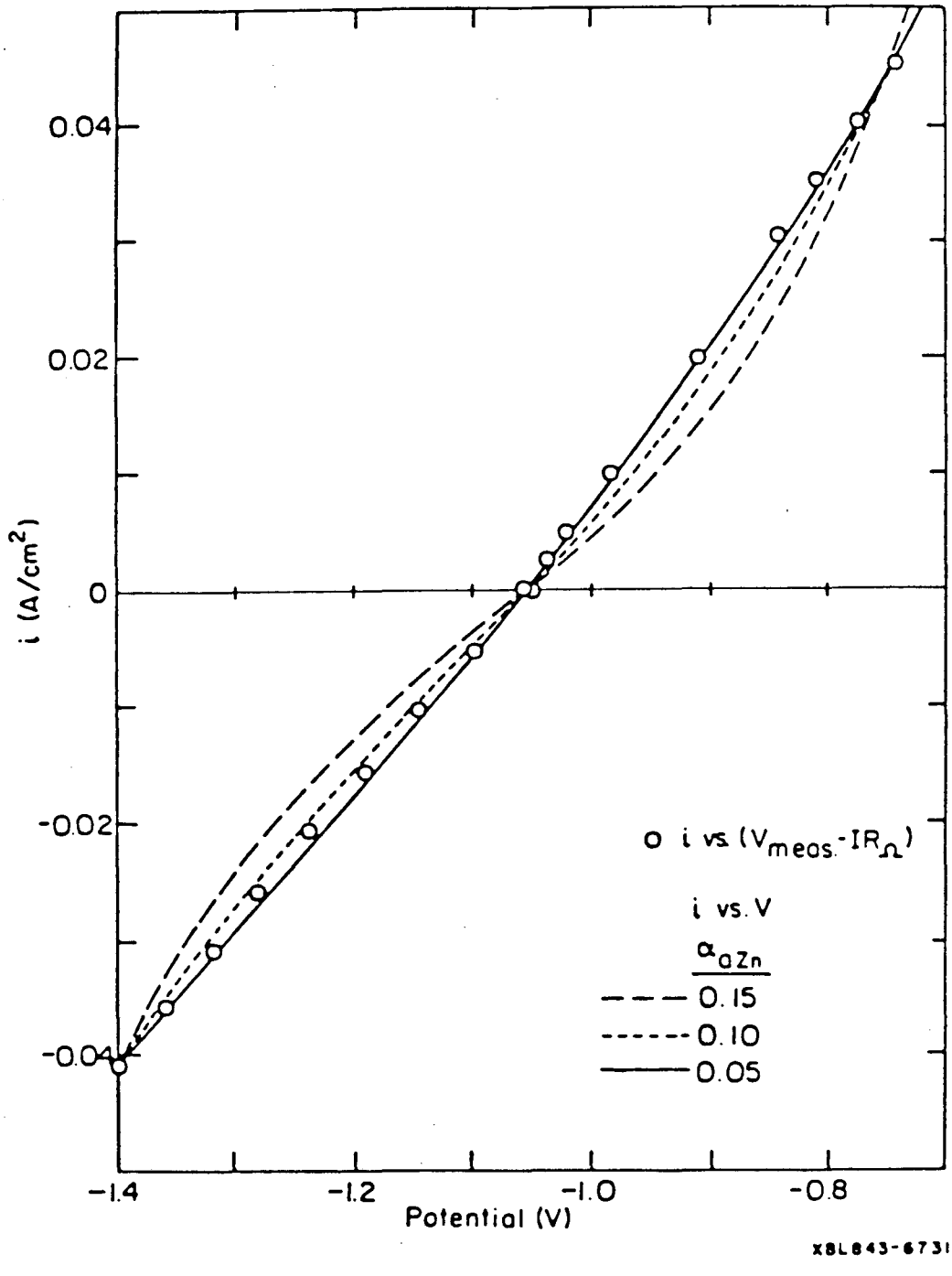

Figure 4–8. Polarization curves generated by parameters using the FIT routine. The experimentally determined potentiodynamic polarization curve for the corrosion of zinc in 1 M HCl and 1600 rpm is also shown.

physical reality is troublesome. The details of this approach and all of the kinetic parameters used in figure 4–8 are summarized in appendix E.

Table 4–2. Kinetic parameters for the zinc reaction from the anodic polarization curve for the zinc corrosion process in 1 M HCl as obtained by FIT.

$b_a = \frac{2.303RT}{\alpha_{a\,Zn}F}$	$\alpha_{a\,Zn}$	$\log(2Fk_{a,Zn})$	k_a
1.183 V	0.050	−0.5115	1.596×10^{-6} mol / cm^2–s

Table 4–3. Kinetic parameters for the hydrogen reaction from the cathodic polarization curve for the zinc corrosion process in 1 M HCl as obtained by FIT.

$b_c = \frac{2.303RT}{-\alpha_{c\,H_2}F}$	$\alpha_{c\,H_2}$	$\log(Fk_{c,H_2}c^*_{H,0})$	k_c
1.849 V	0.032	−1.976	1.095×10^{-4} cm / s

5.5. Kinetic Parameters for the Reverse Reactions

Kinetic parameters for the reverse or back reactions may be calculated by applying thermodynamics to the electrochemical reactions. The determination of the transfer coefficients and rate constants will be discussed here.

There is a reason to expect that the sum $\alpha_a + \alpha_c$ has an integral value. We have shown by assuming reactions 4–9 and 4–12 are single elementary steps that the sum of the anodic and cathodic transfer coefficients is simply equal to the number of electrons n transferred in the reaction. The transfer coefficient for the zinc cathodic reaction is obtained from $\alpha_c = n - \alpha_a$ to be 1.950. The anodic transfer coefficient for the hydrogen reaction is 0.968 assuming a one electron–transfer process.

Next, it is necessary to obtain the cathodic rate constant for the zinc reaction and the anodic rate constant for the hydrogen reaction. Equation 3–57 derived in chapter 3

$$\ln\left[\frac{k_c'}{k_a'}\right]_{Zn} = \frac{2F}{RT}\,U^{\circ}_{Zn/RC} + 2\ln\frac{c'^{\,\varepsilon}_{Cl^-,sat}}{\rho_0} \tag{4–26}$$

is used to determine the thermodynamic equilibrium ratio $\frac{k_c'}{k_a'}$ for the zinc reaction to be 2.414×10^{-34} kg/mol at 25°C and for a saturated chloride species concentration of 4.1 M. The density of pure solvent water ρ_0 is 1 gm/cm^3. Equation 3–59

$$\ln\left[\frac{k_c'}{k_a'}\right]_{H_2} = \frac{F}{RT}\,U^{\circ}_{H_2/RC} + \ln\left[\frac{c'^{\,\varepsilon}_{Cl^-,sat}}{\rho_0}\right] \tag{4–27}$$

gives 1.228×10^{-4} atm$^{\frac{1}{2}}$–kg / mol for the equilibrium ratio of the hydrogen reaction. Equation 3–74

$$\left[\frac{k_c}{k_a}\right]_j = \left[\frac{k_c'}{k_a'}\right]_j \frac{f_{i,Cl^-}}{\rho_0'} \tag{4–28}$$

relates the equilibrium constants that were just given with the desired ratio of the cathodic and anodic kinetic rate constants for reaction j and species i. The density of water ρ_0' is 0.001 kg/cm^3. The cathodic kinetic constant for the zinc reaction therefore is determined to be 4.942×10^{-38} cm/ s using 0.1283 for the activity coefficient of the zinc species relative to the chloride ion. The large difference in the magnitudes of the zinc rate constants implies that the back or deposition reaction occurs at a small rate. Equations 4–26 and 4–27 are used to obtain 3.658×10^{-4} mol / cm^2–s –atm$^{\frac{1}{2}}$ for the hydrogen reaction anodic kinetic constant. The activity coefficient of the hydrogen ion relative to the chloride ion is 2.438 using equation 3–29 and data given in reference 1. The thermodynamic and kinetic rate constant ratios are given in table 4–4.

Table 4–4. Thermodynamic and kinetic parameters for the zinc and hydrogen reactions in the zinc corrosion process.

	$\frac{k_c'}{k_a'}$	$\frac{k_c}{k_a}$	$f_{i,Cl}$
Zn	2.414×10^{-34} kg / mol	3.097×10^{-32} cm^3/ mol	0.1283
H_2	1.228×10^{-4} atm^{½}–kg / mol	2.994×10^{-1} atm^{½}–cm^3/ mol	2.438

6. Discussion of Results

The experimentally determined kinetic parameters obtained in this work are significantly different from what was expected based on other values reported in the literature. In this section, comparisons will be made with the results of other researchers for the zinc and hydrogen reactions, followed by an attempt to explain the differences.

6.1. Kinetic Parameters

Zinc Reaction

The anodic Tafel constant b_a given in section 5.4. for the zinc dissolution in 1 M HCl is 592 mV/decade of current. Kim and Jorné[37] and Chin and Venkatesh[38] give values of 108.5 mV and 125 mV in 0.5 M $ZnCl_2$ solutions with pH of 2 and 4, respectively. In the same reference, Jorné gives the anodic Tafel slopes for 1 M and 2 M $ZnCl_2$ solutions with a pH of 2 as 94.4 and 90.6 mV, respectively. My Tafel slope follows Jorné's reported trend of increasing slope with increasing zinc chloride concentration; however, my value of b_a is still unexpectedly quite large, reflecting a less steep slope on the current–potential curve which also implies a larger polarization resistance. The change in the anodic slope with zinc chloride concentration

is unexpected, because the anodic current density should be independent of concentration according to the proposed model. Therefore, these unexpected differences in the anodic slope with zinc chloride concentration may perhaps be accounted for by a reaction mechanism different from the one-step two-electron-transfer reaction assumed here. More work to confirm this should be done.

The anodic Tafel constant given here implies an anodic transfer coefficient of 0.1 assuming a two electron-transfer reaction. This value is significantly different from what is reported by other investigators. Jorné and Chin's data give approximately (using 118 mV/decade) a value of one for the anodic and cathodic transfer coefficients. Landau[39] in his theoretical model for zinc dendritic growth uses 0.5 for the transfer coefficient in an assumed one electron-transfer reaction. West[40] gives a range of Tafel slopes between 30 and 60 mV/decade so that the arithmetic mean yields an anodic transfer coefficient of 1.3. Sunu and Bennion[41] in their mathematical model of the zinc battery electrode use a value of 1.5. Hsie and Selman[42] determined the electrode-kinetic properties of zinc deposition from potential-time curves in the galvanostatic mode by assuming $\alpha_a = 1.5$ and $\alpha_c = 0.5$. These anodic transfer coefficients of 1.5 imply a slope of 49 mV.

A drastic difference results between 0.1 and 1.5 for the anodic transfer coefficient. If the zinc reaction is taken as a two electron-transfer single elementary step, then the symmetry factor for these two cases is 0.95 and 0.25, respectively. This means that 95% of the applied potential promotes the cathodic reaction instead of an expected 25%. Therefore, when polarizing in the anodic direction since only 5% of the potential goes to the anodic reaction, more applied overpotential is required to overcome the activation energy.

Another interesting point that should be considered is the fact that zinc dissolution may not follow Faraday's law. Johnson *et al.* [43] showed that the weight loss of zinc during electrolysis is greater than that calculated from Faraday's law using the normal valency of the metal cations in solution. Apparent valencies of less than two for zinc ions in the presence of oxidizing anions, in particular NO_3^-, are given and attributed to a combined effect of self–dissolution and disintegration that accompany anodic dissolution. These effects would cause the anodic Tafel slope to be larger than expected if Faraday's law were obeyed. However, it is not anticipated that the reasoning here can explain the discrepancy between my work and that of other researchers, because there should not be anything in the solution which can reduce the zinc, *i.e.* NO_3^-.

The physical significance of the zinc Tafel constants reported here and in the literature has been discussed. The differences may perhaps be accounted for by considering the experimental conditions and inherent problems associated with making the measurements. These difficulties will be presented in section 6.2. following a discussion of the kinetic parameters for the hydrogen reaction.

Hydrogen Reaction

The cathodic Tafel constant b_c for the hydrogen reaction is 592 mV/decade. However, the commonly accepted value of b_c for the hydrogen reaction on most metals is 118 mV/decade. The larger b_c reported here represents a less steep slope and implies that a greater resistance exists for the cathodic polarization.

A cathodic transfer coefficient of 0.1 results from my slope for the hydrogen reaction, whereas cathodic and anodic transfer coefficients of 0.5 obtained from Tafel slopes of $b_{c,H_2} = 118$ mV/decade are most frequently

reported. West[40] gives 0.5 for the cathodic transfer coefficient of hydrogen evolution on zinc in noncomplexing solution. Bard[9] reports $\alpha_{cH_2} = 0.5$ in sulfuric acid over a wide pH range (0.01 N to 10 N) as well as being close to 0.5 in alkaline solutions.

Assuming a one electron–transfer reaction, a symmetry factor of 0.1 also results from my hydrogen data. The symmetry factor β represents the fraction of the applied potential which promotes the cathodic reaction. Frequently, it is assumed that β should have the value ½, although the theoretical justification for this is not completely rigorous. The kinetics of hydrogen overpotential with $\beta = ½$ generally conform to the slow discharge reaction as the rate–controlling mechanism. Since β is 0.1, the cathodic reaction requires more applied overpotential to achieve the same cathodic activation energy and to obtain the same current. Because the experimentally determined value reported here is less than a half, a different mechanism may possibly be taking place, even though this is unlikely. The reason for the difference may perhaps be better explained by attributing the discrepancy to experimental difficulties that were encountered.

6.2. Experimental Difficulties

First, when questioning the results, one may ask whether Tafel regions for the zinc and hydrogen reaction were really obtained. To answer this, one simply needs to repeat the experiments polarizing the electrode much further in the anodic and cathodic directions. However, as the electrode is polarized, other problems result. Polarization into the anodic Tafel region significantly enhances the corrosion rate, which causes the electrode surface to change, affecting both the active surface area and to a smaller extent the hydrodynamics of the rotating zinc disk. The roughened surface results in an increased corrosion rate, and the original surface no longer

exists. Polarization into the cathodic hydrogen Tafel region disrupts the hydrodynamic boundary layer near the disk due to hydrogen nucleation and bubble evolution which have not been controlled.

Another experimental difficulty, the effect of the solution ohmic drop on the scan rate, is considered next. It may not have a direct effect on why the Tafel slopes given here are not as steep as is expected, but it is an important concern when doing polarization measurements. For this reason, discussing this effect is justified. Hopefully, other researchers will consider it as a problem and will confirm its significance (or better yet, the lack of) in their work.

It was pointed out previously that it is possible to correct an experimental polarization curve for the ohmic drop by subtracting the uncompensated ohmic potential after the test using a set value for R_Ω. However, this procedure does not eliminate the effect of the IR_Ω drop on the effective scan rate.† Again, the uncompensated ohmic drop not only alters the shape of the polarization curve, but produces a varying effective scan rate which depends on the potential. Because of this, the electrochemical system of interest does not actually "see" the potential that the potentiostat is trying to maintain. Therefore, one will inevitably interpret the experimental current response differently from that as if the scan rate were not affected. This could easily lead to gross errors when drawing conclusions based on such data.

The relative error of the scan rate due to uncompensated ohmic potential may be quantified by Mansfeld's[31] equation (6)

$$\frac{S_{app} - S_{eff}}{S_{app}} = \frac{R_\Omega}{R_\Omega + R_p} \qquad (4\text{–}29)$$

R_p can be calculated for any point on the polarization curve according to

† The proper choice of scan rate was discussed in section 4.2 of this chapter, and ac–impedance data confirmed that the 1 mV/s sweep used in the present study is well below the maximum rate that ensures a quasi–steady–state scan.

$$\frac{\partial i}{\partial V} = (\pi r \beta R_p)^{-1} = i_{corr} \frac{\alpha_{a\,Zn} F}{RT} \exp\left[\frac{\alpha_{a\,Zn} F}{RT} (V - V_{corr}) \right] + i_{corr} \frac{\alpha_{c\,H_2} F}{RT} \exp\left[- \frac{\alpha_{c\,H_2} F}{RT} (V - V_{corr}) \right] \qquad (4\text{–}30)$$

provided the kinetics of the zinc and hydrogen reactions are adequately governed by equation 4–25. This form of the Stern–Geary equation is in terms of the corrosion–current density given by

$$i_{corr} = 2F k_{a\,Zn} \left[\frac{k_{c\,H_2} C_{H^+}}{2 k_{a\,Zn}} \right]^{\frac{\alpha_{a\,Zn}}{(\alpha_{a\,Zn} + \alpha_{c\,H_2})}} . \qquad (4\text{–}31)$$

and the measured open–circuit potential. The corrosion–current density used in this equation was obtained from figure 4–6 to be 1.2×10^{-2} A/ cm^2.

Figure 4–9 is a plot of the relative error of the scan rate due to ohmic drop as a function of the potential driving force as one polarizes the electrode away from the open–circuit potential. The relative error curves shown by the solid and dashed lines are generated using the kinetic parameters given in tables 4–2 and 4–3 for $\alpha_{a\,Zn} = 0.05$. The solid line is for an assumed primary current distribution where $R_\Omega = 2.35\ \Omega$ is given by equation 4–5 with ε equal to one. A uniform current distribution at the center of the disk yields a resistance $R'_\Omega = 2.99\ \Omega$ that is $4/\pi$ times that of the primary resistance. The percent error due to the ohmic drop for the uniform current distribution and $\alpha_{a\,Zn} = 0.05$ is shown by the dashed line. The uniform current distribution curve shown by the dotted line is fortuitously symmetric due to the fact that it is generated using $\alpha_{a\,Zn} = \alpha_{c\,H_2} = 2(1 - \beta_{Zn}) = \beta_{H_2} = 0.1$. The results given in this figure demonstrate the small effect that ohmic resistance has on the effective scan rate for this system. However, the importance of this effect in other systems led Mansfeld[31] to state that most anodic potentiodynamic polarization curves in 1 M H_2SO_4 for systems with high corrosion rates and high critical current densities reported in the literature are invalid.

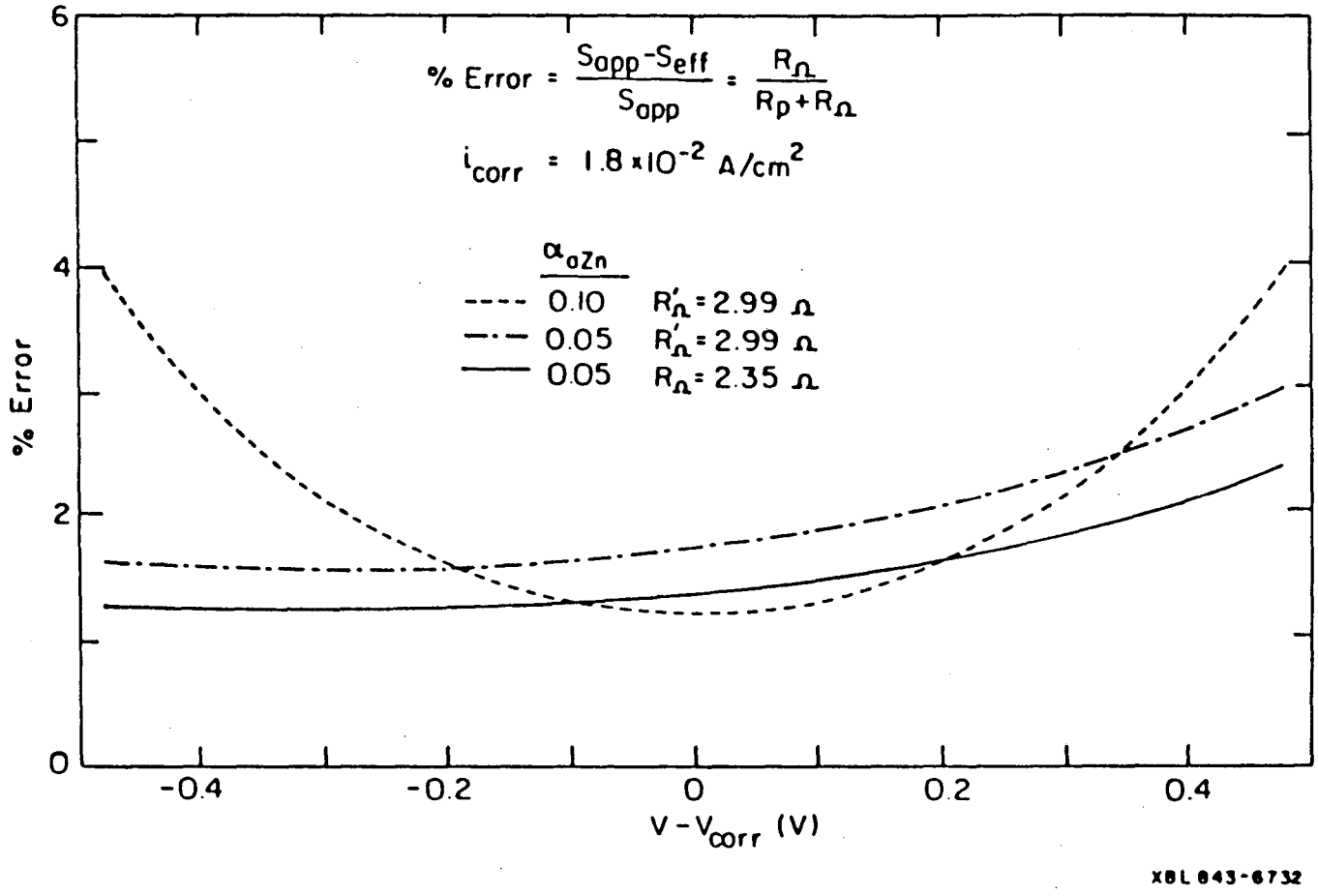

Figure 4–9. Relative error of scan rate due to ohmic drop as a function of the potential driving force.

Let us continue our discussion of experimental difficulties. Impurities are probably the most important reason for the differences in the kinetic parameters reported by researchers and are responsible for the significant changes in the corrosion rate. Little has been said about the corrosion rate up to this point, since we have been concerned only with the kinetics of the individual reactions contributing to the corrosion process. More discussion will be given in the next chapter pertaining to the corrosion rate and factors that enhance or prohibit it. At this time, we will only mention the effect that impurities have on the hydrogen evolution reaction and hence the corrosion rate.

It is well known that impurities can obscure the measurement of the electrode kinetics of the hydrogen reaction on many metals. Impurities in the zinc disk and in the electrolyte are therefore the most probable source of error on the kinetics of the hydrogen reaction. Lead, iron, and cadmium are natural impurities in special high grade zinc as ordinarily produced. The 99.99% analytical grade zinc used in this study may contain up to 0.007%, 0.005%, and 0.005% of them, respectively. Cadmium and especially iron have relatively high hydrogen exchange–current densities and increase the rate of hydrogen evolution. Ettel *et al.* [44] state that As, Sn, Se, Co, Ni, Sb, and Ge may catalyze the hydrogen discharge reaction. The concentrated hydrochloric acid used contains 3×10^{-7} % arsenic, but one should like to think that this is insignificant.

6.3. Verification of Kinetic Parameters

The kinetic parameters given above were determined based on the assumption that no concentration gradients exist across the cell so that the diffusion potential is zero. This first approximation for determining the kinetic parameters may be checked using the results of the model presented in chapter 5. These parameters will be used initially in the model to

determine the surface concentrations of zinc and hydrogen. The diffusion potential may then be calculated, and the results in figure 4–6 will be replotted versus a better approximation for $V = \Phi_m - \Phi_{RC,0}$ taking into account concentration variations across the diffusion–boundary layer. New kinetic parameters then may be determined and compared to the first set. These effects however are expected to be small relative to the other, more drastic effects mentioned in this chapter.

7. Conclusions and Recommendations

The kinetic parameters that have been presented are significantly different from those reported by other investigators, and little confidence should be placed in the data until the experiments are repeated with better control of certain variables. In particular, instead of using reagent grade hydrochloric acid, new solutions for each experiment should be made up using analytical grade hydrochloric acid. Other conditions should be examined so that a more thorough understanding of the causes of the deviations of the parameters that are reported here from those reported in the literature may be obtained. Different rotation speeds should be used so that mass–transfer effects on the corrosion rate and individual reaction kinetic parameters may be studied. Different zinc chloride concentrations and different pH solutions should be used to verify their effects on the Tafel slopes as well as on the corrosion rate. Polarization further into the anodic and cathodic regions should be carried out with the realization, however, that doing so will alter the original electrode surface intended to be studied. The hold time of the experiment should be varied, again to see its effect on the corrosion rate and kinetic parameters. Better IR_Ω compensation and computerized data acquisition methods could also be employed.

Finally, ac impedance techniques should be used to study the corrosion of zinc, because of their ease of application for obtaining mechanistic data.

A knowledge of the corrosion mechanism and the time dependence of the corrosion rate would make it possible to predict the metal lifetime from tests of relatively short duration. These accelerated corrosion tests should prove to be very important in future research.

Chapter 5. Theoretical Analysis of the Corrosion of Zinc

1. Introduction

The experimental work presented in the previous chapter will be treated theoretically so that a better understanding of the corrosion process of zinc may be obtained. First, the corrosion process is described in general terms followed by the development of a mathematical model of steady-state anodic metal dissolution in the presence of fluid flow to a rotating disk. The results of the numerical determination of the corrosion current and potential are given and compared with the Tafel approximation for the corrosion current. The effect of different parameters on the corrosion behavior of the rotating disk are also studied with the aid of the model. The results are shown graphically in a general way and may be used to describe many corrosion systems.

1.1. Background

In general, a corrosion process consists of two or more reactions occurring simultaneously. Each of the simultaneous processes may consist of multiple steps, but it is best to treat the reactions as one overall anodic reaction and another overall reaction which proceeds cathodically. In the case of a zinc rotating disk, it is assumed that the overall anodic zinc dissolution reaction

$$Zn \rightarrow Zn^{2+} + 2e^- \qquad (5-1)$$

occurs on the same surface at the same time and at the same potential as the reduction of some species present in the electrolyte. Cathodic hydrogen evolution reactions occur when hydrogen ions or water act as oxidizing agents. The hydrogen ion is consumed by the following reaction

$$2\,H^+ + 2e^- \rightarrow H_2 \quad 0.0\ V, \tag{5-2}$$

and water reacts according to

$$2H_2O + 2e^- \rightarrow H_2 + 2OH^- \quad -0.828\ V. \tag{5-3}$$

The latter decomposition of water reaction is not as thermodynamically favored as the reduction of hydrogen ions, and therefore has a more negative standard reduction potential than reaction 5-2. Oxygen, if it is present, serves as a much stronger oxidizing agent than hydrogen ions. Oxygen is easily reduced by the following reactions

$$\tfrac{1}{2}O_2 + 2H^+ + 2e^- \rightarrow H_2O \quad +1.229\ V, \tag{5-4}$$

or

$$\tfrac{1}{2}O_2 + H_2O + 2e^- \rightarrow 2OH^- \quad +0.401\ V. \tag{5-5}$$

Both are more thermodynamically favorable than the hydrogen evolution reactions due to their positive reduction potentials.

Following Wagner and Traud,[5] the local (net) current density at each point on the disk surface is the sum of the anodic and cathodic current densities given by

$$i_{net} = i_{Zn} + i_{H_2} \ . \tag{5-6}$$

At open circuit where there is no external current to the rotating disk, the reaction rates of zinc and hydrogen are of equal magnitude. The total net current on the disk should be zero resulting in

$$i_{Zn} = -i_{H_2} = i_{corr} \ . \tag{5-7}$$

where i_{corr} is the corrosion-current density at the mixed or corrosion potential. This relation defines the coupling of simultaneous corrosion reactions on an isolated homogeneous† metal surface. Under these conditions, the open-circuit potential is not an equilibrium potential corresponding to any one of these reactions, but is the corrosion potential lying between the zinc and hydrogen reversible potentials.

†For a nonhomogeneous metal surface, only the net current is zero as opposed to the current density.

Polarization of the metal slightly either anodic or cathodic to the corrosion potential produces a net current. As the potential of the zinc electrode is driven more positive, anodic dissolution becomes the dominant reaction with hydrogen evolution being negligible. The oxidation reaction given by equation 5–1 produces electrons and causes an increase in the valence of the zinc by producing cations (positively charged ions). When the zinc is polarized to a more negative potential than its open–circuit potential, hydrogen evolution is promoted and no zinc reaction occurs unless there are zinc ions in solution which are able to be reduced. Electrons are consumed in the cathodic hydrogen evolution reaction given by 5–2 causing a net decrease in the hydrogen valence state. This reduction reaction takes place on the locally more noble (positive) sites of the zinc surface and dissolution occurs on the locally active (negative) sites.

2. Model Development

A mathematical model of steady–state anodic metal dissolution in the presence of fluid flow to a rotating disk is developed. As was stated in chapter 4, this particular corrosion system is attractive for analysis because the hydrodynamic flow[20],[21],[22] is well known near a rotating disk, and one can calculate the current and potential distribution for this geometry.[24]

Active dissolution occurs at the electrode surface with a rate which varies with location along the anode owing to ohmic, mass transport, and charge–transfer processes. For a primary current distribution, the metal dissolution rate depends only on the potential distribution between electrodes. The electrodes are taken to be equipotential surfaces; thus polarization is neglected, and the potential varies according to solution conductivity and electrode size. Generally, this distribution shows that the more inaccessible parts of the electrode receive a lower current density resulting in a highly nonuniform current. A secondary distribution accounts

for slow electrode–reaction kinetics. The general effect of electrode polarization is to make the current distribution somewhat more uniform than the primary distribution.

For the problem at hand, concentration changes occur adjacent to the metal surface and must be considered along with the charge–transfer resistance and the ohmic potential drop in the solution. The Péclet number $Pe = vr / D_i$, where v is a characteristic velocity, r is the radial distance from the center of the disk, and D_i is the diffusion coefficient, is assumed to be large for the conditions investigated here. Then the concentration variations are confined to a thin mass–transfer boundary layer near the electrode surface since the fluid flow acts to wash reaction products away from the disk rapidly.

2.1. Governing Equations

Mass transfer in an electrolytic solution requires a description of the movement of mobile ionic species, material balances, current flow, electroneutrality, and fluid mechanics. With a known velocity profile, the concentration and potential distribution may be determined from four equations. The first describes the flux of each dissolved species as

$$\mathbf{N}_i = -z_i u_i F c_i \nabla\Phi - D_i \nabla c_i + \mathbf{v} c_i \quad , \tag{5–8}$$

according to dilute solution theory. The flux is due to migration in an electric field $-\nabla\Phi$ if the species is charged, diffusion in a concentration gradient ∇c_i, and convection with the fluid velocity $\mathbf{v}$. The quantity z_i is the valence of the ion; thus, $z_i F$ is the charge per mole on a species. The mobility u_i denotes the average velocity of a species in the solution when acted upon by a force of 1 newton/mol, independent of the origin of the force. The material balance for species i is

$$\frac{\partial c_i}{\partial t} = -\nabla \cdot \mathbf{N}_i + R_i \quad , \tag{5-9}$$

where the production per unit volume R_i involves homogeneous chemical reactions, but not any electrode reactions, which occur at the boundaries of the solution. The current density $\mathbf{i}$ is

$$\mathbf{i} = F \sum_i z_i \mathbf{N}_i \quad . \tag{5-10}$$

Finally, the electrolytic solution is electrically neutral

$$\sum_i z_i c_i = 0 \quad , \tag{5-11}$$

to a good approximation except in a thin double-charge layer of the order of 10 to 100 Å which is part of the electrode-electrolyte interface. These four equations provide a consistent description of transport processes in electrolytic solutions accounting for migration in laminar diffusion layers with forced convection.

For the region outside the diffusion layer, all concentrations have their bulk values $c_i = c_{i,\infty}$, and one must solve Laplace's equation

$$\nabla^2 \Phi = 0 \quad , \tag{5-12}$$

for the potential. The solution of this equation must allow the current density at the boundary to agree with the rate of the electrode reaction. Hence, the boundary condition requires a knowledge of the kinetics of the charge-transfer reactions. The electrode reaction j is represented by

$$\sum_i s_{ij} M_i^{z_i} \rightarrow n_j e^- \quad , \tag{5-13}$$

where s_{ij} is the stoichiometric coefficient of species i, and n_j is the number of electrons transferred in reaction j. The flux of species i is related to the Faradaic current density i_j of reaction j by

$$\mathbf{N}_i = -\sum_j \frac{s_{ij}}{n_j F} \mathbf{i}_j \quad . \tag{5-14}$$

The equations describing the potential dependence of the kinetics of the specific electrochemical reactions will be given in the following sections.

Finally, the material balances in the diffusion layer and Laplace's equation in the bulk medium must be calculated simultaneously since the current density and the concentration at the electrode surface must adjust themselves to balance the overpotential available after the ohmic potential drop in the bulk medium is subtracted from the potential applied to the cell.

2.2. Assumptions

Because rigorous calculations can sometimes be cumbersome, various simplifications have been introduced into the physical picture described above. The following assumptions retain the salient features of the system being studied, but also avoid unwanted numerical complications.

1. Steady–state and isothermal conditions exist so charging currents are negligible. The steady–state assumption is justified in the dynamic corrosion process, because the diffusion layer response time is short relative to the time scale over which the surface changes as the potential is swept.

2. The double layer is assumed to be infinitely thin so that it may be ignored.

3. It is simplest to regard the overall anodic and cathodic reactions in the corrosion process as they occur independently, consequently the net current density is the sum of the Faradaic current densities due to the two reactions.

4. A modified form of the Butler–Volmer kinetic equation is used to describe the potential dependence of the current densities over the entire polarization range.

5. The Reynolds number $Re = r^2\Omega/\nu$, where Ω is the rotation speed in rad/s and ν is the kinematic viscosity in cm^2/s, is less than the critical value 2×10^5 so that the entire disk is assumed to be in the laminar flow region.

6. The model only will be valid rigorously for a given point on the disk surface, *i.e.*, the center of the disk, and radial variations along the disk will not be accounted for.

7. The surface of the disk remains uniformly smooth and accessible during anodic dissolution so that the hydrodynamic boundary layer is not disturbed.

8. The Schmidt number $Sc = \nu / D_i$ is large, so the mass–transfer boundary layer at the active surface is thin with respect to the disk radius and also with respect to the hydrodynamic boundary–layer thickness. Diffusion along the direction of flow is negligible in comparison with convection in the same direction.

9. A stagnant Nernst–diffusion–layer thickness will be used for the zinc divalent ion, the hydrogen ion, and molecular hydrogen.

10. The metal ions formed by dissolution do not undergo hydrolysis, and all other complexing by chemical reaction are assumed to be in equilibrium because their reactions occur infinitely fast.

11. Migration of dissolved metal species is assumed to be negligible owing to the presence of supporting electrolyte.

12. The electrolyte is a Newtonian fluid, and infinitely–dilute solution theory applies.

13. The physical and transport properties of the solution are assumed to be constant depending only on the bulk composition.

2.3. Electrolytic–Solution Treatment

2.3.1. Homogeneous Reactions

The anodic dissolution of zinc in the presence of chloride ions results in complexing of the zinc species. It has been shown in the literature[9] that

four different complexed species may exist in addition to the zinc divalent ion depending on the concentration of the chloride ions. The reactions are as follows:

$$(a) \quad Zn^{2+} + Cl^- \rightarrow ZnCl^+ \tag{5-15}$$

$$(b) \quad ZnCl^+ + Cl^- \rightarrow ZnCl_2 \tag{5-16}$$

$$(c) \quad ZnCl_2 + Cl^- \rightarrow ZnCl_3^- \tag{5-17}$$

$$(d) \quad ZnCl_3^- + Cl^- \rightarrow ZnCl_4^{2-} . \tag{5-18}$$

Each reaction may be represented by

$$\sum_i \nu_{ij} M_i = 0 \quad , \tag{5-19}$$

where ν_{ij} is the stoichiometric coefficient of species i in reaction j and is defined as being positive for products. The rate of the chemical reaction j is given by the generalized equations

$$R_j = k_j c_i c_6 - k_{-j} c_{i+1} = k_j \left[c_i c_6 - \frac{c_{i+1}}{K_j} \right] \quad , \tag{5-20}$$

for the four chemical reactions given by equations 5–15 through 5–18. There are five different zinc species; c_1 through c_5 are the concentrations of Zn^{2+}, $ZnCl^+$, $ZnCl_2$, $ZnCl_3^-$, $ZnCl_4^{2-}$, respectively, and c_6 represents the chloride ion concentration. In more generalized notation, species $i = j$ is the zinc reactant in reaction j and species $i+1$ is produced in reaction j. The expression on the right of equation 5–20 is written in terms of the forward rate constant k_j and the equilibrium constant K_j for the homogeneous reaction j. K_j is defined as k_j / k_{-j}, where the forward rate constant is expressed in cm^3/mol–s and the reverse rate constant k_{-j} has units of s^{-1}. This equilibrium constant, expressed in cm^3/mol, may be related to molality equilibrium constant K_j by $K_j = K_j / \rho_0'$, where ρ_0' is 0.001 kg/cm^3 for the pure solvent and K_j is given by equation 3–55. Finally, the rate of production of species i, which is included in the material balance equation

5–9, is given by

$$R_i = \sum_j \nu_{ij} R_j = R_{j-1} - R_j$$
$$= k_{j-1}\left[c_{i-1}c_8 - \frac{c_i}{K_{j-1}}\right] - k_j\left[c_i c_8 - \frac{c_{i+1}}{K_j}\right] \quad (5\text{–}21)$$

for the five chemical species i participating in the reactions a through d. When $i = j = 1$, the resulting k_0 must be zero, because the first zinc species Zn^{2+} is taken to participate in only one homogeneous reaction.

The material balance equations 5–9, with i representing the five zinc species, hydrogen gas, hydrogen and chloride ions, along with the electroneutrality equation 5–11, are nine equations sufficient to solve for the eight unknown concentrations and potential. Provided kinetic data are available for the zinc homogeneous reactions, no additional assumptions must be made to solve this problem. The homogeneous production terms, R_{H^+} and R_{H_2}, are zero for the two hydrogen species.

The total zinc material balance may be obtained by summing the five individual zinc species balances yielding

$$\frac{\partial(c_1 + c_2 + c_3 + c_4 + c_5)}{\partial t} = -(\nabla\cdot N_1 + \nabla\cdot N_2 + \nabla\cdot N_3 + \nabla\cdot N_4 + \nabla\cdot N_5) \quad (5\text{–}22)$$

The general conservation of species equation 5–9 was shown in a previous section to contain the production rate R_i, however, the sum of the R_i's is zero for the five zinc species. Therefore, the divergence of the total zinc flux, $\nabla\cdot\mathbf{N}_{Zn} = \sum_{i=1}^{5} \nabla\cdot\mathbf{N}_i$, is zero at steady state, without having to make any assumptions about the rates of the homogeneous reactions. It should be pointed out, however, that it still is necessary to specify rates of the chemical reactions using equation 5–21 when writing the material balances for the four other zinc species and for the chloride ion. These nine equations are again sufficient to solve the problem at hand accounting for finite rates of the homogeneous reactions.

If the complexing reactions are assumed to be fast, then the rate constants k_j and k_{-j} are implied to be large. As $k_j \to \infty$, the term in parenthesis in equation 5–20 approaches zero. The concentrations therefore satisfy the equilibrium relation

$$K_j = \frac{c_{i+1}}{c_i c_\beta} \quad , \tag{5–23}$$

where K_j is taken to be independent of position and the activity coefficients have been ignored. It should be pointed out that even if the concentration of the species are in equilibrium with each other, the rate of chemical reaction R_j and the production rate of the individual species R_i are not necessarily equal to zero. Nevertheless, these four equilibrium relationships between the zinc species and chloride ions in reactions a to d may be used to replace four of the zinc species material balances.

Conservation of charge

$$\nabla \cdot \mathbf{i} = F \sum_{i=1}^{\beta} z_i \nabla \cdot \mathbf{N}_i = 0 \tag{5–24}$$

implies that the current density must be independent of position in a one dimensional system. This equation may replace the material balance equation 5–9 for the chloride ion.

Equations 5–11, 5–22, 5–24, equation 5–23 for the four complexing reactions, and equation 5–9 with $R_i = 0$ for the two hydrogen species are another set of nine independent equations that may be used to solve for the eight concentrations and the potential using the rapid equilibrium assumption. These equations should be solved subject to the following two boundary conditions: (i) the average concentration is c_∞ outside the diffusion boundary layer far from the surface; (ii) all species fluxes are specified at the interface.

The general dilute–solution equations governing the zinc corrosion process have been outlined above. Two approaches have been given for

solving the steady–state model for simultaneous zinc dissolution and hydrogen evolution at a rotating disk. One of the mathematical developments accounts for the finite rates of the homogeneous zinc reactions, and the other assumes the complexing reactions reach equilibrium rapidly. We would now like to examine specific special cases, where the equations may be further simplified.

The flux for species i given by equation 5–8 reduces to

$$\mathbf{N}_i = - D_i \nabla c_i \quad , \tag{5–25}$$

for a stagnant diffusion layer and if migration is neglected due to excess supporting electrolyte. Combining this equation with the steady–state conservation of species equation 5–9 yields

$$D_i \frac{d^2 c_i}{dy^2} + R_i = 0 \quad , \tag{5–26}$$

when the concentrations are taken to vary only in the y–direction and the diffusion coefficient of species i is independent of concentration and constant. The steady–state material balance for total zinc reduces to

$$- \nabla \cdot \mathbf{N}_{Zn} = \sum_{i=1}^{5} \nabla \cdot (D_i \nabla c_i) = D_{Zn} \sum_{i=1}^{5} \nabla^2 c_i = D_{Zn} \frac{d^2 c_{Zn}}{dy^2} = 0 \quad , \tag{5–27}$$

if all the individual diffusion coefficients have the same value, D_{Zn}. This implies a constant concentration gradient exists for total zinc when migration and convection are neglected.

Equations 5–26 and 5–27 have been written without having to specify the rates of the homogeneous reactions. Finite reaction rates, even for the case of equal diffusion coefficients, yield in general nonlinear concentration profiles for the individual zinc species. Now, if we choose to assume that the complexing reactions occur infinitely fast and that all the diffusion coefficients are the same D_{Zn}, then $R_i = 0$. Physically this means that all complexing occurs adjacent to the surface, and no homogeneous reaction takes place in the diffusion–boundary layer. This simplifies the analysis,

because only the complexed species diffusing outward across the boundary layer need to be accounted for. The diffusion–layer thickness will also be the same for all the species if the diffusion coefficients are the same.

Let us now mathematically describe the case for infinitely fast homogeneous reactions and all D_i the same. As previously stated, all concentrations variations are taken to occur within the diffusion layer of thickness δ, and outside this region, the concentrations are equal to their bulk values. Because the divergence of the flux is zero, the flux of each species is constant and may be rewritten for a one–dimensional model for the boundary layer as

$$N_i = - D_i \frac{(c_\infty - c_0)_i}{\delta_i} \quad , \tag{5–28}$$

following the classical Nernst[1] diffusion theory. The diffusion–layer thickness for a rotating disk is given by Levich[2] as

$$\delta_i = 1.6117 D_i^{1/3} \nu^{1/6} \Omega^{-1/2} . \tag{5–29}$$

Therefore, a linear concentration profile results for each of the species, when the diffusion coefficients are the same and rapid equilibrium is assumed.

Next, let us examine more closely the implications of using linear profiles for each of the species. Because the flux of species not participating in charge–transfer reactions must be zero at the electrode, the constant flux assumption for the complexed species therefore cannot remain valid all the way up to the electrode surface. The equilibrium assumption must be relaxed near the electrode. Instead, a reaction zone exists where the fluxes of the species are not constant, and nonlinear concentration profiles result given by

$$c_i = - \int_0^{\bar{}} D_i^{-1} \int_0^{\bar{}} R_i \, dy \, dy \quad . \tag{5–30}$$

The steady–state concentration profiles are determined by the kinetics of

the homogeneous reactions. To justify using equation 5–28 for all the species throughout the diffusion layer, it must be shown that the reaction front does not penetrate very far into the diffusion layer. The penetration depth of the homogeneous reactions depends on the magnitude of the rate constants and the diffusion coefficients.

2.3.2. Perturbation Formulation

It was shown in the previous section that the electrolytic solution needs to be treated as two regions: (i) the homogeneous reaction zone, where the flux is not constant and the concentrations are distributed nonlinearly, and (ii) the diffusion layer where the flux is constant resulting in linear concentration profiles. We have achieved a rigorous justification of the separation of the electrolytic solution into two regions by means of a singular–perturbation expansion of the concentration. A singular perturbation consists of two perturbation expansions valid respectively in the region far from the interface and close to the interface. Since these are two expansions of the same function, they must match in an intermediate region. In other words, the outer limit of the inner expansion coincides with the inner limit of the outer expansion. Again, the reason for constructing two such perturbation expansions is that different approximations are valid in the two regions. In the outer region (in the diffusion–boundary layer), one can neglect the rates of the chemical complexing reactions assuming infinitely fast equilibration as a first approximation, so only linear concentration profiles need to be accounted for. In the inner region (near the interface), it is necessary to consider the finite rates of the homogeneous reactions. As in the previous description of the system, convection and migration are assumed to be negligible in both regions.

The perturbation parameter $\xi = \delta_{rxn} / \delta_i$ represents a ratio of the penetration depth (characteristic of the homogeneous reaction zone next to

the surface) to a length characteristic of the thickness of the diffusion layer. If $\xi \ll 1$, then the assumption that the reactions occur simultaneously next to the surface is valid. This allows us to use the simplified conservation of species equation with R_i equal to zero because equilibrium conditions would prevail. If the two characteristic lengths are of the same magnitude ($\xi \geq 1$), then the results of the work to be presented cannot be justified.

The homogeneous reaction thickness δ_{rxn} is given by Levich[45] as $\sqrt{D_i / k_j}$. It is necessary to understand the nature of the zinc complexing reaction to obtain a value for the forward rate constant k_j. The zinc complexing reaction in water occurs via an outer–sphere complex intermediate[3] given as

$$Zn(H_2O)_6^{2+} + Cl^- = Zn(H_2O)_6^{2+},Cl^- = Zn(H_2O)_5Cl^+ + H_2O \quad . \qquad (5\text{–}31)$$

Formation of the aquo complex is a diffusion–controlled process with a bimolecular rate constant of the order of 10^9 to $10^{10}\ M^{-1}s^{-1}$. Next, the outer–sphere complex is converted into an inner–sphere complex. The rate constant for the chloride ligand substitution of water is $3 \times 10^7\ s^{-1}$. Hence, the rate–determining step of the overall reaction is the removal of a water molecule from the inner coordination sphere and its replacement by a particle in the second coordination sphere.

The penetration depth for homogeneous reaction 5–15 is 4.86×10^{-7} cm, when $0.71 \times 10^{-5}\ cm^2/s$ and $3 \times 10^7\ s^{-1}$ are used for the diffusion coefficient of the zinc divalent ion and rate constant, respectively. A diffusion–layer thickness of 1.16×10^{-3} cm for the zinc species is large relative to the reaction zone, so that the perturbation parameter of 4.2×10^{-4} is significantly less than 1. Hence, developing a perturbation expansion accounting for the finite chemical reaction zone next to the electrode is not necessary.

2.4. Kinetics of Multiple Electrode Reactions

The equations given above describe the mass transfer within the diffusion–boundary layer to and from the electrode surface. Next it is necessary to describe the electrode–electrolyte interface. The electrode reactions serve as the boundary conditions for the one–dimensional model being described. The net current density is the sum of the zinc and hydrogen current densities as was given earlier by equation 5–6. That equation may be obtained by substituting Faraday's law given by equation 5–14 into equation 5–10 for the net current density in terms of the ionic fluxes. If a kinetic relation between the zinc and hydrogen current densities and the potential is known, one can determine the corrosion current and potential when the kinetic expressions are coupled to the mass–transport equations 5–28 and 5–29.

The polarization curve of zinc is a function of several variables such as the zinc divalent–ion concentration and the chloride ion concentration. The polarization curve of the hydrogen reaction is a function of the partial pressure of hydrogen gas and the pH of the solution. There are many kinetic expressions from which to choose, but a modified Butler–Volmer relationship is best for the application at hand since the kinetic parameters used in this equation have been determined by methods given in chapter 4. To characterize the overall response of the disk electrode undergoing anodic polarization, the kinetics of the assumed one–step, zinc reaction are described by the following equation

$$i_{Zn} = 2Fk_{a,Zn} \exp\left[\frac{\alpha_{a\,Zn}F}{RT} V\right] - 2Fk_{c,Zn}\, c_{Zn^{2+},0} \exp\left[-\frac{\alpha_{c\,Zn}F}{RT} V\right] \quad (5\text{–}32)$$

The expression for the cathodic evolution of hydrogen, derived from a two step mechanism given in chapter 4, is

$$i_{H_2} = Fk_{a,H_2} p_{H_2,0}^{\gamma} \exp\left[\frac{\alpha_{aH_2}F}{RT} V\right] - Fk_{c,H_2} c_{H^+,0} \exp\left[-\frac{\alpha_{cH_2}F}{RT} V\right] \quad (5\text{–}33)$$

Both kinetic equations are presumed to apply over the entire polarization range. The electrode potential relative to an ideal reference electrode of a given kind placed just outside the double layer is used as the electric driving force $V = \Phi_m - \Phi_{RC,0}$ in these kinetic rate expressions. Because the zinc and hydrogen reactions 5–1 and 5–2 are taken to be the overall net anodic and cathodic reactions, respectively, overall transfer coefficients α are used as opposed to individual–reaction–step symmetry factors β as introduced in chapter 3. Possible effects of mass–transfer limitations are accounted for by including the concentration dependence of the reactants in the kinetic expression. The reaction orders of equations 5–32 and 5–33 are taken to be proportional to the reactions' stoichiometry, and rate constants k are independent of concentration. These assumptions must be validated by experimentation. Concentrations at the surface are needed in both kinetic expressions; therefore, mass transfer to the disk should be taken into account. The results of these considerations will be presented here for a one–step electrode reaction mechanism.

2.5. Resulting Kinetic–Diffusion Equations

The governing equations for the electrolytic solution and the electrode interface have been presented in the previous sections. Simplified equations assuming the homogeneous complexing reactions are in equilibrium are given in addition to the formulation of the more generalized perturbation expansion accounting for chemical reactions with finite rates. Now it is possible to combine the results of the electrode interface and electrolytic solution to obtain an adequate description of the entire system.

Typically under the assumption that homogeneous reactions do not take place, conservation of species within the boundary layer yields a uniform

flux at steady state. Even for homogeneous reactions with finite rates, we have shown with equation 5–22 that the gradient of the total zinc flux is zero at steady state, *i.e.*, $dN_{Zn}/dy = 0$. Equation 5–28 for the flux of species i across a stagnant, Nernst diffusion layer may be rewritten for total zinc and then equated with the flux at the electrode surface given by equation 5–14 yielding

$$\frac{i_{Zn}}{2F} = D_{Zn}\frac{c_{Zn,\infty} - c_{Zn,0}}{\delta_{Zn}} = \sum_{i=1}^{5}\frac{D_i}{\delta_i}(c_\infty - c_0)_i \quad . \tag{5–34}$$

The right side of equation 5–34 represents the sum of the individual zinc species fluxes. Again, making the assumptions that the chemical reaction rate constants are large and that the diffusivities of all the zinc species are equal implies $R_j = 0$. Therefore, the equilibrium relationship equation 5–20 allows the zinc species to be related to each other as follows:

$$c'_2 = K_1 c'_1 c'^2_6/\rho_0 \quad , \tag{5–35}$$

$$c'_3 = K_1 K_2 c'_1 c'^2_6/\rho_0^2 \quad , \tag{5–36}$$

$$c'_4 = K_1 K_2 K_3 c'_1 c'^3_6/\rho_0^3 \quad , \tag{5–37}$$

$$c'_5 = K_1 K_2 K_3 K_4 c'_1 c'^4_6/\rho_0^4 \quad , \tag{5–38}$$

where the activity coefficients have been ignored and the equilibrium constants given by equation 3–54. The chloride ion concentration c_6 is also required to be uniform in order to write equations 5–35 through 5–38. Each species is simply a function of the chloride ion and Zn^{2+} ion concentrations. Therefore, the ratio of the zinc divalent ion species to total zinc is given by $c_{Zn^{2+}}/c_{Zn} = (1+Q)^{-1}$, where

$$Q = \frac{c'_{a^-}}{\rho_0}\left[K_1 + K_1K_2\frac{c'_{a^-}}{\rho_0} + K_1K_2K_3\frac{c'^2_{a^-}}{\rho_0^2} + K_1K_2K_3K_4\frac{c'^3_{a^-}}{\rho_0^3}\right] \quad . \tag{5–39}$$

Equation 5–34 may be rewritten as

$$\frac{i_{Zn}}{2F} = \frac{-D_{Zn}}{\delta_{Zn}}(1+Q)(c_{Zn^{2+},\infty} - c_{Zn^{2+},0}) \quad . \tag{5–40}$$

Here we have related the Faradaic zinc current density to the surface

concentration of the zinc divalent ions accounting for complexing. This equation may be substituted into the zinc kinetic expression 5–32 and after rearrangement gives the following

$$\frac{i_{Zn}}{2F} = \frac{k_{a,Zn} \exp\left[\frac{\alpha_{a\,Zn} F}{RT} V\right] - \frac{k_{c,Zn}\, c_{Zn,\infty}}{(1+Q)} \exp\left[-\frac{\alpha_{c\,Zn} F}{RT} V\right]}{1 + \left[\frac{\delta}{D}\right]_{Zn} \frac{k_{c,Zn}}{(1+Q)} \exp\left[-\frac{\alpha_{c\,Zn} F}{RT} V\right]} \quad . \qquad (5\text{–}41)$$

The current density for the zinc reaction is a function only of the potential driving force $V = \Phi_m - \Phi_{RC,0}$ provided the other variables in the equation are known input parameters.

An expression for the current density of the hydrogen reaction may be obtained in a similar way. However, first a relationship for the solubility of hydrogen is needed. The chemical potentials of hydrogen in the vapor and liquid phases are equated as

$$\mu^{\circ}_{H_2} + RT \ln p_{H_2} = \mu^{a}_{H_2} + RT \ln m_{H_2} \quad , \qquad (5\text{–}42)$$

where the fugacity and activity coefficients have been ignored. After rearrangement and the use of the NBS Technical Note 270–3,[18] equation 5–42 yields

$$\frac{m_{H_2}}{p_{H_2}} = \exp\left[\frac{\mu^{\circ}_{H_2} - \mu^{a}_{H_2}}{RT}\right] = 8.34 \times 10^{-4} \frac{mol/kg}{atm} \quad . \qquad (5\text{–}43)$$

The concentration of hydrogen is related to the molality by the solvent density $\rho_0 = c_i / m_i$, so that using 1.00 gm/cm^3 for water gives

$$s_{H_2} = \frac{c_{H_2}}{p_{H_2}} = 8.34 \times 10^{-7} \frac{mol/cm^3}{atm} \quad . \qquad (5\text{–}44)$$

This may be compared to $7.52 \times 10^{-7} \frac{mol/cm^3}{atm}$ reported by Newman and Hsueh,[4] and the latter value is used in the model. Equations 5–14 and 5–28 are used with the solubility to obtain the following expression for the partial pressure of molecular hydrogen at the surface

$$p_{H_2,0} = p_{H_2,\infty} - \frac{i_{H_2}}{2F}\left[\frac{\delta}{D\,s}\right]_{H_2} . \qquad (5-45)$$

which then is substituted into the kinetic equation 5–33 for the hydrogen reaction. The surface concentration of the hydrogen ion is given by

$$c_{H^+,0} = c_{H^+,\infty} + \frac{i_{H_2}}{F}\left[\frac{\delta}{D}\right]_{H^+} . \qquad (5-46)$$

and also is substituted into equation 5–33, yielding

$$i_{H_2} = \frac{-2C}{B + \sqrt{B^2 - 4AC}} . \qquad (5-47)$$

for the hydrogen reaction rate expression where

$$A = 1 + 2k_c\left[\frac{\delta}{D}\right]_{H^+}\exp\left[-\frac{\alpha_{c\,H_2}F}{RT}V\right] + k_c^2\left[\frac{\delta}{D}\right]_{H^+}^2\exp\left[-\frac{2\alpha_{c\,H_2}F}{RT}V\right] \qquad (5-48)$$

and

$$B = \frac{Fk_{a,H_2}^2}{2}\left[\frac{\delta}{D\,s}\right]_{H_2}\exp\left[\frac{2\alpha_{a\,H_2}F}{RT}V\right] + 2Fk_{c,H_2}\,c_{H^+,\infty}\left[\frac{\delta}{D}\right]_{H^+}\exp\left[-\frac{\alpha_{c\,H_2}F}{RT}V\right] + 2Fk_c^2 c_{H^+,\infty}\exp\left[-\frac{2\alpha_c F}{RT}V\right] . \qquad (5-49)$$

and

$$C = F^2k_{c,H_2}^2\,c_{H^+,\infty}^2\exp\left[-\frac{2\alpha_{c\,H_2}F}{RT}V\right] - F^2k_{a,H_2}^2p_{H_2,\infty}\exp\left[\frac{2\alpha_{c\,H_2}F}{RT}V\right] \qquad (5-50)$$

If the concentration of the hydrogen ion is assumed to remain constant across the diffusion boundary layer, then $A = 1$, and the last term on the right of equation 5–49 is neglected. Again, the current density is only a function of potential and is no longer written in terms of unknown surface concentrations.

2.6. Method of Solution

The governing equations 5–41, 5–47, and 5–7 are solved by a Newton–Raphson numerical technique. The potential is iterated on until equation 5–7 is satisfactorily met with the correct value of the corrosion potential and corresponding corrosion current. The four additional

dependent variables, i_{Zn}, i_{H_2}, $c_{Zn^{2+},0}$, $p_{H_2,0}$, are then determined. Table 5–1 gives the values of the input variables for the model. A listing of the code is given in appendix F.

3. Model Results

The principal value of the model is a generalized and overall description of the total current from a rotating–metal–disk electrode during anodic polarization accounting for concentration variations across the boundary layer. The model first is used to justify the assumptions that were made earlier so that kinetic parameters could be obtained directly from experimental, rotating–disk data. Next, the exchange–current density and corrosion–current density may be determined as functions of the active species surface concentrations. The corrosion–current density obtained from this model will be compared to the simplified estimates of the corrosion–current density given in the next chapter. The magnitudes of the exchange and corrosion current densities may be seen on the polarization

Table 5–1. Values of the kinetic–diffusion model parameters for the corrosion of zinc in 1 M HCl.

species	$D_i \times 10^5$ cm^2/s	$c_{i,\infty} \times 10^3$ mol/cm^3
Zn^{2+}	0.71	0.0
H^+	9.312	1.0
Cl^-	2.032	1.0
K^+	1.957	0.0
H_2	4.0	$p_{i,\infty}$ = 0.0 atm
κ = 0.4261 $(\Omega\text{–cm})^{-1}$	$\nu = 1.3 \times 10^{-2}$ cm^2/s	

curves generated by the model as well as the regions of kinetic and mass–transfer control.

3.1. Comparison of Experimental and Theoretical Polarization Curves

Figure 5–1 is a linear current–potential plot of the results of the model using the best kinetic parameters obtained from the FIT routine given in tables 4–2 and 4–3. The kinetic constants are summarized in table 5–2. The theoretical polarization curve, i_{net} versus V, is represented with triangles, and the experimental curve, i_{meas} versus $V_{meas} - IR_{\Omega}$, is illustrated with a dashed line through the circles. The calculated curve shows good agreement with that obtained experimentally in the anodic Tafel region. However, substantial discrepancy results near the corrosion potential and especially on the cathodic sweep.

Let us examine each contribution to the net current density before giving an explanation for the discrepancy. The forward and reverse reaction terms of both the zinc and hydrogen reactions are shown. Beginning with the zinc current density, it should be pointed out that initially with no zinc ions in the solution, the zinc reversible potential is negative infinity. However, zinc ions are formed immediately after the electrode is placed in the solution. An averaged experimental rest potential of -1.054 V is shown where the net zinc current density balances the net hydrogen current density. A corrosion–current density of 3.80×10^{-2} A/cm^2 results. The zinc exchange–current density at these corrosion conditions is 3.81×10^{-2} A/cm^2. The corresponding thermodynamic zinc potential is -1.073 V according to equation 3–22, when evaluated at the surface concentration of 0.0165 M for the zinc divalent ion at the corrosion conditions.

As anodic polarization begins, the anodic zinc current density increases with the potential V. The dissolution process also causes an increase in the zinc ion concentration. This enables the cathodic back reaction to take place

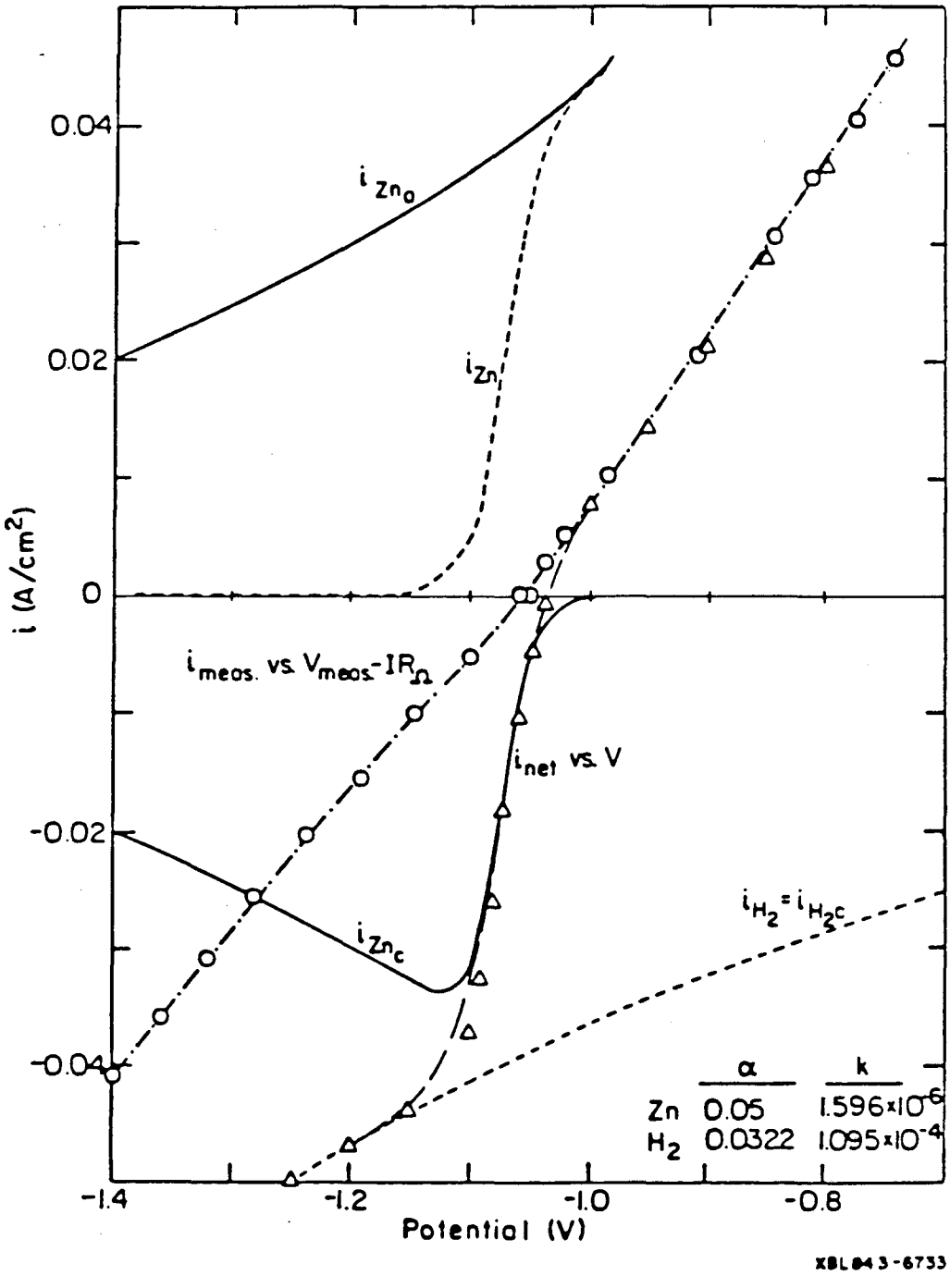

Figure 5–1. Results for the zinc and hydrogen reactions as generated by the kinetic–diffusion model accounting for complexing for the corrosion of zinc shown on a linear plot near the corrosion potential. The net current density is plotted versus V and is given by the triangles. The experimental data are shown with circles.

Table 5–2. Kinetic parameters for the zinc and hydrogen reactions in the zinc corrosion process in 1 M HCl.

	Zn	H_2
α_a	0.050	0.9678
α_c	1.950	0.0322
k_a	1.596×10^{-6} mol / cm^2–s	3.658×10^{-4} mol / cm^2–s –atm^{½}
k_c	4.942×10^{-38} cm / s	1.095×10^{-4} cm / s

yielding an increasing cathodic zinc current density. Because of the finite zinc divalent ion concentration, $i_{Zn^{2+},c}$ is finite at low anodic voltages, but is reduced both by the homogeneous complexation reactions and by increasing anodic polarization. At large anodic potentials, only the anodic term contributes significantly to the zinc current density.

For the range of potentials given, the anodic hydrogen term is, for all practical purposes, negligible. The hydrogen anodic reaction is insignificant because the corrosion potential lies so far from the hydrogen reversible potential of -0.2422 V when evaluated at the corrosion conditions and is not shown in the figure. The calculated net current density will approach the measured current density far into the cathodic Tafel region, but this is not shown in the figure.

Disagreement between experimental and calculated net current density results on the cathodic sweep away from the corrosion potential. This is a consequence of the large contribution of the zinc cathodic reaction and is shown to be most significant in the vicinity of the corrosion potential. One possible factor that causes the calculated net current to deviate from the experimental curve is the relatively large zinc ion concentration. However, the most probable source for the lack of agreement is the experimentally determined transfer coefficient. The measured anodic transfer coefficient is

small, which makes the anodic sweep approximately linear. The predicted scan in the cathodic direction exhibits a high degree of bowing following from the extremely large cathodic transfer coefficient that results. Even though the curves generated by the kinetic–diffusion model are not in agreement with the experimental data using the set of kinetic parameters obtained by program FIT, we will continue the analysis using these parameters to determine the concentration effects on the kinetic parameters.

3.2. Concentration Effects on Kinetic Parameters

We would like to justify the assumption that was made in chapter 4 concerning the neglect of concentration variations as a first approximation for determining the kinetic parameters. The following analysis will demonstrate the magnitude of the concentration effect by using the parameters in tables 5–1 and 5–2 to calculate the diffusion potential.

The simulated experimental potential V^* is given by

$$V^* = V + \Delta\Phi_{ohm} + \Delta\Phi_{diff} + U^{\circ}_{RG/RR,*} \quad . \tag{5–51}$$

The theoretical potential driving force which was used in the Tafel kinetic expression 4–11 and 5–31 was transformed from the experimentally measured cell potential V_{meas} simply by subtracting the solution ohmic–potential drop given by equation 4–2 and 4–3. The last two terms on the right of equation 5–51, the diffusion and liquid–junction potentials, respectively, were neglected as a first approximation so that the kinetic parameters could be obtained. Now, with the aid of the model accounting for concentration variations, the diffusion potential given by equation 4–15 can be calculated using the known surface concentrations. The liquid–junction potential is given by equation 4–16. The potential V^* given above may be evaluated without having to neglect any of the terms and may be compared to the potential when the diffusion and liquid–junction potentials are not

considered.

Figure 5–2 is given in order to compare the simulated measured potentials, V^* and V^*_z, given by equation 5–51, with and without the calculated concentration dependent terms, respectively. The (i versus $V^* - V_{corr}$) and (i versus $V^*_z - V_{corr}$) curves are shown by the same dotted line, because the difference between these simulated experimental potentials as shown in this figure is negligible. At current densities of 10 and 30 mA/cm^2, the percent difference between the two potential differences are 4.29 and 1.27 %, respectively. Therefore, the simulated potential difference, $V^* \approx V + IR_\Omega$, is simply the sum of the theoretical kinetic driving force V and the ohmic drop IR_Ω. The solution resistance is shown in the figure. The effect of the diffusion and liquid–junction potentials on the overall polarization curve is so small that the rate constants and transfer coefficients would not be significantly different provided the concentration variations had been accounted for. Therefore, since these differences are within experimental reproducibility, the set of kinetic parameters given in table 5–2 will be used without further modification.

Also given in figure 5–2 are the experimentally measured data (i versus $V_{meas} - V_{oc}$), which are represented with triangles and are connected by the solid line. Because potential differences are being directly compared, it is necessary to remove the effect of the arbitrary choice of the reference electrode. The measured open–circuit potential V_{oc} has been subtracted from V_{meas} in order to compare this curve to the simulated measured potential, V^* and V^*_z, curves. The theoretical corrosion potential is subtracted from the latter curves. Again, this is done solely for the purpose of comparing the measured data with the computer–generated current–potential curves at a given current density. Finally, good agreement between the measured and theoretical curves is shown in the

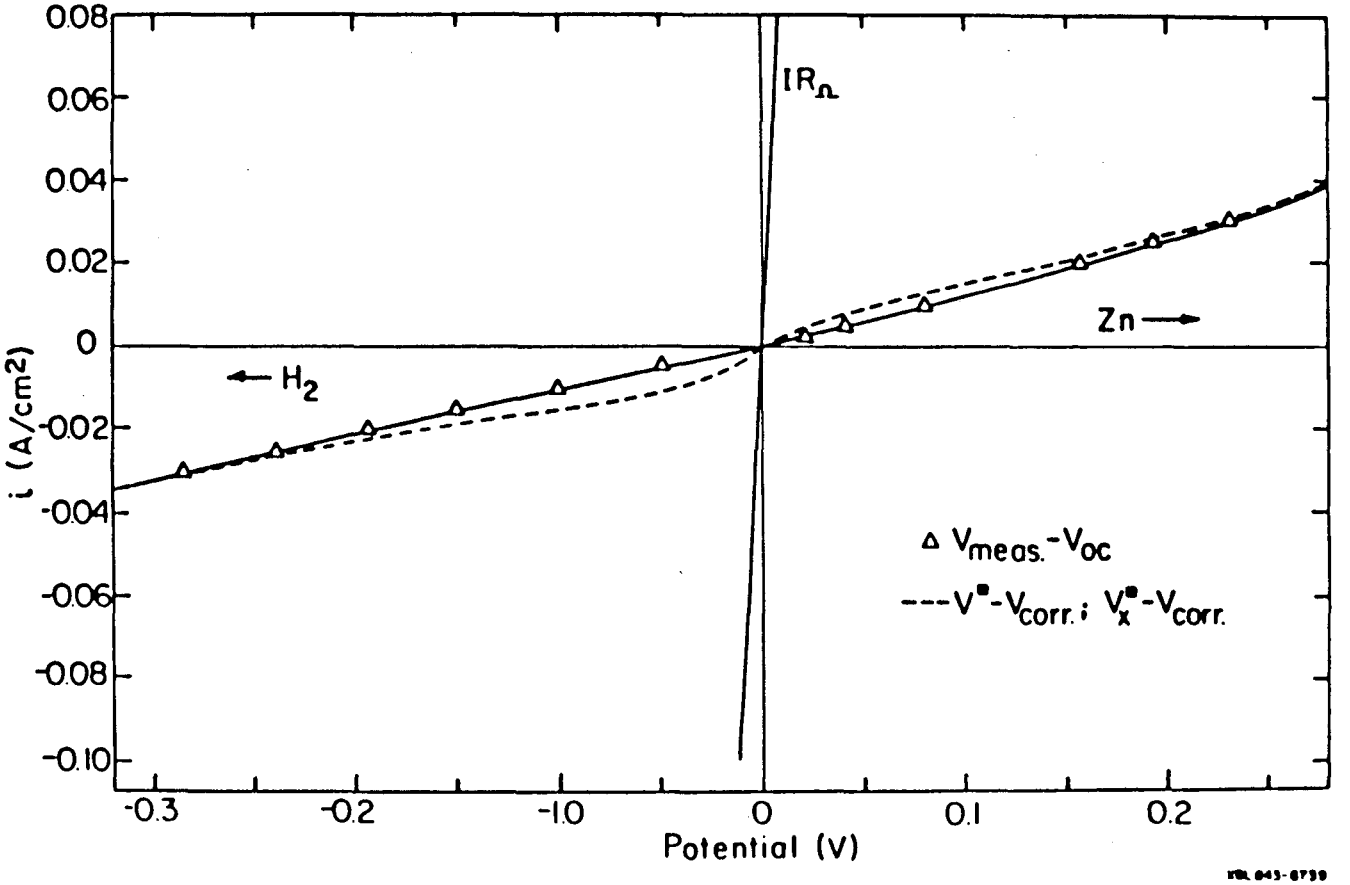

Figure 5-2. Experimental current-potential curve. Simulated measured potential is shown as well as actual data.

Tafel regions, but deviations occur near the corrosion potential. We should like to examine these curves further so a better understanding of what causes the disagreement may be ascertained.

In order to show a larger variation of the magnitudes of current densities and potentials, a log–log current–potential plot of the results shown in figure 5–2 is given in figure 5–3. The separate contributions to the simulated experimental potential difference V^* are given. The theoretical potential driving force, $V = \eta_{sj} + U'_{j/RC,0}$, the diffusion potential $\Delta\Phi_{diff}$, the liquid–junction potential $\Delta\Phi_{LJ}$, and the ohmic–potential difference $\Delta\Phi_{ohm}$ are included. Only the sum of the surface overpotential and the thermodynamic potential is shown because each of these will be shown separately in the next section.

The measured potential differences minus the open–circuit potential, $V_{meas} - V_{oc}$, are shown for the anodic and cathodic potentiodynamic polarization sweeps by the symbols o and Δ, respectively. The kinetic potential driving force, $V - V_{corr}$, for the zinc and hydrogen reactions contribute the most to the simulated overall potential difference V^* and are shown by the solid and dotted lines, respectively. The remaining potential differences given by equation 5–51 are less significant.

The ohmic drop is the largest contributor to the difference between the simulated measured potential V^* and the theoretical potential driving force V. Both the primary and uniform current distributions have been considered, and the electrolyte resistances are given by R_Ω and R'_Ω, respectively. At current densities of 40 and 60 mA/cm^2, the percent differences between the potentials corrected for ohmic drop $V + IR_\Omega - V_{corr}$ and $V + IR'_\Omega - V_{corr}$ are 0.46 and 0.51 for the primary and uniform resistance, respectively. Again, these are well within experimental reproducibility. Because there is no significant difference between the ohmic drop calculated

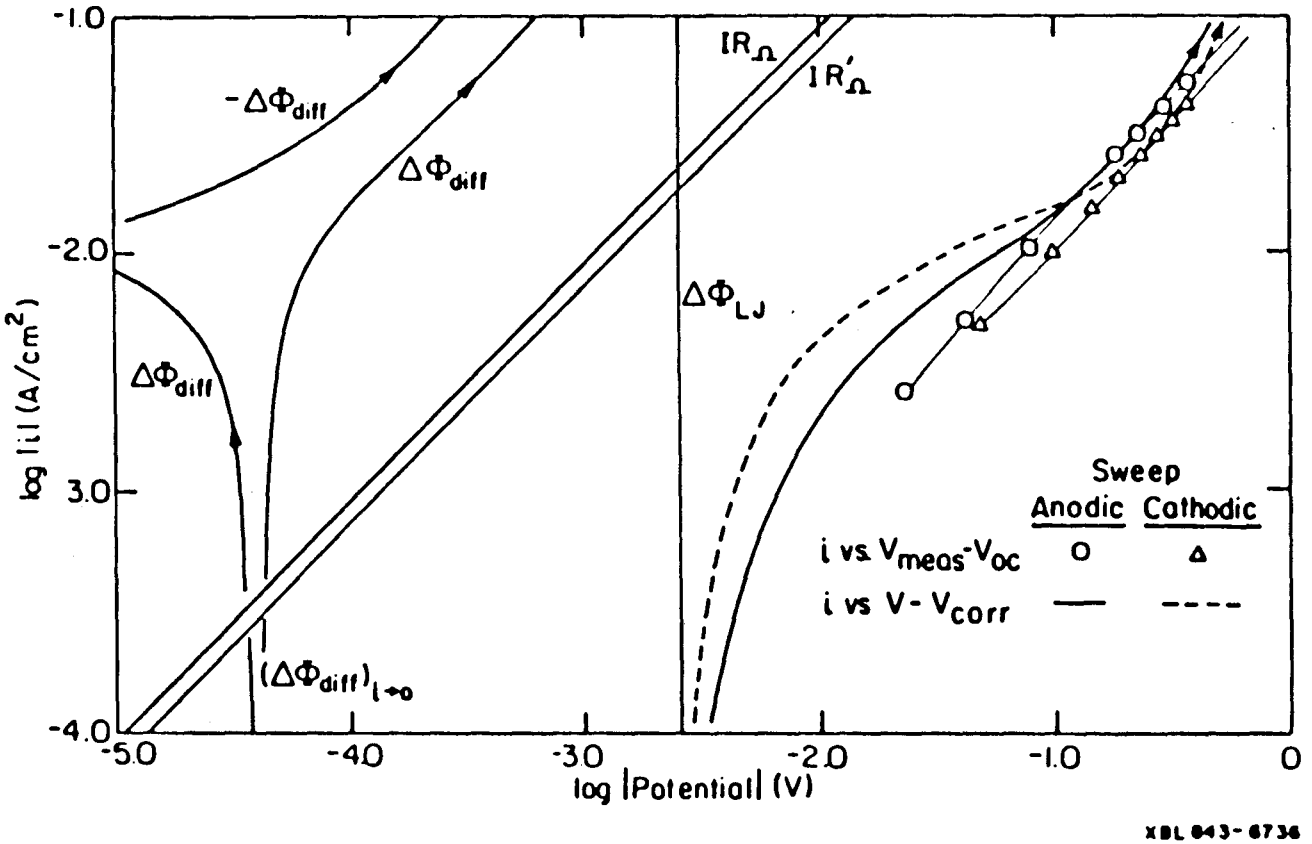

Figure 5–3. Experimental log–log current–potential plot showing break down of different potentials.

using a primary or uniform current distribution evaluated at the center of the disk, the primary resistance will continue to be used, and this justifies the use of the primary resistance up to this point.

The diffusion potential as shown in figure 5–3 contributes to the total potential difference in an interesting manner. In the absence of current, there is a finite potential difference as a result of concentration gradients. At the open–circuit potential, i_{net} is zero, and the diffusion potential is equal to 3.8×10^{-5} V. The diffusion potential is shown to increase with increasing current density on the cathodic sweep away from the open–circuit potential. On the anodic sweep, the diffusion potential decreases with increasing current until $\Delta\Phi_{diff}$ passes through zero. The diffusion potential continues to decrease with anodic polarization, which is shown by $-\Delta\Phi_{diff}$ increasing. If all the diffusion coefficients were equal, the diffusion potential would be zero by electroneutrality. However, the diffusion potential is still small, even though there is a large difference between the coefficients of zinc and hydrogen, This is so, because the species' concentration differences across the boundary layer are small. Finally, the liquid junction potential as calculated by the Henderson equation is a constant 2.5×10^{-3} V, since the concentrations in the bulk of the solution and the reference electrode compartment are assumed not to vary.

Exchange–Current Density

Because modification of the kinetic parameters for concentration effects is not required, the exchange–current densities of the zinc and hydrogen reactions may be determined using the kinetic parameters given in table 5–2. The exchange–current density for the zinc reaction is given by equation 3–75

$$i_{0Zn} = 2Fk_a^{a_c/2} k_c^{a_c/2} c_{Zn^{2+},0}^{a_a/2} , \qquad (5\text{–}52)$$

written here in terms of the transfer coefficients instead of the symmetry

factor β. A surface concentration of 0.0165 M for the zinc divalent ion at the corrosion conditions yields an apparent exchange–current density of 3.813×10^{-2} A/ cm^2 accounting for complexing. The results for these parameters at the corrosion conditions are summarized in table 5–3. The following equation

$$i_{0Zn} = i_{0Zn,ref} \left[\frac{c_{Zn^{2+}}}{c_{Zn^{2+},ref}} \right]^{\alpha_a / 2} , \qquad (5\text{–}53)$$

allows i_0 to be estimated for other zinc concentrations provided an exchange current is known at a reference concentration, and where $\alpha_a / 2 = 0.025$.

The exchange–current density for the hydrogen reaction at the corrosion conditions may be determined by using

$$i_{0H_2} = F k_a^{\alpha_c} k_c^{\alpha_a} p_{H_2,0}^{\alpha_c} c_{H^+,0}^{\alpha_a} , \qquad (5\text{–}54)$$

and the experimentally determined kinetic parameters. An exchange–current density of 1.415×10^{-2} A/cm^2 results after substituting 0.99 M and 13.54 atm for the surface composition of the hydrogen ions and molecular hydrogen, respectively. The calculated results for the hydrogen reaction at the corrosion conditions are summarized in table 5–4.

3.3. Theoretical Polarization Curves of the Corrosion Process

We will continue to use the model as if the parameters did match the experimental data so that a better understanding of the corrosion process may be obtained. The logarithm of the zinc and hydrogen current densities

Table 5–3. Calculated zinc reaction parameters using the kinetic parameters given in table 5–2.

$c_{Zn^{2+},corr} = 1.646 \times 10^{-5}$ mol / cm^3	
$i_{0Zn,corr} = 3.813 \times 10^{-2}$ A/ cm^2	$U'_{Zn/RG,corr} = -1.073$ V

Table 5–4. Hydrogen reaction parameters as determined using the experimental kinetic parameters given in table 5–2.

$c_{H^+,corr} = 9.88 \times 10^{-4}$ mol / cm^3	$p_{H_2,corr} = 13.54$ atm
$i_{0H_2,corr} = 1.415 \times 10^{-3}$ A / cm^2	$U'_{H_2/RC,corr} = -0.2422$ V

and the logarithm of the concentrations of the zinc divalent ion, the hydrogen ion, and the hydrogen partial pressure are plotted in figure 5–4 versus the electrode potential V relative to a saturated calomel electrode. The same steady–state kinetic–diffusion model results were shown in figure 5–1 also in terms of the theoretical potential difference $V = \Phi_m - \Phi_{RC,0}$. Let us examine the zinc curves first.

One can see that V is the sum of the thermodynamic potential $U_{Zn/RC,0}$ and the surface overpotential $\eta_{s,Zn}$. The two regions of kinetic and diffusion control are shown on this plot. The electrode potential given by a solid line must be driven more positive than the thermodynamic potential shown by the dotted line in order to force an anodic current through the cell. As the electrode is polarized anodically, the concentration of zinc ions at the disk surface exponentially increases as the potential increases. Noble of -1.1 V, the corrosion process becomes diffusion limited by the zinc ions. Therefore, the electrode potential is essentially governed by the Nernst equation 3–19. The conclusions concerning the two regions of control may be verified mathematically by using equation 5–41. As the second term in the denominator becomes much greater than 1, the process becomes diffusion limited. When the term is less than 1, the kinetics of the reaction are important.

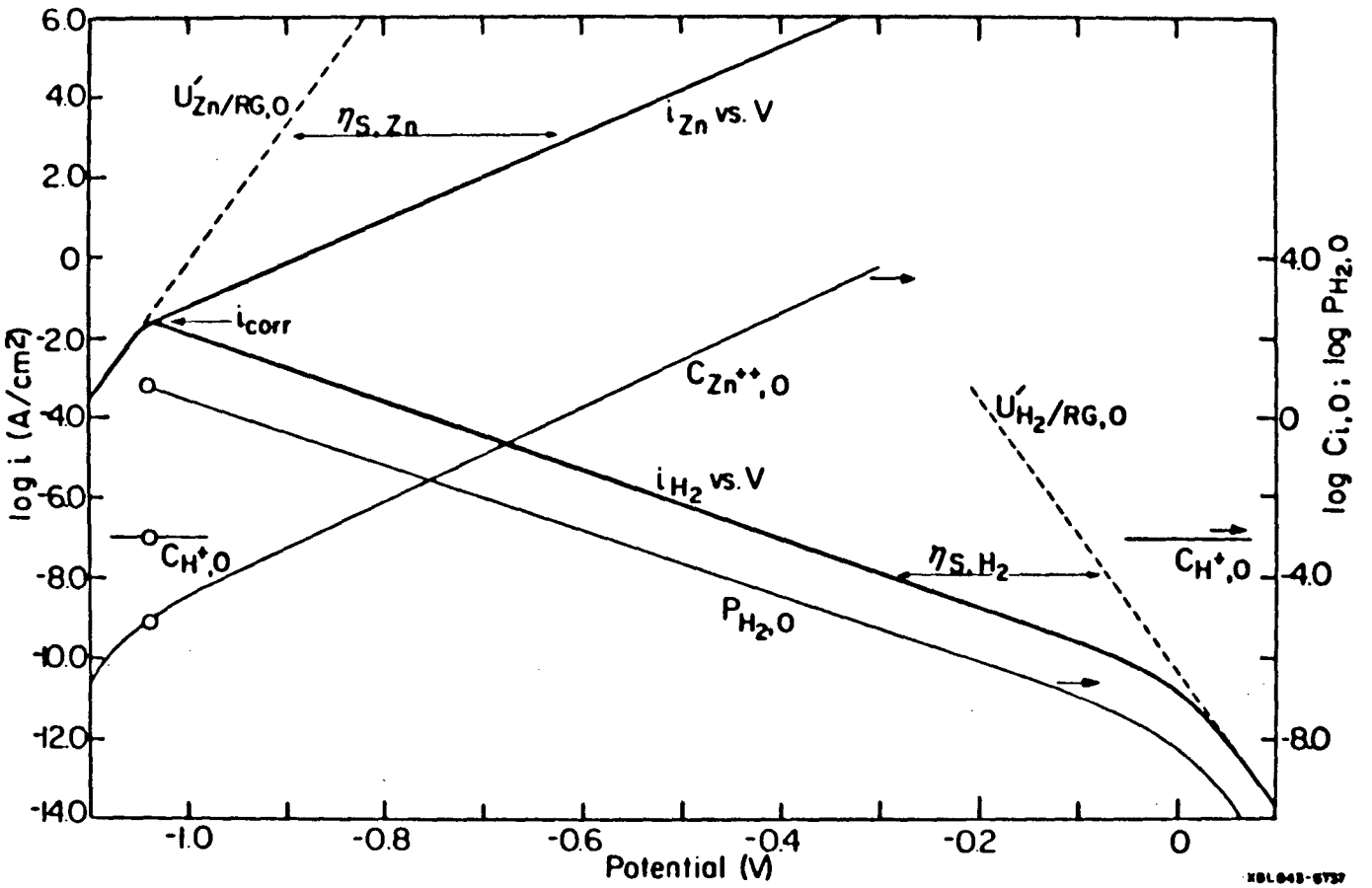

Figure 5–4. Results for the zinc and hydrogen reactions using the kinetic–diffusion model for the corrosion of zinc in 1 M HCl. The logarithms of the current densities are plotted versus the potential V shown by a heavy solid line. The thermodynamic potential evaluated at the surface concentrations of the zinc and hydrogen ion concentrations are given by dashed lines. Both kinetic and diffusion controlled regimes are shown.

The results of the rotating–disk, kinetic–diffusion model for the hydrogen reaction also are shown in figure 5–4. The electrode potential of the disk given by a solid line must be driven more negative than the thermodynamic potential shown by the dotted line in order to force a cathodic current through the cell. As the electrode is polarized cathodically, the partial pressure of hydrogen at the disk surface exponentially increases as the potential becomes more negative. The hydrogen ion concentration at the surface decreases as polarization in the cathodic direction increases. If polarized far enough, the H^+ concentration would go to zero resulting in the hydrogen reaction limiting current. The equation is

$$\frac{c_{H^+,0}}{c_{H^+,\infty}} = 1 - \frac{i_{H_2}}{i_{H_2,lim}} \quad , \tag{5–55}$$

where

$$i_{H_2,lim} = -c_{H^+,\infty}\frac{D_{H^+}F}{\delta_{H^+}} = -3.28\ A/cm^2 \tag{5–56}$$

The hydrogen ion concentration remains essentially constant over the polarization range shown. For potentials more positive than -0.15 V, the corrosion process becomes mass–transfer limited by the amount of hydrogen reaching the surface by diffusion. Again, as for zinc in the mass–transfer controlled region, the Nernst equation 3–25 for the hydrogen reaction governs the cell potential.

Graphical results of the kinetic–diffusion model have been discussed separately for the zinc and hydrogen reactions. Each has an effect on the overall zinc corrosion process. The intersection of the zinc and hydrogen current densities yields a corrosion–current density of 3.80×10^{-2} A/cm^2 and a corresponding corrosion potential of -1.039 V. As was previously stated, the surface concentrations of the zinc ions, hydrogen ions, and the partial pressure of hydrogen are at the corrosion conditions 1.65×10^{-5} mol/cm^3, 9.88×10^{-4} mol/cm^3, and 13.54 atm, respectively.

4. Discussion of Results

The lack of agreement between the model and the experimental data near the corrosion potential is due to the large contribution of the cathodic zinc current density relative to the total zinc current density. This is a result of the exceptionally large cathodic transfer coefficient that is used in the model. The unrealistic original experimental data are again the source of the problem. Even with these problems, the exchange–current densities and corrosion–current density will be discussed in the following sections.

4.1. Exchange–Current Density

Because of the nonuniform primary current distribution for the disk electrode, Tiedemann, Newman, and Bennion[5] have shown that a correction might be necessary to obtain the true exchange–current density. From their figure 1, no correction is necessary for a value of 0.174 for the dimensionless parameter J introduced in chapter 4. The exchange–current density therefore remains the same due to the high conductivity and essentially uniform current density.

Zinc

Equation 5–52 allows for the zinc exchange–current density to be estimated for other zinc concentrations provided an exchange current is known at a reference concentration. Therefore, assuming the surface concentration of zinc ions to be the same as the bulk concentration in a 0.5 M acidic zinc chloride solution, the exchange current–density is 41.5 mA/cm^2 accounting for complexing. This result may be compared to that obtained by Jorné[37] and Chin[38] for zinc in 0.5 M $ZnCl_2$ with pH of 2 and 4. They determined i_0 to be 1.36 mA/cm^2 and 19 mA/cm^2, respectively. Hsie and Selman[42] report for zinc deposition at low pH that the exchange–current densities are in the range of 20.6 to 30.6 mA/cm^2. West[40]

gives 0.001 mA/cm^2 as a mean value for the zinc exchange–current density. Standard deviations of 10 or 20 percent in exchange–current–density values are common, indicating that electrode kinetics are, in general, neither predictable nor reproducible on solid electrodes.[1]

Hydrogen

There is a discrepancy between the value of the hydrogen exchange–current density reported here and that in the literature. However, it is difficult to make comparisons because of the wide range of values reported. The differences are caused in part by the fact that the hydrogen overpotential measurements on zinc are very sensitive to impurities in the zinc electrode and in the solution. Fontana and Green[6] use 10^{-9} A/cm^2 for the hydrogen exchange–current density in an example problem. Bard[9] gives values for the hydrogen exchange–current density as 10^{-9} A/cm^2 on impure zinc and 10^{-12} A/cm^2 on amalgamated zinc in a 0.1 M zinc chloride solution at a pH of 5. Standard kinetic texts[7], [8], [9], [10] and review articles[11] which give the hydrogen overpotential on metals do not give values for zinc at all due to these variations.

A low value of the hydrogen exchange current on zinc relative to the other active metals in the absence of impurities is a direct consequence of the weak interaction between zinc and hydrogen. Because of the weak hydrogen interaction, zinc is essentially free from a chemisorbed layer of atomic hydrogen, and hydride formation even at high overpotentials should not occur on zinc. These properties of hydrogen on zinc yield such low corrosion rates in neutral environments, pure zinc is often used as protective coatings and in cathodic protection processes.

4.2. Corrosion–Current Density

Up to this point, we have discussed what affects each of the reactions that participate in the corrosion process. In chapter 4 the kinetic parameters for the zinc and hydrogen reactions were presented and discussed. In this chapter theoretical polarization curves illustrating the corrosion process have been given as results of the kinetic–diffusion model, and in the previous section we discussed the relative significance of the zinc and hydrogen exchange–current densities. Now we would like to discuss what other factors directly affect the overall corrosion process and more specifically the corrosion–current density.

The corrosion rate of zinc in aqueous deoxygenated solutions depends on pH, composition of the solution, flow rate, temperature, surface roughness, and the metal composition. Figure 5–5 is a qualitative sketch of the zinc corrosion process illustrating the effects of the first two variables. Both the zinc and hydrogen current densities are plotted versus the theoretical potential driving force V on a linear scale for several conditions. Such a plot is useful for obtaining a general overview of the corrosion process and useful for determining what are the most important concentration factors affecting the corrosion–current density.[69]

Zinc Ion Concentration

The anodic part of the zinc current–density is independent of the zinc divalent ion concentration as was shown by the modified Butler–Volmer equation 5–30. Since the cathodic back reaction is a function of the zinc ion concentration, the zinc exchange–current density is as well. As the zinc ion concentration is decreased, then i_{0Zn} also decreases. However, we expect only an indirect effect of zinc concentration on the kinetics of the corrosion process, because as the electrode is polarized anodically the rate of the reaction essentially becomes independent of concentration.

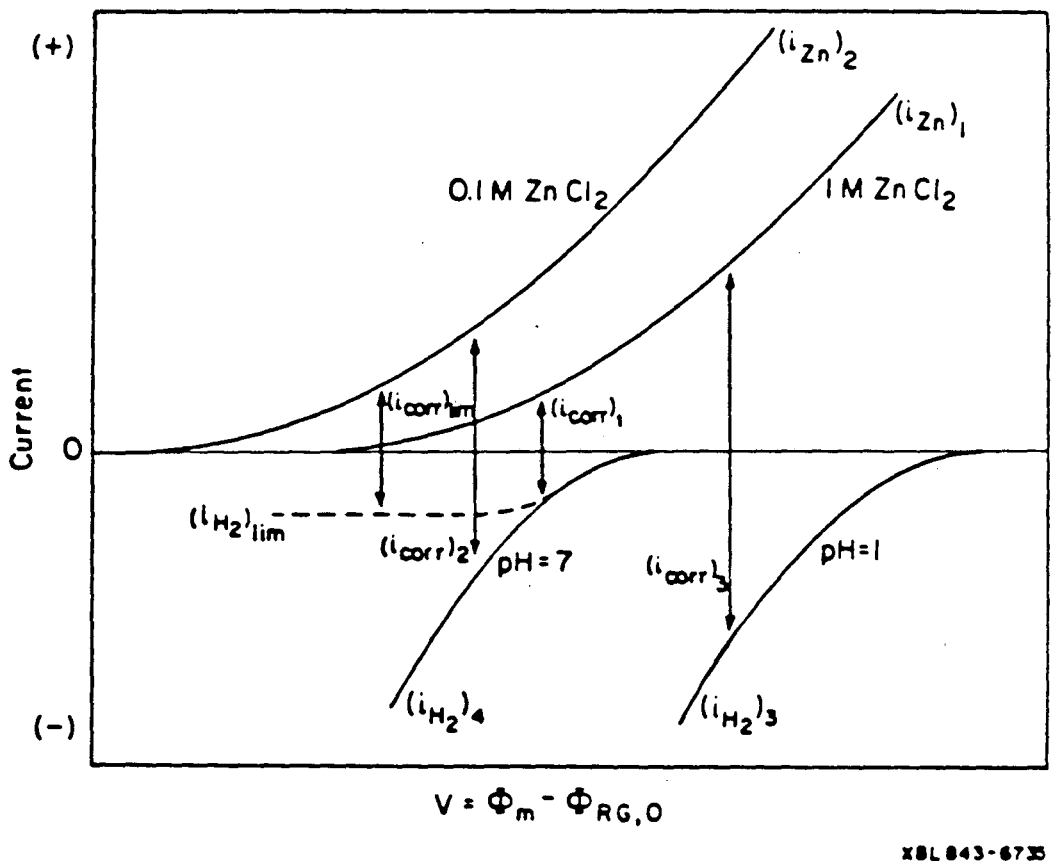

Figure 5–5. Qualitative plot of the corrosion of zinc illustrating the effect of concentration on the zinc dissolution and hydrogen evolution reactions.

The concentration of the zinc divalent ion affects the reversible zinc potential. As the zinc ion concentration goes to zero, the potential approaches negative infinity. This affects the corrosion process by shifting the thermodynamic driving force of the zinc reaction relative to hydrogen. In figure 5–5 as the zinc concentration decreases, the anodic zinc curve 1 is shifted to the left to curve 2 as the thermodynamic potential shifts. The corrosion–current density $(i_{corr})_2$ for curve 2 at smaller zinc ion concentrations is larger than $(i_{corr})_1$ using curve 4 for the hydrogen current density. This effect is much more significant than that of the decreasing zinc exchange–current density with a decrease in concentration.

pH

Increasing the hydrogen ion concentration was shown by equation 5–54 to cause an increase in the hydrogen exchange–current density. The same concentration effect shifts the hydrogen reversible potential in the positive direction increasing the thermodynamic driving force of the hydrogen reaction relative to zinc for the overall corrosion process. The corrosion–current density increases as a result of each of these effects. This concentration dependence of the corrosion–current density is shown in figure 5–5 for the hydrogen reaction by curves 3 and 4 for a pH of 1 and 7, respectively. When the 1 M zinc chloride curve is used for comparison for solutions with different pH, corrosion–current density 3 is significantly larger than 1, because the H^+ concentration affects the kinetic and thermodynamic aspects of the corrosion process in the same way. The dashed line in the figure represents a hydrogen ion mass–transfer limited curve. This situation may arise by rotating the electrode at a lower rotation speed. All of the other curves are for the same rotation speed. The corrosion current is shown to be significantly less for this limiting case than when there is an excess of hydrogen ions at the surface.

Other Factors

Other factors affecting the corrosion rate are rotation speed, conductivity, size of the disk, and temperature. The velocity of the disk has no direct effect on the rate of corrosion of metals, but stirring does have indirect effects. The rate of diffusion of the corrosive species to the metal and the rate of diffusion of the corrosion products away from the metal will be increased resulting in increased corrosion rates. As the conductivity of the solution increases, the corrosion rate becomes more uniform on the surface of the disk. This is expected, because increasing the conductivity will decrease the ohmic potential, and the potential becomes more uniform. Consequently, the corrosion rate should be uniform too. The size of the disk is an important factor in the corrosion rate. Increasing the radius of the disk has a tendency to increase the nonuniformity of the corrosion rate. However, for the small disk and high solution conductivity used in this study, the whole area is in the laminar region, and, consequently, the corrosion rate is uniform. Surface roughness is another variable that changes the corrosion rate of the metals. Usually the corrosion rate of a rough surface is higher than that of a polished one due to the increased surface area. Temperature is a factor that increases the corrosion rate by promoting the rate of electrochemical reaction on the surface of the metal.

Next, a discussion of the merits of the model for determining the corrosion–current density is pertinent. The corrosion–current density as determined by the model accounting for complexing is 3.80×10^{-2} A/ cm^2 using the experimentally determined parameters for the zinc and hydrogen reactions found in table 5–2. The extrapolation of the experimental Tafel curves shown in figure 4–5 for the anodic zinc and cathodic hydrogen reactions back to their intersection gives a corrosion–current density of 1.2×10^{-2} A/cm^2. It should be noted that if the regression fitted parameters

given in tables E–1 and E–2 are used, then the kinetic–diffusion corrosion–current density is 1.105×10^{-2} A/cm^2. This is only 8.6 % less than the result of the graphical method. The kinetic FIT parameters given by case 1 yield a corrosion–current density that is 68.5 % greater than the graphical i_{corr}. This should be expected since the graphical result is based solely on the Tafel regions of the curves as are the regression parameters; whereas, the FIT parameters are slightly modified to match best the experimental data over the entire polarization range. Because the intersection of the zinc and hydrogen current densities occurs in the Tafel region of the hydrogen reaction and near the Tafel region for the zinc reaction, the difference between the Tafel approximation and the full kinetic expression for each reaction when the regression Tafel parameters are used is hardly significant. However, for other systems the difference, as will be shown in the next section, may be much greater.

Copper Dissolution

Because the corrosion kinetics of copper in sulfuric acid is the same as the two–electron transfer reaction for zinc in hydrochloric acid, the developed model may be used to predict the corrosion–current density for the copper system. Smyrl's data[12] for the dissolution of a copper disk rotating at 1000 rpm in 0.1 N sulfuric acid have been reduced and summarized in table 5–5. These parameters are used in the model, and the results are given in figure 5–6. The intersection of the copper and hydrogen current densities lies between the thermodynamic potentials of the two reactions and in the mass–transfer controlled region of the copper reaction. The Tafel graphical estimation used to determine the corrosion–current density results in a 78% error. Therefore, the developed model is necessary for copper dissolution in sulfuric acid if the corrosion current is to be determined accurately.

Table 5–5. Kinetic parameters for the copper and hydrogen reactions in the copper corrosion process in 0.1 N H_2SO_4.

	Cu	H_2
α_a	1.655	0.5
α_c	0.345	0.5
k_a	2.073×10^{-9} mol / cm^2–s	9.40×10^{-11} mol / cm^2–s –$atm^{½}$
k_c	7.737×10^{-3} cm / s	1.15×10^{-11} cm / s

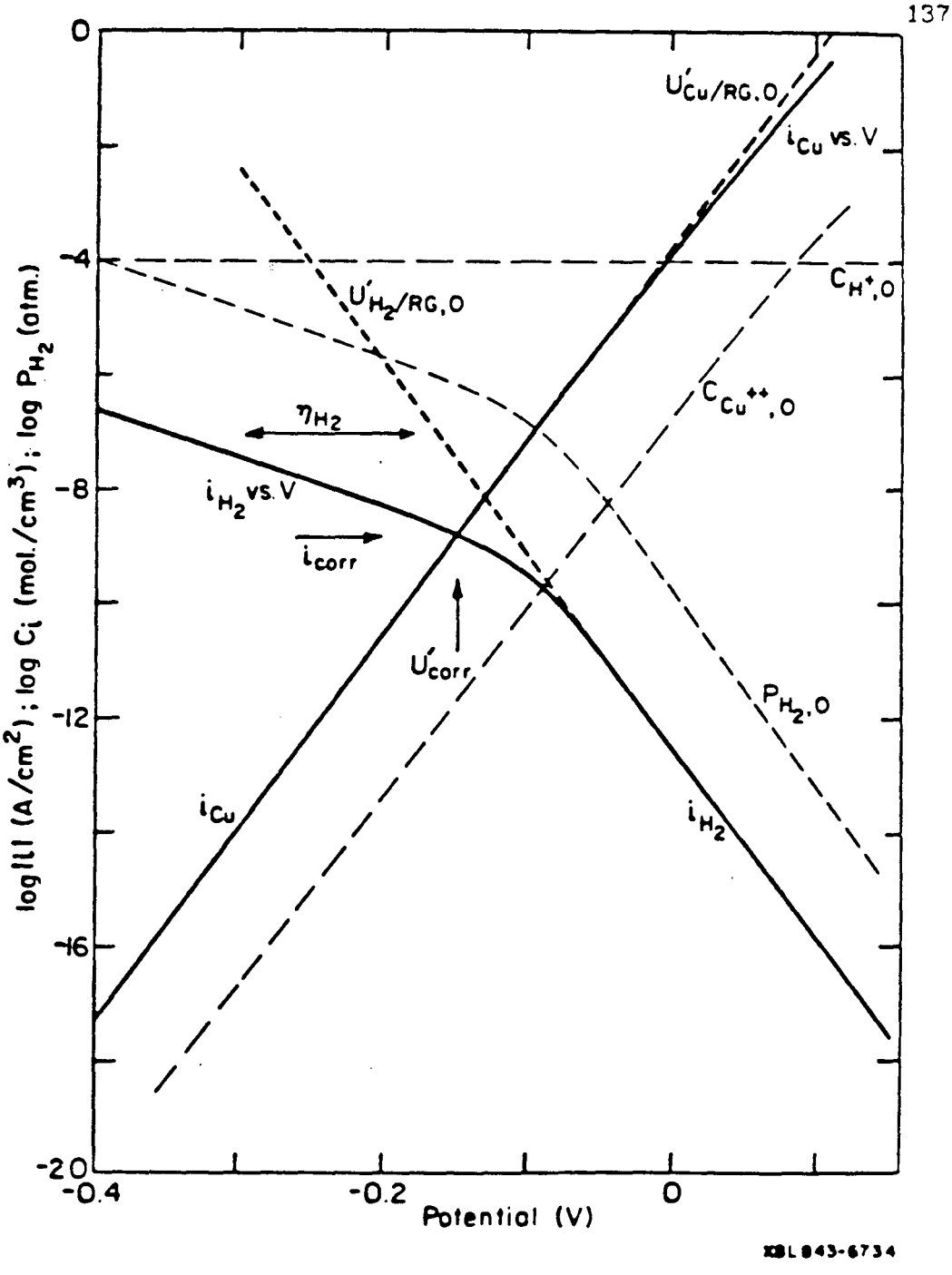

Figure 5–8. Results for the copper and hydrogen reactions using the kinetic–diffusion model for the corrosion of copper in 1 M hydrochloric acid. The logarithms of the current densities are plotted versus the potential V shown by a solid line. The thermodynamic potentials evaluated at the surface concentrations of the species are shown by heavy dotted lines and the copper and hydrogen ion concentrations and hydrogen partial pressure are given by light dashed lines. Both kinetic and diffusion controlled regimes are shown.

5. Conclusions and Recommendations

For certain systems a model such as presented in this chapter is necessary if the corrosion current is to be predicted accurately from polarization measurements. However, analysis of the zinc data given in chapter 4 shows that the experimental results are questionable, leading one to doubt the validity of a calculated corrosion current. If the initial set of rate constants and transfer coefficients had matched the experimental polarization curve approximately, then the parameters could of been slightly modified in an attempt to correct for concentration variations that were originally neglected. However, because of the differences between the model results using the given set of parameters and the experimental data, the small concentration effects as shown in the previous section will not significantly modify the parameters. Thus, good data are necessary, no matter how sophisticated a developed model is. Nonetheless, if one were to make modifications, migration and a nonstagnant diffusion layer should be accounted for in a nonsteady–state model. This might enable better agreement with the experimental data.

It is instructive to have dimensionless parameters that characterize a corrosion process in generalized terms. These parameters may be related to electrode size and rotation speed, solution conductivity, and characteristic reaction parameters such as the transfer coefficients and rate constants. The previously given expressions that mathematically describe the process may yield the desired polarization parameters. With such a set of dimensionless variables, many corrosion systems may be more easily and better understood.

The nonuniform ohmic–potential drop to a disk electrode may result in errors in the measurement of electrode kinetic parameters.[49] The correction for the exchange–current density should be expanded to include

either Tafel or Butler–Volmer kinetics. The kinetic parameters obtained using a rotating disk and corrected for by this procedure should be experimentally verified by using a rotating–hemispherical electrode. The advantage of this geometry is its uniform primary current distribution for which the measured average current is representative of the total surface. Nisancioğlu and Newman[13] have given the results theoretically, but experiments to confirm the theories would be useful.

The work that has been presented is of a fundamental nature. This study has applications for understanding corrosion processes in general, even though only the specific problem of examining the protective nature of zinc is presented. Such a study, to be complete, should be expanded to include ac impedance methods. This technique is a useful tool in corrosion research due to its capability of elucidating electrode kinetics and other interfacial phenomena in electrochemical systems. From a theoretical point of view, ac models could be developed which have relevance in the interpretation of time dependent measurements which give mechanistic information about the processes occurring at the electrode–solution interface.

For example, an ac model could be extended to incorporate a protective zinc based porous paint coating over a metal substrate. Knowledge of the mechanism of corrosion on such a painted metal would provide a good basis for the development of a rapid test method for anticorrosion paints. Such a method is urgently needed, as even in this case the conventional field tests require too long exposure times and the accelerated test methods now being employed are often far from representative of the exposure in practice. In fact a quick and reliable method for the evaluation of anticorrosion paints will be almost essential for rational development work in this field.

Chapter 6. Limitations of Polarization Methods

1. Introduction

Polarization resistance methods have been widely used to measure corrosion rates electrochemically. The corrosion–current density is determined from the slope of the current–voltage curve in the vicinity of the corrosion potential, provided Tafel slopes of the anodic metal reaction and cathodic reactions are known. This technique was first described by Wagner and Traud,[5] and then simplifying approximations were given by Stern *et al.* [6], [14] It is necessary to present the generalized formulation, and then show the simplifications that have been introduced so that the corrosion current may be obtained by the Stern–Geary polarization method. First, however, a discussion concerning the use of the exchange–current density is necessary since previous work uses this notation.

2. Kinetic Equations in Terms of the Exchange–Current Density

Numerous publications previously reported have elucidated electrode kinetics in terms of exchange–current densities. The exchange–current density for the one–step, zinc reaction was derived in chapter 3 from a kinetic expression similar to that given by equation 5–31. At equilibrium, the net–current density is zero, and the forward and back rate terms of the modified Butler–Volmer equation are equal. The equilibrium potential for the zinc reaction $V_0 = (\Phi_m - \Phi_{RC,0})_{equil}$ may be written as

$$V_0 = \frac{RT}{2F}\left[\ln \frac{k_c}{k_a} + \ln c_{Zn^{2+},0}\right] , \qquad (6-1)$$

and is used to obtain the exchange–current density

$$i_0 = 2Fk_a^{a_c/2} k_c^{a_a/2} c_{Zn^{2+},0}^{a_a/2} . \qquad (6-2)$$

A problem may result, however, if the experimental kinetic data are reported

in terms of the exchange–current density. A different expression for the exchange–current density is obtained provided a different mechanism is assumed. A given expression for i_0 does not necessarily have a unique mechanism attributed to it.

For example, let us assume that a two step zinc reaction mechanism occurs as follows:

$$(1) \quad Zn = Zn^{+} + e^{-} \quad , \tag{6–3}$$

$$(2) \quad Zn^{+} = Zn^{2+} + e^{-} \quad . \tag{6–4}$$

Modified Butler–Volmer equations are used to describe each reaction and are given as

$$i_1 = Fk_{a1} \exp\left[\frac{(1-\beta_1)F}{RT} V\right] - Fk_{c1} c_{Zn^{+},0} \exp\left[-\frac{\beta_1 F}{RT} V\right], \tag{6–5}$$

and

$$i_2 = Fk_{a2} c_{Zn^{+},0} \exp\left[\frac{(1-\beta_2)F}{RT} V\right] - Fk_{c2} c_{Zn^{2+},0} \exp\left[-\frac{\beta_2 F}{RT} V\right]. \tag{6–6}$$

The net current density for the zinc reaction is the sum of the two equations

$$i_{Zn} = i_1 + i_2 \quad . \tag{6–7}$$

At equilibrium $i_{Zn} = 0$, and the exchange–current density is given by

$$i_0 = i_1 = -i_2 \quad . \tag{6–8}$$

A formality problem results here, because the exchange–current density cannot be solved analytically in terms of the kinetic parameters and surface concentrations. Various approximations may be used to obtain the exchange–current density. Often an exchange–current density similar to equation 5–52 is given for each reaction step in the mechanism. This has the problem of not being able to measure each separately. What is measured is an overall exchange–current density for the combined individual reactions.

If one step is relatively fast compared to the other, then making the quasi-equilibrium assumption is possible for the fast reaction. Newman[1]

gives the results of this procedure for a copper reaction assuming that the first step of a two–step mechanism is in equilibrium. In terms of the notation used here for the zinc reaction, the overall kinetic expression obtained by combining equations 6–5 and 6–6 is of the same form as the Butler–Volmer equation 3–73 with $\alpha_a = 2 - \beta_2$ and $\alpha_c = \beta_2$. The surface overpotential for the overall two–step reaction is given by $\eta_s = V - V_0$, where the equilibrium potential is

$$V_0 = \frac{RT}{2F} \ln \left[\frac{k_{c2} k_{c1}}{k_{a2} k_{a1}} c_{Zn^{2+},0} \right] \quad . \tag{6–9}$$

The exchange–current density is

$$i_0 = 2F k_{c2} \left[\frac{k_{a2} k_{a1}}{k_{c2} k_{c1}} \right]^{\beta_2/2} c_{Zn^{2+},0}^{(2-\beta_2)/2} \quad . \tag{6–10}$$

In most cases where multiple step mechanisms are required, a rigorously correct form of the exchange–current density is not used. When the equilibrium assumption is not made for the two–step mechanism given above, the following equation for the current density of the overall zinc reaction is obtained

$$i = \frac{i_0 \left\{ \exp\left[\frac{(2-\beta_2)F}{RT} \eta_s \right] - \exp\left[-\frac{\beta_2 F}{RT} \eta_s \right] \right\}}{1 + \frac{k_{a2}}{k_{c1}} \left[\frac{k_{c2} k_{c1}}{k_{a2} k_{a1}} c_{Zn^{2+},0} \exp\left(\frac{2F}{RT} \eta_s \right) \right]^{(1+\beta_1-\beta_2)/2}} \quad . \tag{6–11}$$

The surface overpotential η_s for the zinc reaction is given by

$$\eta_s = V - V_0 \quad , \tag{6–12}$$

and i_0 is defined in equation 6–10, but no physical significance should be placed on this set of parameters. Ratios of the anodic and cathodic rate constants for each reaction may be determined from thermodynamics as was done in chapter 4. Hence, it is necessary to measure the slopes and intercepts of the two Tafel regions of a potentiodynamic anodic polarization

sweep, so that all of the kinetic parameters may be determined. This approach is a fruitful alternative to using exchange–current densities. The kinetics of the overall reaction are best characterized in terms of the rate constants and transfer coefficients without the confusing introduction of a not–so–well–defined i_0.

Nevertheless, a kinetic equation used often in the literature to characterize the corrosion behavior of the disk is a Butler-Volmer relationship. The rate equation for the zinc reaction is

$$i = i_0 \exp\left[\frac{\alpha_a F}{RT} (\Phi_m - \Phi_{RC,0} - U^{'}_{j/RC,0}) \right] - i_0 \exp\left[- \frac{\alpha_c F}{RT} (\Phi_m - \Phi_{RC,0} - U^{'}_{j/RC,0}) \right] , \quad (6-13)$$

where i_0 is the exchange–current density evaluated at the zinc species surface concentration, and α_a and α_c are overall anodic and cathodic transfer coefficients, respectively. The electric driving force in equation 6–13 is the local surface overpotential which is given for reaction j by the general expression

$$\eta_{sj} = V - U^{'}_{j/RC,0} = \Phi_m - \Phi_{RC,0} - U^{'}_{j/RC,0} , \quad (6-14)$$

where Φ_m is the potential of the zinc rotating disk, and $\Phi_{RC,0}$ is an ideal reference electrode of a given kind placed just outside the diffuse–double layer. For this work, a saturated calomel electrode is used. $U^{'}_{j/RC,0}$ is the theoretical thermodynamic potential given by equation B–11 between reaction j and the mercury–mercurous chloride reaction. It is assumed that no liquid junction exists in this highly idealized cell. The kinetics of the molecular hydrogen reaction also are presumed to follow that of equation 6–13, where the hydrogen exchange–current density is evaluated at the surface concentrations of hydrogen and hydrogen ions.

3. Mathematical Description of the Corrosion Process

The Butler–Volmer equation written for the zinc and hydrogen current densities may be substituted into equation 5–6 to give an expression for the local current density on the disk. At open circuit or zero net current, equation 5–7 for the corrosion current may be rewritten using equation 6–13 yielding

$$\begin{aligned} i_{corr} &= i_{0Zn,corr} \exp\left[\frac{\alpha_{aZn} F}{RT} \left(U'_{corr} - U'_{Zn/RG,corr} \right) \right] \\ &\quad - i_{0Zn,corr} \exp\left[- \frac{\alpha_{cZn} F}{RT} \left(U'_{corr} - U'_{Zn/RG,corr} \right) \right] \\ i_{corr} &= - i_{0H_2,corr} \exp\left[\frac{\alpha_{aH_2} F}{RT} \left(U'_{corr} - U'_{H_2/RG,corr} \right) \right] \\ &\quad + i_{0H_2,corr} \exp\left[- \frac{\alpha_{cH_2} F}{RT} \left(U'_{corr} - U'_{H_2/RG,corr} \right) \right] \end{aligned} \qquad (6\text{–}15)$$

This set of equations cannot be solved analytically for the theoretical corrosion potential, $U'_{corr} = (\Phi_m - \Phi_{RG})_{corr}$. Instead, a numerical procedure must be used to obtain the corrosion potential and current density.

3.1. Tafel Approximation

Many times one makes the Stern–Geary approximation that the zinc and hydrogen reactions are governed by Tafel kinetic equations. Assume that the zinc current density may be expressed by the Tafel kinetic equation given by the first term on the right of equation 6–13. The Tafel equation for the hydrogen current density is given by the second term on the right of the same equation. The net current density is then given by

$$i_{net} = i_{0Zn} \exp\left[\frac{\alpha_{aZn} F}{RT} \eta_{sZn} \right] - i_{0H_2} \exp\left[- \frac{\alpha_{cH_2} F}{RT} \eta_{sH_2} \right] . \qquad (6\text{–}16)$$

At zero current, an analytic expression for the corrosion potential may be obtained from

$$i_{corr} = i_{0Zn,corr} \exp\left[\frac{\alpha_{aZn}F}{RT}(U'_{corr} - U'_{Zn/RG,corr})\right] = i_{0H_2,corr} \exp\left[-\frac{\alpha_{cH_2}F}{RT}(U'_{corr} - U'_{H_2/RG,corr})\right] \quad (6-17)$$

The corrosion potential is identified as

$$U'_{corr} = \frac{\alpha_{aZn}U'_{Zn/RG,corr} + \alpha_{cH_2}U'_{H_2/RG,corr} + \frac{RT}{F}\ln\frac{i_{0H_2,corr}}{i_{0Zn,corr}}}{(\alpha_{aZn} + \alpha_{cH_2})} \quad (6-18)$$

which corrects the sign of the first term on the right side of the equation that Smyrl *et al.* [87] report. The corrosion potential may be eliminated from equation 6–17 by substituting equation 6–18 into it. The following expression for the corrosion–current density results

$$i_{corr} = i_{0Zn,corr}^{\frac{\alpha_{cH_2}}{\alpha_{aZn}+\alpha_{cH_2}}} i_{0H_2,corr}^{\frac{\alpha_{aZn}}{\alpha_{aZn}+\alpha_{cH_2}}} \times \exp\left[\frac{\alpha_{aZn}\alpha_{cH_2}}{(\alpha_{aZn} + \alpha_{cH_2})}\frac{F}{RT}(U'_{H_2/RG,corr} - U'_{Zn/RG,corr})\right] \quad (6-19)$$

It is in terms of kinetic parameters which are functions of the species concentrations at the corrosion conditions. The equation for the net current density in terms of the corrosion–current density and corrosion potential may now be written

$$i_{net} = i_{corr} \exp\left[\frac{\alpha_{aZn}F}{RT}(\Phi_m - \Phi_{RG,0} - U'_{corr})\right] - i_{corr} \exp\left[-\frac{\alpha_{cH_2}F}{RT}(\Phi_m - \Phi_{RG,0} - U'_{corr})\right] \quad (6-20)$$

3.2. Linear Polarization Method

The expansion of equation 6–20 into a series which is then truncated after the linear term has been used previously in the literature even though there is no theoretical reason for polarization curves to be linear over the range of potentials. Equation 6–17 which is valid at the corrosion potential then is rewritten as

$$i_{corr} = \alpha_{a\,Zn} i_{0Zn,corr} \frac{F}{RT}\left[U'_{corr} - U'_{Zn/\,RG,corr}\right] = \alpha_{c\,H_2}\, i_{0H_2,corr} \frac{F}{RT}\left[U'_{corr} - U'_{H_2/\,RG,corr}\right] \quad , \tag{6-21}$$

for the linear assumption. The corrosion potential is given as

$$U'_{corr} = \frac{\alpha_{a\,Zn} i_{0Zn,corr} U'_{Zn/\,RG,corr} - \alpha_{c\,H_2,corr} i_{0H_2,corr}\, U'_{H_2/\,RG,corr}}{\alpha_{a\,Zn} i_{0Zn,corr} - \alpha_{c\,H_2} i_{0H_2,corr}} \quad , \tag{6-22}$$

and is used to determine the corrosion–current density yielding

$$i_{corr} = \frac{\alpha_{a\,Zn} i_{0Zn,corr} \alpha_{c\,H_2} i_{0H_2,corr}}{\alpha_{0Zn} i_{0Zn,corr} - \alpha_{c\,H_2} i_{0H_2,corr}} \frac{F}{RT}\left[U'_{Zn/\,RG,corr} - U'_{H_2/\,RG,corr}\right] \tag{6-23}$$

Oldham and Mansfeld[15] show that the polarization curve is not linear and must display curvature in the vicinity of the corrosion potential. They point out that the misconception of the inappropriately named Stern–Geary linear polarization method probably arose as a result of the linearization approximation similar to equation 6–23 which is customarily used.

3.3. Stern–Geary Polarization Resistance Method

The form of the equation for the corrosion–current density given by equation 6–19 is somewhat different from that of the Stern–Geary equation. Differentiation of equation 6–20 with respect to the electrode potential V relative to an ideal saturated reference electrode placed just outside the double layer yields

$$\left[\frac{\partial i}{\partial V}\right]_{U'_{corr}} = \left[\frac{\alpha_{a\,Zn} F}{RT} + \frac{\alpha_{c\,H_2} F}{RT}\right] i_{corr} \quad , \tag{6-24}$$

when evaluated at the corrosion potential U'_{corr}. The slope of the theoretical polarization curve at zero current given by equation 6–24 is equal to $1/\pi r_0^2 R_{ct}$, where R_{ct} is the theoretical charge–transfer resistance. The usual, but seldom valid, assumption for the Stern–Geary analysis is that the ohmic drop and concentration variations are neglected. This implies that the slope $1/R_p = (\partial i/\partial V)_{V_{corr}}$ of the experimental current–potential polarization curve at the corrosion potential must equal $1/R_{ct}$. Hence,

equation 6–24 is commonly rewritten for the corrosion–current density as

$$i_{corr} = \frac{K}{\pi r_0^2 R_p} \quad . \tag{6–25}$$

where K is given by

$$K = \frac{b_{a\,Zn} b_{c\,H_2}}{2.303\left(b_{a\,Zn} + b_{c\,H_2} \right)} \quad . \tag{6–26}$$

The Tafel slopes $b_{a\,Zn}$ and $b_{c\,H_2}$ are defined by equations 4–18 and 4–20. This equation is valid only when the corrosion potential is remote from the reversible potentials $U'_{Zn/\,RC,corr}$ and $U'_{H_2/\,RC,corr}$ of the two oxidation–reduction processes which are responsible for the corrosion. The number of assumptions that are required for the Stern–Geary treatment should make its use quite limited, even though that is not the case.

3.4. Modification of the Stern–Geary Polarization Resistance Method

Mansfeld and Oldham[8] show how the Stern–Geary equation has to be modified for cases where the corrosion potential lies close to either of the reversible potentials $U'_{Zn/\,RC}$ or $U'_{H_2/\,RC}$. They begin their analysis with the more general equation for the net current density obtained by summing equation 6–13 for the zinc and hydrogen reaction instead of using equation 6–16. Their result for the corrosion–current density in terms of the measured slope of the experimental polarization curve $1/R_p$, consists of a more generalized form of equation 6–26 which is a function of the difference between the corrosion potential and the reversible potentials $\Delta U'_j$. Mansfeld's equation 18 for the corrosion–current density rewritten in the notation of this text is given by

$$i_{corr} = (\pi r_0^2 R_p)^{-1} \times$$
$$\left\{ \frac{2.303}{b_{a\,Zn}} + \frac{2.303}{b_{c\,H_2}} + \frac{2F}{RT}\left[\exp\left(\frac{2F\Delta U'_{Zn}}{RT} \right) - 1 \right]^{-1} + \frac{F}{RT}\left[\exp\left(-\frac{F\Delta U'_{H_2}}{RT} \right) - 1 \right]^{-1} \right\}^{-1} \tag{6–27}$$

where

$$\Delta U'_{Zn} = U'_{corr} - U'_{Zn/RG,corr} \qquad (6\text{–}28)$$

and

$$\Delta U'_{H_2} = U'_{corr} - U'_{H_2/RG,corr} \qquad (6\text{–}29)$$

Finally, Mansfeld[16] proposes a method of determining the polarization resistance R_p, the Tafel slopes ($b_{a\,Zn}$ and $b_{c\,H_2}$), and the corrosion–current density from polarization curves in the non–Tafel region in the vicinity of the corrosion potential. The starting point for this analysis is the Stern–Geary equation 6–25 and 6–20. Sophisticated computer programs, CORFIT[17] and POLCURR,[18] developed for the analysis of polarization data are introduced.

4. Results and Discussion

The corrosion–current density may be estimated many different ways as was pointed out in the previous section. Results of each of the different methods will be compared to the corrosion–current density, 3.80×10^{-2} A/ cm^2, obtained by the kinetic–diffusion model using the kinetic parameters that best match the overall experimental curves. The FIT parameters are given in tables 4–2 and 4–3 which are based on an anodic transfer coefficient of 0.05. Equation 6–19, which uses the Tafel approximation, gives 3.93×10^{-2} A/ cm^2 for i_{corr} which is 3.32 % higher than the i_{corr} as determined by the kinetic–diffusion model. The Tafel graphical method was discussed in chapter 5. Equation 6–23 uses the linear approximation, and i_{corr} is given as 1.937×10^{-2} A/ cm^2, which is 151 % lower than the actual i_{corr}. These results are summarized in table 6–1.

Polarization resistance measurements probably are the most widely used electrochemical method for determining the corrosion–current density. The corrosion–current density may be determined using the slopes of the current–potential curve at the corrosion potential as given by the

Table 6–1. Estimation and comparison of the various methods for the determination of the corrosion–current density using the experimentally determined kinetic data.

Method	i_{corr} A/cm^2	$\Delta\% \left[\frac{i_{corr} - (i_{corr})_{K-D}}{(i_{corr})_{K-D}} \right]$
Kinetic–Diffusion Model	3.80×10^{-2}	0.0
Tafel Approximation equation 6–19	3.93×10^{-2}	3.32
Linear Approximation equation 6–23	1.94×10^{-2}	-150.9

Stern–Geary polarization resistance equation 6–25. The experimental data for the zinc and hydrogen curves given in figure 4–6 indicate an average slope of 47.5 Ω at the corrosion potential. This value for the polarization resistance yields a value of 3.35×10^{-2} A/cm^2, which is 11.9 % lower than the actual corrosion–current density. The corrosion–current density as calculated by Mansfeld's correction to the Stern–Geary equation is 68.0 % less than the Stern–Geary equation when a polarization resistance R_p of 47.5 Ω is used. The results given here based on the polarization resistance R_p are not very good estimations for the corrosion–current density. For this case, Mansfeld's modification is unexpectantly worse than the Stern–Geary equation.

The experimental dc work was confirmed by independent ac–impedance measurements. The impedance data[19] for the corrosion of zinc in 1 M hydrochloric acid gave 18 Ω for the polarization resistance. This value used in equations 6–25 and 6–27 gives 132 and -15 % error for the Stern–Geary method and Mansfeld's modification, respectively. Again, the polarization resistance does not lend itself to useful results. It should be pointed out

however, that for the set of ac data, the modified Stern–Geary equation yields a better estimation for the corrosion–current density than the Stern–Geary equation. This is expected because the Stern–Geary equation was shown by Mansfeld to give up to 30 % error for other corrosion systems at such conditions. This is due to the thermodynamic potential of the zinc reaction lying so close to the corrosion potential for which conditions the Stern–Geary equation is not valid. Because the modified equation is of a more general nature, confidence should be placed in the ac data more so than using the slope of the polarization curve. The estimations for the corrosion–current density based on R_p are summarized in table 6–2.

From the same impedance data, a charge–transfer resistance of 16 Ω is obtained using a simple Randles[20] circuit.† If this value for R_{ct} is used in equations 6–25 and 6–27 in the place of R_p, the corrosion–current density is determined to be 9.95×10^{-2} and 3.62×10^{-2} A/ cm^2 with an error of 161 and -5 %, respectively. Again, the modified equation is better. The

Table 6–2. Estimation of the corrosion–current density and comparison with the actual $i_{corr} = 3.80 \times 10^{-2}$ A/cm^2 based on the experimental data using the Stern–Geary equation 6–25 and its modification given by equation 6–27. The polarization resistance R_p is used.

	Stern–Geary		Modification	
Determination of R_p	i_{corr} A/cm^2	% Difference	i_{corr} A/cm^2	% Difference
Slope of figure 4–4 at V_{corr}, R_p = 47.5 Ω	3.35×10^{-2}	−11.9%	1.38×10^{-2}	−58.3%
AC Impedance, R_p = 18 Ω	8.85×10^{-2}	132%	3.22×10^{-2}	−15%

†This equivalent circuit is composed of the charge–transfer resistance R_{ct} and capacitance C connected in parallel, with the ohmic resistance R_Ω attached to this in series. On a complex plane plot of the imaginary and real components of the electrochemical impedance, the intercept of the semicircle with the abscissa at the high–frequency end defines R_Ω while that of the low–frequency end is determined by the sum of R_Ω and R_{ct}.

charge–transfer resistance also gives better results than R_p.

Next, $\pi r_0 R_{ct}$ may be approximated graphically from dc data by taking the slope of the $i-V$ polarization curve at the corrosion potential. The potential V is the measured potential corrected for the ohmic drop assuming the diffusion potential and liquid–junction potential are negligible. The $I, V_{meas} - IR_\Omega$ curve in figure 4–6 is used to obtain a R_{ct} of 45.15 Ω. The results of using this R_{ct} in equations 6–25 and 6–27 give an i_{corr} of 3.53×10^{-2} and $1.28 \times {}^{-2}$ A/cm^2 and a corresponding -7 and -66 % difference from the actual i_{corr}. These results are not as good as when R_{ct} from the ac data is used, but both are better than using the polarization resistance.

Finally, the charge–transfer resistance is given by[21]

$$R_{ct} = \frac{RT}{nFi_0\pi r_0^2} \quad . \tag{6–30}$$

R_{ct} is 1.72 Ω using the exchange–current given by equation 5–56 and the

Table 6–3. Estimation of the corrosion–current density and comparison with the actual $i_{corr} = 3.80 \times 10^{-2}$ A/cm^2 using the Stern–Geary equation 6–25 and its modification given by equation 6–27. The charge transfer resistance R_{ct} is used instead of the polarization resistance R_p.

	Stern–Geary		Modification	
Determination of R_{ct}	i_{corr} A/cm^2	% Difference	i_{corr} A/cm^2	% Difference
Slope of figure 4–4 at V_{corr}, R_{ct} = 45.15 Ω	3.53×10^{-2}	-7 %	1.28×10^{-2}	-66 %
AC Impedance, R_{ct} = 16Ω	9.95×10^{-2}	161 %	3.62×10^{-2}	-5 %
R_{ct} (i_{0Zn}) = 1.72 Ω	9.28×10^{-1}	2338 %	3.37×10^{-1}	786 %
R_{ct} ($i_{0,Hg}$) = 9.25 Ω	1.72×10^{-1}	352 %	6.26×10^{-1}	64 %

results of the model for the two–electron transfer zinc reaction. This value of R_{ct} gives corrosion–current densities of 9.3×10^{-1} and 3.4×10^{-1} A/cm^2 using equations 6–25 and 6–27, respectively. The difference between these i_{corr} and the actual are 2338 and 786 %, respectively. The results of using the charge–transfer resistance are summarized in table 6–3.

5. Conclusions

It is difficult to draw conclusions concerning the validity of the numerous methods for determining the corrosion–current density when the experimental data are questionable. However, it is possible to discuss qualitatively advantages and disadvantages of the various methods based on the present work. First, the resistance polarization method should be used on a very limited basis. A number of restrictions must be applied in order for the method to be valid. Neglect of solution ohmic drop, neglect of concentration variations, and the use of Tafel kinetics in the place of a Butler–Volmer expression are necessary assumptions. Such restrictions are unrealistic. For example, it is true that in the vicinity near U'_{corr} in a well supported electrolyte, the ohmic potential drop is small; however, as a result of the diffusion potential's finite value at zero net current, the diffusion potential becomes more significant and should not be neglected. Even if these small corrections are not made, the major difficulty with the Stern–Geary equation is that in the vicinity of the corrosion potential the back term or cathodic Tafel expression of the metal dissolution and the anodic Tafel term of the hydrogen evolution reaction are not always negligible. It is quite possible to neglect them at potentials far from the corrosion potential, but the back terms of the zinc and hydrogen reactions must be maintained in the region near U'_{corr} in order to be accurate.

Mansfeld in his earlier paper[8] stated that the Stern–Geary method may lead to erroneous conclusions and proposed a modified equation. The

modification was based on a more general equation for the net current density that has been in the literature for over forty years. The authors suggest the reason that the equation had not been accepted generally is that it is too complex. They then proceed to give simplifications of their modification equation 6–28 in an attempt to maintain simplicity with "sufficient accuracy." The major difficulty with Mansfeld's modification to the Stern–Geary equation is not that it is too complex, but that the sometimes very significant ohmic and concentration variations effects are not considered. As has been seen, these must be taken into account before the corrosion–current density may be determined accurately.

Mansfeld then, failing to use the more general current–density equation, based sophisticated computer programs ironically on the simplified Stern–Geary equation. The FIT routine which has been presented here is similar to these programs since each is based on Tafel equations for the metal dissolution and hydrogen evolution reactions. These routines should be expected to be of limited value since extremely simplified equations are chosen as the starting point. Another generalized curve–fitting program similar to POLCURR should be written based on a Butler–Volmer kinetic equation for each reaction instead of equation 6–16. Such a method should prove to be useful when applied to polarization data utilizing the computer to aid in the analysis of corrosion processes. Until this is done, it is recommended that Tafel slopes and rate constants be obtained from Tafel polarization curves. The kinetic parameters may then be used in the modified Butler–Volmer kinetic–diffusion model to determine the corrosion–current density.

List of Symbols

a	mean diameter of ions, cm
a_i	relative activity of species i, mol/kg
a_i^{ϕ}	property expressing secondary reference state of species i, l/mol
$a_{i,n}^{\phi}$	property expressing secondary reference state relative to species n, l/mol
A	parameter used in the Henderson equation 3–41
A	variable used in the kinetic–diffusion equation 5–47 for the hydrogen reaction and given by equation 5–48
b_a, b_c	anodic and cathodic Tafel slopes, V^{-1}
B	parameter used in the Henderson equation 3–41
B	variable used in the kinetic–diffusion equation 5–47 for the hydrogen reaction and given by equation 5–49
B'	Debye–Hückel parameter, $(l/mol)^{1/2}/A$
c_i	concentration of species i, mol/cm^3
c'_i	concentration of species i, mol/l
C	variable given by equation 5–50 used in the kinetic–diffusion equation 5–47 for the hydrogen reaction
D_p	diffusion coefficient of species p, cm^2/s
e^-	symbol for the electron
f_i	molar activity coefficient of species i
$f_{i,n}$	molar activity coefficient relative to species n
f_{max}	maximum frequency characteristic of scan rate, Hz
F	Faraday's constant, 96,487 C/equiv
G_i^f	Gibbs energy of formation for species i, J/mol
ΔG_m	Gibbs energy for reaction m, J/mol

ΔG_m°	standard Gibbs energy for reaction m, J/mol
$\mathbf{i}$	current density, A/ cm^2
$i_{f,l}$	Faradaic current density of reaction l, A/ cm^2
i_n	normal current density at electrode surface used in equation 3–48, A/ cm^2
i_y	current density in the y direction, A/ cm^2
i_0	exchange current density, A/ cm^2
i_{corr}	corrosion current density, A/ cm^2
i_{avg}	average current density, A/ cm^2
I	net current, A
I	molar ionic strength, mol/l
J	dimensionless linear polarization parameter
k_a, k_c	anodic and cathodic rate constant for charge transfer reaction,
k_j, k_{-j}	forward and back kinetic rate constant for zinc complexing chemical reaction, cm^3/mol–s, s^{-1}
k'_j, k'_{-j}	forward and back kinetic rate constant for zinc complexing chemical reaction, l/mol–s, s^{-1}
$\frac{k'_c}{k'_a}$	thermodynamic equilibrium constant for an electrochemical reaction
K	thermodynamic equilibrium constant for zinc complexing chemical reaction, cm^3/mol
K	thermodynamic equilibrium constant for zinc complexing chemical reaction, kg/mol
m_i	molality of species i, mol/kg
M_i	symbol for the chemical formula of species i
n_j	number of electrons involved in electrode reaction j
n_i	number of moles of species i, mol
n_0	number of moles of the solvent, mol

$\mathbf{N}_i$	flux of species i, mol/ cm^2–s
N	dimensionless rotation speed
p_l	partial pressure of species l, atm
p	pressure, atm
Pe	Péclet number, $Pe = \upsilon r / D_i$
q	charge at electrode, C
Q	zinc complexing parameter given by equation 5–39
r	rate of an electrochemical reaction, mol/cm^2–s
r	radial direction of disk
r_0	radius of disk, cm
R	universal gas constant, 8.3143 J/mol-K
R_i	homogeneous chemical reaction production term, mol/cm^3–s
R_Ω	primary solution resistance, ohm
R'_Ω	uniform solution resistance, ohm
R_p	polarization resistance, ohm
R_{ct}	charge–transfer resistance, ohm
Re	Reynolds number, $r_0^2 \Omega / \nu$
s_{ij}	stoichiometric coefficient of species i in electrode reaction j
s_{iRG}	stoichiometric coefficient of species i in reference electrode reaction RG
s	solubility of a gas in a liquid, $\frac{\text{mol/ cm}^3}{\text{atm}}$
S	polarization scan rate, mV/s
S	surface site for adsorption
Sc	Schmidt number, $Sc = \nu / D_i$
t	time, s

t_p^0	transference number of species p with respect to the velocity of species 0
T	absolute temperature, K
u_i	mobility of species i, cm^2–mol/J–s
$U_{j/RG}$	theoretical thermodynamic potential difference between reaction j and the reference electrode reaction RG, V
$U'_{j/RG}$	thermodynamic potential difference between reaction j and the reference electrode reaction RG corrected for any liquid junctions, V
$U''_{RG/RR.-}$	potential difference across a junction region, V
$U^{\circ}_{j/RG}$	standard thermodynamic potential difference between reaction j and the reference electrode reaction RG, V
U°_j	standard thermodynamic electrode potential of reaction j in water relative to the hydrogen electrode, V
U'_{corr}	theoretical corrosion potential relative to a given reference electrode, V
$\mathbf{v}$	fluid velocity, cm/s
V	theoretical electrode potential relative to given reference electrode placed just outside the diffuse double layer, V
V^0	theoretical equilibrium potential relative to given reference electrode placed just outside the diffuse double layer, V
V_r	potential of a moveable reference electrode relative to a fixed reference electrode, V
V^+	a not so well–defined potential driving force
V^*	simulated experimental electrode potential relative to given reference electrode placed in the bulk solution, V
V^*_{oc}	simulated experimental open-circuit cell potential relative to given reference electrode placed in the bulk solution, V
V_{meas}	actual experimentally measured cell potential, V
V_{PP}	peak–to–peak amplitude of voltage perturbation, V

y	normal direction from electrode, cm
z_i	charge number of species i

Greek symbols:

α_a, α_c	transfer coefficients
α'	Debye-Hückel constant, $(l/mol)^{\frac{1}{2}}$
β	symmetry factor
β'_{ij}	coefficient for ion-ion specific interactions, l/mol
γ_i	molal activity coefficient of species i
$\gamma_{i,n}$	molal activity coefficient of species i relative to species n
Γ_i	molal activity coefficient of species i which is independent of the electrical state of the phase
δ_i	thickness of stagnant diffusion layer for species i, cm
δ_{rxn}	homogeneous reaction penetration depth, cm
δ	dimensionless averaged current
ε	current distribution parameter, equation 4–5
η_{sj}	surface overpotential for reaction j, V
η_{cj}	concentration overpotential, V
Θ_H	surface coverage of adsorbed hydrogen atoms
κ	conductivity, mho/cm
κ_∞	bulk solution conductivity, mho/cm
λ_i	absolute activity of species i
λ_i^ϕ	property expressing secondary reference state, kg/mol
$\lambda_{i,n}^\phi$	property expressing secondary reference state relative to species n, kg/mol
λ_+, λ_-	ionic equivalent conductances, mho–cm^2/ equiv
Λ	equivalent conductance of a single salt, mho–cm^2/ equiv

Λ_p	see equation B–11
μ_i	chemical or electrochemical potential of species i, J/mol
ν	number of ions into which a molecule of electrolyte dissociates
ν_i	number of cations or anions into which a molecule of electrolyte dissociates
ν_{im}	stoichiometric coefficient of species i in chemical reaction m
ν	kinematic viscosity, cm^2/s
ρ_0	density of pure solvent, g/cm^3
ρ_0'	density of pure solvent, kg/cm^3
$\Upsilon_{i,n}$	see equation D–30
φ_l	fugacity coefficient of gaseous species l
Φ	potential, V
Φ_m	potential of metal disk electrode, V
Φ_{RS}	potential of an imaginary reference electrode of the same type as the reaction of interest
Φ_{RC}	potential of an imaginary reference electrode of a given kind
Φ_{RR}	potential of an actual reference electrode of a real kind placed in the bulk solution
Φ_{soln}	a not so well–defined potential of the solution just outside the diffuse double layer, V
$\Delta\Phi_{RS}$	potential difference across the diffusion layer and bulk solution as measured by reference electrodes of the same type as the reaction of interest occurring at the electrode, V
$\Delta\Phi_{RC}$	potential difference across the diffusion layer and bulk solution as measured by reference electrodes of a given kind, V
$\Delta\Phi_{ohm}$	ohmic potential drop across the diffusion layer and bulk solution, V

$\Delta\tilde{\Phi}_{ohm}$	ohmic potential drop across the diffusion layer and bulk solution as if there are no concentration gradients, V
ξ	perturbation parameter
Ω	rotation speed of disk electrode, rad/s

subscripts:

m	at the metal electrode surface
0	solvent
RG	reference electrode of a given kind
RS	reference electrode of the same tpye as the reaction of interest occurring at the electrode
,0	at the electrode surface just outside of the double layer
,∞	in the bulk solution
,sat	saturated conditions
,*	equilibrium conditions

superscripts:

0	pure state
ϑ	secondary reference state at infinite dilution
*	ideal-gas secondary reference state

References

[1]. John Newman, *Electrochemical Systems*, Englewood Cliffs, N. J.: Prentice–Hall, Inc., 1974.

[2]. E. C. Potter, "Corrosion–The Past," *Electrochemistry, The Past Thirty and the Next Thirty Years*, Chapter 13, Harry Bloom and Felix Gutman, eds., New York: New York, 1975, pp. 229–237.

[3]. U. R. Evans and T. P. Hoar, *Proc. R. Soc. 137*, 343– (1932).

[4]. J. N. Agar; see U. R. Evans, *J. Iron Steel Inst. 141*, 221p (1940).

[5]. Carl Wagner and Wilhelm Traud, "Über die Deutung von Korrosionsvorgängen durch Über lagerung von elektrochemischen Teilvorgängen und über die Potentialbildung an Mischelektroden," *Z. Elektrochem.*, *44*, 391–402 (1938).

[6]. M. Stern and A. L. Geary, "Analysis of the Shape of Polarization Curves," *J. Electrochem. Soc.*, *104*, 56–60 (1957).

[7]. J. O'M. Bockris, "Electrode Kinetics," *Modern Aspects of Electrochemistry*, *1*, Chapter 4, J. O'M. Bockris and B. E. Conway, eds. London: Butterworth, 1954, pp. 180–276.

[8]. Florian Mansfeld and Keith B. Oldham, "A Modification of the Stern–Geary Linear Polarization Equation," *Corrosion Science*, *11*, 787–796 (1973).

[9]. L. L. Shreir, *Corrosion, Volume 1, Metal/Environment Reactions*, Boston: Newnes–Butterworth Inc., 1976.

[10]. R. J. Brodd and V. E. Leger, "Zinc," *Encyclopedia of the Elements*, Chapter V-I, Allen J. Bard, ed., 1981, pp. 1–67.

[11]. L. L. Shreir, *Corrosion, Volume 2, Corrosion Control*, Boston: Newnes–Butterworth Inc., 1976.

[12]. Einar Mattsson, *Electrochemistry, The Past Thirty and the Next Thirty Years*, Chapter 14, Harry Bloom and Felix Gutman, eds., New York: Plenum Press, 1975, pp. 239–256.

[13]. Henry S. Rawdon, *Protective Metallic Coatings*, New York: The Chemical Catalog Company, Inc., 1928.

[14]. J. O'M. Bockris and D. M. Drazić, "The Stability of Metals," *Electro–chemical Science*, Chapter 9, London: Taylor & Francis LTD, 1972.

[15]. William H. Smyrl and John Newman, "Potentials of Cells with Liquid Junctions," *Journal of Physical Chemistry*, *72*, 4660–4671 (1968).

[16]. P. Henderson, "Zur Thermodynamik der Flüssigkeitsketten," *Zeitschrift für physikalische Chemie*, *59*, 118–127 (1907).

[17]. J. A. Trainham and J. Newman, "A thermodynamic estimation of the minimum concentration attainable in a flow–through porous electrode reactor," *Journal of Applied Electrochemistry*, *7*, 287–297 (1977).

[18]. D. D. Wagman, W. H. Evans, V. B. Parker, I. Halow, S. M. Bailey, and R. H. Schumm, *Selected Values of Chemical Thermodynamic Properties, Tables for the First Thirty–Four Elements in the Standard Order of Arrangement*, NBS Technical Note 270–3, Washington, D.C.: National Bureau of Standards, 1968.

[19]. H. Eyring, S. Glasstone, and K. J. Laidler, "Application of the Theory of Absolute Reaction Rates to Overvoltage," *J. Chem. Phys.*, *7*, 1053

(1939).

[20]. Th. V. Karman, *Z. angew. Math. Mechanik*, *1*, 233 (1921).

[21]. W. G. Cochran, "The flow due to a rotating disc," *Proc. Cambridge Phil. Soc.*, *30*, 365 (1934).

[22]. Ralph White, Charles M. Mohr, Jr., and John Newman, "The Fluid Motion to a Rotating Disk," *J. Electrochem. Soc.*, *123*, 383–385 (1976).

[23]. L. Hseuh and John Newman, "Mass Transfer and Polarization at a Rotating Disk Electrode," *Electrochimica Acta*, *12*, 429–438 (1967).

[24]. John Newman, "Current Distribution below the Limiting Current," *J. Electrochem. Soc.*, *13*, 501–510 (1966).

[25]. A. C. Riddiford, "The Rotating Disk System," *Advances in Electrochemistry and Electrochemical Engineering*, *4*, P. Delahay and C. W. Tobias, eds., New York: Interscience, 1966, pp. 47–116.

[26]. John Newman, "Resistance for Flow of Current to a Disk," *J. Electrochem. Soc.*, *113*, 501–502 (1966).

[27]. Florian Mansfeld and Martin Kendig, "Concerning the Choice of Scan Rate in Polarization Measurements," *Corrosion*, *37*, 545–546 (1981).

[28]. Florian Mansfeld, "The Effect of Uncompensated IR–Drop on Polarization Resistance Measurements," *Corrosion*, *32*, 143–146 (1976).

[29]. John Newman, "Ohmic Potential Measured by Interrupter Techniques," *J. Electrochem. Soc.*, *117*, 507–508 (1970).

[30]. G. W. Walter, "The Effect of IR–Drop on Corrosion Rates Calculated from Low Polarization Data," *Corrosion Science*, *18*, 927–945 (1978).

[31]. Florian Mansfeld, "The Effect of Uncompensated Resistance on the True Scan Rate in Potentiodynamic Experiments," *Corrosion*, *38*, 556–559 (1982).

[32]. John Newman, "The Fundamental Principles of Current Distribution and Mass Transport in Electrochemical Cells," *Electroanalytical Chemistry*, *6*, Allen J. Bard, ed., New York: Marcel Dekker, Inc., 1973, pp. 187–352.

[33]. Leonard Nanis and Wallace Kesselman, "Engineering Applications of Current and Potential Distributions in Disk Electrode Systems," *J. Electrochem. Soc.*, *118*, 454–461 (1971).

[34]. Peter Pierini and John Newman, "Potential Distribution for Disk Electrodes in Axisymmetric Cylindrical Cells," *J. Electrochem. Soc.*, *126*, 1348–1352 (1979).

[35]. Clarence G. Law, Jr., and John Newman, "A Model for the Anodic Dissolution of Iron in Sulfuric Acid," *J. Electrochem. Soc.*, *126*, 2150–2155 (1979).

[36]. Philip P. Russell and John Newman, "Experimental Determination of the Passive–Active Transition for Iron in 1 M Sulfuric Acid," *J. Electrochem. Soc.*, *130*, 547–553 (1983).

[37]. Jung Taek Kim and Jacob Jorné, "The Kinetics and Mass Transfer of Zinc Electrode in Acidic Zinc–Chloride Solution," *J. Electrochem. Soc.*, *127*, 8–15 (1980).

[38]. D–T. Chin and S. Venkatesh, "A–C Modulation of a Rotating Zinc Electrode in an Acid Zinc–Chloride Solution," *J. Electrochem. Soc.*, *128*, 1439–1442 (1981).

[39]. U. Landau, *Roughness Evolution and Dendritic Growth in Zinc Electrodeposition from Halide Electrolytes*, EPRI EM–2937, Project 1198–3, Final Report, 1983.

[40]. John M. West, *Basic Corrosion and Oxidation*, Chichester: Ellis Horwood Limited, 1980.

[41]. W. G. Sunu and D. N. Bennion, "Transient and Failure Analysis of the Porous Zinc Electrode, I. Theoretical" *J. Electrochem. Soc.*, *127*, 2007–2016 (1980).

[42]. W. C. Hsie and J. R. Selman, *Zinc Electrodeposition and Dendritic Growth from Zinc Halide Electrolytes*, EPRI EM–2393, Project 1198–3. Final Report, Page 10–3, May 1982.

[43]. J. W. Johnson, Y. C. Sun, and W. J. James, "Anodic Dissolution of Zn in Aqueous Salt Solutions," *Corrosion Science*, *11*, 153–159 (1971).

[44]. V. A. Ettel and B. V. Tilak, "Electrolytic Refining and Winning of Metals," *Comprehensive Treatise of Electrochemistry*, *2*, Chapter 6, J. O'M. Bockris, Brian E. Conway, Ernest Yeager, and Ralph E. White, eds., New York: Plenum Publishing Corporation, 1981, p. 364.

[45]. W. Nernst, *Z. Physikal. Chem.*, *47*, 52 (1904).

[46]. V. G. Levich, *Physicochemical Hydrodynamics*, Englewood Cliffs, New Jersey: Prentice–Hall, 1962.

[47]. Fred Basolo and Ralph G. Pearson, *Mechanisms of Inorganic Reactions, A Study of Metal Complexes in Solution*, New York: John Wiley and Sons, Inc., Second Edition, pp. 154–156, 1967.

[48]. John Newman and Limin Hsueh, "Currents Limited by Gas Solubility," *Industrial and Engineering Chemistry Fundamentals*, *9*, 677–679

(1970).

[49]. William H. Tiedemann, John Newman, and Douglas N. Bennion, "The Error in Measurements of Electrode Kinetics Caused by Nonuniform Ohmic-Potential Drop to a Disk Electrode," *J. Electrochem. Soc.*, *120*, 256–258 (1973).

[50]. Mars G. Fontana and Norbert D. Green, *Corrosion Engineering*, New York: McGraw–Hill Book Company, 1967.

[51]. Klaus J. Vetter, *Electrochemical Kinetics, Theoretical and Experimental Aspects*, New York: Academic Press Inc., 1967.

[52]. Tibor Erdy–Grúz, *Kinetics of Electrode Processes*, New York: Wiley–Interscience Division, John Wiley and Sons, Inc., 1972.

[53]. J. O'M Bockris, *Textbook of Electrochemistry*, New York: Academic Press Inc., 1951.

[54]. J. O'M Bockris, "Parameters of Electrode Kinetics" *Electrochemical Constants*, NBS Circular 524, 1953, p. 243.

[55]. N. Tanaka and R. Tamamushi, "Kinetic Parameters of Electrode Reactions," *Electrochimica Acta*, *9*, 963–989 (1964).

[56]. William H. Smyrl, "Electrochemistry and Corrosion on Homogeneous and Heterogeneous Metal Surfaces," *Comprehensive Treatise of Electrochemistry*, *4*, Chapter 2, J. O'M. Bockris, Brian E. Conway, Ernest Yeager, and Ralph E. White, eds., New York: Plenum Publishing Corporation, 1981, pp. 97–149.

[57]. Kemal Nisancioğlu and John Newman, "Current Distribution on a Rotating Sphere below the Limiting Current," *J. Electrochem. Soc.*, *121*, 241–246 (1974).

[58]. Milton Stern, "The Electrochemical Behavior, Including Hydrogen Overvoltage, of Iron in Acid Environments," *J. Electrochem. Soc.*, *14*, 609–616 (1955).

[59]. Keith B. Oldham and Florian Mansfeld, "On the So–Called Linear Polarization Method for Measurement of Corrosion Rates," *Corrosion*, *27*, 434–435 (1973).

[60]. Florian Mansfeld, "Simultaneous Determination of Instantaneous Corrosion Rates and Tafel Slopes from Polarization Resistance Measurements," *J. Electrochem. Soc.*, *120*, 515–518 (1973).

[61]. Florian Mansfeld, "Tafel Slopes and Corrosion Rates from Polarization Resistance Measurements," *Corrosion*, *29*, 397–402 (1973).

[62]. Sol M. Gerchakov, Lanny R. Udley, and Florian Mansfeld, "An Improved Method for Analysis of Polarization Resistance Data" *Corrosion*, *37*, 696–700 (1981).

[63]. Alan Kent Hauser and John Newman, "Impedance Measurements of the Corrosion of Zinc in Acidic Chloride Solutions," unpublished data, Department of Chemical Engineering, University of California, Berkeley, CA 94720 (1983).

[64]. J. E. B. Randles, "Kinetics of Rapid Electrode Reactions," *Discuss. Faraday Soc.*, *1*, 11–19 (1947).

[65]. Allen J. Bard and Larry R. Faulkner, *Electrochemical Methods*, New York: John Wiley & Sons, Inc., 1980.

[66]. John Newman, *Chemical Engineering Thermodynamics*, Chemical Engineering 141 Course Notes, University of California, Berkeley, 1981.

[67]. Thomas W. Chapman and John Newman, "A Compilation of Selected Thermodynamic and Transport Properties of Binary Electrolytes in Aqueous Solution," UCRL–17767, May, 1968.

[68]. William H. Symrl and John Newman, "Current and Potential Distributions in Plating Corrosion Systems," *J. Electrochem. Soc.*, *123*, 1423–1432 (1976).

[69]. John Newman, "Mass Transport and Potential Distribution in the Geometries of Localized Corrosion" *Localized Corrosion*, *NACE–3*, 45–61 (1974).

[70]. T. Erdey–Grúz and M. Volmer, *Z. physik. Chem.*, *150 A*, 203 (1930).

[71]. J. Tafel, *Z. physik. Chem.*, *50*, 641 (1905).

[72]. I. Langmuir, *J. Am. Chem. Soc.*, *40*, 1361 (1918).

Appendix A. Chemical and Electrochemical Potentials

The absolute activity λ_i of an ionic or neutral species is defined by[1],[86]

$$\mu_i = RT \ln \lambda_i \quad . \tag{A-1}$$

For a solute species in a solution of a given solvent at a given temperature and pressure, the chemical potential is given by

$$\mu_i = \mu_i^\phi + RT \ln m_i \gamma_i \quad . \tag{A-2}$$

The electrochemical potential of an ionic species is given by the same equation. For aqueous solutions, the molality m_i is the number of moles of solute per kilogram of solvent and γ_i is the dimensionless activity coefficient of component i. The principal composition dependence of the chemical potential is given by the molality m_i in equation A-2, and the activity coefficient γ_i is required to describe any departures from this simple composition dependence. The standard state chemical potential is given by $\mu_i^\phi = RT \ln \lambda_i^\phi$, where λ_i^ϕ is a property expressing the secondary reference state given in kg/mol. Each is independent of composition and electrical state, but characteristic of the solute species and the solvent and dependent on temperature and pressure.

The value of the chemical or electrochemical potential μ_i is set by the primary reference state for component i. The tables[18] of the National Bureau of Standards are based on zero values for the elements in their stable forms at 25°C and one atmosphere (or on the ideal gas state if the element is a gas under these conditions). A secondary reference state, also known as a standard state, is defined in terms of an extrapolation of actual data to infinite dilution. Therefore, λ_i^ϕ and μ_i^ϕ are values related to this secondary reference state. For a solute in aqueous solution, the standard state is taken as the hypothetical ideal solution of unit molality.

Many electrochemical engineering applications of thermodynamics use molar concentrations of expressing the composition. The chemical potential of a solute in terms of the molar concentration c_i' is written

$$\mu_i = RT \ln (a_i^{\phi} c_i' f_i) \tag{A-3}$$

where f_i is a dimensionless activity coefficient and a_i^{ϕ} characterizes the secondary reference state expressed in l/mol, again taken to be infinite dilution. Equating the two expressions for the chemical potential yields

$$\lambda_i^{\phi} m_i \gamma_i = a_i^{\phi} c_i' f_i \tag{A-4}$$

Since λ_i depends on electrical state for an ionic species, the activity coefficients γ_i and f_i must also depend on this state because m_i, λ_i^{ϕ} and c_i', a_i^{ϕ} are taken to be independent of electrical state. The following definition of the secondary reference states for ionic species specifies that certain combinations of activity coefficients approach unity in infinitely dilute solutions; namely,

$$\prod_i (\gamma_i)^{\nu_i} \to 1 \quad \text{as} \quad \sum_{i \neq 0} m_i \to 0 \tag{A-5}$$

$$\prod_i (f_i)^{\nu_i} \to 1 \quad \text{as} \quad \sum_{i \neq 0} c_i' \to 0 \tag{A-6}$$

where ν_i is the number of ions into which a molecule of electrolyte dissociates and for a neutral species, $\sum_i \nu_i z_i = 0$. From these definitions, λ_i^{ϕ} and a_i^{ϕ} are related by $\lambda_i^{\phi} = \rho_0 a_i^{\phi}$, where ρ_0 is the density of the pure solvent with units of g/cm^3 if λ_i^{ϕ} is in kg/mol and a_i^{ϕ} is in l/mol.

The chemical potential of a real gas in a multicomponent system is given by

$$\mu_i = \mu_i^{\circ}(T) + RT \ln (p_i \varphi_i) \quad , \tag{A-7}$$

where $p_i = y_i p$ is the partial pressure of species i. The secondary reference state quantity $\mu_i^{\circ}(T)$ is the temperature dependent part of the chemical potential of pure component i in the ideal–gas state. It is an integral of the ideal–gas limit of the heat capacity of i, and its numerical value depends on

the primary reference states chosen for both the enthalpy and the entropy of the pure component i.[66] The fugacity coefficient φ_i describes departures from the ideal state and approaches one in low–pressure mixtures.

The chemical potential of an alloy, amalgam, or solvent is given by

$$\mu_i = \mu^0 + RT \ln a_i \quad , \tag{A-8}$$

where the activity a_i describes departures from the standard state of species i. For a pure phase, the activity is one, and the chemical potential becomes

$$\mu_i = \mu_i^0 \quad . \tag{A-9}$$

Table A–1 summarizes the results in this appendix giving an expression for μ_p for species p as a pure phase, as an alloy, amalgam, or solvent, as a gas, and as a solute species in solution.

Table A–1. Thermodynamic definitions of absolute activities and electrochemical potentials.

species p	λ_p	$\mu_p = RT \ln \lambda_p$
pure phase k	λ_k^0	μ_k^0
amalgam, alloy, solvent k	$a_k \lambda_k^0$	$\mu_k^0 + RT \ln a_k$
gas l	$p_l \varphi_l \lambda_l^*$	$\mu_l^* + RT \ln p_l \varphi_l$
solute i	$m_i \gamma_i \lambda_i^\phi$	$\mu_i^\phi + RT \ln m_i \gamma_i$
solute i	$c_i' f_i a_i^\phi$	$\mu_i^\phi + RT \ln c_i' f_i / \rho_0$

Appendix B. General Expression for the Thermodynamic Cell Potential without a Liquid Junction

An expression may be derived for the finite thermodynamic potential difference between the electrode undergoing reaction j and an ideal reference electrode of a given kind (saturated calomel electrode)

$$U_{j/RG}^{\cdot} = \Phi_{RS} - \Phi_{RG} \qquad \text{(B-1)}$$

by mentally constructing an electrochemical cell. A schematic representation of this hypothetical cell is as follows:

α	φ	ε	λ	δ	β	α'
Pt	Hg(s)	Hg_2Cl_2(s)	4.1 M KCl saturated in H_2O	--- solution	electrode	Pt

The cell consists of two imaginary reference electrodes so that the dashed line does not denote a junction region. It must be assumed that the electrical states of phases λ and δ are equal if a thermodynamic treatment of the cell is going to be applied. The two reference electrodes are also assumed to be placed adjacent to each other at a given position in the solution being measured so that there is no ohmic drop between the two. Defining the imaginary reference electrodes in this way implies that there are no junction regions in this fictitious cell.

If true chemical equilibrium were to exist in the cell, then the cell potential would be zero. However, this is not the case for the cell potential $U_{j/RG}^{\cdot}$, because of the potential difference of electrons in the two different reactions. In order to calculate finite cell potentials, thermodynamic arguments may be used for the chemical nonequilibrium situations by

applying the concept of local equilibrium. An expression for the cell potential may be derived if the following assumptions are made[17]:

(1) Equilibrium exists between the reacting species and the metal.

(2) The molecular and ionic forms of the reacting species are known.

Thus, the first step in making a calculation of the cell potential is to establish a unique, well-defined reaction for each electrode. They are in generalized form as follows:

$$\sum_i s_{ij} M_i^{z_i} = n_j e^- \tag{B-2}$$

for the working electrode reaction at the right and

$$\sum_i s_{iRC} M_i^{z_i} = n_{RC} e^- \tag{B-3}$$

for the reference electrode reaction at the left. The electrochemical potentials of reactants and products at the right and left electrodes are related by

$$\sum_i s_{ij} \mu_i = n_j \mu_{e^-j} \tag{B-4}$$

and

$$\sum_i s_{iRC} \mu_i = n_{RC} \mu_{e^-RC} \quad , \tag{B-5}$$

respectively.

The cell potential is the difference in potential of electrons between the α' and α phases. The cell potential U in this work will denote the potential of the right electrode relative to the left electrode given by

$$U = \Phi^{\alpha'} - \Phi^{\alpha} \quad . \tag{B-6}$$

Substitution of the electrochemical potential of the electrons,

$$\mu_{e^-} = z_{e^-} F \Phi \tag{B-7}$$

for the electrical potential of electrons in equation B-6 results in

$$FU = \mu_{e^-}^{\alpha} - \mu_{e^-}^{\alpha'} \quad . \tag{B-8}$$

The cell potential can be rewritten using the local equilibrium conditions expressed by equations B-4 and B-5 as

$$FU'_{j/RC} = \frac{1}{n_{RC}} \sum_i s_{iRC}\mu_i - \frac{1}{n_j} \sum_i s_{ij}\mu_i \quad . \tag{B-9}$$

This hypothetical cell with no junction region can be treated by thermodynamics alone. To express the electrochemical potential in terms of concentrations, it is necessary to use the definitions given in table 1 in appendix A for the chemical and electrochemical potential of species p. Equation B-9 for the cell potential becomes

$$\begin{aligned} FU'_{j/RC} = {} & \frac{1}{n_{RC}} \sum_p s_{pRC}\mu_p^\phi - \frac{1}{n_j} \sum_p s_{pj}\mu_p^\phi \\ & + \frac{RT}{n_{RC}} \left[\sum_k s_{kRC} \ln a_k + \sum_l s_{lRC} \ln p_l\varphi_l + \sum_i s_{iRC} \ln \left[\frac{c_i f_i}{\rho_0} \right] \right] \\ & - \frac{RT}{n_j} \left[\sum_k s_{kj} \ln a_k + \sum_l s_{lj} \ln p_l\varphi_l + \sum_i s_{ij} \ln \left[\frac{c_i f_i}{\rho_0} \right] \right] \end{aligned} \tag{B-10}$$

This expression can be rewritten

$$U'_{j/RC} = U^\phi_{j/RC} + \frac{RT}{Fn_{RC}} \left[\sum_p s_{pRC} \ln \Lambda_p \right] - \frac{RT}{Fn_j} \left[\sum_p s_{pj} \ln \Lambda_p \right] \quad . \tag{B-11}$$

where

$$\begin{aligned} U^\phi_{j/RC} = {} & U^\phi_j - U^\phi_{RC} \\ = {} & \frac{1}{Fn_{RC}} \left[\sum_k s_{kRC}\mu_k^0 + \sum_l s_{lRC}\mu_l^* + RT \sum_i s_{iRC} \ln \lambda_i^\phi \right] \\ & + \frac{1}{n_j F} \left[\sum_k s_{kj}\mu_k^0 + \sum_l s_{lj}\mu_l^* + RT \sum_i s_{ij} \ln \lambda_i^\phi \right] \quad . \end{aligned} \tag{B-12}$$

Λ_p is used simply as an abbreviation for writing a_k, $p_l\varphi_l$, or $c_i f_i / \rho_0$ depending on whether species p is an alloy, gas, or solute. Λ_p should not be thought of as the activity for a solute since the individual activity coefficients of each solute would have ambiguous meaning. A more general expression with well-defined activity coefficients is derived in appendix C

where a reference species must be chosen. Nevertheless, equation B–11 is a useful expression for the cell potential of a hypothetical cell that contains no liquid junction. Once equation B-11 is written for specific electrode reactions, it can then be rewritten in terms of the neutral combination of activity coefficients given by

$$f_{i,n} = f_i \,/\, f_n^{z_i/z_n} \quad , \tag{B-13}$$

where species n is the chosen reference ion.

When activity coefficients are ignored, equation B–11 is a form of the so–called Nernst equation, relating cell potentials to the logarithms of ionic concentration. The Nernst equation can be used when there is an excess of inert electrolyte of nearly uniform concentration and the reactant species are present at much smaller concentrations. In writing the Nernst equation, both the liquid–junction potential and the ionic activity coefficient are discarded. It would be somewhat inconsistent to retain one but not the other in view of their dependence upon the choice of species n.

Appendix C. General Expression for the Cell Potential with a Liquid Junction Using the Quasi-Electrostatic Potential

An expression may be derived for the potential difference,

$$U''_{j/RR} = \Phi_{RS} - \Phi_{RR} \quad , \tag{C-1}$$

by mentally constructing an electrochemical cell. A schematic representation of this cell is as follows:

α	φ	ε	κ		δ	β	α'
Pt	Hg(s)	Hg_2Cl_2(s)	4.1 M KCl saturated in H_2O	junction region	solution	electrode	Pt

The hypothetical cell consists of an imaginary reference electrode of the same type as the reaction of interest j occurring at the working electrode and an actual reference electrode of potential Φ_{RR} shown on the left. The two reference electrodes are assumed to be placed adjacent to each other at some given position so that there is no ohmic drop between the two. However, the actual reference electrode is different in composition from the solution in which the two reference electrodes are placed. The result is a transition region in which concentration gradients exist between the δ and κ phases. The treatment of the potential of cells of this nature involves first the description of phase equilibria between the electrodes and the solutions or solids adjacent to them, followed by a consideration of the junction region that is likely to exist between the solutions adjacent to the electrodes.

Just as in appendix B, thermodynamic arguments may be used to start this analysis, if the reactants and products in the immediate vicinity of an electrode are assumed to be in local equilibrium. Next the molecular and

ionic forms of the reacting species must be known.

The reactions at the right and left electrodes are given by the following generalized expressions:

$$\sum_i s_{ij} M_i^{z_i} = n_j e - \tag{C-2}$$

and

$$\sum_i s_{iRR} M_i^{z_i} = n_{RR} e^- \quad . \tag{C-3}$$

respectively. The local equilibrium relationship for each reaction is as follows:

$$\sum_i s_{ij} \mu_i = n_j \mu_{e^-j} \tag{C-4}$$

and

$$\sum_i s_{iRR} \mu_i = n_{RR} \mu_{e^-RR} \tag{C-5}$$

The thermodynamic cell potential, $U''_{j/RR} = \Phi_{RS} - \Phi_{RR}$, taken to denote the potential of the right electrode relative to the left becomes

$$FU''_{j/RR} = \mu^a_{e^-RR} - \mu^a_{e^-j} \tag{C-6}$$

with the substitution of the electrochemical potential of the electrons,

$$\mu_{e^-} = z_{e^-} F \Phi \tag{C-7}$$

for the electrical potential of electrons in equation C-1. Substitution of the phase equilibrium equations C-4 and C-5 into equation C-6 gives

$$FU''_{j/RR} = \frac{1}{n_{RR}} \sum_i s_{iRR} \mu_i - \frac{1}{n_j} \sum_i s_{ij} \mu_i \tag{C-8}$$

for the cell potential. However, unlike the cell given in appendix B, the cell potential given by equation C–8 can not be written in terms of neutral species because of the region of changing composition. Also, thermodynamics alone does not provide the means for evaluating this difference since the junction region basically involves the irreversible process of diffusion and must be treated by the laws of transport in electrolytic solutions.

It is appropriate to assess conditions in this junction region of non-uniform composition by means of electrochemical potentials rather than by the usual concept of an electric potential. The electrochemical potential μ_i can be related to the electrical state of a phase by using the quasi–electrostatic potential Φ introduced by Newman.[1],[15] By selecting an ionic species n, the potential can be defined as

$$\mu_n = RT \ln c_n + z_n F\Phi \qquad \text{(C-9)}$$

Then, the electrochemical potential of any other species can be expressed as

$$\mu_i = RT \ln (c_i f_{i,n} a_{i,n}^{\ominus}) + z_i F\Phi \qquad \text{(C-10)}$$

where

$$f_{i,n} = f_i \,/\, f_n^{z_i/z_n} \qquad \text{(C-11)}$$

and

$$a_{i,n}^{\ominus} = a_i^{\ominus} \,/\, a_n^{\ominus z_i/z_n} \qquad \text{(C-12)}$$

Next, it is necessary to express equation C–10 in terms of $\lambda_i^{\ominus}$ so that the tables of standard potentials given by Newman[1] may be used. By our definition of the secondary reference states, $a_i^{\ominus} = \lambda_i^{\ominus}/\rho_0$. Therefore,

$$a_{i,n}^{\ominus} = \lambda_{i,n}^{\ominus} \,/\, \rho_0^{(1 - z_i/z_n)} \qquad \text{(C-13)}$$

where

$$\lambda_{i,n}^{\ominus} = \lambda_i^{\ominus} \,/\, \lambda_n^{\ominus z_i/z_n} \qquad \text{(C-14)}$$

Now the electrochemical potential of solute i is given by

$$\mu_i = RT \ln \left[c_i f_{i,n} \lambda_{i,n}^{\ominus} \,/\, \rho_0^{(1 - z_i/z_n)} \right] + z_i F\Phi \qquad \text{(C-15)}$$

Because the activity is defined as $a_i = \lambda_i \,/\, \lambda_i^{\ominus}$, it is useful to rewrite equation C-1 as

$$\mu_i = RT \ln \lambda_i^{\ominus} + RT \ln \left[\frac{c_i f_{i,n}}{\lambda_n^{\ominus z_i/z_n} \rho_0^{(1 - z_i/z_n)}} \right] + z_i F\Phi \qquad \text{(C-16)}$$

and this implies

$$a_i = \left[\frac{c_i' f_{i,n}}{\rho_0 (\lambda_n^\phi / \rho_0)^{z_i / z_n}} \right] \exp \left[\frac{z_i F}{RT} \Phi \right] . \qquad \text{(C-17)}$$

The activity of species i is dependent on the choice of the reference species n and the quasi-electrostatic potential of the phase. The activities and electrochemical potentials of all other species are summarized in table C–1.

These results for the solute are somewhat different from those given in table A–1 for the absolute activities and electrochemical potentials of species p.

Substitution of the electrochemical potential μ_i for species i given in table C–1 directly into equation C–8 allows an expression for the potential difference $U''_{j/RR}$ to be obtained. Also, one may use $\mu_i = RT \ln \lambda_i$ in equation C–8 to give

$$FU''_{j/RR} = \frac{RT}{n_{RR}} \sum_i s_{iRR} \ln \lambda_i - \frac{RT}{n_j} \sum_i s_{ij} \ln \lambda_i \qquad \text{(C-18)}$$

where $\lambda_i = a_i \lambda_i^\phi$. Hence equation C-18 may be rewritten resulting in

Table C–1. Definitions of relative activities and electrochemical potentials.

species i	a_i	$\mu_i = \mu_i^\phi + RT \ln a_i$
pure solid phase	1	μ_i^0
amalgam, alloy, solvent	a_i	$\mu_i^0 + RT \ln a_i$
gas	$y_i p \varphi_i$	$\mu_i^\circ(T) + RT \ln y_i p \varphi_i$
solute:		
reference species n	$\frac{c'_n}{\lambda_n^\phi} \exp \left(\frac{z_n F}{RT} \Phi \right)$	$RT \ln c'_n + z_n F \Phi$
solute i	equation C–17	$RT \ln (c_i' f_{i,n} a_{i,n}^\phi) + z_i F \Phi$ or equation C–16

$$U''_{j/RR} = U^{\phi}_{j/RR} + \frac{RT}{Fn_{RR}}\left[\sum_p s_{pRC} \ln a_p\right] - \frac{RT}{Fn_j}\left[\sum_p s_{pj} \ln a_p\right] \qquad \text{(C-19)}$$

where

$$U^{\phi}_{j/RR} = U^{\phi}_j - U^{\phi}_{RR} = \frac{1}{Fn_j}\sum_i s_{iRR}\mu^{\phi}_i - \frac{1}{Fn_{RR}}\sum_i s_{ij}\mu^{\phi}_i \qquad \text{(C-20)}$$

and a_i and μ^{ϕ}_i are given in table C-1 for all species i.

The academic exercise presented in this appendix is for the purpose of demonstrating that the electrochemical potential and the activity of a solute are neither independent of the other species in solution nor the electrical state of the phase. Even though the electrochemical potential is quite often separated into an electrical term and a chemical term for computational purposes, it has been shown here that the quasi–electrostatic potential is related unambiguously to the electrochemical potentials conforming to our usual concept of electrostatic potential. The arbitrariness of the definition of Φ is apparent from the need to select a particular ionic species n. This is evident in equation C–17 where the activity of solute is expressed relative to species n.

Appendix D. Reaction Equilibrium Constants

The purpose of this appendix is to develop general expressions for the equilibrium constants of a chemical and an electrochemical reaction. The fundamental definitions of the chemical and electrochemical potentials introduced in appendix A will be used.

1. Chemical Reaction Equilibrium Constant

Symbolic representation of a chemical reaction m may be made as follows:

$$0 = \sum_i \nu_{im} M_i^{z_i} \quad , \tag{D-1}$$

where M_i represents a chemical formula, ν_{im} are stoichiometric coefficients, and z_i are the charge numbers for species i. If a species is neutral, z_i is zero. The stoichiometric coefficients are negative for a reactant and positive for a product. The change in the total Gibbs energy of a system at constant temperature and pressure due to a chemical reaction m is given by

$$\Delta G_m = \sum_i \nu_{im} \mu_i \quad , \tag{D-2}$$

where μ_i is the chemical potential of species i. A criterion of chemical-reaction equilibrium is

$$\sum_i \nu_{im} \mu_i = 0 \quad , \tag{D-3}$$

implying ΔG_m must equal zero at equilibrium. Also at equilibrium, all driving forces due to concentration, temperature, and pressure differences must equal zero. This means at constant temperature and pressure, the surface and bulk concentrations are the same. This is written $c_{i,0} = c_{i,\infty} = c_{i,*}$, where * represents the equilibrium state.

1.1. Standard Gibbs Energy

The chemical or electrochemical potentials μ_i of species i are given in table A-1 and may be substituted into the chemical reaction equilibrium equation D-3. If equation A-2

$$\mu_i = \mu_i^\circ + RT \ln (m_i \gamma_i) \tag{D-4}$$

for μ_i of a solute in solution is substituted into equation D-3, then

$$\sum_i \nu_{im} \mu_i^\circ = -RT \sum_i \ln (m_i \gamma_i)^{\nu_{im}} \tag{D-5}$$

is obtained. The left side of equation D-5 is the standard Gibbs-function change for reaction m

$$\Delta G_m^\circ = \sum_i \nu_{im} \mu_i^\circ = \sum_i \nu_{im} G_i^f \tag{D-6}$$

and G_i^f is the Gibbs energy of formation of species i in the secondary reference state. Equation D-5 may be rewritten as

$$\Delta G_m^\circ = - RT \, K_m \tag{D-7}$$

where K_m is the equilibrium constant for the chemical reaction m given by

$$K_m = \prod_i (m_i \gamma_i)^{\nu_{im}} = \prod_i \left[\frac{c_i f_i}{\rho_0} \right]^{\nu_{im}} . \tag{D-8}$$

Of course if species other than solutes are part of the chemical reaction, then a_i or $y_i p \varphi_i$ may be substituted for $m_i \gamma_i$ if the species is an alloy, amalgam, or solvent, or a gas, respectively. Another expression for the equilibrium constant is

$$K_m = \prod_i (\lambda_i^\circ)^{-\nu_{im}} . \tag{D-9}$$

1.2. Standard Electrode Potentials

Electrochemical Reactions

The fundamental equations for chemical reaction equilibria have been reviewed. However, it is of interest to express the results of the chemical equilibrium analysis in terms of electrochemical reactions and the

corresponding electrode potentials. The general form of an electrochemical reaction may be given by

$$\sum_i s_{ij} M_i^{z_i} = n_j e^- \quad , \tag{D-10}$$

where s_{ij} is the stoichiometric coefficient of species i in the electrochemical reaction j. The coefficient is positive for the reactants in the oxidation reaction, reducing agents, and is negative for the oxidation products. The number of electrons e^- transferred in the reaction is n_j. The equilibrium expression for reaction j is

$$\sum_i s_{ij} \mu_i = n_j \mu_{e^-j} \tag{D-11}$$

where μ_{e^-j} is the electrochemical potential of the electrons participating in reaction j.

A chemical reaction equation may be obtained by subtracting electrochemical reaction l from j[†]

$$\sum_i s_{ij} M_i^{z_i} - \sum_i s_{il} M_i^{z_i} = n_j e^- - n_l e^- = 0 \quad . \tag{D-12}$$

Since the stoichiometric coefficients in the electrochemical reactions are related to the coefficients in the chemical reaction by

$$s_{ij} - s_{il} = -\nu_{im} \quad , \tag{D-13}$$

equation D-2 for the Gibbs energy for reaction m may be rewritten

$$\Delta G_m = -\sum_i (s_{ij} - s_{il})\mu_i = -n(\mu_{e^-j} - \mu_{e^-l}) \quad . \tag{D-14}$$

From equation D-3, we know that ΔG_m is zero at equilibrium implying that the electrochemical potential of electrons is equivalent in the two reactions.

Electrode Potentials

Next, it is necessary to relate the electrode potentials U_j and U_l of the electrochemical reactions that make up chemical reaction m to ΔG_m. The

[†] In order to obtain a chemical reaction, the stoichiometry coefficients of the electrochemical reactions must be multiplied by a constant so that the number of electrons in each reaction will be the same.

electrode potential $U_{j/l}$ will denote the potential of the electrode reaction j minus the potential of electrode reaction l. Substitution of the electrochemical potential of the electrons,

$$\mu_{e^-} = z_{e^-} F U_j \quad , \tag{D-15}$$

for the electrode potential results in

$$F U_{j/l} = F(U_j - U_l) = -(\mu_{e^-,j} - \mu_{e^-,l}) \, . \tag{D-16}$$

The cell potential given by equation D-16 can be rewritten using the equilibrium condition expressed by equation D-11 as

$$F U_{j,l} = -\frac{1}{n} \sum_i (s_{ij} - s_{il}) \mu_i \quad . \tag{D-17}$$

The stoichiometric coefficients of the electrochemical reactions j and l are related to those of a chemical reaction by equation D-13, and it should be pointed out again that ν_{im} is positive for products and negative for reactants. Therefore,

$$F U_{j/l} = \frac{1}{n} \sum_i \nu_{im} \mu_i \, , \tag{D-18}$$

implying

$$\Delta G_m = n F U_{j/l} \tag{D-19}$$

when equation D-2 is substituted into D-18. At chemical equilibrium,

$$\Delta G_m = n F U_{j/l,\bullet} = 0 \quad . \tag{D-20}$$

ΔG_m equals zero so that the equilibrium cell potential will always be zero when two electrochemical reactions are equilibrated on one electrode.

Since we know that each electrochemical reaction has with it an associated standard electrode potential, we would like to relate the chemical reaction equilibrium constant to the standard potentials of the electrochemical reaction that go into making up the chemical reaction. The equilibrium expression D-11 for an electrochemical reactions can be written for its standard states as

$$\sum_i s_{ij}\mu_i^\circ = n_j\mu_{e^-,j}^\circ \quad . \tag{D-21}$$

From arguments similar to those going into equation D-15,

$$\mu_{e^-,j}^\circ = -FU_j^\circ \quad , \tag{D-22}$$

thereby, allowing D-21 to yield

$$\sum_i s_{ij}\mu_i^\circ = -n_j FU_j^\circ \quad . \tag{D-23}$$

When the electrochemical reaction l is subtracted from reaction j to obtain chemical reaction m, the following expression may be obtained

$$\Delta G_m^\circ = nF(U_j^\circ - U_l^\circ) = \sum_i \nu_{im}\mu_i^\circ \quad . \tag{D-24}$$

Using equation D-7 that relates the equilibrium constant to ΔG_m°, we obtain

$$K_m = \exp\left[\frac{-nF(U_j^\circ - U_l^\circ)}{RT}\right], \tag{D-25}$$

where the equilibrium constant K_m is for the chemical reaction

$$\sum_i s_{ij}M_i^{z_i} - \sum_i s_{il}M_i^{z_i} = 0. \tag{D-26}$$

The standard potential for reaction j, U_j°, is given by equation D-23 where $\mu_i^\circ = RT \ln \lambda_i^\circ$ and may be found in standard chemical thermodynamic tables. The standard electrode potentials U_j° found in Newman[1] are relative to the normal hydrogen electrode given by†

$$FU_j^\circ = -(\mu_{e^-,j}^\circ - \mu_{e^-,H_2}^\circ) \tag{D-27}$$

or rewritten to be

$$FU_j^\circ = \tfrac{1}{2}\mu_{H_2}^\circ - RT \ln \lambda_{H^+}^\circ - \frac{1}{n_j}\sum_i s_{ij}\mu_i^\circ \quad . \tag{D-28}$$

Hence,

$$FU_{j/l}^\circ = F(U_j^\circ - U_l^\circ) = -\left[\frac{1}{n_j}\sum_i s_{ij}\mu_i^\circ - \frac{1}{n_l}\sum_i s_{il}\mu_i^\circ\right] \quad . \tag{D-29}$$

which is the same as equation D-24 if $n_j = n_l$, and ν_{im} is substituted for $-(s_{ij} - s_{il})$.

---

† For consistency, we should write U_{j/H_2}° instead of U_j°, but since we will always use standard states to be referenced to the hydrogen reaction, the $/ H_2$ is dropped for brevity.

2. Electrochemical Reaction Equilibrium Constant

We now want to determine a general expression for the equilibrium constant of an electrochemical reaction. This can be done by starting with a general expression for the potential $U''_{j/RR}$ of an electrode reaction j relative to a real reference electrode. Such an equation was developed in appendix C using the electrochemical potentials and activities in table C–1. We will begin this development with a similar equation given by

$$FU''_{j/RR} = FU^{\phi}_{j/RR} + \frac{RT}{n_{RR}} \sum_{i \neq n} s_{iRR} \ln \Upsilon^{\lambda}_{i,n} - \frac{RT}{n_j} \sum_{i \neq n} s_{ij} \ln \Upsilon^{\beta}_{i,n} + (\Phi^{\delta} - \Phi^{\lambda}) \quad . \tag{D-30}$$

The last term on the right is the liquid–junction potential, $\Delta\Phi_{LJ}$. $\Upsilon_{i,n}$ is similar to Λ_p used in appendix B. It is simply an abbreviation for writing a_i, $p_i\varphi_i$, or $c'_i f_{i,n}/\rho_0$. The activity a_i of any alloy or amalgam, and the partial pressure of any gas and its fugacity coefficient $p_i\varphi_i$ are accounted for in reactions j and RR, as well as the concentration of solute i and its activity coefficient relative to species n, $c'_i f_{i,n}/\rho_0$. Again, $\Upsilon_{i,n}$ should not be thought of as the activity for a solute, since it does not contain the quasi–electrostatic potential Φ. The true activities of species i are given in table C–1. If species n is chosen so that it participates in the reference electrode reaction, then $f_{i,n} = 1$ for species n in the reference electrode term of equation (D-30). This equation may be rewritten

$$FU''_{j/RR} = RT \ln \left[\frac{k'_c}{k'_a}\right]_j - \frac{RT}{n_j} \sum_{i \neq n} s_{ij} \ln \Upsilon^{\beta}_{i,n} \ln \left[a_i p_i \varphi_i \left(\frac{c'_i f_{i,n}}{\rho_0} \right) \right]^{\delta} + (\Phi^{\delta} - \Phi^{\alpha}) \tag{D-31}$$

where

$$\ln \left[\frac{k'_c}{k'_a}\right]_j = \frac{n_j F}{RT} U^{\phi}_{j/RR} + \frac{n_j}{n_{RR}} s_{nRR} \ln \frac{c'^{\kappa}_n}{\rho_0} + \frac{n_j}{n_{RR}} \sum_{i \neq n} s_{iRR} \ln \Upsilon^{\kappa}_{i,n} \tag{D-32}$$

For a reference electrode reaction such as the calomel electrode, there is

but one solute species participating in the reaction. If it is the chosen reference species n, the last term in equation D–32 would not appear. Again it should be noted, the expression for the equilibrium constant for reaction j depends on the choice of the reference species n, but is independent of the concentration of species that participate in reaction j.

The equilibrium ratio given by equation D–32 is not generally dimensionless. Equation D–31 may be rewritten as

$$\frac{\left[\frac{k_c^{\cdot}}{k_a^{\cdot}}\right]_j}{\prod_i \left[\Upsilon_{i,n}\right]^{\nu_{ij}}} = \exp\left[\frac{n_j F}{RT}\left(U_{j/RR}^{\cdot\cdot} - \Delta\Phi_{Lj}\right)\right] . \qquad \text{(D-33)}$$

The right side of this equation is dimensionless, making the equilibrium constant have reciprocal units of the activities of species i participating in reaction j raised to their stoichiometric coefficient power.

Appendix E. Curve Fitting

1. Regression Fit

We should like to determine the kinetic parameters that may be used to best fit the experimental polarization curves. The first method is simply to apply linear regression to the linear or Tafel region of the polarization curve. The second approach is a routine based on the Stern–Geary equation to best fit the the experimental curves over the entire polarization range. This method will be discussed in the next section.

The Tafel slope of the anodic zinc dissolution curve in figure 4–7 is determined by linear regression to be 1.715 V^{-1} or b_a = 583 mV/ decade. The anodic transfer coefficient is given by

$$\alpha = \frac{2.303RT}{bF} \quad , \tag{E-1}$$

which yields 0.102. The anodic Tafel expression 4–21 allows the anodic rate constant to be determined for the zinc dissolution reaction from the y–intercept of figure 4–7. The anodic rate constant $k_{a,Zn}$ for the zinc dissolution is 4.450 × 10^{-6} mol/ cm^2–s. Because the proper rate constant is very sensitive to slight changes in the Tafel slope, round–off errors must be considered. When the transfer coefficient is rounded to 0.10, a corrected value of the rate constant is determined using

$$k_{a\,Zn} = \frac{i_1}{2F \exp\left[\frac{\alpha_{a\,Zn}F}{RT} V_1\right]} \quad , \tag{E-2}$$

where (V_1, i_1) is a selected pivot point in the anodic zinc Tafel region of the experimental polarization curve. When α_a = 0.10, the new $k_{a,Zn}$ is 4.272 × 10^{-6} mol/ cm^2–s using -0.75 V for V_1 in equation E–2. This adjusted value of the rate constant provides good agreement between the theoretical

and experimental curves. These kinetic parameters obtained by modifying the regression fit of the Tafel region of figure 4–7 are summarized in table E–1 for the zinc reaction.

Table E–1. Kinetic parameters for the zinc reaction from the anodic polarization curve for the zinc corrosion process in 1 M HCl.

$b_a = \frac{2.303RT}{\alpha_{a\,Zn}F}$	$\alpha_{a\,Zn}$	$\log(2Fk_{a,Zn})$	k_a
0.592 V	0.100	-8.387×10^{-2}	4.272×10^{-6} mol / cm^2–s

The kinetic parameters reaction may be determined in a similar fashion for the hydrogen evolution reaction. The Tafel slope of the cathodic hydrogen curve in figure 4–7 is 643 mV/decade, which yields a cathodic transfer coefficient of 0.092. The regression best fit gives 2.814×10^{-6} cm / s for the cathodic rate constant of the hydrogen reaction assuming the surface concentration of the hydrogen ions is the same as the bulk concentration of 0.001 mol/cm^3. When the transfer coefficient is rounded up to 0.1 and the same rate constant is used from the regression analysis, a 10 % difference results between the predicted and experimental current–densities. The following equation

$$k_{c\,H_2} = \frac{i_2}{Fc_{H^+,\infty} \exp\left[-\frac{\alpha_{c\,H_2}F}{RT} V_2\right]} \quad \text{(E–3)}$$

is used to adjust the rate constant using a V_2 of -1.4 V. The kinetic parameters obtained from rounding off the transfer coefficient and making the adjustment for the rate constant in figure 4–7 are summarized in table E–2 for hydrogen evolution.

Table E–2. Kinetic parameters for the hydrogen reaction from the cathodic polarization curve for the zinc corrosion process in 1 M HCl.

$b_c = \frac{2.303RT}{-\alpha_{c\,H_2}F}$	$\alpha_{c\,H_2}$	$\log(Fk_{c,H_2}c_{H_2,0})$	k_c
0.592 V	0.10	-3.755×10^{0}	1.823×10^{-6} cm / s

2. Stern–Geary Program FIT

In the previous section, kinetic parameters were determined for a first approximation using only the Tafel equations E–2 and E–3 for the zinc and hydrogen reactions, respectively. The anodic transfer coefficient and the rate constant for the zinc reaction were found by neglecting the effects of the hydrogen reaction as well as not considering the zinc cathodic back reaction, the second term on the right of equation 4–11. The cathodic kinetic parameters for the hydrogen reaction were in turn determined by neglecting the zinc reaction altogether and by neglecting the hydrogen anodic reaction, the first term on the right of equation 4–16. The procedure described there assures one of obtaining a reasonable fit of about 5% in the Tafel regions of the respective reactions, but as shown in figure 4–7 this method is not successful in obtaining parameters that when used to generate the polarization curve match the experimental data over the entire potential range.

A curve fitting program, FIT, based on the Stern–Geary[6] equation is used to obtain new parameters that will predict the entire polarization curve. Stern and Geary in 1938 showed that to a good approximation the net current density in de–aerated solutions is the sum of the Tafel term of the anodic metal dissolution reaction and the Tafel term of the cathodic evolution of hydrogen reaction. Equations E–2 and E–4 are summed giving

$$i_{net} = 2Fk_{a,Zn}\exp\left[\frac{\alpha_{a\,Zn}F}{RT}V\right] - Fk_{c,H_2}c_{H^+,0}\exp\left[-\frac{\alpha_{c\,H_2}F}{RT}V\right], \qquad \text{(E-4)}$$

for the net current density when the transfer coefficients are used in place of symmetry factors. We are interested in the using this equation to determine the kinetic parameters for the entire curve. Three experimental data points may be incorporated into this equation by using $i-V$ points of the zinc and hydrogen Tafel regions and zero current at the corrosion potential. Three equations result in terms of the transfer coefficients and rate constants of the zinc and hydrogen reactions. A trial and error procedure is used by initially assuming a value for the anodic zinc transfer coefficient. The anodic and cathodic rate constants for the zinc and hydrogen reactions then may be determined iteratively. An assumed value for the cathodic hydrogen transfer coefficient enables k_a and k_c to be calculated using the data from the Tafel regions. The value of α_c is iterated upon using

$$(\alpha_c)_{calc} = -\alpha_a - \frac{RT}{FV_{corr}}\ln\left[\frac{2k_{Zn}}{k_{H_2}c_{H^+,\infty}}\right], \qquad \text{(E-5)}$$

until the guessed value is within 10^{-9} of the calculated value. Equation E-5 is obtained by using equation E-4, zero current, and the corrosion potential. For the given α_a, we have the best set of parameters that match the experimental data at the given points. A range of anodic transfer coefficients are used, and the above iterative procedure is repeated each time to determine the other three parameters. The polarization curves generated using the FIT routine are plotted in figure 4-8 and are compared to the experimental curves to determine the best set of kinetic parameters. The set of parameters obtained from the FIT routine used to generate the curves in figure 4-7 are given in table E-3.

Table E–3. Kinetic parameters obtained from FIT.

	Case Number					
	1		*2*		*3*	
	α	k	α	k	α	k
Zn	0.05	1.596×10^{-6}	0.10	4.856×10^{-6}	0.15	1.913×10^{-5}
H_2	0.032	1.095×10^{-4}	0.079	6.264×10^{-6}	0.124	4.931×10^{-7}

A reasonable fit for the entire polarization curve is obtained from set 2, which is determined based on a transfer coefficient of 0.10. This set of parameters should be compared to the set of parameters obtained directly from the regression fit and adjusting for roundoff which were given in tables E–1 and E–2 for the zinc and hydrogen reactions, respectively. The curve generated by the latter set with an anodic transfer coefficient of 0.10 was shown in figure 4–6 and is not shown again in figure 4–7. However, it does not fit the experimental data as well as set 2 in figure 4–7. The FIT routine is also used to determine the best set of kinetic parameters based on transfer coefficients of 0.15 and 0.05. The larger α_a implies a larger Tafel slope and yields poor agreement with the experimental data. An anodic transfer coefficient of 0.05 surprisingly gives the best fit. Therefore, set 1 should be used in the model that is developed in chapter 5.

Appendix F. Computer Programs

1. Program FIT

Program FIT determines the best kinetic parameters that match the experimental polarization curve based on a given value of the zinc transfer coefficient. The cathodic hydrogen transfer coefficient, and anodic and cathodic rate constants for the zinc and hydrogen reactions, respectively are iteratively calculated and then used to generate the polarization curve for the corrosion process.

The input required by FIT is:

ALFAM = anodic transfer coefficient of zinc, α_{aZn}

ALFCH = initial guess for cathodic hydrogen transfer coefficient, α_{cH_2}

V1, I1 = experimental potential, current data point in anodic Tafel region of polarization curve

V2, I2 = experimental potential, current data point in cathodic Tafel region of polarization curve

VCOR = experimental open–circuit potential

The subroutine necessary to run FIT is:

Subroutine FTN - Computes the net current density using the Tafel equations for the zinc and hydrogen reactions.

2. Program FIRST

Program FIRST calculates the the corrosion potential and current density, generates the polarization curves for the corrosion process, and compares the results of the kinetic–diffusion model to the corrosion rates as predicted by conventional corrosion analysis techniques: linear approximation, Tafel approximation, and polarization resistance methods.

The input required by FIRST are:

1. Kinetic parameters determineed by FIT including ALFAM, RKAM, ALFCH2, and RKCH2 for the transfer coefficient and rate constant of the metal dissolution and hydrogen evolution reactions, respectively.

2. Zinc complexing equilibrium constants given by RK1P, RK2P, RK3P, and RK4P.

3. Bulk concentrations of metal ions, hydrogen ions, and hydrogen partial pressure given by CMTB, CHB, and PH2B, respectively.

4. Diffusion coefficients of metal ions, hydrogen ions, and hydrogen given by DM, DH, DH2, respectively, and the solubility of hydrogen, SH2.

5. Rotation speed of the disk electrode RPM, kinematic viscosity RNU, and the density of the pure solvent water RHO.

6. Polarization resistance RP.

The subroutines necessary to run FIRST are:

1. Subroutine NRM - Calculates the corrosion current and potential using a Newton–Raphson iterative technique.

2. Subroutine FTNY - Generates the polarization curves for the corrosion process based on the kinetic–diffusion model that is presented in chapter 5.

3. Subroutine FTNMBV - Generates the polarization curves for the corrosion process based on modified Butler–Volmer equations assuming constant concentrations at the surface over the entire polarization range.

4. Subroutine FTNBV - Generates the polarization curves for the corrosion process based on Butler–Volmer equations assuming constant exchange–current densities with polarization.

5. Functions CM, CH, PH2 - Computes the surface concentrations of the divalent metal ions, hydrogen ions, and hydrogen assuming a stagnant Nernst diffusion–layer thickness with no migration.

6. Subroutine ACTIVC - Calculates activity coefficients.

7. Subroutine KS - Calculates the thermodynamic equilibrium constant of an electrochemical reaction and the kinetic rate constant of the back reaction.

8. Subroutine UJGO - Calculates the thermodynamic reversible cell potential of an electrochemical reaction relative to the saturated calomel reference electrode.

9. Subroutine IO - Evaluates the exchange–current density of an electrochemical reaction as a function of the kinetic parameters and concentration.

10. Subroutine RKAPA - Calculates the conductivity of an electrolytic solution.

11. Subroutine POTLJ - Calculates the liquid–junction potential.

12. Subroutine DIFPOT - Calculates the diffusion potential.

13. Subroutines OHMR, OHMPOT - Calculates the ohmic resistance and potential, respectively.

14. Subroutines VSQFN, VSQXFN - Calculates the simulated measured cell potential relative to an actual saturated calomel electrode with and without concentration variations, respectively.

15. Subroutine CORR - Calculates the corrosion–current density and potential using linear and Tafel approximations as a function of the reversible potentials and exchange current densities.

16. Subroutine SGPM - Calculates the corrosion–current density using the Stern–Geary polarization method and Mansfeld's modifications of it as a

function of the Tafel slopes and polarization resistance.

17. Subroutine IRSCAN - Calculates the relative error of the scan rate due to ohmic resistance of the solution.

3. Program Listings

```
      PROGRAM FIT(INPUT,OUTPUT)
      REAL KAM,KCH
      REAL I1,I2
      COMMON/IN/F,R,T,FF
      COMMON/PARAMM/ALFAM,KAM
      COMMON/PARAMH/ALFCH,KCH,CHB
      READ 130, IAP,ICP
      READ 100, NI,NA,NC
      READ 115, DELVA,DELVC
      READ 115, ALFAM,ALFCH
      READ 115, V1,I1
      READ 115, V2,I2
      READ 115, VCOR,V0
      READ 105, F,R,T
      READ 120, CHB
C
C     DETERMINE THE KINETIC PARAMETERS THAT BEST FIT THE DATA
C     1.  ASSUME A VALUE FOR ALFAM AND LET IT REMAIN CONSTANT
C     2.  MAKE AN INITIAL GUESS FOR ALFCH
C     3.  CALCULATE KAM AND KCH ASSUMING THE BACK REACTION IS NEGLIBLE
C     4.  USE EXPERIMENTAL POINTS (V1,I1) & (V2,I2) FROM TAFEL REGION
C     5.  THIS FORCES THE CURVE THROUGH BOTH POINTS
C     6.  CALCULATE ALFCH SO THAT CURVE IS FORCED THROUGH (VCOR,0)
C     7.  GENERATE I-V CURVE FOR THE SET OF CALCULATED PARAMETERS
C     8.  CONFIRM THE CHOICE FOR ALFAM, PICK A NEW VALUE IF NECESSARY
C     9.  RERUN PROGRAM
C
      FF=F/(R*T)
      VA1=ALFAM*FF*V1
      VA2=ALFAM*FF*V2
      A1=2.0*F*EXP(VA1)
      A2=2.0*F*EXP(VA2)
      AD=A2/A1
C
C     CURVE FITTING METHOD FOR DETERMINATION OF ALFCH
C     1.  X VALUES REPRESENT ALFCH
C     2.  Y VALUES REPRESENT THE ERROR ASSOCIATED WITH A GIVEN X
C
      XB=0.0
      YB=0.0
      XHI=0.0
      YHI=1.0E+5
      XLO=0.0
      YLO=-1.0E+5
C
      PRINT 200
      PRINT 202, NI,IAP,ICP
      PRINT 204, NA,NC
      PRINT 180
      DO 50 I=1,NI
C
```

```
        VC1=-ALFCH*FF*V1
        VC2=-ALFCH*FF*V2
        B1=-F*CHB*EXP(VC1)
        B2=-F*CHB*EXP(VC2)
C
        KCH=(I2-AD*I1)/(B2-AD*B1)
        KAM=(I1-B1*KCH)/A1
C
        ACCALC=-ALFAM-(1.0/(FF*VCOR))*ALOG(2.0*KAM/(KCH*CHB))
C
        Y=ACCALC-ALFCH
C
        IF (I.EQ.1) XB=ALFCH
        IF (I.EQ.1) YB=Y
        XSAVE=ALFCH
        YSAVE=Y
        IF (ABS(Y).GT.ABS(YB)) GO TO 25
        XSAVE=XB
        YSAVE=YB
        XB=ALFCH
        YB=Y
 25     IF (Y.LT.0.0) GO TO 30
        IF (Y.GT.YHI) GO TO 30
        XHI=ALFCH
        YHI=Y
 30     IF (Y.GT.0.0 .OR. Y.LT.YLO) GO TO 35
        XLO=ALFCH
        YLO=Y
 35     IF (I.EQ.1) GO TO 40
        ALFCH=XB-(XSAVE-XB)*YB/(YSAVE-YB)
        IF (ABS(Y).LT.1.0E-10) GO TO 55
        IF (XHI*XLO.EQ.0.0) GO TO 50
        IF ((ALFCH-XHI)*(ALFCH-XLO).LT.0.0) GO TO 50
        ALFCH=0.5*(XHI+XLO)
        GO TO 50
 40     ALFCH=ALFCH+0.05
 50     PRINT 185, XB,YB,XSAVE,YSAVE,ALFCH,Y
        PRINT 195,I,NI
 55     PRINT 190
        PRINT 193, KCH,KAM,ALFAM,ALFCH,XB,Y,YB
C
C     THE BEST SET OF PARAMETERS HAS BEEN DETERMINED FOR THE GIVEN ALFAM
C     GENERATE THE THEORETICAL I-V CURVE USING 'BEST' PARAMETERS
C
        PRINT 400
        PRINT 410
C
        IF (IAP.EQ.1) GO TO 2
        VA=V0
        DO 60 I=1,NA
         IF (I.EQ.1) GO TO 61
```

```
          VA=VA+DELVA
 61       X=FF*VA
          CALL FTN(X,YMAA,YH2A,YA)
          PRINT 430,VA,YA,YMAA,YH2A
 60      CONTINUE
C
 2       IF(ICP.EQ.1) GO TO 3
C
C        GENERATE KINETIC-DIFFUSION POLARIZATION CURVE
C        CATHODIC SWEEP
C
         PRINT 500
         PRINT 410
C
         VC=V0
         DO 70 I=1,NC
          IF (I.EQ.1) GO TO 71
          VC=VC-DELVC
 71       X=FF*VC
          CALL FTN(X,YMCC,YH2C,YC)
          PRINT 430,VC,YC,YMCC,YH2C
 70      CONTINUE
 3       CONTINUE
C
C        READ FORMATS
C
 100     FORMAT(3I3)
 105     FORMAT(3(1PE10.3))
 115     FORMAT(2(1PE10.3))
 120     FORMAT(1(1PE10.3))
 130     FORMAT(2I2)
C
C        PRINT FORMATS
C
 180     FORMAT(1H ,/*    XB     YB      XSAVE     YSAVE      ALFCH      Y */)
 185     FORMAT(1H ,6(1PE10.3))
 190     FORMAT(1H , * THE BEST SET OF PARAMETERS *,
     1   /*       KCH      KAM      ALFAM      ALFCH      XB      Y      YB  *)
 193     FORMAT(1H ,7(1PE10.3))
 195     FORMAT(1H ,/*  NOT CONVERGED,  I=*,I4,*  NI=*,I4)
C
 200     FORMAT(1H ,*PROGRAM FIT IS FOR */(3X,*1.  THE DETERMINATION OF
     1THE BEST KINETIC PARAMETERS*)/(3X,*2.  THE GENERATION OF A METAL
     2DISSOLUTION/HYDROGEN EVOLUTION POLARIZATION CURVE*))
C
 202     FORMAT(1H ,/*I-V CURVE PARAMETERS*/(1X,*   NI= *,I2)/(10X,*
     1 IAP, ICP= 0 OR 1*)
     2/(10X,*IAP= *,I2,3X,*ICP= *,I2)/
     3/(1X,10X,*[1 IMPLIES THAT SECTION OF PROGRAM IS BYPASSED]*))
C
 204     FORMAT(1H ,/*NUMBER OF POLARIZATION POINTS,  NA= *,I2,*    NC= *,
```

```
     1I2)
C
 400    FORMAT(1H ,/*GENERATION OF ANODIC KINETIC-DIFFUSION POLARIZATION
     1 CURVE * )
 410    FORMAT(1H ,*    V     INET       IMTA       IH2TC*)
 430    FORMAT(1H , F6.3,3(1PE10.3))
 500    FORMAT(1H ,///*GENERATION OF KINETIC-DIFF POLARIZATION CURVE*/
     1 * CATHODIC SWEEP * )
C
        STOP
        END
C
        SUBROUTINE FTN(X,YM,YH2,Y)
        REAL KAM,KCH
        REAL I1,I2
        COMMON/IN/F,R,T,FF
        COMMON/PARAMM/ALFAM,KAM
        COMMON/PARAMH/ALFCH,KCH,CHB
C       ALFAM=0.1
C       ALFCH=0.1
C       KAM=4.272E-6
C       KCH=1.823E-6
        YM=2.0*F*KAM*EXP(ALFAM*X)
        YH2=-F*KCH*CHB*EXP(-ALFCH*X)
        Y=YM+YH2
        RETURN
        END
```

```
      PROGRAM FIRST(INPUT,OUTPUT)
      COMMON/I/ ITAF,INRM,IAP,ICP,IXPR
      COMMON/IN/ NLIM,V1,F,R,T,FF,RHO
      COMMON/PARAMM/ ALFAM,ALFCM,RKAM,RKCMF,DM,CMTB,DELM
      COMMON/PARAMH/ALFAH2,ALFCH2,RKAH2F,RKCH2,DH,DH2,SH2,CHB,PH2B,
     1 DELH,DELH2
C     COMMON/H2/B1,C1,BC,EP,QUAD
      COMMON/M/YMA,YMC,YMCD
      COMMON/U/UMTH,UHTH,URGTH,UMGTH,UHGTH
      COMMON/CONC/CCLB,CCLSAT
      COMMON/CC/CMC,CHC,PH2C
      COMMON/FIN/FMCL,FHCL
      COMMON/ETA/ETASM,ETASH2
      COMMON/RII/RIOM,RIMA,RIMC,RIM,RI
      COMMON/RIH/RIOH2,RIH2A,RIH2C,RIH2
      COMMON/RILOG/RIMALG,RIMCLG,RIMLG,RIHALG,RIHCLG,RIHLG,RILG
      COMMON/YLG/YMLG,YHLG,YLG
      COMMON/OHM/RO,RKAPAB,ROHM,ROHMU
      COMMON/POT/VCOR,DPHDIF,DPHLJ
      COMMON/B/BAM,BCH,A
      COMMON/KK/RKKPM,RKKM,RKKPH,RKKH
      COMMON/X/XX,XXX,COMPLX
      COMMON/CMCPLX/CM2,CM3,CM4,CM5
      COMMON/RKKP/RK1P,RK2P,RK3P,RK4P
      READ 100, NLIM,NA,NC
      READ 105, HH,DELVA,DELVC
      READ 105, F,R,T
      READ 115, ALFAM,RKAM
      READ 115, CMTB,DM
      READ 115, ALFCH2,RKCH2
      READ 120, CHB,PH2B,DH,DH2,SH2
      READ 105, RPM,RNU,RHO
      READ 105, V0,V1,V1BV
      READ 135, INRM,IAP,ICP,IBVPC,IMBVPC,IRSR
      READ 130, ITAF
      READ 130, IXPR
      READ 130, M
      READ 125, COMPLX
      READ 105, UMTH,UHTH,URGTH
      READ 115, CCLB,CCLSAT
      READ 140, RK1P,RK2P,RK3P,RK4P
C
      RKAPAB=RKAPA(M,CHB)
C
      FF=F/(R*T)
      DELM=DEL(DM,RNU,RPM)
      DELH2=DEL(DH2,RNU,RPM)
      DELH=DEL(DH,RNU,RPM)
C
      CALL OHMR
      CALL ACTIVC(0.001,CHB,0.002)
```

```
      CALL ACTIVC(0.0005,0.0001,0.0006)
      CALL ACTIVC(CMTB,CHB,CCLB)
      CALL KS
C
      ALFCM=2.0-ALFAM
      ALFAH2=1.0-ALFCH2
C
      PRINT 202, NLIM,INRM,IAP,ICP
      PRINT 204, NA,NC
      PRINT 203, COMPLX
      PRINT 206, DELVA,DELVC
      PRINT 208
      PRINT 210, V0
      PRINT 212, R,F,T
      PRINT 214, M, ALFAM,ALFCM,ALFAH2,ALFCH2
      PRINT 216, RKAM,RKCMF,RKAH2F,RKCH2
      PRINT 218, DM,DH
      PRINT 220, CMTB,DH2
      PRINT 222, SH2
      PRINT 224, CHB
      PRINT 226, PH2B
      PRINT 228, RPM,RNU,RKAPAB
      PRINT 230, DELM
      PRINT 232, DELH
      PRINT 234, DELH2
      PRINT 236, RKKPM,RKKM
      PRINT 238, RKKPH,RKKH
      PRINT 240, ROHM,ROHMU
      PRINT 242, RO,A
      PRINT 250
      PRINT 255, 0.001,CHB,0.002,FMCL,FHCL
      PRINT 255, 0.0005,0.0001,0.0006,FMCL,FHCL
      PRINT 255, CMTB,CHB,CCLB,FMCL,FHCL
C
      CALL POTLJ(DPHLJ)
C
      X1=V0*FF
C
      IF(INRM.EQ.1) GO TO 1
C
      IF(ITAF.EQ.1) GO TO 10
C
      IBV=1
      X=X1
C
      CALL NRM(IBV,X,YTCORM,YTCORH,YT0,DYT)
C
      VTCOR=X/FF
      YT0LG=ALOG10(ABS(YT0))
      YTCORML=ALOG10(ABS(YTCORM))
      YTCORHL=ALOG10(ABS(YTCORH))
```

```
      CMCORT=CM(YTCORM)
      CHCORT=CH(YTCORH)
      PHCORT=PH2(YTCORH)
C
 10   CONTINUE
      IBV=0
      X=X1
C
      CALL NRM(IBV,X,YCORM,YCORH,YO,DY)
C
      VCOR=X/FF
      PDIFT=PDIF(YTCORM,YCORM)
      YOLG=ALOG10(ABS(YO))
      YCORML=ALOG10(ABS(YCORM))
      YCORHL=ALOG10(ABS(YCORH))
      CMC=CM(YCORM)
      CHC=CH(YCORH)
      PH2C=PH2(YCORH)
C
      PRINT 300
      PRINT 302
      PRINT 305, VCOR,VTCOR
      PRINT 310, YO,YOLG,YTO,YTOLG
      PRINT 320, YCORM,YCORML,YTCORM,YTCORML,PDIFT
      PRINT 330, YCORH,YCORHL,YTCORH,YTCORHL
      PRINT 340, CMC,CMCORT
      PRINT 350, CHC,CHCORT
      PRINT 360, PH2C,PHCORT
C
      CALL UJGO(CMC,CHC,PH2C,UMGO,UHGO)
      CALL IO
      PRINT 600
      PRINT 610
      PRINT 615, CMC,CHC,PH2C,CCLB,CCLSAT
      PRINT 620
      PRINT 630, UMTH,URGTH,UMGTH,UMGO,FMCL
      PRINT 630, UHTH,URGTH,UHGTH,UHGO,FHCL
      PRINT 640
      PRINT 645, RIOM,RIOH2
C
      CALL CORR(UMGO,UHGO,UCOR,UCORL,RICOR,RICORL)
      CALL SGPM(UMGO,UHGO,RK1,RKP,EXM,EXH,EXM1,EXH1,DELPM)
      PDIFL=PDIF(RICORL,YCORM)
      PDIFT=PDIF(RICOR,YCORM)
      PRINT 510
      PRINT 512, UCORL,RICORL,PDIFL
      PRINT 514, UCOR,RICOR,PDIFT
      PRINT 516
      PRINT 518, BAM,BCH,RK1,RKP
C
      PRINT 615, EXM,EXH,EXM1,EXH1,DELPM
```

```
C
      READ 130, NRP
      DO 25 K=1,NRP
      READ 125, RP
C
      RICSG=1.0/(RP*A*RK1)
      RICSGM=1.0/(RP*A*RKP)
      PDIFSG=PDIF(RICSG,YCORM)
      PDIFM=PDIF(RICSGM,YCORM)
C
      PRINT 520, RP
      PRINT 522, RICSG,PDIFSG
      PRINT 524, RICSGM,PDIFM
 25   CONTINUE
C
 1    IF(IAP.EQ.1) GO TO 2
C
C     GENERATE KINETIC-DIFFUSION POLARIZATION CURVE
C     ANODIC SWEEP
C
      PRINT 400
      PRINT 402
      PRINT 404
      PRINT 410
      PRINT 416
      PRINT 411
      PRINT 412
      PRINT 414
      PRINT 413
      PRINT 415
C
      IDUM=1
      VA=V1
      DO 50 I=1,NA
      IF (I.EQ.1) GO TO 15
      IBV=0
       VA=VA+DELVA
 15    X=FF*VA
       CALL FTNY(IBV,IDUM,X,YMAA,YH2A,YA,DY)
       YLGAS=YLG
       YMLGAS=YMLG
       YHLGAS=YHLG
C
       CMAS=CM(YMAA)
       CHAS=CH(YH2A)
       PH2AS=PH2(YH2A)
       CALL FTNMBV(VA,CMAS,CHAS,PH2AS)
       DPHDIF=DIFPOT(CMAS,CHAS,PH2AS)
      CALL OHMPOT(YA,YRA,YRUA)
      CALL UJGO(CMAS,CHAS,PH2AS,UMGO,UHGO)
      ETASM=VA-UMGO
```

```
      ETASH=VA-UHGO
      CALL VSQXFN(VA,VMA,YRA,VSQXA,VSQXMA)
      CALL VSQXFN(VA,VMA,YRUA,VSQXUA,VSQXUMA)
      CALL VSQFN(VA,VMA,YRA,VSQA,VSQMA)
      CALL VSQFN(VA,VMA,YRUA,VSQUA,VSQUMA)
C
       IF(ITAF.EQ.1) GO TO 20
C
       IBV=1
       CALL FTNY(IBV,IDUM,X,YMT,YH2T,YT,DYT)
       YTAMLG=YMLG
       YTCHLG=YHLG
C
  20   PRINT 450,VA,RI,RIM,RIMA,RIMC
       PRINT 450,VA,RI,RIH2,RIH2A,RIH2C
       PRINT 420,VA,YA,YMAA,YMT,YH2A,YH2T
       PRINT 420,VA,YLGAS,YMLGAS,YTAMLG,YHLGAS,YTCHLG
       PRINT 430,VA,CMAS,CHAS,PH2AS
       PRINT 420,VA,CMAS,CM2,CM3,CM4,CM5
       PRINT 420,VA,YA,YRA,YRUA,DPHDIF,DPHLJ
       PRINT 440,VA,ETASM,ETASH,UMGO,UHGO
       PRINT 450,VA,VSQXA,VSQXUA,VSQA,VSQUA
       PRINT 460,VMA,VSQXMA,VSQXUMA,VSQMA,VSQUMA
 50    CONTINUE
C
C
  2    IF(ICP.EQ.1) GO TO 3
C
C      GENERATE KINETIC-DIFFUSION POLARIZATION CURVE
C      CATHODIC SWEEP
C
       IDUM=1
C
       PRINT 500
       PRINT 402
       PRINT 404
       PRINT 410
       PRINT 416
       PRINT 411
       PRINT 412
       PRINT 414
       PRINT 413
       PRINT 415
C
       VC=V1
       DO 75 I=1,NC
       IF (I.EQ.1) GO TO 35
       IBV=0
        VC=VC-DELVC
  35    X=FF*VC
        CALL FTNY(IBV,IDUM,X,YMCC,YH2C,YC,DY)
```

```
C
          YMLGCS=YMLG
          YHLGCS=YHLG
          YLGCS=YLG
          CMCS=CM(YMCC)
          CHCS=CH(YH2C)
          PH2CS=PH2(YH2C)
          CALL FTNMBV(VC,CMCS,CHCS,PH2CS)
         DPHDIF=DIFPOT(CMCS,CHCS,PH2CS)
         CALL OHMPOT(YC,YRC,YRUC)
         CALL UJGO(CMCS,CHCS,PH2CS,UMGO,UHGO)
         ETASM=VC-UMGO
         ETASH=VC-UHGO
         CALL VSQXFN(VC,VMC,YRC,VSQXC,VSQXMC)
         CALL VSQXFN(VC,VMC,YRUC,VSQXUC,VSQXUMC)
         CALL VSQFN(VC,VMC,YRC,VSQC,VSQMC)
         CALL VSQFN(VC,VMC,YRUC,VSQUC,VSQUMC)
C
          IF(ITAF.EQ.1) GO TO 30
C
          IBV=1
          CALL FTNY(IBV,IDUM,X,YMT,YH2T,YT,DY)
          YTAMLG=YMLG
          YTCHLG=YHLG
C
  30     PRINT 450, VC,RI,RIM,RIMA,RIMC
         PRINT 450, VC,RI,RIH2,RIH2A,RIH2C
         PRINT 420,VC,YC,YMCC,YMT,YH2C,YH2T
         PRINT 420,VC,YLGCS,YMLGCS,YTAMLG,YHLGCS,YTCHLG
         PRINT 430,VC,CMCS,CHCS,PH2CS
         PRINT 420,VC,CMCS,CM2,CM3,CM4,CM5
         PRINT 420,VC,YC,YRC,YRUC,DPHDIF,DPHLJ
         PRINT 440,VC,ETASM,ETASH,UMGO,UHGO
         PRINT 450,VC,VSQXC,VSQXUC,VSQC,VSQUC
         PRINT 460,VMC,VSQXMC,VSQXUMC,VSQMC,VSQUMC
 75      CONTINUE
C
 3       CONTINUE
         READ 130, NCONC
         NN=NCONC+1
         DO 4000 II=1,NN
         IF (INRM.EQ.0) GO TO 1000
         READ 105, CMC,CHC,PH2C
 1000    CONTINUE
         INRM=1
         IF (IBVPC.EQ.1) GO TO 2000
C
C        GENERATE B-V POLARIZATION CURVE
C
         CALL UJGO(CMC,CHC,PH2C,UMGO,UHGO)
         CALL IO
```

```
      PRINT 600
      PRINT 610
      PRINT 615, CMC,CHC,PH2C,CCLB,CCLSAT
      PRINT 620
      PRINT 630, UMTH,URGTH,UMGTH,UMG0,FMCL
      PRINT 630, UHTH,URGTH,UHGTH,UHG0,FHCL
      PRINT 640
      PRINT 645, RI0M,RI0H2
C
C     ANODIC SWEEP FROM THE CORROSION POTENTIAL
C
      PRINT 650
      PRINT 710
      PRINT 655
      V=V1BV
      CALL FTNBV(V)
      PRINT 660, V,RI,RIM,RIMA,RIMC,ETASM
      PRINT 660, V,RILG,RIMLG,RIMALG,RIMCLG,ETASM
      PRINT 680, V,RI,RIH2,RIH2A,RIH2C,ETASH2
      PRINT 680, V,RILG,RIHLG,RIHALG,RIHCLG,ETASH2
      DO 80 I=2,NA
      V=V+DELVA
      CALL FTNBV(V)
      PRINT 660, V,RI,RIM,RIMA,RIMC,ETASM
      PRINT 660, V,RILG,RIMLG,RIMALG,RIMCLG,ETASM
      PRINT 680, V,RI,RIH2,RIH2A,RIH2C,ETASH2
      PRINT 680, V,RILG,RIHLG,RIHALG,RIHCLG,ETASH2
 80   CONTINUE
C
C     CATHODIC SWEEP FROM THE CORROSION POTENTIAL
C
      PRINT 650
      PRINT 720
      PRINT 655
      V=V1BV
      CALL FTNBV(V)
      PRINT 660, V,RI,RIM,RIMA,RIMC,ETASM
      PRINT 660, V,RILG,RIMLG,RIMALG,RIMCLG,ETASM
      PRINT 680, V,RI,RIH2,RIH2A,RIH2C,ETASH2
      PRINT 680, V,RILG,RIHLG,RIHALG,RIHCLG,ETASH2
      DO 85 I=2,NC
      V=V-DELVC
      CALL FTNBV(V)
      PRINT 660, V,RI,RIM,RIMA,RIMC,ETASM
      PRINT 660, V,RILG,RIMLG,RIMALG,RIMCLG,ETASM
      PRINT 680, V,RI,RIH2,RIH2A,RIH2C,ETASH2
      PRINT 680, V,RILG,RIHLG,RIHALG,RIHCLG,ETASH2
 85   CONTINUE
 2000 IF (IMBVPC.EQ.1) GO TO 3000
C
C     GENERATE MODIFIED B-V POLARIZATION CURVES
```

```
C
      CALL UJGO(CMC,CHC,PH2C,UMGO,UHGO)
      CALL IO
      PRINT 600
      PRINT 610
      PRINT 615, CMC,CHC,PH2C,CCLB,CCLSAT
      PRINT 620
      PRINT 630, UMTH,URGTH,UMGTH,UMGO,FMCL
      PRINT 630, UHTH,URGTH,UHGTH,UHGO,FHCL
      PRINT 640
      PRINT 645, RIOM,RIOH2
C
C     ANODIC SWEEP FROM THE CORROSION POTENTIAL
C
      PRINT 700
      PRINT 710
      PRINT 655
C     V=V1BV
      CALL FTNMBV(V,CMC,CHC,PH2C)
      PRINT 660, V,RI,RIM,RIMA,RIMC,ETASM
      PRINT 660, V,RILG,RIMLG,RIMALG,RIMCLG,ETASM
      PRINT 680, V,RI,RIH2,RIH2A,RIH2C,ETASH2
      PRINT 680, V,RILG,RIHLG,RIHALG,RIHCLG,ETASH2
      DO 90 I=2,NA
      V=V+DELVA
      CALL FTNMBV(V,CMC,CHC,PH2C)
      PRINT 660, V,RI,RIM,RIMA,RIMC,ETASM
      PRINT 660, V,RILG,RIMLG,RIMALG,RIMCLG,ETASM
      PRINT 680, V,RI,RIH2,RIH2A,RIH2C,ETASH2
      PRINT 680, V,RILG,RIHLG,RIHALG,RIHCLG,ETASH2
 90   CONTINUE
C
C     CATHODIC SWEEP FROM THE CORROSION POTENTIAL
C
      PRINT 700
      PRINT 720
      PRINT 655
C     V=V1BV
      CALL FTNMBV(V,CMC,CHC,PH2C)
      PRINT 660, V,RI,RIM,RIMA,RIMC,ETASM
      PRINT 660, V,RILG,RIMLG,RIMALG,RIMCLG,ETASM
      PRINT 680, V,RI,RIH2,RIH2A,RIH2C,ETASH2
      PRINT 680, V,RILG,RIHLG,RIHALG,RIHCLG,ETASH2
      DO 95 I=2,NC
      V=V-DELVC
      CALL FTNMBV(V,CMC,CHC,PH2C)
      PRINT 660, V,RI,RIM,RIMA,RIMC,ETASM
      PRINT 660, V,RILG,RIMLG,RIMALG,RIMCLG,ETASM
      PRINT 680, V,RI,RIH2,RIH2A,RIH2C,ETASH2
      PRINT 680, V,RILG,RIHLG,RIHALG,RIHCLG,ETASH2
 95   CONTINUE
```

```
 3000   CONTINUE
 4000   CONTINUE
C
        IF (IRSR.EQ.1)  GO TO 4
        PRINT 750
        PRINT 240, ROHM,ROHMU
        PRINT 752
        VDIF=-0.60
        DO 40 I=1,40
        VDIF=VDIF+0.04
        CALL IRSCAN(YCORM,VDIF,ROHM,ROHMU,RPP,ERROR,ERRORU)
        PRINT 755, VDIF,RPP,ERROR,ERRORU
 40     CONTINUE
 4      CONTINUE
C
C       READ FORMATS
C
 100    FORMAT(3I3)
 105    FORMAT(6(1PE10.3))
 110    FORMAT(7(1PE10.3))
 115    FORMAT(2(1PE10.3))
 120    FORMAT(5(1PE10.3))
 125    FORMAT(1PE10.3)
 130    FORMAT(I2)
 135    FORMAT(6I2)
 140    FORMAT(4(1PE10.3))
C
C       PRINT FORMATS
C
 200    FORMAT(1H ,*PROGRAM FIRST IS FOR */(3X,*1.  THE DETERMINATION
     1OF THE CORROSION POTENTIAL*)/(3X,*2.  THE GENERATION OF A METAL
     2DISSOLUTION/HYDROGEN EVOLUTION POLARIZATION CURVE*))
C
 202    FORMAT(1H ,/*PROGRAM PARAMETERS*/(1X,*NRM-    NLIM= *,I2)/(10X,*
     1INRM, IAP, ICP= 0 OR 1*)
     2/(10X,*INRM= *,I2,3X,*IAP= *,I2,3X,*ICP= *,I2)/
     3/(1X,*FTNY-    IDUM= 0 OR 1     [1 IMPLIES THAT SECTION OF PROGRAM
     4 IS BYPASSED]*))
C
 203    FORMAT(1H ,/*COMPLX=*,F3.1,/*  [0.0 IMPLIES CALCULATIONS WITH
     1 COMPLEXING ARE NOT MADE]*)
 204    FORMAT(1H ,/*NUMBER OF POLARIZATION POINTS,  NA= *,I2,*    NC= *,
     1I2)
C
 206    FORMAT(1H ,/*POLARIZATION MESH SIZE,  DELVA= *,F6.3,*   DELVC= *
     1,F6.3)
C
 208    FORMAT(1H ,/*RATE CONSTANTS FOR BACK RXNS,   RKCM=0,    RKAH2=0,
     1      FOR TAFEL APPROXIMATION*)
C
 210    FORMAT(1H ,/*CORROSION POTENTIAL INTIAL GUESS,   V0= *,F6.3)
```

```
C
 212    FORMAT(1H ,/*PHYSICAL PARAMETERS*/(1X,*R= *,1PE10.3,4X,*F= *,
     1E10.3,4X,*T= *,E10.3))
C
 214    FORMAT(1H ,/*M.DATA     M= 1, 2, OR 3*/(12X,*1.  CU IN H2SO4*)
     1/(12X,*2.  ZN IN HCL*)//
     2(20X,*M= *,I2,20X,*H2*)//(1X,*ALF  A&C= *
     3,4F10.4))
C
 216    FORMAT(1H ,*RK   A&C= *,4(1PE10.3))
C
 218    FORMAT(17H             DM= ,1PE10.3,6X,*DH= *,E10.3)
 220    FORMAT(17H           CMTB= ,1PE10.3,6X,*DH2= *,E10.3)
 222    FORMAT(33X,*SH2= *,1PE10.3)
 224    FORMAT(33X,*CHB= *,1PE10.3)
 226    FORMAT(33X,*PH2B= *,1PE10.3)
 228    FORMAT(1H ,/*RPM= *,F8.2,2X,*RNU= *,1PE10.3,2X,*RKAPAB= *,E10.3)
 230    FORMAT(1H ,/*CALCULATIONS*,//7H DELM= ,1PE15.6)
 232    FORMAT(7H DELH= ,1PE15.6)
 234    FORMAT(8H DELH2= ,1PE15.6/)
 236    FORMAT(1H ,/*RKKPM= *,1PE10.3,2X,*RKKM= *,E10.3)
 238    FORMAT(1H ,/*RKKPH= *,1PE10.3,2X,*RKKH= *,E10.3)
 240    FORMAT(1H ,/*ROHM=*,1PE10.3,2X,*ROHMU=*,E10.3)
 242    FORMAT(1H ,/*RO=*,1PE10.3,2X,*A=*,E10.3)
 249    FORMAT(1H ,/*    ACTIVITY COEFFICIENTS *)
 250    FORMAT(1H ,/*     CM        CH        CCL        FMCL
     1 FHCL *)
 255    FORMAT(1H ,5(1PE10.3))
C
 300    FORMAT(1H ,//*CORROSION POTENTIAL, CURRENT AND CONCENTRATIONS*)
 302    FORMAT(1H ,/10X,*BUTLER-VOLMER*,20X,*TAFEL*)
 305    FORMAT(7H VCOR= ,F10.8,F20.8)
 310    FORMAT(7H ITOT= ,4(1PE15.6))
 320    FORMAT(8H ICORM= ,5(1PE15.6))
 330    FORMAT(8H ICORH= ,4(1PE15.6)/)
 340    FORMAT(8H CMCOR= ,2(1PE15.6))
 350    FORMAT(8H CHCOR= ,2(1PE15.6))
 360    FORMAT(9H PH2COR= ,2(1PE15.6)//)
 400    FORMAT(1H ,/*GENERATION OF ANODIC KINETIC-DIFFUSION POLARIZATION
     1 CURVE * )
 402    FORMAT(1H ,/*   V    RI       RIM       RIMA       RIMC *)
 404    FORMAT(1H ,*   V    RI       RIH2      RIH2A      RIH2C *)
 410    FORMAT(1H ,*   V    INET      IM       IMTA      IH2     IH2TC*)
 411    FORMAT(1H ,*   V    CM        CH        PH2 *)
 412    FORMAT(1H ,*   V    INET      IR        IRU       DPHDIF
     1DPHLJ *)
 413    FORMAT(1H ,*   V    VSQX      VSQXU     VSQ       VSQU *)
 414    FORMAT(1H ,*   V    ETASM     ETASH     UMGO      UHGO *)
 415    FORMAT(1H ,*   VM   VSQXM     VSQXUM    VSQM      VSQUM *)
 416    FORMAT(1H ,*   V    YLG       YMLG      YTAMLG    YHLG    YTCHLG
     1 *)
```

```
 420    FORMAT(1H , F6.3,5(1PE10.3))
 430    FORMAT(1H , F6.3,3(1PE10.3))
 440    FORMAT(1H , 3F6.3,2(1PE10.3))
 450    FORMAT(1H , F6.3,4(1PE10.3))
 460    FORMAT(1H , F6.3,4(1PE10.3)/)
 500    FORMAT(1H ,///*GENERATION OF KINETIC-DIFF POLARIZATION CURVE*/
     1 * CATHODIC SWEEP * )
C
 510    FORMAT(1H ,/*      CORROSION-CURRENT CALCULATIONS*//
     1 *        LINEAR APPROXIMATION*)
 512    FORMAT(1H ,*  UCORL=*,1PE10.3,5X,*RICORL=*,1PE10.3,5X,*PDIFL=*,
     1  1PE10.3)
 514    FORMAT(1H ,/*        TAFEL APPROXIMATION*/
     1 *  UCOR=*,1PE10.3,5X,*RICOR=*,1PE10.3,5X,*PDIFT=*,1PE10.3)
 516    FORMAT(1H ,/*     STERN-GEARY POLARIZATION METHODS*)
 518    FORMAT(1H ,/*BAM=*,1PE10.3,5X,*BCH=*,1PE10.3,//
     1 *RK1=*,1PE10.3,5X,*RKP=*,1PE10.3)
 520    FORMAT(1H ,/*RP OR RT=*,1PE10.3)
 522    FORMAT(1H ,/*S-G;                RICSG=*,1PE10.3,5X,*PDIFSG=*,
     1  1PE10.3)
 524    FORMAT(1H ,*S-G, MODIFICATION;  RICSGM=*,1PE10.3,5X,*PDIFM=*,
     1   1PE10.3)
C
 600    FORMAT(1H ,/1H ,*DATA FOR BUTLER-VOLMER AND MODIFIED B-V KINETIC
     1 POLARIZATION CURVES*)
 610    FORMAT(1H ,/1H ,*    CMC       CHC         PH2C         CCLB
     1CCLSAT*,/)
 615    FORMAT(1H ,5(1PE10.3))
 620    FORMAT(1H ,/1H ,*    UJTH    URGTH    UJGTH     UJGO
     1FIN*,/)
 630    FORMAT(1H ,5(1PE10.3))
 640    FORMAT(1H ,/1H ,*    RIOM      RIOH2*)
 645    FORMAT(1H ,2(1PE10.3 ))
 650    FORMAT(1H1,/1H ,*  GENERATION OF THE B-V KINETIC POLARIZATION
     1CURVE*)
 655    FORMAT(1H ,/*           V       INET        I         IA
     1IC     ETA*)
 660    FORMAT(1H ,*ZINC    *,F6.3,4(1PE10.3),0PF6.3)
 680    FORMAT(1H ,*HYDROGEN*,F6.3, 4(1PE10.3),0PF6.3)
 700    FORMAT(1H1,/1H ,*GENERATION OF MODIFIED BUTLER-VOLMER KINETIC
     1POLARIZATION CURVES*)
 710    FORMAT(1H ,*       ANODIC SWEEP*)
 720    FORMAT(1H ,*       CATHODIC SWEEP*)
 750    FORMAT(1H ,/*EFFECT OF IR ON SCAN RATE*)
 752    FORMAT(1H ,//*   VDIF     RPP     ERROR      ERRORU  */)
 755    FORMAT(1H ,4(1PE10.3))
        STOP
        END
C
        SUBROUTINE NRM(IBV,X,YM,YH2,Y,DY)
        COMMON/I/ ITAF,INRM,IAP,ICP,IXPR
```

```
      COMMON/IN/ NLIM,V1,F,R,T,FF,RHO
C     COMMON/H2/B1,C1,BC,EP,QUAD
      COMMON/M/YMA,YMC,YMCD
C
      N=1
      PRINT 800, IBV
      PRINT 805
      PRINT 810, N,V1
C
      DO 50 N=2,NLIM
       IDUM=0
       CALL FTNY(IBV,IDUM,X,YM,YH2,Y,DY)
       X=X-(Y/DY)
       V=X/FF
       PRINT 820, N,V,Y,YM,YH2,DY
  50  CONTINUE
C
C
 800  FORMAT(1H ,/*CORROSION POTENTIAL DETERMINATION*/(1X,*NRM
     1 ITERATIONS      IBV= *,I2))
 805  FORMAT(1H ,//*  N      V                INET                IM
     1           IH2               DI*)
 810  FORMAT(1H ,I2,F14.10)
 820  FORMAT(1H ,I2,F14.10,4(1PE18.10))
C
C
      RETURN
      END
C
C
      SUBROUTINE FTNY(IBV,IDUM,X,YM,YH2,Y,DY)
      COMMON/I/ ITAF,INRM,IAP,ICP,IXPR
      COMMON/IN/ NLIM,V1,F,R,T,FF,RHO
      COMMON/PARAMM/ ALFAM,ALFCM,RKAM,RKCMF,DM,CMTB,DELM
      COMMON/PARAMH/ALFAH2,ALFCH2,RKAH2F,RKCH2,DH,DH2,SH2,CHB,PH2B
     1              ,DELH,DELH2
C     COMMON/H2/B1,C1,BC,EP,QUAD
      COMMON/M/YMA,YMC,YMCD
      COMMON/YLG/YMLG,YHLG,YLG
      COMMON/CONC/CCLB,CCLSAT
      COMMON/X/XX,XXX,COMPLX
      COMMON/CMCPLX/CM2,CM3,CM4,CM5
      COMMON/RKKP/RK1P,RK2P,RK3P,RK4P
C
      RKCM=RKCMF
      RKAH2=RKAH2F
C
      IF (IBV.EQ.0) GO TO 10
C
      RKCM=0.0
      RKAH2=0.0
```

```
C
 10     CONTINUE
C
C       FTN YM(IBV,X)
C
C       COMPLX=0.0 FOR NO COMPLEXING, COMPLEX=1.0 FOR COMPLEXING
C
        RK1P=RK1P*COMPLX
        CCLBP=CCLB*1000.0
        CCL=CCLBP/RHO
        XX=CCL*(RK1P+RK1P*RK2P*CCL+RK1P*RK2P*RK3P*CCL**2
     1     +RK1P*RK2P*RK3P*RK4P*CCL**3)
        XXX=1.0/(XX+1.0)
C
        CMB=CMTB* XXX
        YMA=2.0*F*RKAM*EXP(ALFAM*X)
        YMC=-2.0*F*CMB*RKCM*EXP(-ALFCM*X)
C       YMCD=(DELM/DM)*RKCM*EXP(-ALFCM*X)
C
        YMCD= XXX *(DELM/DM)*RKCM*EXP(-ALFCM*X)
C
        YM=(YMA+YMC)/(1.0+YMCD)
C
C
C       FTN YH2(IBV,X)
C
        DD=DELH2/DH2
        A1H2=2.0*RKCH2*DD*EXP(-ALFCH2*X)
        A2H2=(RKCH2*DD)**2*EXP(-2.0*ALFCH2*X)
        A2=1.0+A1H2+A2H2
C
        B1H2C=2.0*F*RKCH2*CHB*EXP(-ALFCH2*X)
        B1H2A=((F*(RKAH2**2))*DELH2/(2.0*DH2*SH2))*EXP(2.0*ALFAH2*X)
        B2H2C=2.0*F*(RKCH2**2)*CHB*DD*EXP(-2.0*ALFCH2*X)
C       B1=B1H2A+B1H2C
        B2=B1H2A+B1H2C+B2H2C
C
        C1H2A=-PH2B*((F*RKAH2)**2)*EXP(2.0*ALFAH2*X)
        C1H2C=((F*RKCH2*CHB)**2)*EXP(-2.0*ALFCH2*X)
        C1=C1H2A+C1H2C
C
C       BC=B1*B1-4.0*C1
C       QUAD=0.0
        QUAD2=0.0
        IF (IBV.EQ.1) GO TO 20
C       EP=2.0*B1H2C*B1H2A+B1H2A**2+4.0*(-C1H2A)
        EP2=B1H2A**2+2.0*B1H2C*B1H2A
     1     +2.0*B1H2A*B2H2C-4.0*(C1H2A+A1H2*C1H2A
     2     +A2H2*C1H2A)
C       QUAD=SQRT(EP)
        QUAD2=SQRT(EP2)
```

```
C
 20     CONTINUE
C
C       YH2=(-2.0*C1)/(B1+QUAD)
        YH2=(-2.0*C1)/(B2+QUAD2)
C
C       FTN Y(IBV,X,)
C
        Y=YM+YH2
C
        YMLG=ALOG10(ABS(YM))
        YHLG=ALOG10(ABS(YH2))
        YLG=ALOG10(ABS(Y))
C
        IF(IXPR.EQ.1) GO TO 40
C
        PRINT 900, B1,C1,BC,QUAD,YH2
        PRINT 910, YMA,YMC,YMCD,YM
C
 900    FORMAT(1H ,*B1=*,1PE20.12,3X,*C1=*,E20.12,3X,*BC=*,E20.12,3X,
     1  *QUAD=*,E15.6,3X,*YH2=*,E15.6)
 910    FORMAT(1H ,*YMA=*,1PE15.6,3X,*YMC=*,E15.6,3X,*YMCD=*,E15.6,3X,
     1  *YM=*,E15.6)
C
 40     IF(IDUM.EQ.1) RETURN
C
C       FTN DY(IBV,X,)
C
        DYMA=ALFAM*YMA
        DYMC=ALFCM*YMC
        DYMCD=-ALFCM*YMCD
C
        DYM=((1.0+YMCD)*(DYMA+DYMC)-(YMA+YMC)*DYMCD)/(1.0+YMCD)**2
C
        DC1=-2.0*ALFCH2*C1H2C-2.0*ALFAH2*C1H2A
C       DB1=-ALFCH2*B1H2C+2.0*ALFAH2*B1H2A
        DB2=-ALFCH2*B1H2C+2.0*ALFAH2*B1H2A-2.0*ALFCH2*B2H2C
        DA2=-ALFCH2*A1H2-2.0*ALFCH2*A2H2
        DA2C1=A2*DC1+C1*DA2
C
C       DQUAD=0.0
        DQUAD2=0.0
        IF (IBV.EQ.1) GO TO 30
C       DQUAD=0.5*(QUAD**(-0.5))*(2.0*B1*DB1-4.0*DC1)
        DQUAD2=0.5*(QUAD2**(-1.0))*(2.0*B2*DB2-4.0*DA2C1)
 30     CONTINUE
C
C       DYH2=(-(B1+QUAD)*2.0*DC1+2.0*C1*(DB1+DQUAD))/(B1+QUAD)**2
        DYH2=(-(B2+QUAD2)*2.0*DC1+2.0*C1*(DB2+DQUAD2))/(B2+QUAD2)**2
C
        DY=DYM+DYH2
```

```
C
      RETURN
      END
C
      SUBROUTINE FTNBV(V)
      COMMON/I/ ITAF,INRM,IAP,ICP,IXPR
      COMMON/IN/ NLIM,V1,F,R,T,FF,RHO
      COMMON/PARAMM/ ALFAM,ALFCM,RKAM,RKCMF,DM,CMTB,DELM
      COMMON/PARAMH/ALFAH2,ALFCH2,RKAH2F,RKCH2,DH,DH2,SH2,CHB,PH2B
     1              ,DELH,DELH2
C     COMMON/H2/B1,C1,BC,EP,QUAD
      COMMON/M/YMA,YMC,YMCD
      COMMON/U/UMTH,UHTH,URGTH,UMGTH,UHGTH
      COMMON/CONC/CCLB,CCLSAT
      COMMON/CC/CMC,CHC,PH2C
      COMMON/FIN/FMCL,FHCL
      COMMON/ETA/ETASM,ETASH2
      COMMON/RII/RIOM,RIMA,RIMC,RIM,RI
      COMMON/RIH/RIOH2,RIH2A,RIH2C,RIH2
      COMMON/RILOG/RIMALG,RIMCLG,RIMLG,RIHALG,RIHCLG,RIHLG,RILG
C
      RKCM=RKCMF
      RKAH2=RKAH2F
C
      CALL UJGO(CMC,CHC,PH2C,UMGO,UHGO)
      ETASM=V-UMGO
      RIMA=RIOM*EXP(ALFAM*FF*ETASM)
      RIMC=-RIOM*EXP(-ALFCM*FF*ETASM)
      RIM=RIMA+RIMC
C
      ETASH2=V-UHGO
      RIH2A=RIOH2*EXP(ALFAH2*FF*ETASH2)
      RIH2C=-RIOH2*EXP(-ALFCH2*FF*ETASH2)
      RIH2=RIH2A+RIH2C
C
      RI=RIM+RIH2
C
      RIMALG=ALOG10(ABS(RIMA))
      RIMCLG=ALOG10(ABS(RIMC))
      RIMLG=ALOG10(ABS(RIM))
      RIHALG=ALOG10(ABS(RIH2A))
      RIHCLG=ALOG10(ABS(RIH2C))
      RIHLG=ALOG10(ABS(RIH2))
      RILG=ALOG10(ABS(RI))
      RETURN
      END
C
C
      SUBROUTINE FTNMBV(V,CMC,CHC,PH2C)
      COMMON/I/ ITAF,INRM,IAP,ICP,IXPR
      COMMON/IN/ NLIM,V1,F,R,T,FF,RHO
```

```
      COMMON/PARAMM/ ALFAM,ALFCM,RKAM,RKCMF,DM,CMTB,DELM
      COMMON/PARAMH/ALFAH2,ALFCH2,RKAH2F,RKCH2,DH,DH2,SH2,CHB,PH2B
     1              ,DELH,DELH2
C     COMMON/H2/B1,C1,BC,EP,QUAD
      COMMON/M/YMA,YMC,YMCD
      COMMON/U/UMTH,UHTH,URGTH,UMGTH,UHGTH
      COMMON/CONC/CCLB,CCLSAT
      COMMON/FIN/FMCL,FHCL
      COMMON/ETA/ETASM,ETASH2
      COMMON/RII/RIOM,RIMA,RIMC,RIM,RI
      COMMON/RIH/RIOH2,RIH2A,RIH2C,RIH2
      COMMON/RILOG/RIMALG,RIMCLG,RIMLG,RIHALG,RIHCLG,RIHLG,RILG
C
 10   CONTINUE
C
      RKCM=RKCMF
      RKAH2=RKAH2F
C
      CALL UJGO(CMC,CHC,PH2C,UMGO,UHGO)
      ETASM=V-UMGO
      RIMA=2.0*F*RKAM*EXP(ALFAM*FF*V)
      RIMC=-2.0*F*RKCM*CMC*EXP(-ALFCM*FF*V)
      RIM=RIMA+RIMC
C
      ETASH2=V-UHGO
      RIH2A=F*RKAH2*PH2C**(1.0/2.0)*EXP(ALFAH2*FF*V)
      RIH2C=-F*RKCH2*CHC*EXP(-ALFCH2*FF*V)
      RIH2=RIH2A+RIH2C
C
      RI=RIM+RIH2
C
      RIMALG=ALOG10(ABS(RIMA))
      RIMCLG=ALOG10(ABS(RIMC))
      RIMLG=ALOG10(ABS(RIM))
      RIHALG=ALOG10(ABS(RIH2A))
      RIHCLG=ALOG10(ABS(RIH2C))
      RIHLG=ALOG10(ABS(RIH2))
      RILG=ALOG10(ABS(RI))
      RETURN
      END
C
      FUNCTION CM(YM)
      COMMON/IN/ NLIM,V1,F,R,T,FF,RHO
      COMMON/PARAMM/ ALFAM,ALFCM,RKAM,RKCMF,DM,CMTB,DELM
      COMMON/CONC/CCLB,CCLSAT
      COMMON/X/XX,XXX,COMPLX
      COMMON/CMCPLX/CM2,CM3,CM4,CM5
      COMMON/RKKP/RK1P,RK2P,RK3P,RK4P
C
C     CM IS ZINC ++ ION CONCENTRATION AT THE SURFACE
C     CMTB IS TOTAL ZINC CONCENTRATION IN THE BULK
```

```
C       CMB IS ZINC ++ ION CONCENTRATION IN THE BULK
C
        CCLBP=1000.0*CCLB
        RK1P=RK1P*COMPLX
C
        CM= XXX *(CMTB+(YM*DELM)/(2.0*F*DM))
C
        CM2=RK1P*CM*CCLBP/RHO
        CM3=RK1P*RK2P*CM*(CCLBP/RHO)**2
        CM4=RK1P*RK2P*RK3P*CM*(CCLBP/RHO)**3
        CM5=RK1P*RK2P*RK3P*RK4P*CM*(CCLBP/RHO)**4
C
        RETURN
        END
C
C
C
C
        FUNCTION CH(YH2)
        COMMON/IN/ NLIM,V1,F,R,T,FF,RHO
        COMMON/PARAMH/ALFAH2,ALFCH2,RKAH2F,RKCH2,DH,DH2,SH2,CHB,PH2B
     1  ,DELH,DELH2
C
C       USE LATER WHEN CH DOES NOT EQUAL CHB
        CH=CHB+YH2*DELH/(F*DH)
C
C       CH=CHB
C
        RETURN
        END
C
C
        FUNCTION PH2(YH2)
        COMMON/IN/ NLIM,V1,F,R,T,FF,RHO
        COMMON/PARAMH/ALFAH2,ALFCH2,RKAH2F,RKCH2,DH,DH2,SH2,CHB,PH2B,DEL
     1  ,DELH2
C
        PH2=PH2B-YH2*DELH2/(2.0*F*DH2*SH2)
C
        RETURN
        END
C
C
        FUNCTION DEL(D,RNU,RPM)
C
        ROT=RPM*2.0*3.14159/60.0
C
        DEL=1.6117*(D**(1.0/3.0))*(RNU**(1.0/6.0))/SQRT(ROT)
C
        RETURN
        END
```

```
C
      SUBROUTINE KS
      COMMON/IN/ NLIM,V1,F,R,T,FF,RHO
      COMMON/PARAMM/ ALFAM,ALFCM,RKAM,RKCMF,DM,CMTB,DELM
      COMMON/PARAMH/ALFAH2,ALFCH2,RKAH2F,RKCH2,DH,DH2,SH2,CHB,PH2B,
     1 DELH,DELH2
      COMMON/U/UMTH,UHTH,URGTH,UMGTH,UHGTH
      COMMON/CONC/CCLB,CCLSAT
      COMMON/FIN/FMCL,FHCL
      COMMON/KK/RKKPM,RKKM,RKKPH,RKKH
      UMGTH=UMTH-URGTH
      RLKKPM=2.0*FF*UMGTH+2.0*ALOG(CCLSAT*1000.0/RHO)
      RKKPM=EXP(RLKKPM)
      RKKM=RKKPM*1000.0*FMCL/RHO
      RKCMF=RKAM*RKKM
C
      UHGTH=UHTH-URGTH
      RLKKPH=FF*UHGTH+ALOG(CCLSAT*1000.0/RHO)
      RKKPH=EXP(RLKKPH)
      RKKH=RKKPH*1000.0*FHCL/RHO
      RKAH2F=RKCH2/RKKH
      RETURN
      END
C
      SUBROUTINE UJGO(CMO,CHO,PH2O,UMGO,UHGO)
      COMMON/IN/ NLIM,V1,F,R,T,FF,RHO
      COMMON/U/UMTH,UHTH,URGTH,UMGTH,UHGTH
      COMMON/CONC/CCLB,CCLSAT
      COMMON/CC/CMC,CHC,PH2C
      COMMON/FIN/FMCL,FHCL
C
      UMGTH=UMTH-URGTH
C     FMCL=1.0
      UMGO=UMGTH + (1.0/(2.0*FF))*
     1      ALOG( (CMO*1000.0*((CCLSAT*1000.0)**2)*FMCL)/(RHO**3) )
C
      UHGTH=UHTH-URGTH
C     FHCL=1.0
      UHGO=UHGTH+(1.0/FF)
     1      *ALOG ( (CHO*1000.*CCLSAT*1000.*FHCL)/(RHO**2) )
     2      -(1.0/(FF*2.0))*ALOG(PH2O)
C
      RETURN
      END
C
      SUBROUTINE IO
      COMMON/IN/ NLIM,V1,F,R,T,FF,RHO
      COMMON/PARAMM/ ALFAM,ALFCM,RKAM,RKCMF,DM,CMTB,DELM
      COMMON/PARAMH/ALFAH2,ALFCH2,RKAH2F,RKCH2,DH,DH2,SH2,CHB,PH2B,
     1 DELH,DELH2
      COMMON/CC/CMC,CHC,PH2C
```

```
      COMMON/FIN/FINM,FINH2
      COMMON/RII/RIOM,RIMA,RIMC,RIM,RI
      COMMON/RIH/RIOH2,RIH2A,RIH2C,RIH2
C
      RKCM=RKCMF
      RKAH2=RKAH2F
      RIOM=2.0*F*RKAM**(ALFCM/2.0)*RKCM**(ALFAM/2.0)
     1       *CMC**(ALFAM/2.0)
C
      RIOH2=1.0*F*RKAH2**(ALFCH2/1.0)*RKCH2**(ALFAH2/1.0)
     1            *PH2C**(ALFCH2/(2.0*1.0))
     2            *CHC**(ALFAH2/1.0)
C
      RETURN
      END
C
      FUNCTION RKAPA(M,CHB)
      RLAMH=349.8
      RLAMCL=76.34
      RLAMSO=80.0
      RKAPA=CHB*(RLAMH+RLAMCL)
      IF (M.EQ.2) GO TO 20
      RKAPA=2.0*CHB*(RLAMH+RLAMSO)
 20   CONTINUE
      RETURN
      END
C
      SUBROUTINE POTLJ(DPHLJ)
      COMMON/CONC/CCLB,CCLSAT
      COMMON/IN/ NLIM,V1,F,R,T,FF,RHO
      COMMON/PARAMM/ ALFAM,ALFCM,RKAM,RKCMF,DM,CMTB,DELM
      COMMON/PARAMH/ALFAH2,ALFCH2,RKAH2F,RKCH2,DH,DH2,SH2,CHB,PH2B,
     1  DELH,DELH2
      DK=0.00001957
      DCL=0.00002032
      CM1=CMTB
      CM2=0.0
      CH1=CHB
      CH2=0.001
      CCL1=CCLB
      CCL2=CCLSAT
      CK1=0.0
      CK2=CCLSAT
C
      A=2.0*DM*(CM1-CM2)+DH*(CH1-CH2)-DCL*(CCL1-CCL2)+DK*(CK1-CK2)
      B1=4.0*DM*CM1+DH*CH1+DCL*CCL1+DK*CK1
      B2=4.0*DM*CM2+DH*CH2+DCL*CCL2+DK*CK2
C
      DPHLJ=-(R*T/F)*A*ALOG(B1/B2)/(B1-B2)
C
      RETURN
```

```
      END
C
      FUNCTION DIFPOT(CM0,CH0,PH20)
      COMMON/OHM/R0,RKAPAB,ROHM,ROHMU
      COMMON/CONC/CCLB,CCLSAT
      COMMON/IN/ NLIM,V1,F,R,T,FF,RHO
      COMMON/PARAMM/ ALFAM,ALFCM,RKAM,RKCMF,DM,CMTB,DELM
      COMMON/PARAMH/ALFAH2,ALFCH2,RKAH2F,RKCH2,DH,DH2,SH2,CHB,PH2B,
     1 DELH,DELH2
      COMMON/RKKP/RK1P,RK2P,RK3P,RK4P
      COMMON/X/XX,XXX,COMPLX
C
      CCL0=CCLB
      DCL=0.00002032
C
C     DIFPOT=(F/RKAPAB)*(2.0*DM*(CMB-CM0)+DH*(CHB-CH0)-DCL
C    1          *(CCLB-CCL0))
C
C     COMPLX=0.0 FOR NO COMPLEXING
C
      RK1P= COMPLX *RK1P
      CMB=CMTB*XXX
      CCLBP=CCLB*1000.0
      DIFPOT=(F/RKAPAB)*DM*(CMB-CM0)*
     1        (2.0+RK1P*CCLBP/RH0
     2         -RK1P*RK2P*RK3P*(CCLBP/RH0)**3
     3         -2.0*RK1P*RK2P*RK3P*RK4P*(CCLBP/RH0)**4)
     4        +(F/RKAPAB)*(DH*(CHB-CH0)-DCL*(CCLB-CCL0))
      RETURN
      END
C
      SUBROUTINE VSQFN(V,VM,YR,VSQ,VSQM)
      COMMON/POT/VCOR,DPHDIF,DPHLJ
      VM=V-VCOR
      VSQ=V+YR+DPHDIF+DPHLJ
      VSQM=VSQ-VCOR
      RETURN
      END
C
      SUBROUTINE VSQXFN(V,VM,YR,VSQX,VSQXM)
      COMMON/POT/VCOR,DPHDIF,DPHLJ
      VM=V-VCOR
      VSQX=V+YR
      VSQXM=VSQX-VCOR
      RETURN
      END
C
      SUBROUTINE OHMR
      COMMON/B/BAM,BCH,A
      COMMON/OHM/R0,RKAPAB,ROHM,ROHMU
      R0=0.25
```

```
      PI=3.141069
      A=PI*RO**2
      ROHM=1.0/(4.0*RKAPAB*RO)
      ROHMU=ROHM*4.0/PI
      RETURN
      END
C
      SUBROUTINE OHMPOT(Y,DPHOHM,DPHOMU)
      COMMON/B/BAM,BCH,A
      COMMON/OHM/RO,RKAPAB,ROHM,ROHMU
      DPHOHM=Y*A*ROHM
      DPHOMU=Y*A*ROHMU
      RETURN
      END
C
      SUBROUTINE CORR(UMGO,UHGO,UCOR,UCORL,RICOR,RICORL)
      COMMON/PARAMM/ ALFAM,ALFCM,RKAM,RKCMF,DM,CMTB,DELM
      COMMON/PARAMH/ALFAH2,ALFCH2,RKAH2F,RKCH2,DH,DH2,SH2,CHB,PH2B,
     1  DELH,DELH2
      COMMON/IN/ NLIM,V1,F,R,T,FF,RHO
      COMMON/RII/RIOM,RIMA,RIMC,RIM,RI
      COMMON/RIH/RIOH2,RIH2A,RIH2C,RIH2
      UCOR=(ALFAM*UMGO+ALFCH2*UHGO+(1.0/FF)*ALOG(RIOH2/RIOM))/
     1      (ALFAM+ALFCH2)
      UCORL=(RIOM*ALFAM*UMGO-RIOH2*ALFCH2*UHGO)/(ALFAM+ALFCH2)
      RICOR=RIOM**(ALFCH2/(ALFAM+ALFCH2))
     1       *RIOH2**(ALFAM/(ALFAM+ALFCH2))
     2       *EXP(ALFAM*ALFCH2/(ALFAM+ALFCH2)*FF*(UHGO-UMGO))
      RICORL=(ALFAM*RIOM*ALFCH2*RIOH2/(ALFAM*RIOM-ALFCH2*RIOH2))
     1        *FF*(UMGO-UHGO)
      RETURN
      END
C
      SUBROUTINE SGPM(UMGO,UHGO,RK1,RKP,EXM,EXH,EXM1,EXH1,DELPM)
      COMMON/PARAMM/ ALFAM,ALFCM,RKAM,RKCMF,DM,CMTB,DELM
      COMMON/PARAMH/ALFAH2,ALFCH2,RKAH2F,RKCH2,DH,DH2,SH2,CHB,PH2B,
     1  DELH,DELH2
      COMMON/IN/ NLIM,V1,F,R,T,FF,RHO
      COMMON/OHM/RO,RKAPAB,ROHM,ROHMU
      COMMON/POT/VCOR,DPHDIF,DPHLJ
      COMMON/B/BAM,BCH,A
      BAM=2.303/(ALFAM*FF)
      BCH=2.303/(ALFCH2*FF)
      RK=BAM*BCH/(2.303*(BAM+BCH))
      RK1=1.0/RK
      DELPM=VCOR-UMGO
      DELPH=UHGO-VCOR
      EXM=(EXP(2.0*FF*DELPM)-1.0)
      EXM1=2.0*FF*(1.0/EXM)
      EXH=(EXP(FF*DELPH)-1.0)
      EXH1=FF*(1.0/EXH)
```

```
      RKP=RK1+EXM1+EXH1
C     RICSG=RK/(A*RP)
C     RICSGM=1.0/(RP*A*RKP)
      RETURN
      END
C
      FUNCTION PDIF(Y,YCORM)
      PDIF=(Y-YCORM)*100.0/YCORM
      RETURN
      END
C
      SUBROUTINE ACTIVC(CM0,CH0,CCL0)
      COMMON/FIN/FMCL,FHCL
      CMP=1000.0*CM0
      CHP=1000.0*CH0
      CCLP=1000.0*CCL0
      ALPHAP=1.1779
      BPA=1.0
      BETPH=0.27
      BETPM=0.2
      SQRTIP=0.5*(CHP+4.0*CMP+CCLP)
      FM1=-6.0*ALPHAP*SQRTIP/(1.0+BPA*SQRTIP)
      FM2=4.0*BETPH*CHP
      FM3=2.0*BETPM*(2.0*CMP+CCLP)
      ALNFM=FM1+FM2+FM3
      FMCL=EXP(ALNFM)
C
      FH1=-ALPHAP*SQRTIP/(1.0+BPA*SQRTIP)
      FH2=FM2
      FH3=FM3
      ALNFH=FH1+FH2+FH3
      FHCL=EXP(ALNFH)
C
      RETURN
      END
C
      SUBROUTINE IRSCAN(YCORM,VDIF,ROHM,ROHMU,RPP,ERROR,ERRORU)
      COMMON/PARAMM/ ALFAM,ALFCM,RKAM,RKCMF,DM,CMTB,DELM
      COMMON/PARAMH/ALFAH2,ALFCH2,RKAH2F,RKCH2,DH,DH2,SH2,CHB,PH2B,
     1 DELH,DELH2
      COMMON/IN/ NLIM,V1,F,R,T,FF,RHO
      COMMON/B/BAM,BCH,A
      FFM=ALFAM*FF
      FFH=ALFCH2*FF
      ARP1=YCORM*FFM*EXP(FFM*VDIF)+YCORM*FFH*EXP(-FFH*VDIF)
      RPP=1.0/(ARP1*A)
      ERROR=ROHM*100.0/(RPP+ROHM)
      ERRORU=ROHMU*100.0/(RPP+ROHMU)
      RETURN
      END
```

TECHNICAL INFORMATION DEPARTMENT
LAWRENCE BERKELEY LABORATORY
UNIVERSITY OF CALIFORNIA
BERKELEY, CALIFORNIA 94720